Active particles, ratchets and their field theories

a thesis presented for the degree of

Doctor of Philosophy of Imperial College London

and the

Diploma of Imperial College

by

Zigan Zhen

Department of Mathematics

Imperial College

180 Queen's Gate, London SW7 2AZ

March 2023

Declaration of Originality

I declare that the work presented in this thesis is entirely my own work unless stated otherwise. I have acknowledged contributions from collaborators and others according to the standard referencing practices. Further, I have sought permission to reproduce any third-party copyrighted material in this thesis from the copyright holders and collaborators. All permissions are included in the appendix of this thesis.

Zigan Zhen

Copyright Declaration

The copyright of this thesis rests with the author. Unless otherwise indicated, its contents are licensed under a Creative Commons Attribution-Non Commercial 4.0 International Licence (CC BY-NC). Under this licence, you may copy and redistribute the material in any medium or format. You may also create and distribute modified versions of the work. This is on the condition that: you credit the author and do not use it, or any derivative works, for a commercial purpose. When reusing or sharing this work, ensure you make the licence terms clear to others by naming the licence and linking to the licence text. Where a work has been adapted, you should indicate that the work has been changed and describe those changes. Please seek permission from the copyright holder for uses of this work that are not included in this licence or permitted under UK Copyright Law.

Thesis advisor: Dr. Gunnar Pruessner

Active particles, ratchets and their field theories

Zigan Zhen

Abstract

This thesis aims to address problems in active matter by employing techniques in both stochastic processes and statistical field theories. It is mainly divided into two parts: first, applications of stochastic processes to find the entropy production of various exactly solvable models and solve the dynamics of a Run-and-Tumble particle in a piecewise linear potential, and second, applications of field theories to find the optimal shape for maximising currents of a Run-and-Tumble particle perturbatively and probing the particle identities using different field theories. In Chapter 1, I derive various methods and results from stochastic processes that are used in the rest of the thesis. In Chapter 2, I present a self-contained review of entropy production and calculate it from first principles for various exactly solvable models. In Chapter 3, I solve the steady-state dynamics of a Run-and-Tumble particle in a piecewise linear ratchet and calculate various other quantities such as particle current, entropy production and mean first passage time. In Chapter 4, I derive and present Doi-Peliti field theory and response field theory which are used in the rest of the thesis. In Chapter 5, I present a method of solving the probability distribution perturbatively and finding the optimal shape of the potential that maximises the probability current for a Run-and-Tumble particle using Doi-Peliti field theory. In Chapter 6, I identify the mechanism where particle entity is enforced in the context of the Doi-Peliti field theory of a diffusive particle and the response field theory that is derived from Dean's equation.

Thesis advisor: Dr. Gunnar Pruessner

Statement of contribution

The content of this thesis, as far as the scientific foundations are concerned, is a reflection of my understanding of the literature. I have prepared such introductory material specifically for the present thesis. As far as original work is concerned, the thesis is a collection of my work together with my collaborators, as well as my supervisor. Much of these chapters are based on published or jointly prepared manuscripts, which I have copied verbatim to this thesis. To clarify what my contributions are, in particular with respect to the technical work and the scientific writing, I include a summary of my contribution to each chapter.

- Chapter 1: This is an introduction to stochastic processes in general. The derivations and results are heavily based on H. Risken's textbook *The Fokker-Planck equations: Methods of Solution and Applications* [135] and D. Tong's lecture notes on *kinetic theory* [163].
- Chapter 2: This chapter is based on [30], which is itself an introduction to entropy production, based on exactly solvable systems. I contributed mainly to the analysis of driven Brownian particles (Sec. 2.3.9), driven Brownian particles in a harmonic potential (Sec. 2.3.10), driven Brownian particles on a ring with potentials (Sec. 2.3.11 and Sec. 2.3.12), run-and-tumble motion with diffusion on a ring (Sec. 2.3.13) and switching diffusion process on a ring (Sec. 2.135). I also contributed to the writing up of the manuscript.
- Chapter 3: This chapter is a manuscript [137] I recently completed with C. Roberts, independently from my supervisor. C. Roberts and I contributed equally to this chapter. I mainly contributed to the theoretical analysis and C.R. contributed mainly to numerical studies.
- Chapter 4: This is an introduction to field theories. The derivations and results are heavily based on J. Pausch's PhD thesis [119], G. Pruessner's lecture notes [128] and U. Täuber's book *Critical Dynamics: A Field Theory Approach to Equilibrium and Non-Equilibrium Scaling Behavior* [161].
- Chapter 5: This chapter is an (almost) verbatim copy of a manuscript [181] I prepared in collaboration with G. Pruessner. G.P. conceived the project and

supervised the project throughout. I did everything else, including the mathematical derivations, the diagrammatics, identifying symmetries and conservation laws. The writing of this manuscript was done jointly with G.P.

- Chapter 6: This is a chapter on particle entity in field theories, an (almost) verbatim copy of [18]. The research project was in collaboration with M.Bothe, L.Cocconi and G.Pruessner. My contribution to the project consisted of the construction and the derivation of the field theory. I also contributed to the example of two-point correlation functions and proving the particle entity in the Doi-Peliti framework.

Acknowledgments

First and foremost, I thank my supervisor Dr Gunnar Pruessner for his continuous support, guidance and encouragement. His passion for research has always been an inspiration for me to keep going forward. He was always there when I encountered difficulties and was always willing to advise, support and encourage me. A few lines of words are not enough to express my gratitude.

I am grateful to everyone in my research group who provided a supportive and kind environment for research and for the fun time we spent together. I would like to acknowledge all of my co-authors, this thesis would not have been possible without them. I thank all of my fellow students, friends and teachers who have influenced me throughout my education.

A special acknowledgement to a family in Brighton that I was incredibly fortunate to know and that has supported me throughout my years in the UK, family friends who hosted me in the last few years and a gentleman in Edinburgh who has been an inspiration for me outside academia.

Finally, I thank my parents for their love and support.

Contents

Abstract **5**

Acknowledgments **9**

List of figures **15**

List of tables **25**

0 Introduction **27**

1 STOCHASTIC PROCESSES **31**
- 1.1 Stochastic processes . . . 31
- 1.2 Master equations . . . 32
- 1.3 Langevin equations . . . 32
  - 1.3.1 Overdamped Langevin equations . . . 33
- 1.4 Fokker-Planck equations . . . 33
  - 1.4.1 Formal solution and short time transition probability . . . 36
  - 1.4.2 Boundary conditions . . . 38
  - 1.4.3 Path-integral solution . . . 39
- 1.5 First-Passage time problems . . . 40
  - 1.5.1 Formal solution . . . 42
  - 1.5.2 Solution using the adjoint operator . . . 42
  - 1.5.3 BOUNDARY CONDITIONS . . . 43

2 ENTROPY PRODUCTION IN EXACTLY SOLVABLE MODELS **45**
- 2.1 Introduction . . . 46
- 2.2 Review of entropy production . . . 47
- 2.3 Systems . . . 59
  - 2.3.1 Two-state Markov process . . . 59
  - 2.3.2 Three-state Markov process . . . 60
  - 2.3.3 Random walk on a complete graph . . . 63
  - 2.3.4 N independent, distinguishable Markov processes . . . 64
  - 2.3.5 N independent, indistinguishable two-state Markov processes . . . 66
  - 2.3.6 N independent, indistinguishable d-state processes . . . 68
  - 2.3.7 Random Walk on a lattice . . . 72

2.3.8 Random Walk on a ring lattice . . . 76
2.3.9 Driven Brownian particle . . . 77
2.3.10 Driven Brownian particle in a harmonic potential . . . 80
2.3.11 Driven Brownian particle on a ring with potential . . . 82
2.3.12 Run-and-tumble motion with diffusion on a ring . . . 85
2.3.13 Switching diffusion process on a ring . . . 88
2.4 Discussion and concluding remarks . . . 91

3 Run-and-tumble motion on a linear ratchet: analytic solution, power extraction and first-passage properties **95**
3.1 Introduction . . . 96
3.2 Model . . . 98
3.3 Particle densities . . . 102
3.4 Currents . . . 107
3.5 Entropy production . . . 114
3.6 Power output and efficiency . . . 121
3.7 First-passage properties . . . 124
3.8 Conclusion . . . 128

Appendices **131**
Appendix 3.A Derivation of steady-state particle densities $P^{[i]}_{R,L}(x)$ . . . 131
Appendix 3.B Derivation of $D = 0$ steady-state particle densities $p^{[i]}_{R,L}(x)$ and currents $j^{[i]}_{R,L}(x)$ . . . 133
Appendix 3.C Derivation of first-passage properties . . . 137
3.C.1 Mean first-passage times $\tau^{[i]}_{R,L}(x)$ . . . 137
3.C.2 Splitting probabilities $\Pi^{[i]}_{R,L}(x)$ . . . 139
3.C.3 Conditional splitting probabilities $\pi^{[i]}_{X|Y}(x)$ . . . 140

4 Statistical Field Theories **143**
4.1 Doi-Peliti field theory . . . 143
4.1.1 Operator and states . . . 144
4.1.2 Deriving the field theory . . . 145
4.1.3 Path integral representation . . . 146
4.1.4 From Fokker-Planck equations to field theories . . . 150
4.1.5 Generating functions and correlation functions . . . 152
4.2 Response field theory . . . 153
4.2.1 Janssen–De Dominicis response functional . . . 155

Appendices **159**
Appendix 4.A Discretisation and Jacobian . . . 159

5 Optimal Ratchet Potentials for Run-and-Tumble particles **161**

Appendices **173**
Appendix 5.A Numerical optimisation and plotting procedure 173
5.A.1 Optimisation procedure 173
5.A.2 Plotting procedure 175
Appendix 5.B Field theory 178
Appendix 5.C Steady-state density and current 183
5.C.1 General arguments 183
5.C.2 Steady-state density of Run-and-Tumble particles in a periodic potential 186
5.C.3 Steady-state current 191
Appendix 5.D Comparison between the field theory and the exact result [9] for a piece-wise linear potential 193
5.D.1 Radius of convergence in field theory 195
Appendix 5.E Symmetry properties of the steady-state current with no external force 197
5.E.1 The steady-state current J is odd in ν 200
5.E.2 The steady-state current vanishes in potentials with only odd Fourier coefficients 202
5.E.3 The steady-state current vanishes in potentials even about some x^* 204
Appendix 5.F Current for more different ratchet profiles 206
Appendix 5.G Current with an external force 208
Appendix 5.H Entropy production 210
Appendix 5.I Active engine efficiency 211

6 Particle Entity in the Doi-Peliti and Response Field Formalisms **215**
6.1 Introduction 216
6.2 Setting up the formalisms 217
6.2.1 Doi-Peliti field theory 217
6.2.2 Dean's equation in the response field formalism 221
6.2.3 Example: the two-point density correlation function 226
6.3 Probing for particle entity 233
6.4 Particle entity in Doi-Peliti 236
6.5 Particle entity in response field theories: Dean's equation 239
6.6 Conclusion 245

Appendices **247**
Appendix 6.A Induction over connected diagrams 247
Appendix 6.B Multiple starting points 257

Appendix 6.C Integer requirements on initialisation amplitude n_0 260

7 Conclusion **263**

Index **265**

Bibliography **265**

A Right to Reproduce **283**
A.1 Copyright permission 283
A.2 Approval of co-authors 284
A.2.1 Bianca Buturca 284
A.2.2 Marius Bothe 284
A.2.3 Luca Cocconi 285
A.2.4 Rosalba Garcia-Millan 286
A.2.5 Gunnar Pruessner 287
A.2.6 Connor Roberts 287

List of figures

2.1 Two-state Markov chain in continuous time. The black blob indicates the current state of the system. Independently of the choice of α and β, this processes settles into an equilibrium steady-state at long times (in the absence of an external time-dependent diving). 59

2.2 Three-state Markov chain in continuous time. The black blob indicates the current state of the system. Symmetry under cyclic permutation is introduced by imposing identical transition rates α and β for counter-clockwise and clockwise transition, respectively. 61

2.3 Entropy production of the two- and three-state Markov processes (black and grey lines respectively) discussed in Sections 2.3.1 and 2.3.2 as a function of time. For the two-state system we plot Eq. (2.38) with $p = 1$ both for the symmetric, $\alpha = \beta$ (solid lines), and for the asymmetric case, $\alpha \neq \beta$ (dashed lines). In both, the entropy production decays exponentially at long times. For the three-state system, Eq. (2.42), the asymmetric case displays a finite entropy production rate at long times, consistent with Eq. (2.43) and the condition that at stationarity $\dot{S}_i(t) = -\dot{S}_e(t)$. 62

2.4 Random walk on a complete graph of d nodes (here shown for $d = 6$). The black blob indicates the current state of the system. For uniform transition rates, the symmetry under node relabelling leads to an equilibrium, homogeneous steady-state with $P_j = 1/d$ for all j. 63

2.5 Example of $N = 5$ non-interacting, distinguishable processes with $d_1 = 4$, $d_2 = 2$, $d_3 = 3$, $d_4 = 5$ and $d_5 = 5$. The black blobs indicate the current state of each sub-system. 64

2.6 N independent, indistinguishable two-state Markov processes in continuous time. The black blobs indicate the current state of the single-particle sub-system. Since processes are indistinguishable, states are fully characterised by the occupation number of either state, if the total number of particles is known. 66

2.7 N independent, indistinguishable d-state Markov processes (here shown for $d = 6$ and $N = 8$) in continuous time. Black blobs indicate the current state of the single-particle sub-systems. Due to indistinguishably, multi-particle states are fully characterised by the occupation number of an arbitrary subset of $d - 1$ states, if the total number of particles is known. 68

2.8 Simple random walk on an infinite, one-dimensional lattice in continuous time. The black blob indicates the current position of the random walker. The left and right hopping rates, labelled ℓ and r respectively, are assumed to be homogeneous but not equal in general, this leading to a net drift of the average position. 72

2.9 Entropy production of a random walk on a one-dimensional lattice (RW on $\mathbb{Z}$), for symmetric and asymmetric hopping rates, as a function of time, Eq. (2.82) (solid lines). The asymptotic behaviour at large t, Eq. (2.83) (dotted lines), decays algebraically in the symmetric case ($r = \ell$) and converges to a positive constant in the asymmetric case ($r \neq \ell$). 75

2.10 Simple random walk on an periodic, one-dimensional 'ring' lattice in continuous time. This model generalises the three-state Markov chain discussed in Section 2.3.2 to L states. The black blob indicates the current position of the random walker. Due to the finiteness of the state space, this process is characterised by a well defined steady-state, which is an equilibrium one for symmetric rates $\ell = r$. 76

2.11 Driven Brownian particle on the real line. The black blob indicates the particle's current position. 78

2.12 Driven Brownian particle in a harmonic potential. This process reduces to the standard Ornstein-Uhlenbeck process upon rescaling $x \to x' + v/k$. The black blob indicates the particle's current position. The presence of a binding potential implies that the system relaxes to an equilibrium steady-state at long times. 80

2.13 Entropy production of the drift-diffusion process in an external potential, Eq. (2.104), as a function of time for different parameter combinations. For vanishing potential stiffness, $k \to 0$, we recover Eq. (2.94) for a free drift-diffusion particle. In particular, for $v = 0$ the entropy production decays algebraically, while for $v \neq 0$ it converges to the constant value v^2/D. For $k > 0$, the algebraic decay is suppressed exponentially at long times as the process settles into its equilibrium steady-state. 82

2.14 Driven Brownian particle on a ring $x \in [0, L)$ with a periodic potential satisfying $V(x) = V(x + L)$. Any finite diffusion constant $D > 0$ results in a stationary state at long times that is non-equilibrium for $v \neq 0$. The black blob indicates the particle's current position. 83

2.15 Run-and-tumble motion with diffusion on a ring $x \in [0, L)$. A run-and-tumble particle switches stochastically, in a Poisson process with rate α, between two modes 1 and 2 characterised by an identical diffusion constant D but distinct drift velocities v_1 and v_2. The two modes are here represented in black and grey, respectively. For arbitrary positive diffusion constant D or tumbling rate α with $v_1 \neq v_2$ the steady state is uniform but generally non-equilibrium. 85

2.16 Switching diffusion process on a ring $x \in [0, L]$ in continuous time. A switching diffusion process involves a stochastic switching between M modes characterised by an identical diffusion constant D but distinct drifts v_i $(i = 1, 2, \ldots, M)$. The marginal switching dynamics are characterised as an M-state Markov process with transition rates α_{ij} from mode i to mode j. 89

3.1 Schematic representation of RnT particles moving on a periodic ratchet potential $U(x) = U(x + \ell)$, Eq. (3.1), with maximum amplitude $U(a) = h$. Due to the contribution imparted by the external force $-f$, the overall drift of an RnT particle alternates, with rate γ, between $v - f$, corresponding to the right-moving state $\sigma(t) = +1$ (red sphere), and $-(v + f)$, corresponding to the left-moving state $\sigma(t) = -1$ (blue sphere). 99

3.2 By applying an external counterforce $-f$, work W can be extracted from the rectified motion of an RnT particle. 100

3.3 Steady-state particle densities $P(x), P_R(x), P_L(x)$, Eq. (3.4) (top), and particle currents $J, J_R(x), J_L(x), \mathcal{J}_{L\to R}(x)$, Eqs. (3.6)-(3.8) (middle), for a particular ratchet potential $U(x)$, Eq. (3.1), shown in the bottom panel. The vertical dashed lines indicate the position of the ratchet apex, x = a. 105

3.4 Time evolution of the overall particle density $P(x,t) = P_R(x,t) + P_L(x,t)$ obtained from averaging 10^6 stochastic trajectories of an RnT particle on a ratchet. In each realisation, a particle is initialised with equal probability of being a right mover or a left mover at $x = \ell/2$ and $t = 0$, i.e. $P_R(x,0) = P_L(x,0) = \delta(x - \ell/2)/2$, before it is evolved in time by numerically integrating Eq. (3.2) in timesteps of $\mathrm{d}t = 10^{-5}$. At large times $t \to \infty$, the simulated densities converge to the theoretical steady-state density $P(x) = P_R(x) + P_L(x)$, Eq. (3.4). We also numerically integrated Eq. (3.2) in timesteps of $\mathrm{d}t = 10^{-4}$ to check for convergence and obtained the same result. 106

3.5 Mechanism through which the magnitude of the current of each species, i.e. $|J_R(x)|$ and $|J_L(x)|$, is greater close to the potential minimum $x = 0$ due to a "circulating" current effect from particles that tumble before overcoming the potential barrier. When in the right-moving state (red spheres), the particle experiences a smaller effective potential $U_{\text{eff}}(x) = U(x) - (v - f)x$ than when in the left-moving state (blue spheres) $U_{\text{eff}}(x) = U(x) + (v + f)x$. Even in the case where the self-propulsion v is suppressed by the force $U'(x)$ from the ratchet, i.e. $0 < v - f < U'$[1], the asymmetry in $U_{\text{eff}}(x)$ between species will result in, on average, a greater number of right movers diffusing up the slope that return back down the slope as left movers. 108

3.6 Particle current J, Eq. (3.8), as a function of the position of the ratchet apex a for various external forces f. 109

3.7 Position of the ratchet apex a^* resulting in maximum current J for various diffusion constants D and $h = 0.2$. Maximum current occurs for $a = \ell - h/(v + f)$ as $D \to 0$ and monotonically increases with D to $a \to \ell^-$. 110

3.8 Particle current J, Eq. (3.8), as a function of the ratchet height h for various external forces f. For $h = 0$, the current is given by $J = -f/\ell$. The current vanishes for all f as $h \to \infty$, due to the confinement at $x = 0$ being infinitely strong. The peak in the current around $h \approx 4$ reflects a compromise between the degree to which particles are rectified while not being confined too strongly. 112

3.9 Particle current J, Eq. (3.8), as a function of diffusion D for various magnitudes of the slope $U'^{[1]} = h/a$ and for parameter values $a = 0.9$, $v = 1$ and $f = 0.02$. For $D \to \infty$, the current asymptotically approaches $J = -f/\ell$. As $D \to 0$, the value of J depends on whether $v - f < h/a$ and $v + f < h/(\ell - a)$, which are sufficient conditions for vanishing current since the resulting confining force is greater than the combined self-propulsive and external forces. For $v - f > h/a$, it is possible that $J > 0$, even for $D = 0$, as illustrated by the line for $h/a = 0.5$. The inset shows that for $v - f < h/a$, J picks up abruptly in D indicating transport is due to diffusive fluctuations. 113

3.10 Steady-state entropy production density for right movers $\dot{s}_R(x)$, Eq. (3.15), left movers $\dot{s}_L(x)$, tumbling transitions between states $\dot{s}_{R\leftrightarrow L}(x)$, Eq. (3.16) (inset), and their sum $\dot{s}_{\text{int}}(x) = \dot{s}_R(x) + \dot{s}_L(x) + \dot{s}_{R\leftrightarrow L}(x)$. The vertical dashed lines indicate the position of the ratchet apex, $x = a$. 116

3.11 Steady-state entropy production rate $\dot{S}_{\text{int}}$, Eq. (3.21), as a function of the ratchet height h for various external forces f. In the absence of a ratchet, $h = 0$, the entropy production is given by $\dot{S}_{\text{int}} = (v^2 + f^2)/D$ (inset), whilst $\dot{S}_{\text{int}} \to 0$ as $h \to \infty$ for all f. 117

3.12 Steady-state entropy production rate $\dot{S}_{\text{int}}$, Eq. (3.21), as a function of diffusion D for various magnitudes of the slope $U'^{[1]} = h/a$ and for parameter values $a = 0.9$, $v = 1$ and $f = 0$. The entropy production vanishes as $D \to \infty$. For $D \to 0$ (inset), $\dot{S}_{\text{int}}$ diverges or remains finite depending on whether the particle is confined, i.e. whether $v - f < h/a$ and $v + f < h/(\ell - a)$. 119

3.13 Steady-state power output $\dot{W}$, Eq. (3.23), as a function of the external force f for various magnitudes of the slope $U'^{[1]} = h/a$. Maximum power output is observed to occur for a slope around $U'^{[1]} \approx 6$ for the default parameters defined in Sec. 3.2. The power output $\dot{W}$ and thermodynamic efficiency η (inset) are non-zero for external forces $0 < f < f_{\text{stall}}$. The stall forces in this case are $f_{\text{stall}} \approx 0.054, 0.083, 0.112, 0.138$ for each $U'^{[1]} = 4, 5, 6, 7$ respectively. 122

3.14 Steady-state efficiency η as a function of the external force f for various heights h of the ratchet. 123

3.15 Schematic representation of configuration (ii) in Sec. 3.7, used to study the mean first-passage time of RnT particles on a ratchet with a reflecting boundary at $x = \ell$ and an absorbing boundary at $x = 0$. Configuration (i) is the same as configuration (ii) but with the reflecting boundary at $x = \ell$ replaced by an absorbing boundary. 124

3.16 Comparison between simulations and theoretical results for mean first-passage times $\tau_{R/L}(x)$, Eq. (3.25), and splitting probabilities $\Pi_{R/L}(x)$, Eq. (3.26), for initialisation of an RnT particle as a right/left mover. As in Fig. 3.4, simulations were performed by numerically integrating the Langevin equation (3.2) in timesteps of $\mathrm{d}t = 10^{-5}$. The mean first-passage times and splitting probabilities were calculated from the average time it takes the particle to escape the interval, in the case of (a) and (b), and the proportion of times it escapes through $x = 0$, in the case of (c), for 10^5 realisations at each $x = 0, 0.01, \ldots, \ell = 1$. The vertical dashed lines indicate the position of the ratchet apex, $x = a$. The theoretical results are in good agreement with simulations. We also numerically integrated Eq. (3.2) in timesteps of $\mathrm{d}t = 10^{-4}$ to check for convergence and obtained the same result. 126

3.17 Mean first-passage times $\tau(x)$, Eq. (3.25), and corresponding splitting probabilities $\Pi(x)$ (insets), Eq. (3.26), for varying different parameters of the system in the case of absorbing boundaries at $x = 0$ and $x = \ell$. In (b), red (respectively, blue) lines indicate initialisation as a right mover (respectively, left mover) for $h = 0$, as studied in Ref. [105]. In (a) and (b), the vertical dashed lines indicate the position of the ratchet apex, $x = a$. 126

5.0.1 Optimal potential $\widehat{U}(x)/D$ for $f = 0, D = 1$, $w = 1$, $L = 1$ and $\gamma = 1$, so that $Pe = Qe = \kappa = 1$, resulting in the current $\widehat{J}L^2/D = 0.03789\ldots$ to the right and $\widehat{\nu^{<}_{\mathrm{roc}}} = 1.167\ldots$. The details of the numerical scheme employed to produce the plot are discussed in Appendix. 5.A.2. 163

5.0.2 Shapes of potential maximising the steady-state current at the parameter values indicated. Technical details of the plots in Appendix. 5.A.2. 168

5.A.1 Imaginary part of the modes $\widehat{U}_a$ allowing for $A = 50, 100, 150, 200$ modes in the optimisation procedures (filled symbols) and, also, as extracted from the linear interpolation of the potential shown in Fig. 5.0.1 (open squares). Parameters are $D = 1$, $w = 1$, $L = 1$ and $\gamma = 1$, so that $Pe = Qe = \kappa = 1$. 175

5.A.2 The optimal potential $\widehat{U}(x)$ of Fig. 5.0.1 shown with higher resolution of 2000 points and $A = 50, 200$ as indicated. The peaks around $x = 0$ and $x = L$ are likely to be artefacts, as discussed in the text. 176

5.A.3 Detail of the potential $U_B(x)/D$ of Eq. (5.14) around the peak near $x/L = 1$ based on $A = 100$ modes using $B = 20, 40, 60, 80$ and 100 modes respectively in the sum. Parameters: $f = 0, D = 1$, $w = 1$, $L = 1$ and $\gamma = 1$, so that $Pe = Qe = \kappa = 1$. 176

5.D.1 The periodic, piece-wise linear ratchet described by Eq. (5.69) with $\alpha = 0.9$. The ratchet has $U(0) = 0$ rises up to $U(\alpha L) = U_0$ and descends again to $U(L) = 0$. The point $x^* = \alpha L/2$ marks the point where $U(x^* + x) - U(x^*) = U(x^*) - U(x^* - x)$ with $U(x^*) = U_0/2$, Eq. (5.73), Appendix. 5.E. 194

5.D.2 Comparison of the present field-theoretic result (filled circles) for the steady-state current and the exact solution [9] (solid line) for a piece-wise linear ratchet potential Eq. (5.69) with $\alpha = 0.9$ and $U_0 = 1$ as shown in Fig. 5.D.1. The other parameters are $f = 0, w = 1, \gamma = 5$, $D = 1$ and $L = 1$. The field theoretic results are based on 200 Fourier coefficients and up to 75 orders in ν. The agreement is perfect (deviation of less than 0.15% up until $\nu^{<}_{\rm roc} = 4.272\ldots$ the radius of convergence estimated via Eq. (5.12) and shown as a dotted vertical line Beyond that, the current due to the field theory diverges sharply. The coupling ν that produces the best current $\widehat{J} = 0.015739\ldots$ in this potential is $\widehat{\nu} = 3.90\ldots$, where even the shallow part of the potential has a slope greater than the self-propulsion speed, $\widehat{\nu}U_0/(\alpha L) = 3.9 \cdot 1/(0.9 \cdot 1) > w = 1$, indicating that transport is dominated by diffusion. 196

5.D.3 A plot of $\nu^{<}_{\rm roc}$ against D with all other parameters using the first 200 modes of a piece-wise linear ratchet potential Eq. (5.69) with $\alpha = 0.9$ and $U_0 = 1$ as shown in Fig. 5.D.1. The other parameters are $f = 0, w = 1, \gamma = 1$, $D = 1$ and $L = 1$. The field theoretic results are based on 200 Fourier coefficients and up to 75 orders in ν. One can see there is a linear relationship between $\nu^{<}_{\rm roc}$ and D. 197

5.D.4 A plot of $\nu^{<}_{\rm roc}/D$ against Pe and Qe with all other parameters using the first 200 modes of a piece-wise linear ratchet potential Eq. (5.69) with $\alpha = 0.9$ and $U_0 = 1$ as shown in Fig. 5.D.1. The other parameters are $f = 0, \gamma = 1$, $D = 1$ and $L = 1$. The field theoretic results are based on 200 Fourier coefficients and up to 75 orders in ν. 198

5.E.1 Particle density $\rho(x)$ for an RnT particle in the periodic "hurdle" potential $U(x)$ Eq. (5.76) shown in Fig. 5.E.2, based on 100 modes calculated perturbatively to 75th order in ν. Even when the density profiles cannot be related by a simple geometrical transformation, the steady-state currents are simple the negative of each other. Parameters: $f = 0$, $D = 1$, $w = 1$, $L = 1$ and $\gamma = 1$, so that $Pe = Qe = \kappa = 1$. 199

5.E.2 The "hurdle" potential Eq. (5.76), whose resulting RnT particle density is shown in Fig. 5.E.1a. 200

5.E.3 A schematic representation of a "supersymmetric" ratchet. 203

5.F.1 The 2-mode potential from Eq. (5.96). 206

5.F.2 Current produced by the ratchet potential Eq. (5.96) against the coupling parameter ν. The system parameters are $w = 1, \gamma = 1$, $D = 1$ and $L = 1$. The field theoretic results are up to 75 orders in ν. The radius of convergence $\nu_{\text{roc}}^{<} = 4.221\ldots$ estimated via Eq. (5.12) is shown as a dotted vertical line Beyond that, the current due to the field theory diverges sharply. The coupling ν that produces the best current $\widehat{J} = 0.013735\ldots$ in this potential is $\widehat{\nu} = 3.45\ldots$. The optimal current produced by Eq. (5.96) is about 64% smaller versus the optimal current in Fig. 5.0.1. 207

5.F.3 The ratchet potential profile in Eq. (5.97). 207

5.F.4 Current produced by the ratchet potential Eq. (5.97) against the coupling parameter ν. The system parameters are $w = 1, \gamma = 1$, $D = 1$ and $L = 1$. The field theoretic results are up to 75 orders in ν. The radius of convergence $\nu_{\text{roc}}^{<} = 1.5767\ldots$ estimated via Eq. (5.12) is shown as a dotted vertical line Beyond that, the current due to the field theory diverges sharply. The coupling ν that produces the best current $\widehat{J} = 0.011553\ldots$ in this potential is $\widehat{\nu} = 1.525\ldots$. The optimal current produced by Eq. (5.97) is about 69% smaller versus the optimal current in Fig. 5.0.1. 208

5.G.1 Current produced by piece-wise linear ratchet potential Eq. (5.69) against the force f using the perturbative expansion arising from Eq. (5.11). The system parameters are $w = 1, \gamma = 1$, $D = 1$ and $L = 1$. For the piece-wise linear ratchet potential Eq. (5.69), we used $\alpha = 0.9$ and 200 modes. The field theoretic results are up to 75 orders in ν. 209

5.G.2 Current produced by piece-wise linear ratchet potential Eq. (5.69) against the force f using the perturbative expansion arising from Eq. (5.11). The system parameters are $w = 1, \gamma = 1$, $D = 1$ and $L = 1$. For the piece-wise linear ratchet potential Eq. (5.69), we used $\alpha = 0.9$ and 200 modes. The field theoretic results are up to 75 orders in ν. 209

5.I.1 Optimal power output $\mathcal{P}_{\text{out}}$ against the force f. The system parameters are $w = 1, \gamma = 1$, $D = 1$ and $L = 1$. We used 20 modes and the field theoretic results are up to 75 orders in ν. 212

6.2.1 The time-dependent number density $\rho(x,t)$ for a physical point particle undergoing diffusion is expected to remain localised under the dynamics, indicating that the particle can only occupy one position in space at any given time. While this property is preserved under Dean's dynamics (left column), it is generally lost when resorting to effective descriptions, such as the classical diffusion equation (right column). This difference is most obvious when measuring the instantaneous particle number density at two points a finite distance away from each other (bottom row). 225

List of tables

2.1 List of particle systems for which we have calculated their entropy production $\dot{S}_i(t)$. 59

0

Introduction

Active matter is a classic example of far-from-equilibrium systems [130, 106]. They are composed of self-propelling agents that consume energy from the environment to exert mechanical work [59, 29, 84, 54, 113, 124, 109]. Due to the self-propelled motion, active particles are known to break detailed-balance typically by converting fuel into mechanical motion or energy at the individual particle scale. These phenomena can be observed in bacteria [29], cells and artificially made particles, such as Janus particles [171].

Ratchet effects arise by placing a single or interacting Brownian particles under an asymmetric environment that produce a net current by applying an external force or flashing the asymmetric obstacle [42, 102, 9, 121]. A new class of active ratchet systems has been realised by immersing self-propelling particles under asymmetric environments. Such systems demonstrate a rectified unidirectional motion, break time-reversal symmetry and locally produce entropy [132, 54, 109]. Due to the emergence of rectified motion, active ratchet systems can also drive engines that perform work against an external workload [124].

Despite the progress made and the benchmark models discovered in the last few years, addressing general physical quantities such as the probability distribution of active matter or other non-equilibrium systems still remains challenging. In many cases, the

thermodynamical quantities such as free energy or pressure cannot even be defined properly [154], these are known as non-variational systems.

Over of the past few decades, fresh approaches have unveiled universal laws applicable to far-from-equilibrium systems beyond the linear response regime. One approach to studying such non-equilibrium or active matter systems is by the use of stochastic thermodynamics [146]. Stochastic thermodynamics systematically provides a toolbox to extend concepts from equilibrium thermodynamics to far-from-equilibrium systems through Jarzynski relation fluctuation theorems [80, 34]. These results are particularly relevant for the study of distribution functions of quantities such as exchanged heat and entropy production. The entropy production rate is a quantity of particular interest as a non-zero entropy production implies the breaking of time-reversal symmetry, which is the hallmark of a non-equilibrium system. In other words, the system manifests the arrow of time as the future is distinguishable from the past.

Another approach to studying such systems is by employing techniques in statistical field theories [164]. In statistical field theories, the path integral is a powerful and elegant tool allowing us to systematically calculate correlation functions. One class of field theories is Doi-Peliti field theory which is derived from models that can be described as master equations of Markovian Poisson processes. It was built on the work of Masao Doi [43] and Luca Peliti [123]. Doi-Peliti field theory has proven to be a useful and versatile tool in many problems in non-equilibrium statistical mechanics as it is able to capture the particle entity nature of the system and account for interactions. It has been applied in areas including active matter [62, 19, 180], reaction-diffusion processes [119], branching processes [61] and percolations [158, 79]. Another example of field theory is response field theory. It was built on the work by P.C. Martin, E.D. Siggia and H.A. Rose, H.K Janssen and C. De Dominicis [110, 78, 44] which transforms a stochastic process described by Langevin equations into a field theory.

Objectives

By studying various topics in active matter, ratchets and field theories, I hope to accomplish the following objectives:

- To study exactly solvable problems in non-equilibrium settings and entropy pro-

duction rates for both discrete and continuous Markovian processes as well as single and multi-particle systems.

- To expand the current knowledge on models from active matter, such as the probability distributions, probability current, entropy production and first-passage properties for run-and-tumble particles under a piecewise linear ratchet potential using stochastic methods and an arbitrary external potential using field theories.
- To probe and discuss the particle nature of interacting particle systems under different field theoretic frameworks such as Doi-Peliti and response field theory.

Organisation of this thesis

The results of the thesis are presented in Chapters 1-6.

- In Chapter 1, some background knowledge for the rest of the thesis such as stochastic processes, master equations, Langevin Equations, Fokker-Planck equations and so on are introduced and derived.
- In Chapter 2, a review of entropy production is presented and various exactly solvable models such as Markov jump processes, random walks, driven Brownian particles in different potentials and run-and-tumble particles on a ring are presented. Their distribution functions and entropy production rates are calculated and discussed.
- In Chapter 3, a model for a run-and-tumble particle in a piecewise linear potential is introduced. The steady-state probability distribution, probability current, entropy production rate, engine efficiency and first passage properties are calculated and discussed.
- In Chapter 4, a review of field theory is introduced. Some results for Doi-Peliti field theory and response field theory are derived and discussed.
- In Chapter 5, a model for a run-and-tumble particle is introduced. Using Doi-Peliti field theory, the stationary distribution function and the stationary probability current are calculated using a perturbation series. Under a numerical

optimisation scheme, a representation of the optimal potential ratchets that produce the highest current is presented and their design features are discussed.

- In Chapter 6, the Doi-Peliti field theory and the response field theory using Dean's equation both describing non-interacting diffusive particle systems are introduced and compared. The concept of particle entity and related observables to probe it is presented and calculated under both Doi-Peliti and response field theory. A more intuitive probabilistic picture discussing the role of integer particle numbers is also presented.

For each chapter, we start with its own abstract or introduction, where the background and past literature of the content discussed are reviewed. The main results for each chapter are then presented and discussed. We then end with a discussion of the main findings and future problems.

We end the thesis in Chapter 7, where we offer a summary of the thesis and discuss open questions and future research directions.

1

STOCHASTIC PROCESSES

Abstract

The following derivations and results are heavily based on H. Risken's textbook *The Fokker-Planck equations: Methods of Solution and Applications* [135] and D. Tong's lecture notes on *kinetic theory* [163].

In this chapter, we present some results from the theory of stochastic processes which are the main tools employed for the analysis in Chapter 2 and Chapter 3. We first give the definition of a stochastic process, master equations and Langevin equations. We then investigate some of the results in continuous stochastic processes including Fokker-Planck equations, formal solutions to the Fokker-Planck equations and first passage problems.

1.1 Stochastic processes

A stochastic process is a collection of random variables $X = \{X_t; t \in T\}$ with an ordered set T, which can be both discrete and continuous, where, for every $t \in T$, X_t is a measurable function from the sample space Ω to the state space E.

1.2 Master equations

For Markovian systems, the probability density function $P_n(t)$ at time t over a discrete set of states $n \in \Omega$ evolves according to the *Master equation*

$$\frac{\partial P_n(t)}{\partial t} = \dot{P}_n(t) = \sum_m W(m \to n)P_m(t) - W(n \to m)P_n(t) \tag{1.1}$$

where $W(m \to n)$ is the transition rate from state m to n which must be positive. For a continuous variable, the sum needs to be replaced by an integral and the Master equation reads

$$\frac{\partial P(x,t)}{\partial t} = \dot{P}(x,t) = \int \mathrm{d}x' W(x' \to x)P(x',t) - W(x \to x')P(x,t). \tag{1.2}$$

As the system is Markovian, the probability at a later time is completely determined by the probability at time $t = t_0$.

1.3 Langevin equations

Brownian motion is the random motion of particles suspended in a liquid or a gas. The movement of particles is famously caused by the bombardment due to other molecules in the surrounding liquid. Here, we only focus on a single particle with position $x(t)$ at time t in a surrounding medium. Assuming we know the external force L acting on the particle, the motion is then entirely deterministic, which is can be determined by the second order differential equation

$$m\ddot{x} = -\gamma\dot{x} + L \tag{1.3}$$

where the mass of the particle is m and we have included a friction term with coefficient γ. For any specific force L, the path of the particle is fully determined which is in contrast to the random fluctuations in Brownian motion. To reconcile the difference, we split the force L into a deterministic part and a random part

$$L = -V'(x) + f(t), \tag{1.4}$$

where $V(x)$ is a deterministic external potential and $f(t)$ is a random force exerted on the particle from the other molecules in the liquid or gas. The following three properties about the force $f(t)$ are postulated:

1. $f(t)$ can be treated as a stochastic process.
2. The properties of $f(t)$ are independent of the particle position $x(t)$ and the average of the force vanishes,
$$\langle f(t) \rangle = 0. \tag{1.5}$$
3. The collisions of the molecules in the surrounding fluid happen rapidly, which motivates us to postulate the autocorrelation function for the force
$$\langle f(t) f(t') \rangle = 2D\delta(t - t') \tag{1.6}$$

where D is a constant. A term $f(t)$ satisfying the above three properties is generally known as the *white noise* or the *Langevin force* and Eq. (1.3) is known as the *Langevin equation.*

1.3.1 Overdamped Langevin equations

We can simplify the problem further by considering Brownian motion in a very viscous liquid under an external force. This is equivalent to setting the mass $m = 0$ by ignoring the inertial term as the motion is entirely dominated by the friction term in the Langevin equation Eq. (1.3). We are left with the *overdamped* Langevin equation

$$\gamma \dot{x} = -V'(x) + f(t). \tag{1.7}$$

Recall $f(t)$ is the noise term with correlation $\langle f(t) f(t') \rangle = 2D\delta(t - t')$. In the rest of the thesis, we often set the friction term γ to be 1.

1.4 Fokker-Planck equations

We saw previously the Langevin equation Eq. (1.3) which describes the equation of motions of a Brownian particle under an external force or potential. We then try to

derive an equation to describe the probability distribution function.

From the Chapman-Komogorov equation, the probability distribution $P(x, t+\tau)$ at time $t+\tau$ and the probability distribution $P(x,t)$ at time t are related by the transition probability via $W(x, t+\tau|x,t)$,

$$P(x,t+\tau) = \int \mathrm{d}x' W(x,t+\tau|x',t)P(x',t). \tag{1.8}$$

Assuming we know all the moments of

$$M_n(x',t,\tau) = \int \mathrm{d}x\,(x-x')^n W(x,t+\tau|x',t) \tag{1.9}$$

for all $n \geq 1$, we now derive a general expression for the transition probability. We start with the identity

$$W(x,t+\tau|x',t) = \int \mathrm{d}y\,\delta(y-x)W(y,t+\tau|x',t) \tag{1.10}$$

where $\delta(x)$ is the Dirac delta function. We make use of the Taylor series expansion of the Dirac delta function

$$\begin{aligned}
\delta(y-x) =& \delta(x'-x+y-x') && (1.11)\\
=& \sum_{n=0}^{\infty} \frac{(y-x')^n}{n!} \left(\frac{\partial}{\partial x'}\right)^n \delta(x'-x) && (1.12)\\
=& \sum_{n=0}^{\infty} \frac{(y-x')^n}{n!} \left(-\frac{\partial}{\partial x'}\right)^n \delta(x'-x). && (1.13)
\end{aligned}$$

Substituting Eq. (1.13) into Eq. (1.10) yields

$$\begin{aligned}
W(x,t+\tau|x',t) &= \sum_{n=0}^{\infty} \frac{1}{n!} \left(-\frac{\partial}{\partial x}\right)^n \int \mathrm{d}y\,(y-x')^n W(y,t+\tau|x',t)\delta(x'-x)\\
&= \left[1 + \sum_{n=1}^{\infty} \frac{1}{n!} \left(-\frac{\partial}{\partial x}\right)^n M_n(x',t,\tau)\right]\delta(x'-x)\\
&= \left[1 + \sum_{n=1}^{\infty} \frac{1}{n!} \left(-\frac{\partial}{\partial x}\right)^n M_n(x,t,\tau)\right]\delta(x-x'). && (1.14)
\end{aligned}$$

In deriving Eq. (1.14), we have made use of the definition of the moments $M_n(x', t, \tau)$ in Eq. (1.9) and the symmetry of the Dirac delta function $\delta(x) = \delta(-x)$.

Substituting Eq. (1.14) into Eq. (1.8) leads to

$$\begin{aligned} P(x, t+\tau) - P(x,t) &= \frac{\partial P(x,t)}{\partial t}\tau + \mathcal{O}(\tau^2) \\ &= \sum_{n=1}^{\infty} \left(-\frac{\partial}{\partial x}\right)^n \int \mathrm{d}x \, \frac{\delta(x-x')}{n!} M_n(x,t,\tau) P(x',t) \\ &= \sum_{n=1}^{n} \left(-\frac{\partial}{\partial x}\right)^n \frac{M_n(x,t,\tau)}{n!} P(x,t). \end{aligned} \tag{1.15}$$

Now, we assume that all the moments M_n can be Taylor expanded with respect to τ

$$\frac{M_n(x,t,\tau)}{n!} = D^{(n)}(x,t)\tau + \mathcal{O}(\tau^2) \tag{1.16}$$

for $n \geq 1$. The zeroth order term in τ must vanish as the transition probability W has initial value at $\tau = 0$

$$W(x,t|x',t) = \delta(x-x') \tag{1.17}$$

which leads into $M_0 = 0$ by Eq. (1.9). By comparing the linear order term in τ in Eq. (1.15), we find a partial differential equation on the probability distribution $P(x,t)$

$$\frac{\partial P(x,t)}{\partial t} = \sum_{n=1}^{\infty} \left(-\frac{\partial}{\partial x}\right)^n D^{(n)}(x,t) P(x,t) = \mathcal{L}_{\mathrm{KM}} P(x,t), \tag{1.18}$$

where the differential operators act on both $D^{(n)}(x,t)$ and $P(x,t)$. The Kramers-Moyal differential operator is defined by

$$\mathcal{L}_{\mathrm{KM}} = \sum_{n=1}^{\infty} \left(-\frac{\partial}{\partial x}\right)^n D^{(n)}(x,t). \tag{1.19}$$

Eq. (1.18) is the *Kramers-Moyal expansion.*

1.4.1 Formal solution and short time transition probability

Now, we derive a formal solution to the Kramers-Moyal equation (1.18) with the initial conditions given by Eq. (1.17) and the short time transition probability. As the short time transition probability also satisfies Eq. (1.18), the formal solution reads

$$W(x,t|x',t') = e^{\mathcal{L}_{\mathrm{KM}}(x)(t-t')}\delta(x-x'). \tag{1.20}$$

It is important to note that the time-dependent Kramers-Moyal operator does not commute with itself at different times. Via iteration of Eq. (1.18) using Dyson series [46], the general solution to Eq. (1.18) is

$$\begin{aligned} W(x,t|x',t') &= \delta(x-x') + \int_{t'}^{t} \mathrm{d}t_{\,1}\mathcal{L}_{\mathrm{KM}}(x,t_1)\delta(x-x') && (1.21)\\ &+ \int_{t'}^{t}\mathrm{d}t_{\,1}\int_{t'}^{t_1}\mathrm{d}t_{\,2}\mathcal{L}_{\mathrm{KM}}(x,t_1)\mathcal{L}_{\mathrm{KM}}(x,t_2)\delta(x-x') + ... && (1.22)\\ &= \left[1+\sum_{n=1}^{\infty}\int_{t'}^{t}\mathrm{d}t_{\,1}\int_{t'}^{t_1}\mathrm{d}t_{\,2}...\int_{t'}^{t_{n-1}}\mathrm{d}t_{\,n}\mathcal{L}_{\mathrm{KM}}(x,t_1)...\mathcal{L}_{\mathrm{KM}}(x,t_n)\right] && (1.23)\\ &\times \delta(x-x'). && (1.24) \end{aligned}$$

Introducing a time-ordering operator $\mathcal{T}$ to move larger times to the left of the smaller time, Eq. (1.24) then reads

$$W(x,t|x',t') = \mathcal{T}\left[1+\sum_{n=1}^{\infty}\frac{1}{n!}\int_{t'}^{t}\mathrm{d}t_{\,1}\int_{t'}^{t}\mathrm{d}t_{\,2}...\int_{t'}^{t}\mathrm{d}t_{\,n}\mathcal{L}_{\mathrm{KM}}(x,t_1)...\mathcal{L}_{\mathrm{KM}}(x,t_n)\right]\delta(x-x'). \tag{1.25}$$

$$= \mathcal{T}\exp\left[\int_{t'}^{t}\mathrm{d}t''\mathcal{L}_{\mathrm{KM}}(x,t'')\right]\delta(x-x'). \tag{1.26}$$

When the time increment $\tau = t - t'$ is small, Eq. (1.26) becomes

$$W(x,t+\tau|x',t) = [1+\mathcal{L}_{\mathrm{KM}}(x,t)\tau + \mathcal{O}(\tau^2)]\delta(x-x') \tag{1.27}$$

which is consistent with Eq. (1.14).

Truncating the Kramer-Moyal expansion (1.18) and discarding higher order terms

with $n > 3$ yields the *Fokker-Planck* equation in one dimension

$$\frac{\partial P(x,t)}{\partial t} = \mathcal{L}_{\mathrm{FP}} P(x,t), \tag{1.28}$$

$$\mathcal{L}_{\mathrm{FP}} = -\frac{\partial}{\partial x} D^{(1)}(x,t) + \frac{\partial^2}{\partial x^2} D^{(2)}(x,t). \tag{1.29}$$

The Fokker-Planck equation is a special form of the continuous master equation Eq. (1.2).

For an overdamped Langevin dynamics (1.7), the corresponding Fokker-Planck equation is

$$\frac{\partial P(x,t)}{\partial t} = \frac{1}{\gamma}\frac{\partial}{\partial x}(V'(x)P(x,t)) + \frac{D}{\gamma}\frac{\partial^2}{\partial x^2} P(x,t). \tag{1.30}$$

The Fokker-Planck equations Eqs. (1.28) and (1.29) can also be written in the form

$$\frac{\partial P(x,t)}{\partial t} + \frac{\partial J}{\partial x} = 0, \tag{1.31}$$

$$J(x,t) = \left[D^{(1)}(x,t) - \frac{\partial}{\partial x} D^{(2)}(x,t) \right] \tag{1.32}$$

where $J(x,t)$ is the probability current.

Also truncating the Kramers-Moyal differential operator after two terms for the transition probability, Eq. (1.27) yields an expression for the small time transition probability for the Fokker-Planck operator

$$W(x, t+\tau|x', t) = [1 + \mathcal{L}_{\mathrm{FP}}(x,t)\tau + \mathcal{O}(\tau^2)]\delta(x - x') \tag{1.33}$$

with

$$\mathcal{L}_{\mathrm{FP}} = -\frac{\partial}{\partial x} D^{(1)}(x,t) + \frac{\partial^2}{\partial x^2} D^{(2)}(x,t). \tag{1.34}$$

Therefore, the small time transition probability satisfies

$$\begin{aligned} W(x, t+\tau|x', t) &= \left[1 - \frac{\partial}{\partial x} D^{(1)}(x,t)\tau + \frac{\partial^2}{\partial x^2} D^{(2)}(x,t)\tau \right] \delta(x - x') \\ &= \left[1 - \frac{\partial}{\partial x} D^{(1)}(x',t)\tau + \frac{\partial^2}{\partial x^2} D^{(2)}(x',t)\tau \right] \delta(x - x') \\ &= \exp\left[-\frac{\partial}{\partial x} D^{(1)}(x',t)\tau + \frac{\partial^2}{\partial x^2} D^{(2)}(x',t)\tau \right] \delta(x - x') \end{aligned} \tag{1.35}$$

where we have made use of the identity

$$\delta(x-x')f(x') = \delta(x-x')f(x) \tag{1.36}$$

in the second line to replace x by x' in the drift and diffusion coefficients.

Using the Fourier representation of a Dirac delta function

$$\delta(x) = \frac{1}{2\pi}\int \mathrm{d}k\, e^{\mathring{\imath}kx}, \tag{1.37}$$

we rewrite the short-time transition probability

$$\begin{aligned} W(x,t+\tau|x',t) =& \exp\left[-\frac{\partial}{\partial x}D^{(1)}(x',t)\tau + \frac{\partial^2}{\partial x^2}D^{(2)}(x',t)\tau\right]\frac{1}{2\pi}\int \mathrm{d}k\, e^{\mathring{\imath}k(x-x')} \\ =& \frac{1}{2\pi}\int \mathrm{d}k \exp[-\mathring{\imath}kD^{(1)}(x',t)\tau - k^2D^{(2)}(x',t)\tau + \mathring{\imath}k(x-x')] \\ =& \frac{1}{2\sqrt{\pi D^{(2)}(x',t)\tau}}\exp\left(-\frac{[x-x'-D^{(1)}(x',t)\tau]^2}{4D^{(2)}(x',t)\tau}\right). \end{aligned} \tag{1.38}$$

Eq. (1.38) is not only just valid for small time τ but also valid for any $\tau > 0$. It is also important to note that the small time transition probability is not unique to Eq. (1.38), other forms also exist [174].

It is also important to note that one can turn a Langevin equation Eq. (1.3) into a Fokker-Planck Eqs. (1.28) equation formally without going through the Kramer-Moyal expansion. This can be found in [115].

1.4.2 Boundary conditions

In order to study the Fokker-Planck equation and the underlying Langevin equation, we need to specify the Langevin dynamics at the boundary of the domain and, equally, the boundary conditions of the probability distribution. For a Langevin dynamics in one dimension on an interval $[0, L]$, we can consider the following cases:

1. Absorbing boundary conditions: the probability distribution vanishes on the boundary

$$P(0,t) = P(L,0) = 0 \tag{1.39}$$

2. Reflecting boundary conditions: the probability current vanishes on the boundary

$$J(0,t) = J(L,t) = 0 \tag{1.40}$$

3. Periodic boundary conditions:

$$P(0,t) = P(L,t) \tag{1.41}$$

using the probability current defined in Eq. (1.32). Mixed boundary conditions could also arise. For instance, one could have an absorbing boundary at the left end of the interval and a reflecting boundary condition at the right end of the interval:

$$P(0,t) = 0, \quad J(L,t) = 0. \tag{1.42}$$

1.4.3 Path-integral solution

We derive the path-integral solution to the Fokker-Planck equation. Applying the Chapman-Kolmogorov equation Eq. (1.8) repeatedly to the initial probability distribution $P(x_0, t_0)$, we can find the probability distribution at position x and time t after dividing the time interval $t - t_0$ in N increments $\tau = (t - t_0)/N$,

$$\begin{aligned} P(x,t) = \int \mathrm{d}x_{N-1} \int \mathrm{d}x_{N-2} \ldots \int \mathrm{d}x_0 \\ W(x,t|x_{N-1},t_{N-1}) P(x_{N-1},t_{N-1}|x_{N-2,t_{N-2}}) \ldots \\ W(x_1,t_1|x_0,t_0) P(x_0,t_0). \end{aligned} \tag{1.43}$$

Substituting the short time transition probability Eq. (1.38) into the probability distribution Eq. (1.43) in the continuous limit $N \to \infty$ and replacing $x_N = x$, the probability distribution $P(x,t)$ becomes

$$P(x,t) = \lim_{N\to\infty} \int \prod_{i=0}^{N-1} \{\mathrm{d}x_{\,i} [4\pi D^{(2)}(x_i,t_i)\tau]^{-1/2}\} \tag{1.44}$$

$$\times \exp\left(- \sum_{i=0}^{N-1} \frac{[x_{i+1} - x_i - D^{(1)}(x_i,t_i)\tau]^2}{4D^{(2)}(x_i,t_i)\tau} \right) W(x_0,t_0). \tag{1.45}$$

It is important to note that as all terms in front of $P(x_0, t_0)$ in Eq. (1.45) are positive, the probability distribution $P(x, t)$ remains positive if we start with a positive initial probability distribution $P(x_0, t_0)$.

As the interval τ is small, we can write the time derivative of the position

$$\dot{x}(t_i) = \frac{x_{i+1} - x_i}{\tau}, \tag{1.46}$$

and the exponent in the exponential term in Eq. (1.45)

$$-\sum_{i=0}^{N-1} \frac{[x_{i+1} - x_i - D^{(1)}(x_i, t_i)\tau]^2}{4D^{(2)}(x_i, t_i)\tau} = \int_{t_0}^{t} \mathrm{d}t' \frac{[\dot{x}(t') - D^{(1)}(x(t'), t')]^2}{4D^{(2)}(x(t'), t)} \tag{1.47}$$

in the continuous limit $N \to \infty$. The integrand in Eq. (1.47) is called a *generalised Onsager-Machlup* function [116].

1.5 First-Passage time problems

First-passage time is the time required for a stochastic variable $\dot{x}(t)$ to leave a given domain [135, 63]. In biological systems, we are often interested in the time it takes for a diffusing molecule inside a cell to be absorbed at the cell boundaries. Therefore, it is important to calculate quantities such as the first-passage distribution and mean first-passage time. Below, we only consider the one-dimensional case.

We start with the Fokker-Planck equation

$$\frac{\partial P(x, t)}{\partial t} = \mathcal{L}_{\mathrm{FP}} P(x, t) \tag{1.48}$$

with the initial conditions

$$P(x, 0|x', 0) = \delta(x - x') \quad \text{for} \quad x_1 < x < x_2 \tag{1.49}$$

and boundary conditions

$$P(x, t|x', 0) = 0 \quad \text{for} \quad x = x_1 \quad \text{or} \quad x = x_2. \tag{1.50}$$

Initialising at position x', the probability $W(x',t)$ of not reaching one of the boundaries x_1 or x_2 up to time t reads

$$W(x',t) = \int_{x_1}^{x_2} \mathrm{d}x\, P(x,t|x',0). \tag{1.51}$$

Within a small time interval $(t, t+dt)$, the probability of reaching is given by

$$-\mathrm{d}W\,(x',t) = -\int_{x_1}^{x_2} \mathrm{d}x\mathrm{d}t\, \dot{P}(x,t|x',0). \tag{1.52}$$

Therefore, the probability distribution for the first-passage time to escape the region (x_1, x_2) is then given by

$$w(x',T) = -\frac{\mathrm{d}W\,(x',T)}{\mathrm{d}T} = -\int_{x_1}^{x_2} \mathrm{d}x\, \dot{P}(x,T|x',0). \tag{1.53}$$

With the distribution function at hand, the moments $T_n(x')$ for the first-passage time distribution are given by

$$T_n(x') = \int_0^\infty \mathrm{d}T\, T^n w(x',T) = \int_{x_1}^{x_2} \mathrm{d}x\, p_n(x,x') \tag{1.54}$$

where $p_n(x,x')$ is defined by

$$p_n(x,x') = -\int_0^\infty \mathrm{d}T\, T^n \dot{P}(x,T|x'0). \tag{1.55}$$

The zeroth moment is given by

$$p_0(x,x') = -\int_0^\infty \mathrm{d}T\, \dot{P}(x,T|x',0) = P(x,0|x',0) = \delta(x-x'). \tag{1.56}$$

Integrating (1.55) by parts yields

$$p_n(x,x') = n\int_0^\infty \mathrm{d}T\, T^{n-1} P(x,T|x',0) \quad n \geq 1. \tag{1.57}$$

Applying the Fokker-Planck operator on (1.57), we obtain the following recurrence

relation

$$\mathcal{L}_{\mathrm{FP}} p_n(x, x') = -n p_{n-1}(x, x') \quad n \geq 1. \tag{1.58}$$

We can then obtain $p_n(x, x')$ for all n by solving the equations iteratively starting with $n = 1$. The boundary conditions for all p_n are the same as the probability distribution $P(x, t|x', 0)$. In other words,

$$p_n(x, x') = 0 \quad \text{for} \quad x = x_1 \quad \text{or} \quad x = x_2. \tag{1.59}$$

1.5.1 Formal solution

A formal solution to (1.58) to can be found via

$$p_n(x, x') = n![-\mathcal{L}_{\mathrm{FP}}(x)]^{-n} \delta(x - x'). \tag{1.60}$$

This formal solution can also be found by integrating the formal solution of P, in other words,

$$p_n(x, x') = -\int_0^\infty \mathrm{d}t\, t^n \mathcal{L}_{\mathrm{FP}}(x) e^{\mathcal{L}_{\mathrm{FP}}(x)t} \delta(x - x') \tag{1.61}$$

$$= n![-\mathcal{L}_{\mathrm{FP}}(x)]^{-n} \delta(x - x'). \tag{1.62}$$

1.5.2 Solution using the adjoint operator

Because $P(x, t|x', 0) = P(x, 0|x', -t)$ also satisfies the backward Kolmogorov equation

$$\frac{\partial P}{\partial t} = \mathcal{L}^\dagger(x') P. \tag{1.63}$$

We can therefore replace the Fokker-Planck operator $\mathcal{L}_{\mathrm{FP}}(x)$ by its adjoint $\mathcal{L}^\dagger_{\mathrm{FP}}(x')$. If x' is outside of the region (x_1, x_2), the probability must vanish. This is equivalent to solving the adjoint equation (1.63) with boundary conditions

$$P(x, t|x', 0) = 0 \quad \text{for} \quad x' = x_1 \quad \text{and} \quad x' = x_2. \tag{1.64}$$

In the meantime, we can use just the adjoint equation (1.63) to obtain all the moments (1.54) via the recurrence relation

$$\mathcal{L}_{\rm FP}^{\dagger} T_n(x') = -nT_{n-1}(x') \tag{1.65}$$

with the zeroth moment

$$T_0(x') = 1. \tag{1.66}$$

The equation for the mean first-passage time $T_1(x')$ satisfies

$$\mathcal{L}^{\dagger}(x')T_1(x') = -1. \tag{1.67}$$

It is interesting to note that at first glance, Eq. (1.67) seems easier to be solved compared to Eq. (1.58) as Eq. (1.67) only contains one variable. However, to obtain $T(x')$ for some position $x' = x_0$, one has to solve Eq. (1.67) completely for all x' in the domain. On the other hand, one only needs to solve Eq. (1.58) for the case $x' = x_0$.

1.5.3 BOUNDARY CONDITIONS

As the mean first-passage time satisfies the backward equation (1.67), to obtain the full solution, we also need to specify the boundary conditions. We list two types of different boundary conditions, namely

1. Absorbing boundaries at both x_1 and x_2: $T_1(x_1) = 0$ and $T_1(x_2) = 0$.
2. Absorbing boundary at x_1 and reflecting boundary at x_2: $T_1(x_1) = 0$ and $T_1'(x_2) = 0$.

2

ENTROPY PRODUCTION IN EXACTLY SOLVABLE MODELS

Abstract

In this chapter, I present a near-verbatim copy of the peer-reviewed journal article

L. Cocconi, R. Garcia-Millan, Z. Zhen, B. Buturca, and G. Pruessner. Entropy Production in Exactly Solvable Systems [30].

This chapter is based on [30], which is itself an introduction to entropy production, based on exactly solvable systems. I contributed mainly to the analysis of driven Brownian particles (Sec. 2.3.9), driven Brownian particles in a harmonic potential (Sec. 2.3.10), driven Brownian particles on a ring with potentials (Sec. 2.3.11 and Sec. 2.3.12), run-and-tumble motion with diffusion on a ring (Sec. 2.3.13) and switching diffusion process on a ring (Sec. 2.135). I also contributed to the writing up of the manuscript.

The rate of entropy production by a stochastic process quantifies how far the latter is from thermodynamic equilibrium. Equivalently, entropy production captures the degree to which the detailed balance relation and time-reversal symmetry are broken. Despite abundant references to entropy production in the

literature and its many applications in the study of non-equilibrium stochastic particle systems, a comprehensive list of paradigmatic examples illustrating the fundamentals of entropy production is lacking. Here, we present a self-contained review of entropy production and calculate it from first principles in a catalogue of exactly solvable setups, encompassing both discrete- and continuous-state Markov processes, as well as single- and multiple-particle systems. The examples covered in this work provide a stepping stone for further study on entropy production of more complex systems, such as many-particle active matter, as well as a benchmark in the development of alternative mathematical formalisms.

2.1 Introduction

Stochastic thermodynamics has progressively evolved into an essential tool in the study of non-equilibrium systems in light of the connection it establishes between the quantities of interest of traditional thermodynamics, such as work, heat and entropy, and the properties of microscopically-resolved fluctuating trajectories [146, 81, 147]. The possibility of equipping stochastic processes with a consistent thermodynamic and information-theoretic interpretation has resulted in a number of fascinating works, with the interface between mathematical physics and the biological sciences proving to be a particularly fertile ground for new insights ([11, 89, 25, 140, 124], amongst many others). This affinity is not surprising, since it is precisely at the microscopic scale that environmental fluctuations start to play an non-negligible role. The concept of entropy and, more specifically, entropy production has attracted special interest, as a consequence of the quantitative handle it provides on the distinction between equilibrium systems, passive systems relaxing to equilibrium and genuinely non-equilibrium, 'active' systems. While there exist multiple routes to the the mathematical formulation of entropy production [141, 99, 64, 144, 113, 90], the underlying physical picture is consistent: the entropy production associated with an ensemble of stochastic trajectories quantifies the degree of certainty with which we can assess whether a realisation originates from a stochastic process or from a suitably-defined conjugate (usually, its time-reverse). When averaged over long times (or over an ensemble), a non-vanishing entropy production signals time-reversal symmetry breaking at the microscopic scale. In turn this implies, at least for Markovian systems, the existence of steady-state probability currents in the state space, which are odd

under time-reversal. When a thermodynamically consistent description is available, the average rate of entropy production can be related to the rate of energy/information exchange between the system, the heat bath(s) it is connected to, and any other thermodynamic entity involved in the dynamics, such as a measuring device [112, 98, 117]. Whilst the rate of energy dissipation is of immediate interest since it captures how 'costly' it is to sustain specific dynamics (e.g. the metabolism sustaining the development of an organism [138, 155]), it was also found to relate non-trivially to the efficiency and precision of the corresponding process via uncertainty relations [75, 147]. Entropy production along fluctuating trajectories also plays a fundamental role in the formulation of various fluctuation theorems [144].
Given the recent upsurge of interest in stochastic thermodynamics and entropy production in particular, as well as the increasing number of mathematical techniques implemented in the quantification of the latter, it is essential to have access to a few, well-understood reference systems, for which exact results are known. These can play the role of benchmarks for new techniques, while helping newcomers to develop intuition. In this review will exclusively present results in the framework proposed by Gaspard [64], which we review and contextualise in Section 2. The rate of entropy production of the universe is thus defined through the asymmetry between forwards and backwards entropies per unit time of microscopic trajectories and can be expressed exactly. The analysis is initially conducted for processes on a discrete state space (Sections 2.3.1-2.3.8), and is subsequently extended to the continuous case (Sections 2.3.9-2.3.11). Finally, in sections 2.3.12 and 2.3.13 we consider processes that involve both discrete and continuous degrees of freedom. Time is taken as a continuous variable throughout.

2.2 Review of entropy production

Entropy production of Markov jump processes. Shannon [149] first introduced the concept of time-dependent informational entropy associated with a given ensemble of stochastic processes. For an arbitrary probability density function $P_n(t)$ of time t over a discrete set of states $n \in \Omega$, the Shannon entropy is defined as

$$S(t) = -\sum_n P_n(t) \ln P_n(t) \tag{2.1}$$

with the convention of $x \ln x = 0$ for $x = 0$. It quantifies the intrinsic degree of uncertainty about the state of a stochastic process. In the microcanonical ensemble P_n is constant in t and n and upon providing an entropy scale in the form of the Boltzmann constant k_B, Shannon's entropy reduces to that of traditional thermodynamics given by Boltzmann's $S = k_B \ln |\Omega|$, where $|\Omega| = 1/P_n$ is the cardinality of Ω. In Markovian systems, the probability $P_n(t)$ depends on n and evolves in time t according to the master equation

$$\dot{P}_n(t) = \sum_m \left(P_m(t) w_{mn} - P_n(t) w_{nm} \right) \tag{2.2}$$

with non-negative transition rates w_{mn} from state m to state $n \neq m$. Eq. (2.2) reduces to $\dot{P}_n(t) = \sum_m P_m(t) w_{mn}$ by imposing the Markov condition $\sum_m w_{nm} = 0$, equivalently $w_{nn} = -\sum_{m \neq n} w_{nm}$, which we will use in the following. For simplicity we will restrict ourselves to time-independent rates w_{nm} but as far as the following discussion is concerned, generalising to time-dependent rates is a matter of replacing w_{nm} by $w_{nm}(t)$. The rate of change of entropy for a continuous time jump process can be derived by differentiating $S(t)$ in Eq. (2.1) with respect to time and substituting (2.2) into the resulting expression [64, 48], thus obtaining

$$\dot{S}(t) = -\sum_{m,n} P_m(t) w_{mn} \ln \left(P_n(t) \right) = \sum_{m,n} P_n(t) w_{nm} \ln \left(\frac{P_n(t)}{P_m(t)} \right) = \dot{S}_e(t) + \dot{S}_i(t) \tag{2.3}$$

where we define

$$\begin{aligned} \dot{S}_e(t) &= -\frac{1}{2} \sum_{m,n} \left(P_n(t) w_{nm} - P_m(t) w_{mn} \right) \ln \left(\frac{w_{nm}}{w_{mn}} \right) && \text{(2.4a)} \\ &= -\sum_{m,n} P_n(t) w_{nm} \ln \left(\frac{w_{nm}}{w_{mn}} \right) = -\sum_{m,n} \left(P_n(t) w_{nm} - P_m(t) w_{mn} \right) \ln \left(\frac{w_{nm}}{w_0} \right) \\ \dot{S}_i(t) &= \frac{1}{2} \sum_{m,n} \left(P_n(t) w_{nm} - P_m(t) w_{mn} \right) \ln \left(\frac{P_n(t) w_{nm}}{P_m(t) w_{mn}} \right) && \text{(2.4b)} \\ &= \sum_{m,n} P_n(t) w_{nm} \ln \left(\frac{P_n(t) w_{nm}}{P_m(t) w_{mn}} \right) = \sum_{m,n} \left(P_n(t) w_{nm} - P_m(t) w_{mn} \right) \ln \left(\frac{P_n(t) w_{nm}}{w_0} \right) \end{aligned}$$

with arbitrary positive rate w_0 to restore dimensional consistency, that cancel trivially. Here we follow the convention [146] to split the rate of entropy change into two contributions: the first, Eq. (2.4a), commonly referred to as "external" entropy production or entropy flow, is denoted by $\dot{S}_e$. It contains a factor $\ln(w_{nm}/w_{mn})$ corresponding, for systems satisfying local detailed balance, to the net change in entropy of the reservoir(s) associated with the system's transition from state n to state m. For such thermal systems, $\dot{S}_e$ can thus be identified as the rate of entropy production in the environment [94, 141]. The second contribution, Eq. (2.4b), termed "internal" entropy production and denoted by $\dot{S}_i$ is non-negative because $(x-y)\ln(x/y) \geq 0$ for any two real, positive x, y and using the convention $z \ln z = 0$ for $z = 0$. The internal entropy production vanishes when the global detailed balance condition $P_n(t)w_{nm} = P_m(t)w_{mn}$ is satisfied for all pairs of states. In this sense, a non-vanishing $\dot{S}_i$ is the fingerprint of non-equilibrium phenomena. In [142], $\dot{S}_i$ is also interpreted as the entropy production. Defining $\pi_n = \lim_{t\to\infty} P_n(t)$ as the probability mass function at steady-state, the internal entropy production rate can be further decomposed into two non-negative contributions, $\dot{S}_i(t) = \dot{S}_i^{\mathrm{a}}(t) + \dot{S}_i^{\mathrm{na}}(t)$, of the form

$$\dot{S}_i^{\mathrm{a}}(t) = \sum_{m,n} P_n(t) w_{nm} \ln\left(\frac{\pi_n w_{nm}}{\pi_m w_{mn}}\right) \tag{2.5a}$$

$$\dot{S}_i^{\mathrm{na}}(t) = \sum_{m,n} P_n(t) w_{nm} \ln\left(\frac{P_n(t)\pi_m}{P_m(t)\pi_n}\right) = -\sum_n \dot{P}_n(t) \ln\left(\frac{P_n(t)}{\pi_n}\right) . \tag{2.5b}$$

These contributions are usually referred to as adiabatic (or housekeeping) and non-adiabatic (or excess) entropy production rates, respectively [146]. The non-adiabatic contribution vanishes at steady-state, $\lim_{t\to\infty} \dot{S}_i^{\mathrm{na}}(t) = 0$. While these quantities have received attention in the context of fluctuation theorems, they will not be discussed further here. At steady-state, namely when $\dot{P}_n(t) = 0$ for all n, $\dot{S}(t)$ in Eq. (2.3) vanishes by construction, so that the internal and external contributions to the entropy production cancel each other exactly, $\dot{S}(t) = \dot{S}_e(t) + \dot{S}_i(t) = 0$, while they vanish individually only for systems at equilibrium. Equations (2.4) will be used throughout the present work to compute the entropy productions of discrete-state processes.

Entropy production as a measure of time-reversal-symmetry breaking. As it turns out, a deeper connection between internal entropy production and time-reversal symmetry breaking can be established [64]. The result, which we re-derive below, identifies $\dot{S}_i$

as the relative dynamical entropy (*i.e.* the Kullback-Leibler divergence [86]) per unit time of the ensemble of forward paths and their time-reversed counterparts. To see this, we first need to define a path $\mathbf{n} = (n_0, n_1, \ldots, n_M)$ as a set of trajectories starting at time t_0 and visiting states n_j at successive discrete times $t_j = t_0 + j\tau$ with $j = 0, 1, \ldots, M$, equally spaced by a time interval τ. For a time-homogeneous Markovian jump process in continuous time, the joint probability of observing a particular path is

$$\mathcal{P}(\mathbf{n}; t_0, M\tau) = P_{n_0}(t_0) W(n_0 \to n_1; \tau) W(n_1 \to n_2; \tau) \ldots W(n_{M-1} \to n_M; \tau) \tag{2.6}$$

where $P_{n_0}(t_0)$ is the probability of observing the system in state n_0 at time t_0, while $W(n_j \to n_{j+1}; \tau)$ is the probability that the system is in state n_{j+1} time τ after being in state n_j. This probability can be expressed in terms of the transition rate matrix w with elements w_{mn}. It is $W(n \to m; \tau) = [\exp(w\tau)]_{nm}$, the matrix elements of the exponential of the matrix $w\tau$ with the Markov condition imposed. It can be expanded in small τ as

$$W(n \to m; \tau) = \delta_{n,m} + w_{nm}\tau + O(\tau^2) \ , \tag{2.7}$$

where $\delta_{n,m}$ is the Kronecker-δ function. We can now define a dynamical entropy per unit time [149] as

$$h(t_0, \Delta t) = \lim_{M \to \infty} -\frac{1}{\Delta t} \sum_{n_0, \ldots, n_M} \mathcal{P}(\mathbf{n}; t_0, \Delta t) \ln \mathcal{P}(\mathbf{n}; t_0, \Delta t) \ . \tag{2.8}$$

where the limit is to be considered a continuous time limit taken at fixed $\Delta t = t_M - t_0 = M\tau$ [41], thus determining the sampling interval τ, and the sum runs over all possible paths $\mathbf{n}$. Other than τ, the paths are the only quantity on the right-hand side of Eq. (2.8) that depend on M. The dynamical entropy $h(t_0, \Delta t)$ may be considered the expectation of $\ln(\mathcal{P}(\mathbf{n}; t_0, \Delta t))$ across all paths. Similarly to the static Shannon entropy, the dynamical entropy $h(t_0, \Delta t)$ quantifies the inherent degree of uncertainty about the evolution over a time Δt of a process starting at a given time t_0. To compare with the dynamics as observed under time-reversal, one introduces the time-reversed path $\mathbf{n}^R = (n_M, n_{M-1}, \ldots, n_0)$ and thus the time-reversed dynamical entropy

per unit time as

$$h^R(t_0, \Delta t) = \lim_{M\to\infty} -\frac{1}{\Delta t} \sum_{n_0,\ldots,n_M} \mathcal{P}(\mathbf{n}; t_0, \Delta t) \ln \mathcal{P}(\mathbf{n}^R; t_0, \Delta t) \ . \tag{2.9}$$

While similar in spirit to $h(t_0, \Delta t)$, the physical interpretation of $h^R(t_0, \Delta t)$ as the expectation of $\ln(\mathcal{P}(\mathbf{n}^R; \Delta t))$ under the forward probability $\mathcal{P}(\mathbf{n}; t_0, \Delta t)$ is more convoluted since it involves the forward and the backward paths simultaneously, which have potentially different statistics. However, time-reversal symmetry implies precisely identical statistics of the two ensembles, whence $h(t_0, \Delta t) = h^R(t_0, \Delta t)$. The motivation for introducing $h^R(t_0, \Delta t)$ is that the difference of the two dynamical entropies defined above is a non-negative Kullback-Leibler divergence given by

$$h^R(t_0, \Delta t) - h(t_0, \Delta t) = \lim_{M\to\infty} \frac{1}{\Delta t} \sum_{\mathbf{n}} \mathcal{P}(\mathbf{n}; t_0, \Delta t) \ln \left(\frac{\mathcal{P}(\mathbf{n}; t_0, \Delta t)}{\mathcal{P}(\mathbf{n}^R; t_0, \Delta t)} \right) \ . \tag{2.10}$$

Using Eq. (2.6) in (2.10) with Eq. (2.7) provides the expansion

$$h^R(t_0, \Delta t) - h(t_0, \Delta t) = \sum_{nm} P_n(t_0) w_{nm} \ln \left(\frac{P_n(t_0) w_{nm}}{P_m(t_0) w_{mn}} \right) + \mathcal{O}(\Delta t) \ , \tag{2.11}$$

which is an instantaneous measure of the Kullback-Leibler divergence. The limit of $h^R(t_0, \Delta t) - h(t_0, \Delta t)$ in small Δt is finite and identical to the internal entropy production (2.4b) derived above. This result establishes the profound connection between broken global detailed balance, Eq. (2.4), and Kullback-Leibler divergence, Eq. (2.11), both of which can thus be recognised as fingerprints of non-equilibrium systems. In light of this connection, it might not come as a surprise that the steady-state rate of entropy production is inversely proportional to the minimal time needed to decide on the direction of the arrow of time [139].

Entropy production for continuous degrees of freedom. The results above were obtained for Markov jump processes within a discrete state space. However, the decomposition of the rate of change of entropy in Eq. (2.3) into internal and external contributions can be readily generalised to Markovian processes with continuous degrees of freedom, for example a spatial coordinate. For simplicity we will restrict ourselves to processes in one dimension but as far as the following discussion is concerned, generalising to higher dimensions is a matter of replacing spatial deriva-

tives and integrals over the spatial coordinate with their higher dimensional counterparts. The dynamics of such a process with probability density $P(x,t)$ to find it at x at time t are captured by a Fokker-Planck equation of the form $\dot{P}(x,t) = -\partial_x j(x,t)$, with j the probability current, augmented by an initial condition $P(x,0)$. Starting from the Gibbs-Shannon's entropy for a continuous random variable $S(t) = -\int \mathrm{d}x\, P(x,t) \ln(P(x,t)/P_0)$ with some arbitrary density scale P_0 for dimensional consistency, we differentiate with respect to time and substitute $-\partial_x j(x,t)$ for $\dot{P}(x,t)$ to obtain

$$\dot{S}(t) = -\int \mathrm{d}x\, \dot{P}(x,t) \ln\left(\frac{P(x,t)}{P_0}\right) = -\int \mathrm{d}x\, \frac{(\partial_x P(x,t)) j(x,t)}{P(x,t)} \;, \tag{2.12}$$

where the second equality follows upon integration by parts using $\int \mathrm{d}x\, \dot{P}(x,t) = 0$ by normalisation. For the paradigmatic case of an overdamped colloidal particle, which will be discussed in more detail below (Secs. 2.3.9 – 2.3.11), the probability current is given by $j(x,t) = -D\partial_x P(x,t) + \mu F(x,t) P(x,t)$ with local, time-dependent force $F(x,t)$. We can then decompose the entropy production $\dot{S}(t) = \dot{S}_i(t) + \dot{S}_e(t)$ into internal and external contributions as

$$\dot{S}_i(t) = \int \mathrm{d}x\, \frac{j(x,t)^2}{D P(x,t)} \geq 0 \tag{2.13}$$

and

$$\dot{S}_e(t) = -\int \mathrm{d}x\, \frac{\mu}{D} F(x,t) j(x,t) \;, \tag{2.14}$$

respectively. The Kullback-Leibler divergence between the densities of forward and time-reversed paths can be calculated as outlined above for discrete state systems, thus producing an alternative expression for the internal entropy production in the form

$$\begin{aligned} \dot{S}_i(t) &= \lim_{\Delta t \to 0} h^R(t, \Delta t) - h(t, \Delta t) \\ &= \lim_{\tau \to 0} \frac{1}{2\tau} \int \mathrm{d}x \mathrm{d}x' \left(P(x,t) W(x \to x', \tau) - P(x',t) W(x' \to x, \tau)\right) \qquad (2.15) \\ &\quad \times \ln \frac{P(x,t) W(x \to x', \tau)}{P(x',t) W(x' \to x, \tau)} \;. \qquad (2.16) \end{aligned}$$

Here we have introduced the propagator $W(x' \to x, \tau)$, the probability density that

a system observed in state x' will be found at x time τ later. In general, here and above, the density $W(x \to x', \tau)$ depends on the absolute time t, which we have omitted here for better readability. The corresponding expression for the entropy flow is obtained by substituting (2.16) into the balance equation $\dot{S}_e(t) = \dot{S}(t) - \dot{S}_i(t)$, whence

$$\dot{S}_e(t) = -\lim_{\tau\to 0} \frac{1}{2\tau} \int \mathrm{d}x\mathrm{d}x' \left(P(x,t)W(x \to x', \tau) - P(x',t)W(x' \to x, \tau)\right) \ln \frac{W(x' \to x, \tau)}{W(x \to x', \tau)} \ . \tag{2.17}$$

Since $\lim_{\tau\to 0} W(x \to x', \tau) = \delta(x - x')$ [174] and $P(x,t)\delta(x - x') = P(x',t)\delta(x' - x)$ the factor in front of the logarithm in (2.16) and (2.17) vanishes in the limit of small τ, $\lim_{\tau\to 0} P(x,t)W(x \to x';\tau) - P(x',t)W(x' \to x;\tau) = 0$. Together with the prefactor $1/\tau$ this necessitates the use of L'Hôpital's rule

$$\begin{aligned} &\lim_{\tau\to 0} \frac{1}{\tau} \left(P(x,t)W(x \to x';\tau) - P(x',t)W(x' \to x;\tau)\right) \\ =&P(x,t)\dot{W}(x \to x') - P(x',t)\dot{W}(x' \to x) \end{aligned} \tag{2.18}$$

where we used the shorthand

$$\dot{W}(x \to x') := \lim_{\tau\to 0} \frac{\mathrm{d}}{\mathrm{d}\tau} W(x \to x';\tau) \ , \tag{2.19}$$

which is generally given by the Fokker-Planck equation of the process, so that

$$\dot{P}(x,t) = \int \mathrm{d}x' \, P(x',t)\dot{W}(x' \to x) \ . \tag{2.20}$$

In the continuum processes considered below, in particular Sec. 2.3.11, 2.3.12 and 2.3.13, $\dot{W}(x \to x')$ is a kernel in the form of Dirac δ-functions and derivatives thereof, acting under the integral as the adjoint Fokker-Planck operator on $P(x,t)$. With Eq. (2.18) the internal entropy production of a continuous process (2.16) may con-

veniently be written as

$$\begin{aligned}
\dot{S}_i(t) =& \frac{1}{2}\int \mathrm{d}x\mathrm{d}x' \left(P(x,t)\dot{W}(x\to x') - P(x',t)\dot{W}(x'\to x)\right) \\
&\times \lim_{\tau\to 0} \ln\left(\frac{P(x,t)W(x\to x';\tau)}{P(x',t)W(x'\to x;\tau)}\right) && \text{(2.21a)} \\
=& \int \mathrm{d}x\mathrm{d}x'\, P(x,t)\dot{W}(x\to x') \times \lim_{\tau\to 0} \ln\left(\frac{P(x,t)W(x\to x';\tau)}{P(x',t)W(x'\to x;\tau)}\right) && \text{(2.21b)} \\
=& \int \mathrm{d}x\mathrm{d}x' \left(P(x,t)\dot{W}(x\to x') - P(x',t)\dot{W}(x'\to x)\right) \\
&\times \lim_{\tau\to 0} \ln\left(\frac{P(x,t)W(x\to x';\tau)}{W_0 P_0}\right) && \text{(2.21c)}
\end{aligned}$$

with suitable constants W_0 and P_0. Correspondingly, the (external) entropy flow (2.17) is

$$\begin{aligned}
\dot{S}_e(t) =& -\frac{1}{2}\int \mathrm{d}x\mathrm{d}x' \left(P(x,t)\dot{W}(x\to x') - P(x',t)\dot{W}(x'\to x)\right) \\
&\times \lim_{\tau\to 0} \ln\left(\frac{W(x\to x';\tau)}{W(x'\to x;\tau)}\right) && \text{(2.22a)} \\
=& -\int \mathrm{d}x\mathrm{d}x'\, P(x,t)\dot{W}(x\to x') \times \lim_{\tau\to 0} \ln\left(\frac{W(x\to x';\tau)}{W(x'\to x;\tau)}\right) && \text{(2.22b)} \\
=& -\int \mathrm{d}x\mathrm{d}x' \left(P(x,t)\dot{W}(x\to x') - P(x',t)\dot{W}(x'\to x)\right) \\
&\times \lim_{\tau\to 0} \ln\left(\frac{W(x\to x';\tau)}{W_0}\right) . && \text{(2.22c)}
\end{aligned}$$

All of these expressions assume that the limits of the logarithms exist. Naively replacing them by $\ln(\delta(x-x')/\delta(x'-x))$ produces a meaningless expression with a Dirac δ-function in the denominator. Eqs. (2.21) and (2.22) are identically obtained in the same manner as Eqs. (2.4) with the master Eq. (2.2) replaced by the Fokker-Planck Eq. (2.20). All of these expressions, Eq. (2.4), (2.21) and (2.22), may thus be seen as Gaspard's [64] framework.

Langevin description and stochastic entropy. We have seen in Eqs. (2.13) and (2.14) how the notion of entropy production can be extended to continuous degrees of freedom by means of a Fokker-Planck description of the stochastic dynamics. The Fokker-Plank equation is a deterministic equation for the probability density and thus pro-

vides a description at the level of ensembles, rather than single fluctuating trajectories. A complementary description can be provided by means of a Langevin equation of motion, which is instead a stochastic differential equation for the continuous degree of freedom [122]. The presence of an explicit noise term, which usually represents faster degrees of freedom or fluctuations induced by the contact with a heat reservoir, allows for a clearer thermodynamic interpretation. A paradigmatic example is that of the overdamped colloidal particle mentioned above, whose dynamics is described by

$$\dot{x}(t) = \mu F(x,t) + \zeta(t) \tag{2.23}$$

with μ a mobility, $F(x,t)$ a generic force and $\zeta(t)$ a white noise term with covariance $\langle \zeta(t)\zeta(t')\rangle = 2D\delta(t-t')$. For one-dimensional motion on the real line, the force $F(x,t)$ can always be written as the gradient of a potential $V(x,t)$, namely $F(x,t) = -\partial_x V(x,t)$, so that it is conservative. For time-independent, stable potentials, $V(x,t) = V(x)$, this leads at long times to an equilibrium steady-state. This property does not hold in higher dimensions and for different boundary conditions (e.g. periodic), in which case the force $\mathbf{F}(\mathbf{x},t)$ need not have a corresponding potential $V(\mathbf{x},t)$ for which $\mathbf{F}(\mathbf{x},t) = -\nabla V(\mathbf{x},t)$ [173].

The concept of entropy is traditionally introduced at the level of ensembles. However, due to its rôle in fluctuation theorems [146, 94], a consistent definition at the level of single trajectories is required. This can be constructed along the lines of [144] by positing the trajectory-dependent entropy $S(x^*(t),t)$ where $x^*(t)$ is a random trajectory as given by Eq. (2.23) and

$$S(x,t) = -\ln(P(x,t)/P_0)\ . \tag{2.24}$$

Here $P(x,t)$ denotes the probability density of finding a particle at position x at time t as introduced above and P_0 is a scale as used above to maintain dimensional consistency. Given that $x^*(t)$ is a random variable, so is $S(x^*(t),t)$, which may be regarded

as an instantaneous entropy. Taking the total derivative with respect to t produces

$$\begin{aligned}\frac{\mathrm{d}}{\mathrm{d}t}S(x^*(t),t) &= -\left.\frac{\partial_t P(x,t)}{P(x,t)}\right|_{x=x^*(t)} - \left.\frac{\partial_x P(x,t)}{P(x,t)}\right|_{x=x^*(t)} \circ \dot{x}^*(t) \\ &= -\left.\frac{\partial_t P(x,t)}{P(x,t)}\right|_{x=x^*(t)} + \frac{j(x^*(t),t)}{DP(x^*(t),t)} \circ \dot{x}^*(t) - \frac{\mu}{D}F(x^*(t),t)\circ\dot{x}^*(t)\end{aligned} \tag{2.25}$$

where we have used the processes' Fokker-Planck equation $\partial_t P(x,t) = -\partial_x j(x,t)$ with $j(x,t) = \mu F(x,t)P(x,t) - D\partial_x P(x,t)$. The total time derivative has been taken as a conventional derivative implying the Stratonovich convention indicated by $\circ$, which will become relevant below. The term in (2.25) containing $\partial_t P(x,t)$ accounts for changes in the probability density due to its temporal evolution, such as relaxation to a steady state, and any time-dependent driving protocol. The product $F(x^*(t),t)\circ\dot{x}^*(t)$ can be interpreted as a power expended by the force and in the absence of an internal energy of the particle, dissipated in the medium. With Einstein's relation defining the temperature of $T = D/\mu$ of the medium, the last term may be written as

$$\dot{S}_m(t) = \frac{F(x^*(t),t)\circ\dot{x}^*(t)}{T} \tag{2.26}$$

and thus interpreted as the entropy change in the medium. Together with the entropy change of the particle, this gives the total entropy change of particle and medium,

$$\dot{S}_{\mathrm{tot}}(t) = \frac{\mathrm{d}}{\mathrm{d}t}S(x^*(t),t) + \dot{S}_m(t) = -\left.\frac{\partial_t P(x,t)}{P(x,t)}\right|_{x=x^*(t)} + \frac{j(x^*(t),t)}{DP(x^*(t),t)}\circ\dot{x}^*(t)\,, \tag{2.27}$$

which is a random variable, as it depends on the position $x^*(t)$. It also draws on $P(x,t)$ and $j(x,t)$ which are properties of the ensemble. To make the connection to the entropies constructed above we need to take an ensemble average of the instantaneous $\dot{S}_{\mathrm{tot}}(t)$. To do so, we need an interpretation of the last term of (2.27), where the noise $\zeta(t)$ of $\dot{x}^*(t)$, Eq. (2.23), multiplies $j(x^*(t),t)/P(x^*(t),t)$. Equivalently, we need the joint density $P(x,\dot{x};t)$ of position x and velocity $\dot{x}$ at time t. In the spirit of Ito this density trivially factorises into a normally distributed $\dot{x} - \mu F(x,t)$ and $P(x,t)$ as the increment $\dot{x}dt$ on the basis of (2.23) depends only on the particle's current position $x(t)$. However, this is not so in the Stratonovich interpretation of $P(x,\dot{x};t)$, as here the increment depends equally on $x(t)$ and $x(t+dt)$ [146, 145, 125]. Taking the en-

semble average of $\dot{S}_{\mathrm{tot}}$ thus produces

$$\begin{aligned}\langle \dot{S}_{\mathrm{tot}}(t)\rangle &= \int \mathrm{d}x^*\mathrm{d}\dot{x}^*\, \dot{S}_{\mathrm{tot}}(t) P(x^*,\dot{x}^*;t) \\ &= -\int \mathrm{d}x^*\, \frac{\partial_t P(x^*,t)}{P(x^*,t)} \int \mathrm{d}\dot{x}^*\, P(x^*,\dot{x}^*;t) + \int \mathrm{d}x^*\mathrm{d}\dot{x}^*\, \frac{j(x^*,t)}{DP(x^*,t)} \dot{x}^* P(x^*,\dot{x}^*;t)\,,\end{aligned} \tag{2.28}$$

where x^* and $\dot{x}^*$ are now dummy variables. The first term on the right hand side vanishes, because $P(x^*,t) = \int \mathrm{d}\dot{x}^*\, P(x^*,\dot{x}^*;t)$ is the marginal of $P(x^*,\dot{x}^*;t)$ and $\int \mathrm{d}x^*\, \partial_t P(x^*,t) = 0$ by normalisation. The integral over $\dot{x}^*$ in the second term produces the expected particle velocity conditional to its position,

$$\langle \dot{x}^* | x^*, t\rangle = \int \mathrm{d}\dot{x}^*\, \dot{x}^* \frac{P(x^*,\dot{x}^*;t)}{P(x^*,t)} \tag{2.29}$$

in the Stratonovich sense, where it gives rise to the current [144], $\langle \dot{x}^*|x^*,t\rangle = j(x^*,t)/P(x^*,t)$, so that

$$\langle \dot{S}_{\mathrm{tot}}(t)\rangle = \int \mathrm{d}x^*\, \frac{j^2(x^*,t)}{DP(x^*,t)} \geq 0\ , \tag{2.30}$$

which vanishes only in the absence of any probability current, *i.e.* in thermodynamic equilibrium. In the Ito sense, the conditional expectation (2.29) would have instead given rise to the ensemble-independent drift, $\langle \dot{x}^*|x^*,t\rangle = \mu F(x^*,t)$. Comparing to Eq. (2.13), the expectation $\langle \dot{S}_{\mathrm{tot}}(t)\rangle$ turns out to be the internal entropy production $\dot{S}_i(t)$, so that $\dot{S}_{\mathrm{tot}}(t)$ of Eq. (2.27) may be regarded as its instantaneous counterpart.

Path integral methods. An interesting aspect of working with the Langevin description is the possibility of casting probability densities $p([x];t)$ for paths $x(t')$ with $t' \in [0,t]$ into path integrals, for example in the Onsager-Machlup formalism [116, 164]. For the colloidal particle introduced in (2.23), it gives $p([x];t) = \mathcal{N}\exp\left(-\mathcal{A}([x];t)\right)$ with the action functional

$$\mathcal{A}([x];t) = \int_0^t \mathrm{d}t'\, \frac{(\dot{x}(t') - \mu F(x(t'),t'))^{\circ 2}}{4D} - \frac{\mu}{2}\int_0^t \mathrm{d}t'\, \partial_x F(x(t'),t') \tag{2.31}$$

in the Stratonovich discretisation, which differs from the Ito form only by the second term [164, Sec. 4.5], which is the Jacobian of the transform of the noise $\zeta(t)$ to $x(t)$, Eq. (2.23). The Stratonovich form is needed so that the action does not give pref-

erence to a particular time direction [35]. This choice plays a rôle in every product of white noise, as is implicit to $\dot{x}$, and a random variable. We therefore indicate the choice by a $\circ$ also in powers, reminding us that $F(x(t'),t')$ should be read as $F((x(t')+x(t'+\Delta t))/2, t'+\Delta t)$ and $\dot{x}(t')$ as $(x(t'+\Delta t)-x(t'))/2$ with discretisation time step Δt. Evaluating the action for the reversed path $x^R(t') = x(t-t')$ then gives

$$\mathcal{A}([x^R];t) = \int_0^t \mathrm{d}t' \, \frac{(\dot{x}^R(t') - \mu F(x^R(t'),t'))^{\circ 2}}{4D} - \frac{\mu}{2}\int_0^t \mathrm{d}t' \, \partial_x F(x^R(t'),t') \tag{2.32}$$

$$= \int_0^t \mathrm{d}t' \, \frac{(\dot{x}(t') + \mu F(x(t'),t-t'))^{\circ 2}}{4D} - \frac{\mu}{2}\int_0^t \mathrm{d}t' \, \partial_x F(x(t'),t-t') \; . \tag{2.33}$$

If the force is even under time reversal, $F(x,t') = F(x,t-t')$, in particular when it is independent of time, the path probability density obeys

$$\ln \frac{p([x];t)}{p([x^R];t)} = \int_0^t \mathrm{d}t' \, \frac{F(x(t'),t') \circ \dot{x}(t')}{T} = S_m(t) \; , \tag{2.34}$$

with random variables multiplied with Stratonovich convention. With Eq. (2.26), the integral in Eq. (2.34) can be identified as the entropy of the medium. When the driving is time-independent and the system's probability distribution eventually becomes stationary, such that $\lim_{t\to\infty}\langle \dot{S}(x^*,t)\rangle = 0$, Eq. (2.24), the only contribution to the total entropy change is due to change of entropy in the medium, Eq. (2.27). Assuming that the system is ergodic, we have the equivalence $\lim_{t\to\infty} S_m(t)/t = \lim_{t\to\infty}\langle \dot{S}_{\mathrm{tot}}(t)\rangle$, where $\langle\bullet\rangle$ denotes an ensemble average. Using Eqs. (2.13) and (2.30) gives $\lim_{t\to\infty} S_m(t)/t = \lim_{t\to\infty} \dot{S}_i(t)$. Equation (2.34) can therefore be used directly to compute the steady-state internal entropy production rate. The equivalence between the long-time limit $t\to\infty$ and the ensemble average holds only for ergodic systems, whose unique steady-state does not depend on the specific initialisation $x(0)$. This connection between stochastic thermodynamics and field theory has stimulated a number of works aimed at characterising the non-equilibrium features of continuum models of active matter [113, 54]. Extensions of this formalism to systems driven by correlated noise have also been proposed [26].

2.3 Systems

In this section we calculate the entropy production rate on the basis of Gaspard's framework [64], Eqs. (2.4), (2.16) and (2.17), for different particle systems. We cover the systems listed in Tab. 2.1, with both discrete and continuous states and with one or multiple particles.

Table 2.1: List of particle systems for which we have calculated their entropy production $\dot{S}_i(t)$.

	System	$\dot{S}_i(t)$
2.3.1	Two-state Markov process	(2.38)
2.3.2	Three-state Markov process	(2.42)
2.3.3	Random walk on a complete graph	(2.45), (2.46)
2.3.4	N independent, distinguishable Markov processes	(2.53)
2.3.5	N independent, indistinguishable two-state Markov processes	(2.56b)
2.3.6	N independent, indistinguishable d-state processes	(2.69)
2.3.7	Random Walk on a lattice	(2.82)
2.3.8	Random Walk on a ring lattice	(2.86), (2.88)
2.3.9	Driven Brownian particle	(2.94)
2.3.10	Driven Brownian particle in a harmonic potential	(2.104)
2.3.11	Driven Brownian particle on a ring with potential	(2.120d)
2.3.12	Run-and-tumble motion with diffusion on a ring	(2.129)
2.3.13	Switching diffusion process on a ring	(2.135)

2.3.1 Two-state Markov process

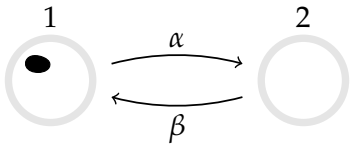


Figure 2.1: Two-state Markov chain in continuous time. The black blob indicates the current state of the system. Independently of the choice of α and β, this processes settles into an equilibrium steady-state at long times (in the absence of an external time-dependent diving).

Consider a particle that hops between two states, 1 and 2, with transition rates $\dot{W}(1 \to 2) = \alpha$ and $\dot{W}(2 \to 1) = \beta$, see Fig. 2.1 [48, 96], and using the notation in Eq. (2.19)

for discrete states. The rate-matrix (see Eq. (2.7)) may thus be

$$w = \begin{pmatrix} -\alpha & \alpha \\ \beta & -\beta \end{pmatrix} , \tag{2.35}$$

with $\mathbf{P}(t) = (P_1(t), P_2(t))$ the probability of the particle to be in state 1 or 2 respectively as a function of time. By normalisation, $P_1(t) + P_2(t) = 1$, with probabilistic initial condition $\mathbf{P}(0) = (p, 1-p)$. Solving the master equation in Eq. (2.2) yields

$$\mathbf{P}(t) = (P_1(t), P_2(t)) = \frac{1}{\alpha+\beta}\left(\beta + r\, e^{-(\alpha+\beta)t}, \alpha - r\, e^{-(\alpha+\beta)t}\right) , \tag{2.36}$$

with $r = \alpha p - \beta(1-p)$, corresponding to an exponentially decaying probability current

$$P_1(t)\alpha - P_2(t)\beta = r\, e^{-(\alpha+\beta)t} . \tag{2.37}$$

The internal entropy production (2.4b) is then

$$\dot{S}_i(t) = [P_1(t)\alpha - P_2(t)\beta] \ln\left[\frac{P_1(t)\alpha}{P_2(t)\beta}\right] = r\mathrm{e}^{-(\alpha+\beta)t} \ln\left[\frac{1 + \frac{r}{\beta}\, e^{-(\alpha+\beta)t}}{1 - \frac{r}{\alpha}\, e^{-(\alpha+\beta)t}}\right] , \tag{2.38}$$

see Fig. 2.3, and the entropy flow (2.4a),

$$\dot{S}_e(t) = -r\,\mathrm{e}^{-(\alpha+\beta)t} \ln\left(\frac{\alpha}{\beta}\right) . \tag{2.39}$$

At stationarity, $\dot{S}_i = \dot{S}_e = 0$ and therefore the two-state Markov process reaches equilibrium. In this example, the topology of the transition network does not allow a sustained current between states, which inevitably leads to equilibrium in the steady state and, therefore, there is production of entropy only due to the relaxation of the system from the initial state.

2.3.2 Three-state Markov process

We extend the system in Sec. 2.3.1 to three states, 1, 2 and 3, with transition rates $\dot{W}(1 \to 2) = \alpha$, $\dot{W}(2 \to 3) = \alpha$, $\dot{W}(3 \to 1) = \alpha$, $\dot{W}(2 \to 1) = \beta$, $\dot{W}(3 \to 2) = \beta$, and $\dot{W}(1 \to 3) = \beta$, see Fig. 2.2, and using the notation Eq. (2.19) for discrete states. The

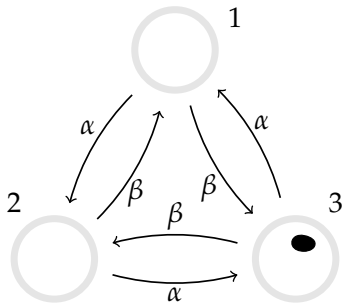


Figure 2.2: Three-state Markov chain in continuous time. The black blob indicates the current state of the system. Symmetry under cyclic permutation is introduced by imposing identical transition rates α and β for counter-clockwise and clockwise transition, respectively.

rate matrix (see Eq. (2.7)) is then

$$w = \begin{pmatrix} -(\alpha+\beta) & \alpha & \beta \\ \beta & -(\alpha+\beta) & \alpha \\ \alpha & \beta & -(\alpha+\beta) \end{pmatrix} . \tag{2.40}$$

Assuming the initial condition $\mathbf{P}(0) = (1, 0, 0)$, the probabilities of states 1, 2 and 3 respectively, evolve according to Eq. (2.2), which has solution

$$P_1(t) = \frac{1}{3}\left(1 + 2\mathrm{e}^{-3\phi t}\cos\left(\sqrt{3}\psi t\right)\right) , \tag{2.41a}$$

$$P_2(t) = \frac{1}{3}\left(1 - 2\mathrm{e}^{-3\phi t}\cos\left(\sqrt{3}\psi t - \pi/3\right)\right) , \tag{2.41b}$$

$$P_3(t) = \frac{1}{3}\left(1 - 2\mathrm{e}^{-3\phi t}\cos\left(\sqrt{3}\psi t + \pi/3\right)\right) , \tag{2.41c}$$

with $\phi = (\alpha+\beta)/2$ and $\psi = (\alpha-\beta)/2$.

The entropy production (2.4b) is then, using (2.41),

$$\begin{aligned} \dot{S}_i(t) = (\alpha-\beta)\ln\frac{\alpha}{\beta} &+ \left(P_1(t)\alpha - P_2(t)\beta\right)\ln\left(\frac{P_1(t)}{P_2(t)}\right) \\ &+ \left(P_2(t)\alpha - P_3(t)\beta\right)\ln\left(\frac{P_2(t)}{P_3(t)}\right) + \left(P_3(t)\alpha - P_1(t)\beta\right)\ln\left(\frac{P_3(t)}{P_1(t)}\right) , \end{aligned} \tag{2.42}$$

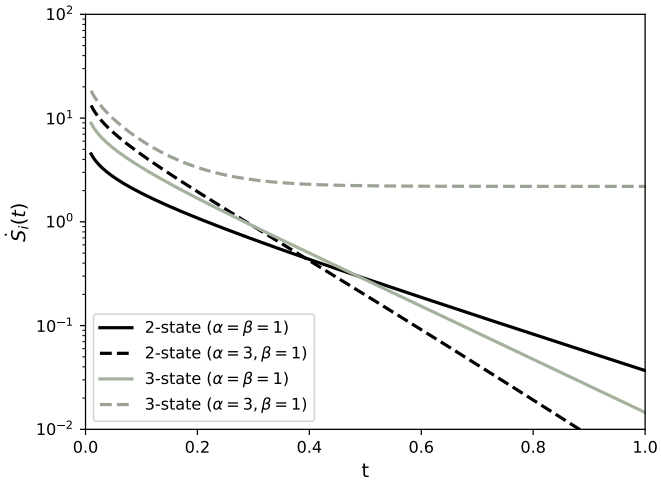


Figure 2.3: Entropy production of the two- and three-state Markov processes (black and grey lines respectively) discussed in Sections 2.3.1 and 2.3.2 as a function of time. For the two-state system we plot Eq. (2.38) with $p = 1$ both for the symmetric, $\alpha = \beta$ (solid lines), and for the asymmetric case, $\alpha \neq \beta$ (dashed lines). In both, the entropy production decays exponentially at long times. For the three-state system, Eq. (2.42), the asymmetric case displays a finite entropy production rate at long times, consistent with Eq. (2.43) and the condition that at stationarity $\dot{S}_i(t) = -\dot{S}_e(t)$.

see Fig. 2.3, and the entropy flow (2.4a),

$$\dot{S}_e(t) = -(\alpha - \beta) \ln \left(\frac{\alpha}{\beta} \right), \tag{2.43}$$

which is constant throughout. At stationarity, the system is uniformly distributed and, if $\alpha \neq \beta$, the entropy production and flow satisfy $\dot{S}_i = -\dot{S}_e \neq 0$. If $\alpha \neq \beta$, the particle has a net drift that sustains a probability current $(\alpha - \beta)/3$ in the system, which prevents the system from reaching equilibrium. This setup can be generalised straightforwardly to M-state Markov processes characterised by the same cyclic structure $\dot{W}(i \to i + 1 \pmod M) = \alpha$ and $\dot{W}(i \to i - 1 \pmod M) = \beta$, to find that the steady-state entropy production is independent of M. These can be seen as simple models of protein conformational cycles driven by instantaneous energy inputs of order $k_B T \ln(\alpha/\beta)$, for example ATP hydrolysis [179].

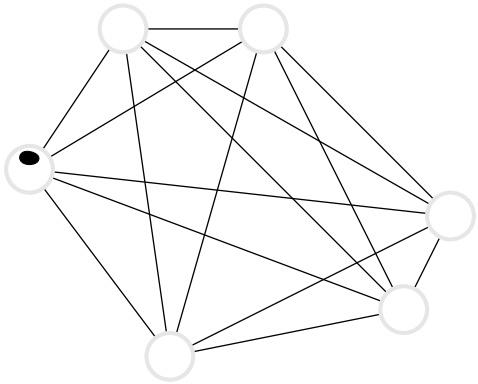


Figure 2.4: Random walk on a complete graph of d nodes (here shown for $d = 6$). The black blob indicates the current state of the system. For uniform transition rates, the symmetry under node relabelling leads to an equilibrium, homogeneous steady-state with $P_j = 1/d$ for all j.

2.3.3 Random walk on a complete graph

Consider a random walker on a complete graph with d nodes, where each node is connected to all other nodes, and the walker jumps from node $j \in \{1, 2, \ldots, d\}$ to node $k \in \{1, 2, \ldots, d\}$, $k \neq j$, with rate w_{jk}, see Fig. 2.4. These are the off-diagonal elements of the corresponding Markov matrix whose diagonal elements are $w_{jj} = -\sum_{i=1, i\neq j}^{d} w_{ji}$. The probability vector $\mathbf{P}(t) = (P_1(t), P_2(t), \ldots, P_d(t))$ has components $P_j(t)$ that are the probability that the system is in state j at time t. The general case of arbitrary transition rates is impossible to discuss exhaustively. In the uniform case, $w_{jk} = \alpha$, the Markov matrix has only two distinct eigenvalues, namely eigenvalue αd with degeneracy $d - 1$ and eigenvalue 0 with degeneracy 1. Assuming an arbitrary initial condition $\mathbf{P}(0)$, the probability distribution at a later time t is

$$P_j(t) = \frac{1}{d} + e^{-d\alpha t}\left(P_j(0) - \frac{1}{d}\right) . \tag{2.44}$$

The steady state, which is associated with the vanishing eigenvalue, is the uniform distribution $\lim_{t\to\infty} P_j(t) = 1/d$ for all $j \in \{1, 2, \ldots, d\}$. The entropy production (2.4b) of the initial state relaxing to the uniform state is

$$\dot{S}_i(t) = \frac{1}{2}\alpha e^{-d\alpha t} \sum_{j,k} \left(P_j(0) - P_k(0)\right) \ln\left(\frac{1 + e^{-d\alpha t}\left(P_j(0)d - 1\right)}{1 + e^{-d\alpha t}\left(P_k(0)d - 1\right)}\right) , \tag{2.45}$$

and the entropy flow (2.4a) is $\dot{S}_e = 0$ throughout. If the walker is initially located on node k, so that $P_j(0) = \delta_{j,k}$, the entropy production simplifies to

$$\dot{S}_i(t) = (d-1)\alpha e^{-d\alpha t} \ln(1 + \frac{de^{-d\alpha t}}{1 - e^{-d\alpha t}}) \,. \tag{2.46}$$

We can see that the system reaches equilibrium at stationarity, since $\lim_{t\to\infty} \dot{S}_i(t) = \dot{S}_e(t) = 0$. At long times ($de^{-d\alpha t} \ll 1$), the asymptotic behaviour of $\dot{S}_i$ is

$$\dot{S}_i(t) = d(d-1)\alpha e^{-2d\alpha t} + \mathcal{O}(e^{-3d\alpha t}) \,, \tag{2.47}$$

by expanding the logarithm in the small exponential.

2.3.4 N INDEPENDENT, DISTINGUISHABLE MARKOV PROCESSES

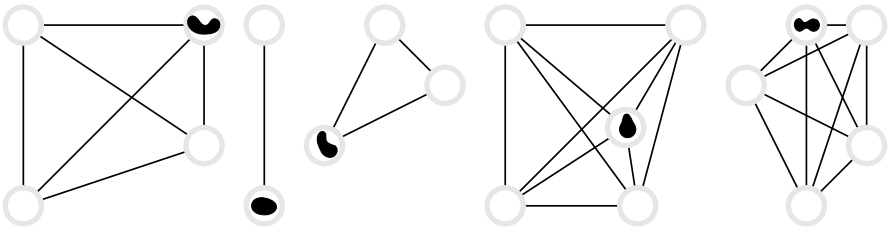


Figure 2.5: Example of $N = 5$ non-interacting, distinguishable processes with $d_1 = 4$, $d_2 = 2$, $d_3 = 3$, $d_4 = 5$ and $d_5 = 5$. The black blobs indicate the current state of each sub-system.

In the following we consider N non-interacting, distinguishable particles undergoing Markovian dynamics on a discrete state space. Each of the N particles carries an index $\ell \in \{1, 2, \ldots, N\}$ and is in state $n_\ell \in \{1, 2, \ldots, d_\ell\}$, so that the state of the entire system is given by an N-particle state $\mathbf{n} = (n_1, n_2, \ldots, n_N)$. Particle distinguishability implies the factorisation of state and transition probabilities into their single-particle contributions, whence the joint probability $P_{\mathbf{n}}(t)$ of an N-particle state $\mathbf{n}$ factorises into a product of single particle probabilities $P^{(\ell)}_{n_\ell}(t)$ of particle ℓ to be in state n_ℓ,

$$P_{\mathbf{n}}(t) = \prod_{\ell=1}^{N} P^{(\ell)}_{n_\ell}(t) \,. \tag{2.48}$$

Further, the Poissonian rate $w_{\mathbf{nm}}$ from N-particle state $\mathbf{n}$ to N-particle state $\mathbf{m} \neq \mathbf{n}$ vanishes for all transitions $\mathbf{n} \to \mathbf{m}$ that differ in more than one component ℓ, *i.e.*

$w_{\mathbf{nm}} = 0$ unless there exists a single $\ell \in \{1, 2, \ldots, N\}$ such that $m_k = n_k$ for all $k \neq \ell$, in which case $w_{\mathbf{nm}} = w^{(\ell)}_{n_\ell m_\ell}$, the transition rates of the single particle transition of particle ℓ.

The entropy production of this N-particle system according to Eq. (2.4b),

$$\dot{S}_i(t) = \frac{1}{2} \sum_{\mathbf{nm}} (P_{\mathbf{n}}(t) w_{\mathbf{nm}} - P_{\mathbf{m}}(t) w_{\mathbf{mn}}) \ln \left(\frac{P_{\mathbf{n}}(t) w_{\mathbf{nm}}}{P_{\mathbf{m}}(t) w_{\mathbf{mn}}} \right) \tag{2.49}$$

simplifies considerably due to $w_{\mathbf{nm}}$, as the sum may be re-written as

$$\sum_{\mathbf{nm}} \ldots w_{\mathbf{nm}} \ldots = \sum_{\mathbf{n}} \sum_{\ell} \sum_{m_\ell} \ldots w_{\mathbf{nm}_\ell} \ldots \tag{2.50}$$

with $\mathbf{m}_\ell = (n_1, n_2, \ldots, n_{\ell-1}, m_\ell, n_{\ell+1}, \ldots, n_N)$ so that $w_{\mathbf{nm}_\ell} = w^{(\ell)}_{n_\ell m_\ell}$ and

$$\dot{S}_i(t) = \frac{1}{2} \sum_{\mathbf{n}} \sum_{\ell=1}^{N} \sum_{m_\ell} \left\{ \left(\prod_{k=1}^{N} P^{(k)}_{n_k}(t) \right) w^{(\ell)}_{n_\ell m_\ell} - \left(\prod_{k=1}^{N} P^{(k)}_{m_k}(t) \right) w^{(\ell)}_{m_\ell n_\ell} \right\} \ln \left(\frac{\prod_{k=1}^{N} P^{(k)}_{n_k}(t) w^{(\ell)}_{n_\ell m_\ell}}{\prod_{k=1}^{N} P^{(k)}_{m_k}(t) w^{(\ell)}_{m_\ell n_\ell}} \right) . \tag{2.51}$$

Since $m_k = n_k$ for any $k \neq \ell$ inside the curly bracket, we may write

$$\prod_{k=1}^{N} P^{(k)}_{n_k}(t) = P^{(\ell)}_{n_\ell}(t) \prod_{\substack{k=1 \\ k \neq \ell}}^{N} P^{(k)}_{n_k}(t) \qquad \text{and} \qquad \prod_{k=1}^{N} P^{(k)}_{m_k}(t) = P^{(\ell)}_{m_\ell}(t) \prod_{\substack{k=1 \\ k \neq \ell}}^{N} P^{(k)}_{n_k}(t) \, . \tag{2.52}$$

The product $\prod_{k \neq \ell}^{N} P^{(k)}_{n_k}(t)$ can thus be taken outside the curly bracket in Eq. (2.51) and be summed over, as well as cancelled in the logarithm. After changing the dummy variables in the remaining summation from n_ℓ and m_ℓ to n and m respectively, the entropy production is

$$\dot{S}_i(t) = \frac{1}{2} \sum_{\ell=1}^{N} \sum_{nm} \left(P^{(\ell)}_{n}(t) w^{(\ell)}_{nm} - P^{(\ell)}_{m}(t) w^{(\ell)}_{mn} \right) \ln \left(\frac{P^{(\ell)}_{n}(t) w^{(\ell)}_{nm}}{P^{(\ell)}_{m}(t) w^{(\ell)}_{mn}} \right) , \tag{2.53}$$

which is the sum of the entropy productions of the single particle $\ell \in \{1, 2, \ldots, N\}$, Eq. (2.4b), irrespective of how each particle is initialised. The same argument applies

to $\dot{S}_e$, the entropy flow Eq. (2.4a). The entropy production and flow obviously simplify to an N-fold product of the single particle expressions if $w_{nm}^{(\ell)}$ do not depend on ℓ and all particles are initialised by the same $P_n^\ell(0)$ independent of ℓ. This result may equally be found from the dynamical entropy per unit time, Eq. (2.8).

2.3.5 N INDEPENDENT, INDISTINGUISHABLE TWO-STATE MARKOV PROCESSES

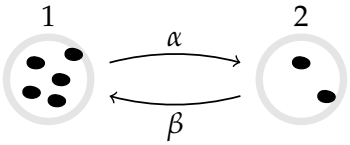


Figure 2.6: N independent, indistinguishable two-state Markov processes in continuous time. The black blobs indicate the current state of the single-particle sub-system. Since processes are indistinguishable, states are fully characterised by the occupation number of either state, if the total number of particles is known.

Suppose that N identical, indistinguishable, non-interacting particles follow the two-state Markov process described in Sec. 2.3.1, Fig. 2.6 [48]. There are $\Omega = N + 1$ distinct states given by the occupation number $n \in \{0, 1, \ldots, N\}$ of one of the two states, say state 1, as the occupation number of the other state follows as $N - n$ given the particle number N is fixed under the dynamics. In the following, $P(n, t)$ denotes the probability of finding n particles in state 1 at time t. The master equation is then

$$\dot{P}(n,t) = -\alpha n P(n,t) + \alpha(n+1)P(n+1,t) - \beta(N-n)P(n,t) + \beta(N-n+1)P(n-1,t) \ . \tag{2.54}$$

The state space and the evolution in it can be thought of as a hopping process on a one-dimensional chain of states with non-uniform rates. Provided $P(n, 0)$ initially follows a binomial distribution, $P(n, 0) = \binom{N}{n} p^n (1-p)^{N-n}$ with probability p for a particle to be placed in state 1 initially, the solution of Eq. (2.54) is easily constructed from the solution $P_1(t)$ in Eq. (2.36) of Sec. 2.3.1 via

$$P(n,t) = \binom{N}{n} P_1^n(t)(1 - P_1(t))^{N-n} \quad \text{for} \quad 0 \leq n \leq N \tag{2.55}$$

with $P_1(0) = p$, as $\dot{P}_1(t) = -\alpha P_1(t) + \beta(1 - P_1(t))$, which can be verified by substituting Eq. (2.55) into Eq. (2.54). Using Eqs. (2.35) and (2.55) in (2.4b) the entropy

production reads

$$\dot{S}_i(t) = \sum_{n=1}^{N} [P(n,t)\alpha n - P(n-1,t)\beta(N-n+1)] \ln\left[\frac{P(n,t)\alpha n}{P(n-1,t)\beta(N-n+1)}\right] \tag{2.56a}$$

$$= N[P_1(t)\alpha - (1-P_1(t))\beta] \ln\left[\frac{P_1(t)\alpha}{(1-P_1(t))\beta}\right] , \tag{2.56b}$$

which is the N-fold multiple of the result of the corresponding single particle system, Eq. (2.38). This result, Eq. (2.56b), depends on the initialisation being commensurable with Eq. (2.55) which otherwise is recovered only asymptotically and only if the stationary distribution is unique. Further, the entropy production of N indistinguishable particles being the N-fold entropy production of a single particle does not extend to the external entropy flow, which lacks the simplification of the logarithm and gives

$$\begin{aligned}\dot{S}_e(t) = &- N[\alpha P_1(t) - \beta(1-P_1(t))]\times \\ &\left\{\ln\left(\frac{\alpha}{\beta}\right) + \sum_{n=0}^{N-1} P_1^n(t)(1-P_1(t))^{N-1-n}\binom{N-1}{n}\ln\left(\frac{n+1}{N-n}\right)\right\}\end{aligned} \tag{2.57}$$

thus picking up a correction in the form of the additional sum in the curly bracket that vanishes only at $N = 1$ or $P_1(t) = 1/2$, but does not contribute at stationarity because of the overall prefactor $\alpha P_1 - \beta(1-P_1)$ that converges to 0. To make sense of this correction in relation to particle indistinguishability, with the help of Eq. (2.55) we can rewrite the difference between the right hand side of Eq. (2.57) and the N-fold entropy flow of a single two-state system (2.39) as

$$\begin{aligned}&-N[\alpha P_1(t) - \beta(1-P_1(t))] \sum_{n=0}^{N-1} P_1^n(t)(1-P_1(t))^{N-1-n}\binom{N-1}{n}\ln\left(\frac{n+1}{N-n}\right) \\ &= -\sum_{n=0}^{N-1}[\alpha(n+1)P(n+1,t) - \beta(N-n)P(n,t)]\ln\left(\frac{n+1}{N-n}\right)\end{aligned} \tag{2.58}$$

which now explicitly involves the net probability current from the occupation number state with $n+1$ particles in state A to that with n particles in state A, as well as a

the logarithm

$$\ln\left(\frac{n+1}{N-n}\right) = \ln\left[\binom{N}{n}\right] - \ln\left[\binom{N}{n+1}\right] \ . \tag{2.59}$$

Written in terms of the same combinatorial factors appearing in Eq. (2.55), the logarithm (2.59) can be interpreted as a difference of microcanonical (Boltzmann) entropies, defined as the logarithm of the degeneracy of the occupation number state if we were to assume that the N particles are distinguishable. With the help of the master Eq. (2.54) as well as Eqs. (2.55) and (2.59), the term Eq. (2.58) may be rewritten to give

$$\dot{S}_e(t) = -N[\alpha P_1(t) - \beta(1-P_1(t))] \ln\left(\frac{\alpha}{\beta}\right) - \sum_{n=0}^{N-1} \dot{P}(n,t) \ln\left[\binom{N}{n}\right] \tag{2.60}$$

This result is further generalised in Eq. (2.71).

2.3.6 N INDEPENDENT, INDISTINGUISHABLE d-STATE PROCESSES

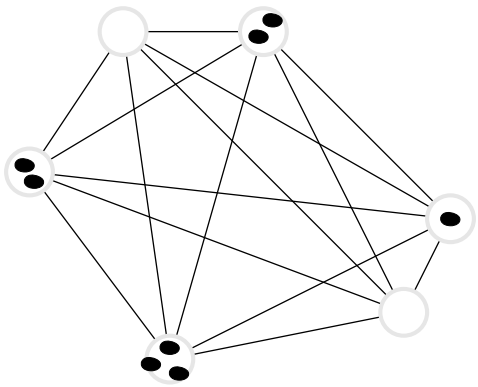


Figure 2.7: N independent, indistinguishable d-state Markov processes (here shown for $d = 6$ and $N = 8$) in continuous time. Black blobs indicate the current state of the single-particle sub-systems. Due to indistinguishably, multi-particle states are fully characterised by the occupation number of an arbitrary subset of $d-1$ states, if the total number of particles is known.

We generalise now the results in Sec. 2.3.3 and Sec. 2.3.5 to N independent d-state Markov processes, see Fig. 2.7. These results represent a special case of those obtained in [71] when the N processes are non-interacting. In this section we consider non-interacting, indistinguishable particles hopping on a graph of d nodes with edge-dependent hopping rates w_{jk}. As in the two-state system in Sec. 2.3.5, we find that

the internal (but not the external) entropy production of the d-state system $\dot{S}_i$ is N times the entropy production of the individual processes assuming the initial condition is probabilistically identical for all single-particle sub-systems. The entropy productions of a single such process according to Eq. (2.4) read

$$\dot{S}_i^{(1)}(t) = \frac{1}{2}\sum_{jk}[P_j(t)w_{jk} - P_k(t)w_{kj}]\ln\left(\frac{P_j(t)w_{jk}}{P_k(t)w_{kj}}\right), \tag{2.61a}$$

$$\dot{S}_e^{(1)}(t) = -\frac{1}{2}\sum_{jk}[P_j(t)w_{jk} - P_k(t)w_{kj}]\ln\left(\frac{w_{jk}}{w_{kj}}\right), \tag{2.61b}$$

where $P_j(t)$ is the time-dependent probability of a single-particle process to be in state j, Sec. 2.3.3. To calculate the entropy production of the N concurrent indistinguishable processes using the occupation number representation, we first derive the probability of an occupation number configuration $\mathbf{n} = (n_1, n_2, \ldots, n_d)$, with $\sum_{j=1}^{d} n_j = N$, which similar to Eq. (2.55) is given by the multinomial distribution

$$P_{\mathbf{n}}(t) = N!\prod_{j=1}^{d}\frac{P_j^{n_j}(t)}{n_j!} \tag{2.62}$$

for the probability $P_{\mathbf{n}}(t)$ of the system to be in state $\mathbf{n}$ at time t assuming that each particle is subject to the same single-particle distribution $P_j(t)$, $j \in \{1, 2, \ldots, d\}$ for all t, *i.e.* in particular assuming that all particles are initialised identically, by placing them all at the same site or, more generally, by placing them initially according to the same distribution $P_j(0)$. Given this initialisation, Eq. (2.62) solves Eq. (2.2)

$$\dot{P}_{\mathbf{n}}(t) = \sum_{\mathbf{m}} P_{\mathbf{m}}(t)w_{\mathbf{mn}} - P_{\mathbf{n}}(t)w_{\mathbf{nm}} \tag{2.63}$$

with the transition rates $w_{\mathbf{mn}}$ discussed below.

For non-interacting processes with a unique stationary distribution, Eq. (2.62) is always obeyed in the limit of long times after initialisation, since the single-particle distributions $P_j(t)$ are identical at steady state. The entropy production Eq. (2.4b) of the entire system has the same form as Eq. (2.49) of Sec. 2.3.4 (N independent, *distinguishable* particles) with $w_{\mathbf{nm}}$ however now the transition rate between the oc-

cupation number state $\mathbf{n} = (n_1, n_2, \ldots, n_d)$ with $0 \leq n_k \leq N$ to occupation number state $\mathbf{m} = (m_1, m_2, \ldots, m_d)$. The rate $w_{\mathbf{nm}}$ vanishes except when $\mathbf{m}$ differs from $\mathbf{n}$ in exactly two distinct components, say $m_j = n_j - 1 \geq 0$ and $m_k = n_k + 1 \geq 1$ in which case $w_{\mathbf{nm}} = n_j w_{jk}$ with w_{jk} the transition rates of a single particle from j to k as introduced above. For such $\mathbf{m}$, the rate obeys $w_{\mathbf{mn}} = m_k w_{kj}$ and the probability $P_{\mathbf{m}}(t)$ fulfills

$$P_{\mathbf{m}}(t) = P_{\mathbf{n}}(t)\frac{P_k(t)n_j}{P_j(t)m_k} = P_{\mathbf{n}}(t)\frac{P_k(t)w_{\mathbf{nm}}w_{kj}}{P_j(t)w_{\mathbf{mn}}w_{jk}} \ , \tag{2.64}$$

which simplifies the entropy production Eq. (2.49) to

$$\begin{aligned}\dot{S}_i(t) &= \frac{1}{2}\sum_{\mathbf{nm}}(P_{\mathbf{n}}(t)w_{\mathbf{nm}} - P_{\mathbf{m}}(t)w_{\mathbf{mn}})\ln\left(\frac{P_{\mathbf{n}}(t)w_{\mathbf{nm}}}{P_{\mathbf{m}}(t)w_{\mathbf{mn}}}\right) \\ &= \frac{1}{2}\sum_{\mathbf{n}}\sum_{jk}(P_{\mathbf{n}}(t)n_j w_{jk} - P_{\mathbf{m}}(t)m_k w_{kj})\ln\left(\frac{P_j(t)w_{jk}}{P_k(t)w_{kj}}\right)\end{aligned} \tag{2.65}$$

where the sum $\sum_{\mathbf{n}}$ runs over all allowed configurations, namely $0 \leq n_j \leq N$ for $j = 1, 2, \ldots, d$ with $\sum_j n_j = N$ and $\mathbf{m} = (n_1, n_2, \ldots, n_j - 1, \ldots, n_k + 1, \ldots, n_d)$ is derived from $\mathbf{n}$ as outlined above. Strictly, $P_{\mathbf{n}}(t)$ has to be defined to vanish for invalid states $\mathbf{n}$, so that the first bracket in the summand of Eq. (2.65) vanishes in particular when $n_j = 0$, in which case $m_j = -1$. To proceed, we introduce the probability

$$\bar{P}_{\bar{\mathbf{n}}_j}(t) = (N-1)!\frac{P_j^{n_j-1}}{(n_j-1)!}\prod_{i=1,i\neq j}^{d}\frac{P_i^{n_i}}{n_i!} \ , \tag{2.66}$$

defined to vanish for $n_j = 0$, so that $P_{\mathbf{n}}(t)n_j = NP_j(t)\bar{P}_{\bar{\mathbf{n}}_j}(t)$. The probability $\bar{P}_{\bar{\mathbf{n}}_j}(t)$ is that of finding n_i particles at states $i \neq j$ and $n_j - 1$ particles at state j. It is Eq. (2.62) evaluated in a system with only $N-1$ particles and configuration $\bar{\mathbf{n}}_j = (n_1, n_2, \ldots, n_{j-1}, n_j - 1, n_{j+1}, \ldots, n_d) = \bar{\mathbf{m}}_k$ a function of $\mathbf{n}$. Eq. (2.65) may now be rewritten as

$$\dot{S}_i(t) = \frac{N}{2}\sum_{jk}\left\{\left(\sum_{\mathbf{n}}\bar{P}_{\bar{\mathbf{n}}_j}(t)\right)P_j(t)w_{jk} - \left(\sum_{\mathbf{n}}\bar{P}_{\bar{\mathbf{m}}_k}(t)\right)P_k(t)w_{kj}\right\}\ln\left(\frac{P_j(t)w_{jk}}{P_k(t)w_{kj}}\right) \tag{2.67}$$

where we have used that the arguments of the logarithm are independent of $\mathbf{n}$ and $\mathbf{m}$.

The summation over $\mathbf{n}$ gives

$$\sum_{\mathbf{n}} \bar{P}_{\bar{\mathbf{n}}_j}(t) = \sum_{\mathbf{n}} \bar{P}_{\bar{\mathbf{m}}_k}(t) = 1 \tag{2.68}$$

so that

$$\dot{S}_i(t) = \frac{N}{2} \sum_{jk} (P_j(t) w_{jk} - P_k(t) w_{kj}) \ln \left(\frac{P_j(t) w_{jk}}{P_k(t) w_{kj}} \right) = N \dot{S}_i^{(1)}(t) \tag{2.69}$$

which is the N-fold entropy production of the single particle system $\dot{S}_i(t)$, Eq. (2.61a), or equivalently that of N distinguishable particles, Eq. (2.53), Sec. 2.3.4. As in Sec. 2.3.5, this dramatic simplification does not carry over to the external entropy flow Eq. (2.4a)

$$\begin{aligned}
\dot{S}_e(t) &= -\frac{N}{2} \sum_{jk} \sum_{\mathbf{n}} \bar{P}_{\bar{\mathbf{n}}_j}(t) (P_j(t) w_{jk} - P_k(t) w_{kj}) \ln \left(\frac{n_j w_{jk}}{(n_k + 1) w_{kj}} \right) \\
&= -\frac{N}{2} \sum_{jk} (P_j(t) w_{jk} - P_k(t) w_{kj}) \ln \left(\frac{w_{jk}}{w_{kj}} \right) \\
&\quad - \frac{N}{2} \sum_{jk} \sum_{\mathbf{n}} \bar{P}_{\bar{\mathbf{n}}_j}(t) (P_j(t) w_{jk} - P_k(t) w_{kj}) \ln \left(\frac{n_j}{n_k + 1} \right) ,
\end{aligned} \tag{2.70}$$

where of the last two terms only the first is the N-fold entropy flow of the single particle system $\dot{S}_e(t)$, Eq. (2.61b). The reason for the second term is the lack of a cancellation mechanism to absorb the n_j and $n_k + 1$ from the logarithm. Rewriting the second term as

$$\begin{aligned}
&- \frac{N}{2} \sum_{jk} \sum_{\mathbf{n}} \bar{P}_{\bar{\mathbf{n}}_j}(t) (P_j(t) w_{jk} - P_k(t) w_{kj}) \ln \left(\frac{n_j}{n_k + 1} \right) \\
&= - \frac{1}{2} \sum_{\mathbf{n}} \sum_{jk} \left(P_{\mathbf{n}}(t) n_j w_{jk} - P_{\mathbf{n}} \left(\frac{P_k(t) n_j}{P_j(t)(n_k + 1)} \right) (n_k + 1) w_{kj} \right) \ln \left(\frac{n_j}{n_k + 1} \right) \qquad (2.71) \\
&= - \sum_{\mathbf{n}} \dot{P}_{\mathbf{n}}(t) \ln \left[\binom{N}{n_1, ..., n_d} \right] , \qquad (2.72)
\end{aligned}$$

using Eq. (2.63) where we re-expressed the logarithm as

$$\ln \left(\frac{n_j}{n_k + 1} \right) = \ln \left[\binom{N}{n_1, \ldots, n_j - 1, \ldots, n_k + 1, \ldots, n_d} \right] - \ln \left[\binom{N}{n_1, \ldots, n_d} \right] , \tag{2.73}$$

shows that the correction term has the same form as the corresponding term in the two-state system, Eq. (2.58), namely that of a difference of microcanonical (Boltzmann) entropies of the multi-particle states. It vanishes when all n_j are either 0 or 1, as expected for $d \gg N$ and also at stationarity when $\dot{P}_{\mathbf{n}}(t) = 0$. In that limit $\dot{S}_e = -\dot{S}_i$ when indeed Eq. (2.61a) gives

$$\lim_{t\to\infty} \dot{S}_i^{(1)}(t) = \frac{1}{2}\sum_k (P_j w_{jk} - P_k w_{kj}) \ln\left(\frac{w_{jk}}{w_{kj}}\right) \ , \tag{2.74}$$

with $P_j = \lim_{t\to\infty} P_j(t)$. As far as the entropy production $\dot{S}_i(t)$ is concerned, we thus recover and generalise the result in Sec. 2.3.5 on indistinguishable particles in a two-state system, which produce N times the entropy of a single particle. In Sec. 2.3.4 it was shown that N *distinguishable* particles have the same entropy production and flow as the sum of the entropy productions of individual particles. In Sec. 2.3.5 and 2.3.6 it was shown that the entropy production of *indistinguishable* particles, which require the states to be represented by occupation numbers, show the N-fold entropy production of the single particle system, provided suitable initialisation, but asymptotically independent of initialisation, provided the stationary state has a unique distribution. The same does not apply to the entropy flow, which generally acquires additional logarithmic terms accounting for the degeneracy of the occupation number states. The extra terms, however, are bound to vanish at stationarity, when $\dot{S}_e(t) = -\dot{S}_i(t)$.

2.3.7 Random Walk on a lattice

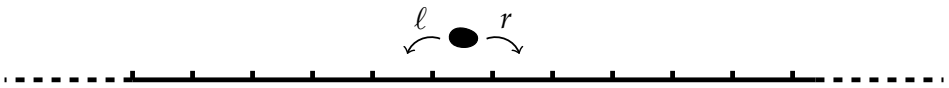


Figure 2.8: Simple random walk on an infinite, one-dimensional lattice in continuous time. The black blob indicates the current position of the random walker. The left and right hopping rates, labelled ℓ and r respectively, are assumed to be homogeneous but not equal in general, this leading to a net drift of the average position.

In this section we study a particle on a one-dimensional lattice that hops to the right nearest neighbouring site with rate r and to the left with rate ℓ, see Fig. 2.8. The case of unequal hopping rates, $\ell \neq r$, is generally referred to as an asymmetric ran-

dom walk and can be seen as a minimal model for the directed motion of a molecular motor on a cytoskeletal filament [88]. The position x of the particle at time t, after $N(t)$ jumps, is

$$x = x_0 + \sum_{i=1}^{N(t)} \Delta x_i, \tag{2.75}$$

where the random hops Δx_i are independent and identically distributed, and x_0 is the initial position at time $t = 0$. If a is the lattice spacing, the distance increments are $\Delta x_i = +a$ with probability $r/(\ell + r)$ and $\Delta x_i = -a$ with probability $\ell/(\ell + r)$. The probability distribution of the particle position is

$$P(x, t; x_0) = \sum_{n=0}^{\infty} H(n, t) P_n(x; x_0)\,, \tag{2.76}$$

where $H(n, t)$ is the probability that by time t, the particle has hopped $N(t) = n$ times, and $P_n(x; x_0)$ is the probability that the particle is at position x after n hops starting from x_0. Since jumping is a Poisson process with rate $r + \ell$, the random variable $N(t)$ has a Poisson distribution,

$$H(n, t) = \frac{((\ell + r)t)^n}{n!} \mathrm{e}^{-(\ell+r)t}\,. \tag{2.77}$$

On the other hand, the distribution of the position x after n jumps is the binomial distribution

$$P_n(x; x_0) = \binom{n}{k_x} \frac{r^{k_x} \ell^{n-k_x}}{(\ell + r)^n}\,, \tag{2.78}$$

where $k_x = (n + (x - x_0)/a)/2$ is the number of jumps to the right, $0 \le k_x \le n$ with (2.78) implied to vanish if k_x is not integer. From Eq. (2.75) the parity of $(x - x_0)/a$ and $N(t)$ are identical. Using (2.77) and (2.78), the probability distribution in (2.76) reads

$$P(x, t; x_0) = \mathrm{e}^{-(\ell+r)t} \left(\frac{r}{\ell}\right)^{\frac{x-x_0}{2a}} \mathcal{I}\left(\frac{|x - x_0|}{a}, 2t\sqrt{r\ell}\right)\,, \tag{2.79}$$

where $\mathcal{I}(n,z)$ is the modified Bessel function of the first kind. * The transition probability is then,

$$W(x \to y;\tau) = \mathrm{e}^{-(\ell+r)\tau}\left(\frac{r}{\ell}\right)^{\frac{y-x}{2a}} \mathcal{I}\left(\frac{|y-x|}{a}, 2\tau\sqrt{r\ell}\right) . \tag{2.80}$$

Using (2.79) and (2.80) to calculate the entropy production (2.4b), we need the following identity for $|y-x|/a = |m| \geq 1$,

$$\lim_{\tau\to 0}\frac{1}{\tau}\mathcal{I}\left(|m|, 2\tau\sqrt{r\ell}\right) = \sqrt{r\ell}\delta_{|m|,1} , \tag{2.81}$$

which follows immediately from the definition of the modified Bessel function (see footnote $*$). It indicates that the only transitions that contribute to the entropy production are those where the particle travels a distance equal to the lattice spacing a. Then, the entropy production reads,

$$\begin{aligned}\dot{S}_i(t) =& \frac{1}{2}(r-\ell)\ln\left(\frac{r}{\ell}\right) + \mathrm{e}^{-(\ell+r)t}\sum_{m=-\infty}^{\infty}\left(\frac{r}{\ell}\right)^{\frac{m}{2}}\mathcal{I}\left(|m|, 2t\sqrt{r\ell}\right) \\ &\times\left[r\ln\left(\frac{\mathcal{I}\left(|m|,2t\sqrt{r\ell}\right)}{\mathcal{I}\left(|m+1|,2t\sqrt{r\ell}\right)}\right) + \ell\ln\left(\frac{\mathcal{I}\left(|m|,2t\sqrt{r\ell}\right)}{\mathcal{I}\left(|m-1|,2t\sqrt{r\ell}\right)}\right)\right] ,\end{aligned} \tag{2.82}$$

see Fig. 2.9. The entropy flow is $\dot{S}_e(t) = -(r-\ell)\ln(r/\ell)$ independent of t, which owes its simplicity to the transition rates being independent of the particle's position. large times t, we cannot calculate the stationary entropy production $\lim_{t\to\infty}\dot{S}_i(t)$. If we naively assume that the sum in Eq. (2.82) converges such that it is suppressed by the exponential $\exp(-(r+\ell)t)$, then the entropy production $\dot{S}_i$ appears to converge to $\frac{1}{2}(r-\ell)\ln(r/\ell)$. If that were the case, $\dot{S} = \dot{S}_i + \dot{S}_e$ would converge to a negative constant, while $S(t)$, Eq. (2.1), which vanishes at $t = 0$ given the initialisation of $P(x,t;x_0) = \delta_{(x-x_0)/a,0}$, is bound to be strictly positive at all finite t. Given that $P(x,t;x_0)$ does not converge, not much else can be said about $S(t)$ or $\dot{S}$. Numer-

* The modified Bessel function of the first kind of $m, z \in \mathbb{C}$ is defined as [103]

$$\mathcal{I}(m,z) = \sum_{j=0}^{\infty}\frac{1}{j!\Gamma(j+m+1)}\left(\frac{z}{2}\right)^{2j+m} .$$

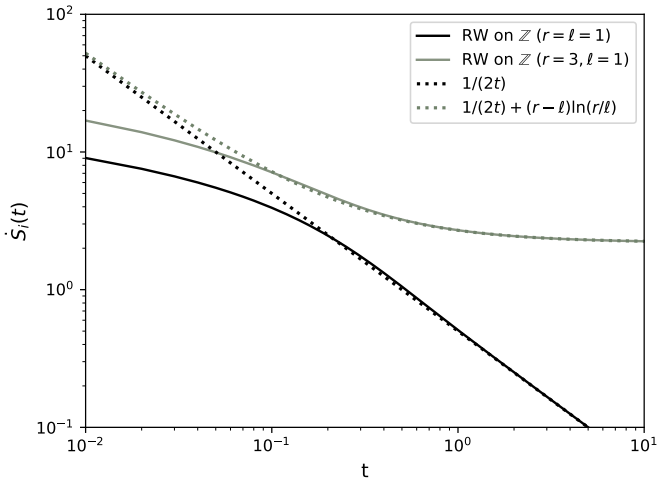


Figure 2.9: Entropy production of a random walk on a one-dimensional lattice (RW on $\mathbb{Z}$), for symmetric and asymmetric hopping rates, as a function of time, Eq. (2.82) (solid lines). The asymptotic behaviour at large t, Eq. (2.83) (dotted lines), decays algebraically in the symmetric case ($r = \ell$) and converges to a positive constant in the asymmetric case ($r \neq \ell$).

ically, using the GNU Scientific Library [60] implementation of Bessel functions, we find that, asymptotically for large times, Eq. (2.82) is

$$\dot{S}_i(t) \simeq (r-\ell)\ln\left(\frac{r}{\ell}\right) + \frac{1}{2t} + \mathcal{O}\left(t^{-2}\right) \tag{2.83}$$

if $r \neq \ell$ and $\dot{S}_i(t) \simeq 1/(2t) + \mathcal{O}\left(t^{-3}\right)$ if $r = \ell$, see Fig. 2.9.

To take the continuum limit $a \to 0$ of the probability distribution (2.79), we define v and D such that $r + \ell = 2D/a^2$ and $r - \ell = v/a$. Using the asymptotic expansion[†] of $\mathcal{I}(m,z)$ in m, we obtain in fact the Gaussian distribution,

$$\lim_{a\to 0} \frac{1}{a} P\left(\frac{x}{a}, t; \frac{x_0}{a}; r(v,D,a), \ell(v,D,a)\right) = \frac{1}{\sqrt{4\pi D t}} \mathrm{e}^{-\frac{(x-x_0-vt)^2}{4Dt}}, \tag{2.84}$$

which corresponds to the distribution of a drift-diffusive particle, which is studied in

[†]We use the asymptotic expansion in m of the modified Bessel function [103]

$$\mathcal{I}(m,z) \sim \frac{\exp(z)}{\sqrt{2\pi z}}\left(1 - \frac{4m^2-1}{8z} + \frac{\left(4m^2-1\right)\left(4m^2-9\right)}{2!(8z)^2} - \frac{\left(4m^2-1\right)\left(4m^2-9\right)\left(4m^2-25\right)}{3!(8z)^3} + \ldots\right),$$

which is valid for $|\arg z| < \pi/2$.

Sec. 2.3.9. Therefore, all results derived in Sec. 2.3.9, apply to the present system in the continuum limit.

2.3.8 Random Walk on a ring lattice

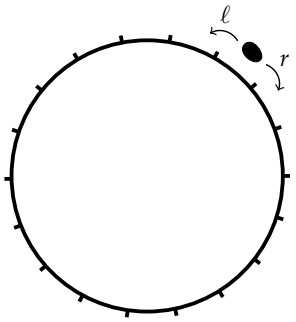


Figure 2.10: Simple random walk on an periodic, one-dimensional 'ring' lattice in continuous time. This model generalises the three-state Markov chain discussed in Section 2.3.2 to L states. The black blob indicates the current position of the random walker. Due to the finiteness of the state space, this process is characterised by a well defined steady-state, which is an equilibrium one for symmetric rates $\ell = r$.

In this section we extend the system in Sec. 2.3.7 to a random walk on a ring lattice of length $L > 2$, so that $1 \leq x \leq L$, see Fig. 2.10. The probability distribution $P_L(x,t)$ of the particle on the ring follows from the distribution on the one-dimensional lattice $P(x,t)$ in (2.79), by mapping all positions $x + jL$ on the one-dimensional lattice to position $x \in \{1, 2, \ldots, L\}$ on the ring with j being the winding number irrelevant to the evolution of the walker. Then, the distribution on the ring lattice reads,

$$P_L(x,t;x_0) = \sum_{j=-\infty}^{\infty} P(x+jL,t;x_0) \tag{2.85}$$

and similarly for the transition probability $W(x \to y,\tau) = P_L(y,\tau;x)$. To calculate the entropy production (2.4b), each pair of points x, y on the lattice is mapped to a pair of points on the ring. For $L > 2$, as $\tau \to 0$ only transitions to distinct, nearest neighbours contribute and the expression for the entropy production simplifies dra-

matically,

$$\begin{aligned}\dot{S}_i(t) =&(r-\ell)\ln\left(\frac{r}{\ell}\right)+\sum_{m=1}^{L/a}P_L(ma,t;x_0)\\ &\left\{r\ln\left(\frac{P_L(ma,t;x_0)}{P_L((m+1)a,t;x_0)}\right)+\ell\ln\left(\frac{P_L(ma,t;x_0)}{P_L((m-1)a,t;x_0)}\right)\right\}\end{aligned} \tag{2.86}$$

and similar for

$$\dot{S}_e(t) = -(r-\ell)\ln\left(\frac{r}{\ell}\right). \tag{2.87}$$

While the entropy flow $\dot{S}_e$ on a ring is thus identical to that of a particle on a one-dimensional lattice, the entropy production $\dot{S}_i$ on a ring is in principle more complicated, but with a lack of cancellations of $\sqrt{r/\ell}$ in the logarithm as found in Sec. 2.3.7 and P_L reaching stationarity comes the asymptote

$$\lim_{t\to\infty}\dot{S}_i(t) = (r-\ell)\ln\left(\frac{r}{\ell}\right). \tag{2.88}$$

This is easily derived from $\lim_{t\to\infty} P_L(x,t;x_0) = 1/L$ taken into the finite sum of Eq. (2.86). It follows that $\dot{S}(t) = \dot{S}_i(t) + \dot{S}_e(t)$ converges to 0 at large t, as expected for a convergent stationary distribution.

The case $L = 2$ and the less interesting case $L = 1$ are not covered above, because of the different topology of the phase space of $L > 2$ compared to $L = 2$. The difference can be observed in the different structure of the transition matrices (2.35) and (2.40). The framework above is based on each site having two outgoing and two incoming rates, $2L$ in total. However, for $L = 2$ there are only two transitions, which cannot be separated into four to fit the framework above, because even when rates of concurrent transitions between two given states are additive, their entropy production generally is not. The case of $L = 2$ is recovered in the two-state system of Sec. 2.3.1 with $\alpha = \beta = r + \ell$, which is at equilibrium in the stationary state.

2.3.9 Driven Brownian particle

In continuum space, the motion of a freely diffusive particle with diffusion constant D and drift v is governed by the Langevin equation $\dot{x} = v + \sqrt{2D}\xi(t)$, where $\xi(t)$ is a

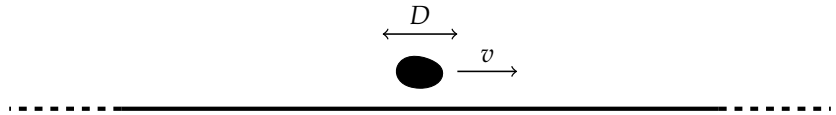


Figure 2.11: Driven Brownian particle on the real line. The black blob indicates the particle's current position.

Gaussian white noise with zero mean, $\langle \xi(t) \rangle = 0$, and covariance $\langle \xi(t)\xi(t') \rangle = \delta(t - t')$, see Fig. 2.11 [165]. The corresponding Fokker-Planck equation for the probability distribution $P(x,t)$ is [135]

$$\partial_t P(x,t) = -v\partial_x P(x,t) + D\partial_x^2 P(x,t)\,. \tag{2.89}$$

Assuming the initial condition $P(x,0) = \delta(x - x_0)$, the solution to the Fokker-Planck equation is the Gaussian distribution

$$P(x,t) = \frac{1}{\sqrt{4D\pi t}} \mathrm{e}^{-\frac{(x-x_0-vt)^2}{4Dt}}\,, \tag{2.90}$$

which is also the Green function of the Fokker-Planck equation (2.89). We therefore also have the transition probability density from state x to state y over an interval τ,

$$W(x \to y, \tau) = \frac{1}{\sqrt{4D\pi\tau}} \mathrm{e}^{-\frac{(y-x-v\tau)^2}{4D\tau}}\,. \tag{2.91}$$

Substituting (2.90) and (2.91) into Eq. (2.16) for the internal entropy production of a continuous system gives,

$$\begin{aligned} \dot{S}_i = \lim_{\tau\to 0} \frac{1}{\tau} \int \mathrm{d}x\mathrm{d}y \, \frac{1}{\sqrt{4D\pi t}} \mathrm{e}^{-\frac{(x-x_0-vt)^2}{4Dt}} \frac{1}{\sqrt{4D\pi\tau}} \mathrm{e}^{-\frac{(y-x-v\tau)^2}{4D\tau}} \times \\ \left(\frac{(y-x_0)^2 - (x-x_0)^2}{4Dt} + \frac{(y-x)v}{2D} \right)\,, \end{aligned} \tag{2.92}$$

where the Gaussian integrals can be evaluated in closed form,

$$\dot{S}_i(t) = \lim_{\tau\to 0} \left(\frac{1}{2t} + \frac{v^2}{D} + \frac{v^2\tau}{2Dt} \right). \tag{2.93}$$

Taking the limit $\tau \to 0$ then gives the entropy production rate [165, 100, 157],

$$\dot{S}_i(t) = \frac{1}{2t} + \frac{v^2}{D}\,, \tag{2.94}$$

see Fig. 2.13. Similarly, following (2.17), the entropy flow reads $\dot{S}_e(t) = -v^2/D$ independent of time t. As $\dot{S}_i(t) \neq 0$, we see that for finite t or $v \neq 0$, the system is out of equilibrium with a sustained probability current, so that there is in fact no steady-state distribution. We can verify Eq. (2.94) for the time-dependent internal entropy production by computing the probability current

$$j(x,t) = (v - D\partial_x)P(x,t) = \left(\frac{v}{2} + \frac{(x - x_0 - vt)}{4t}\right) \frac{e^{-\frac{(x-x_0-vt)^2}{4Dt}}}{\sqrt{\pi D t}} \tag{2.95}$$

and substituting it together with (2.90), into (2.30). As expected, the two procedures return identical results. The independence of the transient contribution $1/(2t)$ to the internal entropy production on the diffusion constant is remarkable although necessary on dimensional grounds, as a consequence of $\dot{S}_i$ having dimensions of inverse time. The diffusion constant characterising the spatial behaviour of diffusion suggests that it is the temporal, rather than spatial features of the process that determine its initial entropy production.

It is interesting to note that when $t = 0$, the entropy production rate $\dot{S}_i$ is infinity. This is because the system has an entropy of $-\infty$. As the entropy S is defined as

$$S = -P(x,t)\log P(x,t), \tag{2.96}$$

using the distribution (2.90), the entropy reads

$$S = -\frac{1}{\sqrt{4\pi D t}}\left(\log\left(\frac{1}{\sqrt{4D\pi t}}\right) - \frac{(x - x_0 - vt)^2}{4Dt}\right) e^{-\frac{(x-x_0-vt)^2}{4Dt}}. \tag{2.97}$$

At $t = 0$ and $x = x_0$, the entropy S has value $-\infty$.

Instead of having a Dirac-δ function as the initial condition, the initial position could also be a distribution. Assuming $P(x,0) = \frac{1}{\sqrt{4D\pi t_0}} e^{-\frac{x^2}{4Dt_0}}$, the solution to the Fokker-

Planck equation is now

$$P(x,t) = \frac{1}{\sqrt{4D\pi(t+t_0)}} e^{-\frac{(x-x_0-vt)^2}{4D(t+t_0)}}. \tag{2.98}$$

and the entropy production rate is therefore

$$\dot{S}_i(t) = \frac{1}{2(t+t_0)} + \frac{v^2}{D}. \tag{2.99}$$

2.3.10 Driven Brownian particle in a harmonic potential

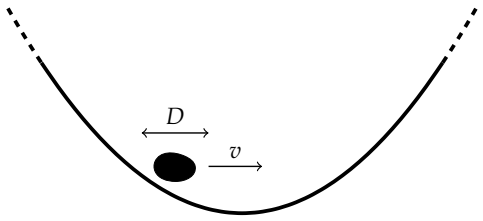


Figure 2.12: Driven Brownian particle in a harmonic potential. This process reduces to the standard Ornstein-Uhlenbeck process upon rescaling $x \to x' + v/k$. The black blob indicates the particle's current position. The presence of a binding potential implies that the system relaxes to an equilibrium steady-state at long times.

Consider a drift-diffusive particle such as in Section 2.3.9 that is confined in a harmonic potential $V(x) = \frac{1}{2}kx^2$, where k is the potential stiffness, see Fig. 2.12 [3]. The Langevin equation is $\dot{x} = v - kx + \sqrt{2D}\xi(t)$, where $\langle \xi(t) \rangle = 0$ and $\langle \xi(t)\xi(t') \rangle = \delta(t-t')$ and the Fokker-Planck equation for $P(x,t)$ is [135]

$$\partial_t P(x,t) = -\partial_x((v - kx)P(x,t)) + D\partial_x^2 P(x,t)\,. \tag{2.100}$$

Assuming the initial condition $P(x,0) = \delta(x - x_0)$, the solution to the Fokker-Plank equation is the Gaussian distribution

$$P(x,t) = \sqrt{\frac{k}{2\pi D(1 - \exp(-2kt))}} \mathrm{e}^{-\frac{(kx - v - (kx_0 - v)\exp(-kt))^2}{2Dk(1-\exp(-2kt))}}, \tag{2.101}$$

corresponding to a probability current $j(x,t) = (v - kx - D\partial_x)P(x,t)$ of the form

$$j(x) = \frac{\sqrt{\frac{k}{2\pi D(1-e^{-2kt})}}e^{-kt}\left(v\left(1-e^{-kt}\right) - k\left(x_0 - xe^{-kt}\right)\right)}{1-e^{-2kt}}\mathrm{e}^{-\frac{(v(1-e^{-kt})-k(x-x_0e^{-kt})^2}{2Dk(1-e^{-2kt})}} . \tag{2.102}$$

The transition probability density within τ is then also of Gaussian form, namely

$$W(x \to y, \tau) = \sqrt{\frac{k}{2\pi D(1-\exp(-2k\tau))}}\mathrm{e}^{-\frac{(ky-v-(kx-v)\exp(-k\tau))^2}{2Dk(1-\exp(-2k\tau))}} . \tag{2.103}$$

Using (2.101) and (2.103) in (2.16) gives the entropy production rate

$$\dot{S}_i = \left(\frac{(v-kx_0)^2}{D} - k\right)\mathrm{e}^{-2kt} + \frac{k\exp(-2kt)}{1-\exp(-2kt)} , \tag{2.104}$$

see Fig. 2.13, and in (2.17) the external entropy flow

$$\dot{S}_e = -\left(\frac{(v-kx_0)^2}{D} - k\right)\mathrm{e}^{-2kt} . \tag{2.105}$$

In the limit $t \to \infty$, the system will reach equilibrium as $P(x,t)$ in Eq. (2.101) converges to the Boltzmann distribution $\sqrt{\frac{k}{2\pi D}}\exp\left(-\frac{(kx-v)^2}{2Dk}\right)$ of the effective potential $\frac{1}{2}kx^2 - vx$ at temperature D. This is consistent with (2.104) and (2.105) since $\lim_{t\to\infty}\dot{S}_i(t) = \lim_{t\to\infty}\dot{S}_e(t) = 0$. Similarly to drift diffusion on the real line, Eq. (2.94), there is a transient contribution to the entropy production that is independent of the diffusion constant D but does now depend on the stiffness k, which has dimensions of inverse time, through the rescaled time kt.

We also note that the steady-state entropy production is 0 if the potential $V(x)$ is confining, that is, $\lim_{|x|\to+\infty}V(x) = +\infty$ as the probability density follows a Boltzmann distribution. In the above example, the drift and the external field can be absorbed into the potential and hence the system can be treated as a thermal system in equilibrium.

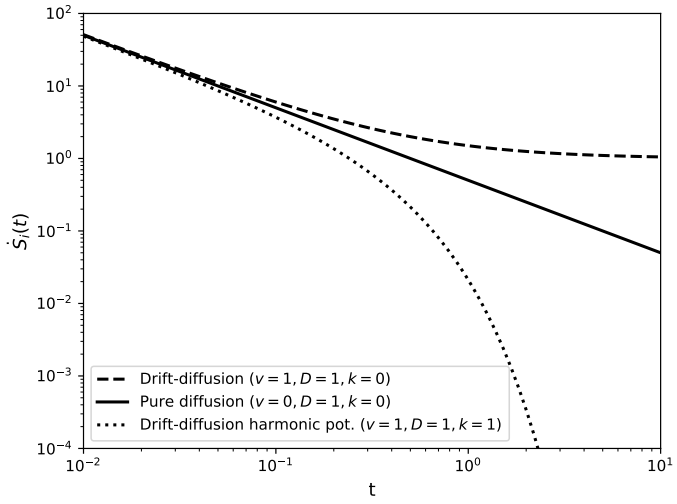


Figure 2.13: Entropy production of the drift-diffusion process in an external potential, Eq. (2.104), as a function of time for different parameter combinations. For vanishing potential stiffness, $k \to 0$, we recover Eq. (2.94) for a free drift-diffusion particle. In particular, for $v = 0$ the entropy production decays algebraically, while for $v \neq 0$ it converges to the constant value v^2/D. For $k > 0$, the algebraic decay is suppressed exponentially at long times as the process settles into its equilibrium steady-state.

2.3.11 Driven Brownian particle on a ring with potential

Consider a drift-diffusive particle on a ring $x \in [0, L)$ in a smooth potential $V(x)$, Fig. 2.14, initialised at position x_0. The Langevin equation of the particle is [134, 126, 114] $\dot{x} = v - \partial_x V(x) + \sqrt{2D}\xi(t)$, where $\xi(t)$ is Gaussian white noise. The Fokker-Planck equation is then

$$\partial_t P(x, t; x_0) = -\partial_x((v - V'(x))P(x, t; x_0)) + D\partial_x^2 P(x, t; x_0) \tag{2.106}$$

with $V'(x) = \frac{d}{dx}V(x)$ and boundary condition $P^{(n)}(0, t; x_0) = P^{(n)}(L, t; x_0)$ for for all $n \geq 0$ derivatives and $t \geq 0$. At stationarity, in the limit $t \to \infty$, where $\partial_t P(x, t; x_0) = 0$, the solution to the Fokker-Planck equation (2.106) is [76, 122, 114]

$$P_s(x) = \lim_{t\to\infty} P(x, t) = \mathcal{Z}\mathrm{e}^{-\frac{V(x)-vx}{D}} \int_x^{x+L} \mathrm{d}y\, \mathrm{e}^{\frac{V(y)-vy}{D}}, \tag{2.107}$$

where $\mathcal{Z}$ is the normalisation constant. The corresponding steady-state probability current $j = (v - \partial_x V)P_s - D\partial_x P_s$ is independent of x by continuity, $0 = \partial_t P = -\partial_x j$,

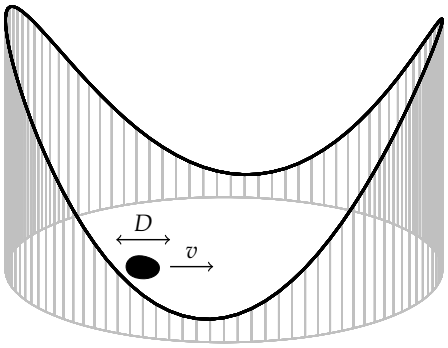


Figure 2.14: Driven Brownian particle on a ring $x \in [0, L)$ with a periodic potential satisfying $V(x) = V(x + L)$. Any finite diffusion constant $D > 0$ results in a stationary state at long times that is non-equilibrium for $v \neq 0$. The black blob indicates the particle's current position.

and reads [135]

$$j = \mathcal{Z}\left(\mathrm{e}^{-\frac{vL}{D}} - 1\right) \ . \tag{2.108}$$

In order to calculate the entropy production according to (2.16) and (2.17) using (2.18), we need $W(x \to y; \tau)$ for small τ. As discussed after Eq. (2.18), $W(x \to y; \tau)$ obeys the Fokker-Planck Eq. (2.106) in the form

$$\partial_\tau W(x \to y; \tau) = -\partial_y \left[(v - V'(y))\, W(x \to y; \tau)\right] + D\partial_y^2 W(x \to y; \tau) \tag{2.109}$$

with $\lim_{\tau \to 0} W(x \to y; \tau) = \delta(y - x)$, so that

$$\dot{W}(x \to y) = \lim_{\tau \to 0} \partial_\tau W(x \to y; \tau) = V''(y)\delta(y - x) - (v - V'(y))\delta'(y - x) + D\delta''(y - x) \tag{2.110}$$

to be evaluated under an integral, where $\delta'(y-x) = \frac{d}{dy}\delta(y-x)$ will require an integration by parts. The derivation of the propagator Eq. (2.110) follows from [174]. In the limit of $\tau \to 0$, the short-time propagator is

$$\lim_{\tau \to 0} W(x \to y, \tau) = \delta(x - y). \tag{2.111}$$

As the short-time propagator also follows the Fokker-Planck equation, we act the

Fokker-Planck operator on the Dirac-δ function, therefore

$$\dot{W}(x \to y) = \lim_{\tau \to 0} \partial_\tau W(x \to y; \tau) = V''(y)\delta(y-x) - (v - V'(y))\delta'(y-x) + D\delta''(y-x). \tag{2.112}$$

As for the logarithmic term, we use [135]

$$W(x \to y; \tau) = \frac{1}{\sqrt{4\pi D\tau}} e^{-\frac{(y-x-\tau(v-V'(x)))^2}{4D\tau}} (1 + \mathcal{O}(\tau)) \tag{2.113}$$

so that

$$\ln\left(\frac{W(x \to y; \tau)}{W(y \to x; \tau)}\right) = \frac{y-x}{2D}(2v - V'(x) - V'(y)) + \mathcal{O}(\tau). \tag{2.114}$$

The entropy flow Eq. (2.17) in the more convenient version Eq. (2.22a) can be obtained easily using Eqs. (2.110) and (2.114),

$$\dot{S}_e(t) = -\int_0^L \mathrm{d}x\mathrm{d}y\, P(x,t)\Big(V''(y)\delta(y-x) - (v - V'(y))\delta'(y-x) + D\delta''(y-x)\Big) \tag{2.115}$$

$$\times \frac{y-x}{2D}(2v - V'(x) - V'(y)) \tag{2.116}$$

$$= -\int_0^L \mathrm{d}x\, P(x,t)\left(\frac{1}{D}(v - V'(x))^2 - V''(x)\right) \tag{2.117}$$

after suitable integration by parts, whereby derivatives of the δ-function are conveniently interpreted as derivatives with respect to y to avoid subsequent differentiation of $P(x,t)$. Since $\delta(y-x)(y-x) = 0$, the factor $(y-x)/(2D)$ needs to be differentiated for a term to contribute. In the absence of a potential, $P(x,t) = 1/L$ at stationarity, so that Eq. (2.117) simplifies to $\dot{S}_e(t) = -v^2/D$ and $\lim_{t\to\infty} \dot{S}_i(t) = v^2/D$, Eq. (2.94). Using the probability current $j(x,t) = -D\partial_x P(x,t) + (v - V'(x))\, P(x,t)$, the entropy flow simplifies further to

$$\dot{S}_e(t) = -\int_0^L \mathrm{d}x\, j(x,t)\frac{v - V'(x)}{D} \tag{2.118}$$

so that at stationarity, when the current is spatially uniform,

$$\lim_{t\to\infty} \dot{S}_e(t) = -\lim_{t\to\infty} j(x,t) vL/D \tag{2.119}$$

as the potential is periodic, entering only via the current.

An equivalent calculation of $\dot{S}_i$ on the basis of (2.21a) gives

$$\dot{S}_i(t) = -\dot{S}_e + \int_0^L \mathrm{d}x\mathrm{d}y\, P(x,t)\Big(V''(y)\delta(y-x) - (v - V'(y))\delta'(y-x) + D\delta''(y-x)\Big) \times \ln\left(\frac{P(x,t)}{P(y,t)}\right) \tag{2.120a}$$

$$= -\dot{S}_e + \int_0^L \mathrm{d}x\, \left\{D\frac{(P'(x,t))^2}{P(x,t)} - P(x,t)V''(x)\right\} \tag{2.120b}$$

$$= -\dot{S}_e - \int_0^L \mathrm{d}x\, j(x,t)\partial_x \ln P(x,t) \tag{2.120c}$$

$$= \int_0^L \mathrm{d}x \frac{j^2(x,t)}{DP(x,t)}\,, \tag{2.120d}$$

with the last line identical to Eq. (2.13).

By considering the functional derivative $\delta Z/\delta V(z)$ in $\int_0^L \mathrm{d}x P(x) = 1$ of Eq. (2.107), one can show that the stationary current $j(x,t)$ Eq. (2.108) is extremal for constant $V(x)$, indicating that the magnitude of the stationary entropy flow Eq. (2.120d) is maximised in a constant potential.

2.3.12 Run-and-tumble motion with diffusion on a ring

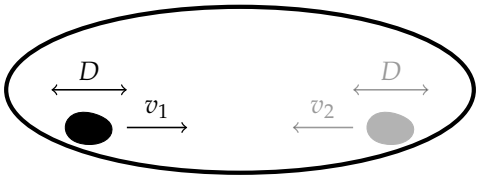


Figure 2.15: Run-and-tumble motion with diffusion on a ring $x \in [0, L)$. A run-and-tumble particle switches stochastically, in a Poisson process with rate α, between two modes 1 and 2 characterised by an identical diffusion constant D but distinct drift velocities v_1 and v_2. The two modes are here represented in black and grey, respectively. For arbitrary positive diffusion constant D or tumbling rate α with $v_1 \neq v_2$ the steady state is uniform but generally non-equilibrium.

Consider the dynamics of a run-and-tumble particle on a ring $x \in [0, L)$ with Langevin equation $\dot{x} = v(t) + \sqrt{2D}\xi(t)$, where the drift $v(t)$ is a Poisson process with rate α that alternates the speed of the particle between the constants v_1 and v_2, and $\xi(t)$

is Gaussian white noise, Fig. 2.15. Run-and-tumble particles are widely studied as a model of bacterial motion [143]. The drift being $v(t) = v_1$ or $v(t) = v_2$ will be referred to as the mode of the particle being 1 or 2 respectively. Defining $P_1(x,t)$ and $P_2(x,t)$ as the joint probabilities that the particle is at position x at time t and in mode 1 or 2 respectively, the coupled Fokker-Planck equations for P_1 and P_2 are

$$\partial_t P_1(x,t) = -v_1 \partial_x P_1(x,t) + D\partial_x^2 P_1(x,t) - \alpha(P_1(x,t) - P_2(x,t)) \tag{2.121a}$$

$$\partial_t P_2(x,t) = -v_2 \partial_x P_2(x,t) + D\partial_x^2 P_2(x,t) - \alpha(P_2(x,t) - P_1(x,t)) \tag{2.121b}$$

whose stationary solution is the uniform distribution $\lim_{t\to\infty} P_1(x,t) = \lim_{t\to\infty} P_2(x) = 1/(2L)$ as is easily verified by direct substitution. The corresponding steady-state probability currents thus read $j_1 = v_1/(2L)$ and $j_2 = v_2/(2L)$.

In the following, we denote by the propagator $W(x \to y, Q \to R; \tau)$ the probability density that a particle at position x in mode Q is found time τ later at position y in mode R. For $Q = R$, this propagation is a sum over all even numbers m of Poissonian switches, that occur with probability $(\alpha\tau)^m \exp(-\alpha\tau)/m!$, which includes the probability $\exp(-\alpha\tau)$ of not switching at all over a total of time τ. For $Q \neq R$, the propagation is due to an odd number of switches.

For $m = 0$, the contribution to $W(x \to y, Q \to R; \tau)$ is thus $\exp(-\alpha\tau)\, W(x \to y; \tau)$, with $W(x \to y; \tau)$ of a drift diffusion particle on a ring, Section 2.3.11, but without potential, approximated at short times τ by the process on the real line, Eq. (2.91) with drift $v = v_1$ or $v = v_2$ according to the particle's mode. For $m = 1$ the contribution is a single convolution over the time $t' \in [0, \tau)$ at which the particle changes mode, most easily done after Fourier transforming. Before presenting this calculation in real space, we argue that any such convolution will result in some approximate Gaussian with an amplitude proportional to $1/\sqrt{\tau}$ multiplied by a term of order $(\alpha\tau)^m$. In small τ, therefore only the lowest orders need to be kept, $m = 0$ for $Q = R$ and $m = 1$ for $Q \neq R$.

More concretely,

$$
\begin{aligned}
&W(x \to y, 1 \to 2; \tau) \\
&= \int_{-\infty}^{\infty} \mathrm{d}z \int_0^{\tau} \mathrm{d}\tau' \frac{1}{\sqrt{4\pi D \tau'}} \mathrm{e}^{-\frac{(z-x-v_1\tau')^2}{4D\tau'}} \mathrm{e}^{-\alpha\tau'} \frac{1}{\sqrt{4\pi D(\tau-\tau')}} \mathrm{e}^{-\frac{(y-z-v_2(\tau-\tau'))^2}{4D(\tau-\tau')}} \mathrm{e}^{-\alpha(\tau-\tau')} + \ldots
\end{aligned} \tag{2.122}
$$

$$
= \frac{\alpha \exp(-\alpha\tau)}{2(v_1 - v_2)} \left[\operatorname{erf}\left(\frac{x - y + v_1\tau}{\sqrt{4D\tau}} \right) - \operatorname{erf}\left(\frac{x - y + v_2\tau}{\sqrt{4D\tau}} \right) \right] + \ldots \tag{2.123}
$$

which in small τ, when $v_{1,2}\tau/\sqrt{4D\tau} \ll 1$, so that $\operatorname{erf}(r+\varepsilon) = \operatorname{erf}(r) + 2\varepsilon\, e^{-r^2}/\sqrt{\pi} + \ldots$, expands to

$$
\begin{aligned}
W(x \to y, 1 \to 2; \tau) &= \frac{\alpha\tau}{\sqrt{4\pi D\tau}} e^{-\frac{(y-x)^2}{4D\tau}} \left(1 + \mathcal{O}(\tau)\right) \\
&= W(x \to y, 2 \to 1; \tau) \,,
\end{aligned} \tag{2.124}
$$

whereas $W(x \to y, Q \to Q; \tau)$, the propagator with an even number of mode switches, is given by Eq. (2.91) to leading order in τ,

$$
W(x \to y, Q \to Q; \tau) = \frac{1}{\sqrt{4\pi D\tau}} e^{-\frac{(y-x-v_Q\tau)^2}{4D\tau} - \alpha\tau} \left(1 + \mathcal{O}(\tau)\right) \,. \tag{2.125}
$$

Much of the calculation of the entropy production follows the procedure in Secs. 2.3.9 and 2.3.11 to be detailed further below. To this end, we also need

$$
\begin{aligned}
\lim_{\tau \to 0} \frac{\mathrm{d}}{\mathrm{d}\tau} W(x \to y, 1 \to 2; \tau) &= \dot{W}(x \to y, 1 \to 2) = \alpha\delta(x - y) \\
&= \dot{W}(x \to y, 2 \to 1) \,.
\end{aligned} \tag{2.126}
$$

As far as processes are concerned that involve a change of particle mode, therefore only the transition rates enter, not diffusion or drift. Given a uniform stationary spatial distribution of particles of any mode, mode changes between two modes cannot result in a sustained probability current, even when the switching rates differ,

$$
\left(P_1 \dot{W}(1 \to 2) - P_2 \dot{W}(2 \to 1) \right) \ln \left(\frac{P_1 \dot{W}(1 \to 2)}{P_2 \dot{W}(2 \to 1)} \right) = 0 \tag{2.127}
$$

for $P_1\dot{W}(1 \to 2) = P_2\dot{W}(2 \to 1)$ at stationarity as in the process discussed in Section 2.3.1. A probability current and thus entropy production can occur when different particle modes result in a different distribution, Section 2.3.10, or when mode switching between more than two modes results in a current in its own rights, Secs. 2.3.2 and 2.3.13.

Since the full time-dependent density is beyond the scope of the present work, we calculate entropy flow and production at stationary on the basis of a natural extension of Eqs. (2.4), (2.17) and (2.22a) to a mixture of discrete and continuous states

$$-\lim_{t\to\infty} \dot{S}_e(t) = \lim_{t\to\infty} \dot{S}_i(t) \tag{2.128}$$

$$= \sum_{Q,R\in\{1,2\}} \int_0^L \mathrm{d}x\mathrm{d}y P_Q(x,t)\dot{W}(x \to y, Q \to R) \lim_{\tau\to 0} \ln\left(\frac{W(x \to y, Q \to R;\tau)}{W(y \to x, R \to Q;\tau)}\right)$$

$$= \frac{v_1^2 + v_2^2}{2D} \tag{2.129}$$

which immediately follows from Secs. 2.3.9 and 2.3.11, as the stationary density is constant, $P_Q = P_R = 1/(2L)$, and only $Q = R$ contribute, with

$$\lim_{\tau\to 0} \ln\left(\frac{W(x \to y, 1 \to 2;\tau)}{W(y \to x, 2 \to 1;\tau)}\right) = 0\ . \tag{2.130}$$

If the drifts are equal in absolute value $|v_1| = |v_2| = v$, then we recover the entropy production of a simple drift-diffusive particle, $\dot{S}_i = v^2/D$. This is because we can think of run-and-tumble as a drift-diffusion particle that changes direction instantly. Since changing the direction produces no entropy, the total entropy production rate should be the same as a drift-diffusion particle. The entropy production can alternatively be derived via (2.30) by computing $\dot{S}_i = \int \mathrm{d}x\,(j_1^2/(DP_1) + j_2^2/(DP_2))$ with the steady-state currents stated above.

2.3.13 Switching diffusion process on a ring

The dynamics of a one-dimensional run-and-tumble particle discussed above can be readily generalised to the so called switching diffusion process [177] by allowing for an extended set $\{v_i\}$ of drift modes $i = 1, \ldots, M$, Fig. 2.16. The corresponding Langevin

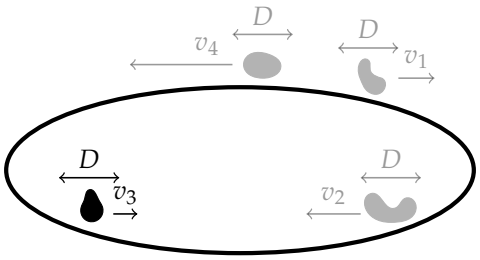


Figure 2.16: Switching diffusion process on a ring $x \in [0, L]$ in continuous time. A switching diffusion process involves a stochastic switching between M modes characterised by an identical diffusion constant D but distinct drifts v_i $(i = 1, 2, \ldots, M)$. The marginal switching dynamics are characterised as an M-state Markov process with transition rates α_{ij} from mode i to mode j.

equation for the particle position on a ring $x \in [0, L]$ is almost identical to that of run-and-tumble, namely $\dot{x} = v(t) + \sqrt{2D}\xi(t)$, with the exception that the process $v(t)$ is now an M-state Markov process. In the general case, a single switching rate α is thus not sufficient and the full transition rate matrix α_{ij} needs to be provided. In this formulation, the run-and-tumble dynamics Sec. 2.3.12 correspond to the choice $M = 2$ with symmetric rates $\alpha_{12} = \alpha_{21} = \alpha$. Defining $P_i(x, t)$ as the joint probability that at time t the particle is at position x and in mode i, thereby moving with velocity v_i, the system (2.121) of Fokker-Planck equations generalises to

$$\partial_t P_i(x,t) = -\partial_x[(v_i - D\partial_x)P_i(x,t)] + \sum_j P_j(x,t)\alpha_{ji} \tag{2.131}$$

where the transmutation rates α_{ij} from mode i to mode j are assumed to be independent of position. To ease notation we use the convention $\alpha_{jj} = -\sum_{i \neq j} \alpha_{ji}$. For non-vanishing diffusion constant, the stationary solution is uniform for all modes and given by $\lim_{t\to\infty} P_i(x,t) = z_i/L$, where z_i is the ith element of the eigenvector $\mathbf{z}$ satisfying $\sum_j z_j = 1$ and the eigenvalue relation $\sum_j z_j \alpha_{ji} = 0$, which we assume to be unique for simplicity.

The calculation of the steady-state entropy production follows very closely that of run-and-tumble presented above. The conditional transition probabilities including

up to one transmutation event read to leading order

$$W(x \to y, i \to j; \tau) = \begin{cases} \frac{e^{\alpha_{ii}\tau}}{\sqrt{4\pi D\tau}} \exp\left(-\frac{(y-x-v_i\tau)^2}{4D\tau}\right)(1+\mathcal{O}(\tau)) & \text{for } i = j \\ \frac{\alpha_{ij}}{2(v_i-v_j)}\left[\operatorname{erf}\left(\frac{x-y+v_i\tau}{\sqrt{4D\tau}}\right) - \operatorname{erf}\left(\frac{x-y+v_j\tau}{\sqrt{4D\tau}}\right)\right](1+\mathcal{O}(\tau)) & \text{for } i \neq j \end{cases}, \tag{2.132}$$

so that

$$\lim_{\tau\to 0}\frac{\mathrm{d}}{\mathrm{d}\tau}W(x \to y, i \to j; \tau) = \begin{cases} D\partial_y^2\delta(y-x) - v_i\partial_y\delta(y-x) + \alpha_{ii}\delta(y-x) & \text{for } i = j \\ \alpha_{ij}\delta(y-x) & \text{for } i \neq j \end{cases}. \tag{2.133}$$

We could perform the calculation of the entropy production using the procedure of Sec. 2.3.9 rather than drawing on the operator for $i = j$, which, however, is used in the following for convenience, see Sec. 2.3.11. Substituting (2.132) and (2.133) into (2.21a) and assuming steady-state densities, we arrive at

$$\begin{aligned} \lim_{t\to\infty}\dot{S}_i(t) &= -\lim_{t\to\infty}\dot{S}_e(t) \\ &= \int_0^L \mathrm{d}x\mathrm{d}y \sum_i \frac{z_i}{L}\left(D\partial_y^2\delta(y-x) - v_i\partial_y\delta(y-x) + \alpha_{ii}\delta(y-x)\right)(y-x)\frac{v_i}{D} \\ &\quad + \int_0^L \mathrm{d}x\mathrm{d}y \sum_{i,j\neq i}\frac{z_i}{L}\alpha_{ij}\delta(y-x)\ln\left(\frac{\alpha_{ij}}{\alpha_{ji}}\right), \end{aligned} \tag{2.134}$$

where we have used Eq. (2.133) in the operators containing the δ-functions and Eq. (2.132) in the logarithms. The term $\ln(\alpha_{ij}/\alpha_{ji})$ is obtained by the same expansion as used in Eq. (2.124), Sec. 2.3.12. Both terms contributing to the entropy production above are familiar from previous sections: the first is a sum over the entropy production of M drift-diffusion processes with characteristic drift v_i, Sec. 2.3.11 without potential, weighted by the steady-state marginal probability z_i for the particle to be in state i; the second is the steady-state entropy production of an M-state Markov process with transition rate matrix α_{ij}, which reduces to Eq. (2.4) after integration. Carrying out all integrals, we finally have

$$\lim_{t\to\infty}\dot{S}_i(t) = \lim_{t\to\infty} -\dot{S}_e(t) = \sum_i z_i\frac{v_i^2}{D} + \frac{1}{2}\sum_{i,j}(z_i\alpha_{ij} - z_j\alpha_{ji})\ln\left(\frac{\alpha_{ij}}{\alpha_{ji}}\right). \tag{2.135}$$

Unlike run-and-tumble, Sec. 2.3.12, the transmutation process in switching diffusion does in general contribute to the entropy production for $M > 2$, since the stationary state generally does not satisfy global detailed balance. However, contributions to the total entropy production originating from the switching and those from the diffusion parts of the process are effectively independent at steady state, as only the stationary marginal probabilities z_i of the switching process feature as weights in the entropy production of the drift-diffusion. Otherwise the parameters characterising the two processes stay separate in Eq. (2.135). Further, the drift-diffusion contributions of the form v_i^2/D are invariant under the time-rescaling $\alpha_{ij} \to T\alpha_{ij}$. This property originates from the steady-state distributions $P_i(x)$ being uniform and would generally disappear in a potential, Sec. 2.3.10.

2.4 Discussion and concluding remarks

In this work we calculate the rate of entropy production within Gaspard's framework [64] from first principles in a collection of paradigmatic processes, encompassing both discrete and continuous degrees of freedom. Based on the Markovian dynamics of each system, where we can, we derive the probability distribution of the particle (or particles) as a function of time $P(x,t)$ from Dirac or Kronecker-δ initial conditions $P(x,0) = \delta(x - x_0)$, from which the transition probability $W(x \to y;\tau)$ follows straightforwardly. In some cases, we determine only the stationary density and the (short-time) propagator $W(x \to y;\tau)$ to leading order in τ. We then use Eq. (2.4) for discrete systems or Eqs. (2.21) and (2.22) for continuous systems to calculate the time-dependent entropy production. We set out to give concrete, exact results in closed form, rather than general expressions that are difficult to evaluate, even when we allowed for general potentials in Sec. 2.3.11. In summary, the ingredients that are needed to calculate the entropy production in closed form in the present framework are: a) the probability (density) $P(x,t)$ to find the system in state x ideally as a function of time t and b) the propagator $W(x \to y;\tau)$, the probability (density) that the system is found at a certain state y after some short time τ given an initial state x. If the propagator is known for any time τ, it can be used to calculate the probability $P(x,t;x_0) = W(x_0 \to x;t)$ for some initial state x_0. However, this full time dependence is often difficult to obtain. The propagator is further needed in two

forms, firstly $\lim_{\tau\to 0}\partial_\tau W(x \to y;\tau)$ when it is most elegantly written as an operator in continuous space, and secondly $\lim_{\tau\to 0}\ln(W(x \to y;\tau)/W(y \to x;\tau))$.

For completeness, where feasible, we have calculated the probability current $j(x,t)$ in continuous systems at position x. The mere presence of such a flow indicates broken time-reversal symmetry and thus non-equilibrium. Our results on the discrete systems (Sec. 2.3.1 to 2.3.8) illustrate two important aspects of entropy production. First, the need of a probability flow $P_A\dot{W}(A \to B) - P_B\dot{W}(B \to A)$ between states: in the two-state system Sec. 2.3.1 there are no transition rates α and β such that there is a sustained probability flow and therefore, the system inevitably relaxes to equilibrium. However, in the three-state system Sec. 2.3.2 the transition rates can be chosen so that there is a perpetual flow $(\alpha - \beta)/3$ between any two states and therefore there is entropy production not only during relaxation but also at stationarity. Hence, we can ascertain these as non-equilibrium steady states in the long time limit due to the non-vanishing rate of internal entropy production. Uniformly distributed steady states can be far from equilibrium as a rigorous analysis on the basis of the microscopic dynamics reveals, although an effective dynamics may suggest otherwise.

Second, we see how the extensivity of entropy production arises in the N-particle systems (Secs. 2.3.4, 2.3.5 and 2.3.6), independently of whether the particles are distinguishable or not. We therefore conclude that the number of particles in the system must be accounted for when calculating the entropy production, and doing otherwise will not lead to a correct result. This is sometimes overlooked, especially when using effective theories. In the continuous systems (Sec. 2.3.9 to 2.3.11), which involve a drift v and a diffusion constant D, we always find the contribution v^2/D to the entropy production emerging one way or another. Moreover, in the case of drift-diffusion on the real line (Sec. 2.3.9) we find that the contribution due to the relaxation of the system $1/(2t)$ is independent of any of the system parameters. Additionally, we note that whenever there is confinement, the system can be treated as a thermal equilibrium system and therefore has 0 steady-state entropy production.

Finally, we have studied two systems (Sec. 2.3.12 and 2.3.13) where the state space has a discrete and a continuous component. The discrete component corresponds to the transmutation between particle species, *i.e.* their mode of drifting, whereas the continuous component corresponds to the particle motion. We find that both pro-

cesses, motion and transmutation, contribute to the entropy production rate essentially independently since any term that combines both processes is a higher-order term contribution in τ, and therefore vanishes in the limit $\tau \to 0$.

This work has applications to the field of active particle systems, where particles are subject to local non-thermal forces. In fact, the systems studied in sections 2.3.2 and 2.3.8 – 2.3.13 are prominent examples of active systems. We have shown that their entropy production crucially relies on the microscopic dynamics of the system, which are captured by the Fokker-Planck equation (or the master equation for discrete systems) and its solution. However, in interacting many-particle systems, such a description is not available in general. Instead, we may choose to use the Doi-Peliti formalism [43, 123, 161, 153, 17, 91, 120, 62] to describe the system, since it provides a systematic approach based on the microscopic dynamics and which retains the particle entity.

Acknowledgement

I would like to thank my collaborators for their permission to present our joint work as a part of my PhD thesis. I have obtained their approval which is shown in Appendix A. The authors would like to thank Letian Chen, Greg Pavliotis and Ziluo Zhang for discussions and kind advice. The authors gratefully acknowledge Kin Tat (Kenneth) Yiu's much earlier, related work [178].

3

Run-and-tumble motion on a linear ratchet: analytic solution, power extraction and first-passage properties

Abstract

In this chapter, I present a near-verbatim copy of the preprint

C. Roberts and Z. Zhen. Run-and-tumble motion in a linear ratchet potential: analytic solution, power extraction and first-passage properties Entropy Production in Exactly Solvable Systems [137].

This chapter is a manuscript [137] I recently completed with C. Roberts, independently from my supervisor. C. Roberts and I contributed equally to this chapter. I mainly contributed to the theoretical analysis and C.R. contributed mainly to numerical studies.

We characterise a system of run-and-tumble (RnT) particles moving on a piecewise linear "ratchet" potential, subject to periodic boundary conditions and non-negligible diffusion, by deriving exact analytical results for its steady-state particle density, current, entropy production rate, power output, and thermodynamic efficiency. In the confining case, where the particles' self-propulsion is suppressed by the force from the ratchet, we find the system's

entropy production rate surprisingly remains finite in the limit of vanishing diffusion. In the final part of this work, we consider RnT motion on a linear ratchet defined over a bounded interval, allowing the derivation of mean first-passage times and splitting probabilities for different boundary and initial conditions. This work falls within the line of research dedicated to exactly solvable models of run-and-tumble motion but is also particularly relevant to the extraction of work from active matter as we provide theoretical insight into the feasibility of active engines. Finally, our results are in full agreement with Monte Carlo simulations.

3.1 Introduction

Active matter systems are composed of self-propelling agents that consume energy from their environment to exert mechanical forces [106]. As these systems operate away from equilibrium, they break detailed balance and are thus impervious to the tools of equilibrium statistical mechanics. As a result, the rich phenomenology exhibited by active matter, even at the single-particle scale, has made active matter models the ideal mathematical playground to explore the broader field of nonequilibrium systems [68].

A paradigmatic active matter model is the run-and-tumble (RnT) particle, suggested to depict the piecewise-ballistic locomotion of *E. coli* [143]. RnT particles, whose dynamics reduce to that of two coupled drift-diffusive particles in 1D, are arguably the simplest of the canonical active particle models. This has led to intensive study of their non-equilibrium steady-state distributions in confining potentials [160, 181, 136, 5, 62, 105, 131, 39, 12, 57, 49, 47], alongside other active particle models such as active Ornstein-Uhlenbeck particles [54, 109, 101], and active Brownian particles [169, 36]. Notably, most results for these models are obtained through simulations or under approximations [101, 49, 47, 54, 109, 56, 51, 107, 82, 108], including recent work studying a mixture of RnT and passive particles subject to a differentiable ratchet potential [38]. Only a handful of exact results are documented in the literature, most of which are attributed to RnT particles in 1D [5, 105, 62, 131, 39, 12, 58, 21].

When immersed in asymmetric environments, active particles display spontaneous unidirectional motion [42, 9, 121, 59, 172, 8, 40, 6, 132, 181]. The emergence of such rectified motion has generated significant interest into the concept of active engines,

whose constituent active agents perform work on an external load to store potential energy [83, 118, 124, 148]. The net current observed in these systems is the hallmark of broken time-reversal symmetry and thus indicates that a system is operating far from equilibrium. Exactly "how far" from equilibrium can be quantified by the system's entropy production rate [54, 62, 30, 109], which was recently calculated for RnT particles confined to an infinite-square well [131], but has yet to be calculated for more general asymmetric potentials such as ratchets.

The nonequilibrium behaviour of active matter results in first-passage properties that are significantly different to equilibrium setups, where the latter depends only on the relative height of a potential barrier [85]. In contrast, the mean first-passage time of active particles can depend on the shape of the potential [109, 175]. Studying the first-passage properties of active matter is particularly relevant to biology, which is often concerned with the time it takes self-motile agents to reach certain locations, such as in chemical reactions, chemotaxis and foraging. For the specific case of RnT particles, first-passage properties have been studied both with [105] and without [7, 93, 4, 5] the presence of additive noise. Even for the more general case of non-negligible noise, it is possible to obtain analytic expressions for the first-passage time density on a semi-infinite line, as well as the splitting probabilities and mean first-passage times on a finite interval [105]. However, the simplifications afforded by the noiseless case allow these results to be extended to partially absorbing boundaries [7, 5], and even encounter-based absorption [22]. Further still, the noiseless case has allowed the derivation of the first-passage properties of RnT particles in symmetric confining potentials [39]. It is of interest to see how asymmetric potentials and the presence of additive noise, both of which are considered here, generalise these known results.

In light of the broad interest and wide applications of RnT particles, in this paper we obtain exact analytical results for RnT particles in the presence of an external piecewise linear "ratchet" potential on a 1D ring. On top of this, we consider the application of an additional external counter force, assuming the role of an external load, to the resulting rectified motion. This allows for the study of work extraction and is therefore of relevance to the design of active engines. This novel model of RnT motion is implemented through the addition of active telegraphic noise to the motion of a Brownian particle in a ratchet. Remarkably, this can describe several physically

equivalent nonequilibrium systems, discussed further in Sec. 3.2.

In what follows, the derivation and discussion of new results begins in Sec. 3.3 with a calculation of the steady-state particle densities, obtained by solving the governing coupled Fokker-Planck equations of the system and verified through Monte Carlo simulations. From these densities, in Sec. 3.4, we go on to obtain the corresponding particle current, and study how it depends on the system's parameters, in particular determining the parameters of the ratchet that optimise the steady-state current. Then, following the formalism outlined in Ref. [144], we derive the steady-state entropy production rate in Sec. 3.5. This paves the way for the study of the power output and thermodynamic efficiency in Sec. 3.6. Finally, in Sec. 3.7, we study the transport properties of this system, namely, the mean first-passage times for the separate cases of absorbing and reflecting boundary conditions and the splitting probabilities for the particle to exit from either end of the ratchet.

Given the large number of observables and quantities of interest, the aim of this work is not to provide a full exploration of the high-dimensional phase space for every observable, but rather to give an overview of the most interesting and relevant features of the system.

3.2 Model

We consider an RnT particle, whose telegraphic motion alternates between self-propulsion speeds $w(t) \in [+v, -v]$ with rate γ, moving at position $x \in [0, \ell)$ on a piecewise-linear ratchet potential of periodicity ℓ. The ratchet has maximum amplitude h at the apex $x = a$. We define the system to have periodic boundary conditions at $x = 0$ and $x = \ell$ so the motion is equivalent to that of an RnT particle moving on a ring of circumference ℓ, see Fig. 3.1, whilst subject to the ratchet potential

$$U(x) = \begin{cases} U^{[1]}(x) \equiv \frac{h}{a}x, & 0 \leq x < a \\ U^{[2]}(x) \equiv \frac{h}{\ell - a}(\ell - x), & a \leq x < \ell \end{cases}. \tag{3.1}$$

Henceforth, any reference to the position $x = 0$ can be assumed to also refer to $x = \ell$, due to the periodicity, and we will thus refer only to the former. Without loss of generality, in Secs. 3.3-3.6, we take $h \geq 0$ since replacing $h \to -h$ simply generates the

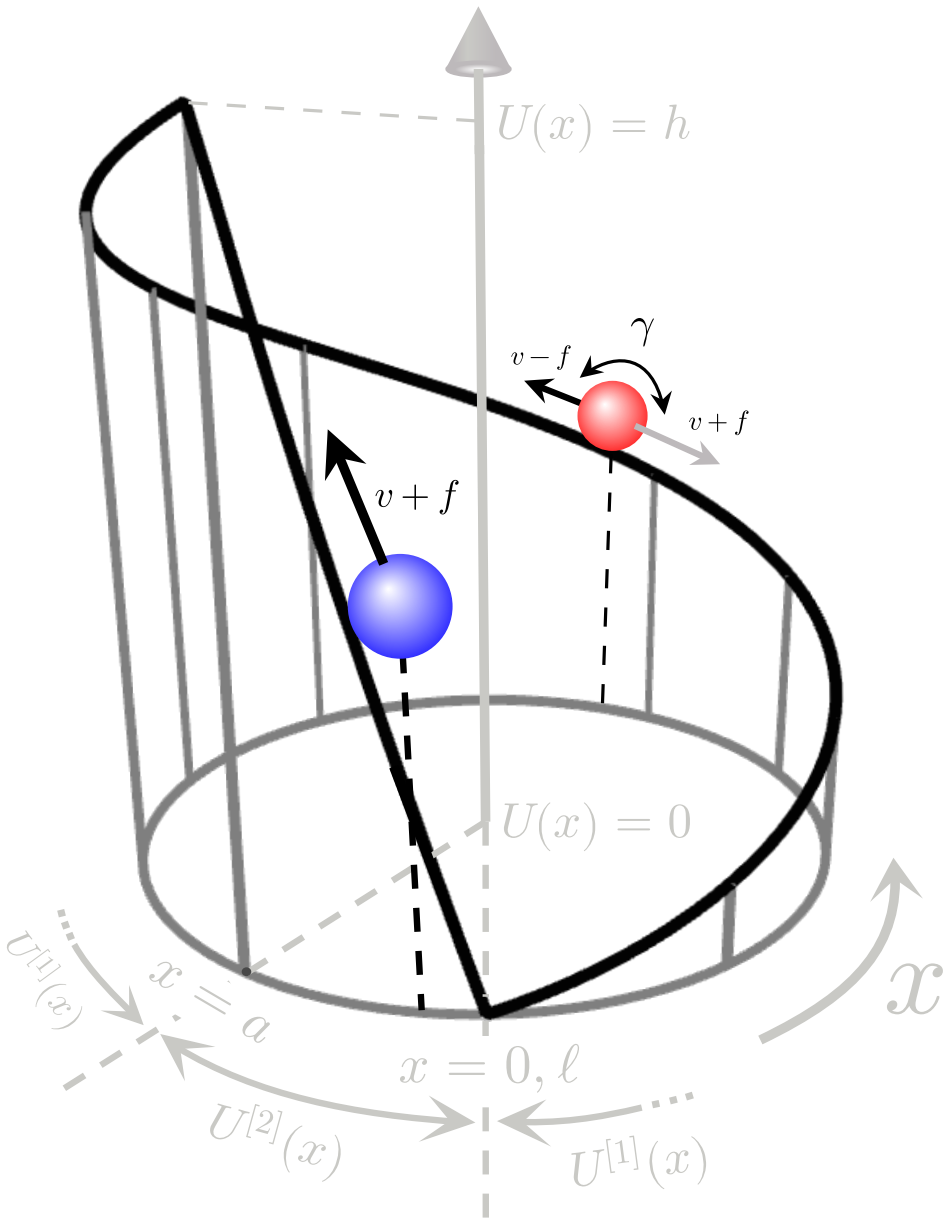


Figure 3.1: Schematic representation of RnT particles moving on a periodic ratchet potential $U(x) = U(x + \ell)$, Eq. (3.1), with maximum amplitude $U(a) = h$. Due to the contribution imparted by the external force $-f$, the overall drift of an RnT particle alternates, with rate γ, between $v - f$, corresponding to the right-moving state $\sigma(t) = +1$ (red sphere), and $-(v + f)$, corresponding to the left-moving state $\sigma(t) = -1$ (blue sphere).

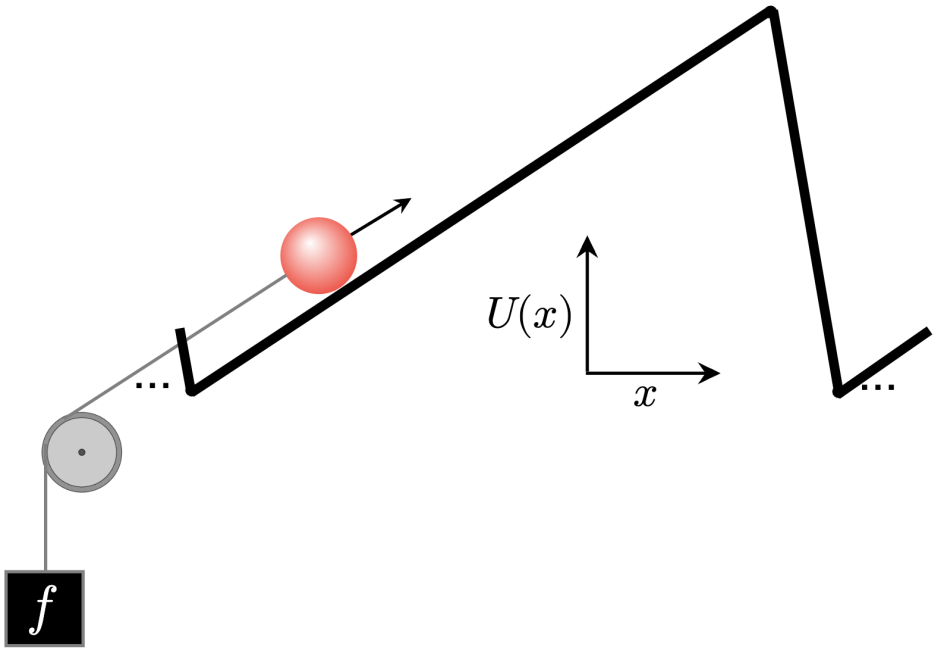


Figure 3.2: By applying an external counterforce $-f$, work W can be extracted from the rectified motion of an RnT particle.

mirror-image of the ratchet, i.e. $a \to \ell - a$, up to an (irrelevant) constant offset $-h$ and after translating space by $x \to x - a$. For $a \neq \ell/2$, the ratchet is asymmetric and can therefore rectify the motion of the RnT particle. The rectified motion results in a current which can be exploited to perform useful work by applying a counter force of magnitude f, such as an external load, see Fig. 3.2. In the following, we take this counterforce to act to the left, i.e. in the $-x$ direction, so that work is done *by* the particle when the current is positive, corresponding to a net drift of particles to the right. We will also work in units where the particle mobility is set to unity. In the overdamped regime, this results in forces, such as from the ratchet $-U'(x)$ and the external load $-f$, having the same dimensions as the particle's self-propulsion velocity $w(t)$. Hence, forces can be interpreted as external drifts in this regime.

The present system has several other physically equivalent interpretations depending primarily on whether the breaking of detailed balance is attributed to external forcing or particle motility. For instance, f has been introduced as a counterforce, but it can also be thought of as an asymmetry parameter of a biased RnT motion with self-propulsion speeds $w(t) \in [v - f, \ -(v + f)]$, Fig. 3.1. Alternatively, f could be

considered a property of the ratchet by defining the potential $V(x) = U(x) + fx$, so that $-f$ becomes the tilt parameter of the tilted ratchet potential $V(x)$ [134, 97]. Similarly, the tumble rate γ could instead be thought of as the switching rate of a time-fluctuating ratchet $V(x,t) \in [U(x) - (v-f)x,\ U(x) + (v+f)x]$ acting on a Brownian particle. The latter is the case for Brownian motors, which work on the principle of rectifying thermal fluctuations through time-fluctuating external forces [104, 9, 118, 102]. Other interpretations of the set-up exist and can also be devised from suitable combinations of the above.

We will occasionally draw on different interpretations when it offers additional insight, but the focus of the present work is on the single perspective of an RnT particle with symmetric self-propulsion $w(t) \in [+v, -v]$ moving on the potential $U(x)$, Eq. (3.1), whilst subject to an additional external counterforce $-f$. Regardless, the results presented in this paper apply to all of the aforementioned interpretations as, in any case, the motion of the particle is governed by the same Langevin equation in the overdamped limit,

$$\dot{x}(t) = -U'(x) + v\sigma(t) - f + \sqrt{2D}\xi(t), \tag{3.2}$$

where t is time, $U'(x)$ is the derivative of $U(x)$ with respect to x, $\sigma(t) \in [+1, -1]$ is telegraphic noise that switches with rate γ, and $\xi(t)$ is delta-correlated Gaussian white noise with associated diffusion constant D. As is the case for thermal fluctuations, the diffusion considered here is translational and therefore superimposed on the self-propelled component of the particle's motion. Henceforth, we will refer to particles as being "right movers" or in the "right-moving state" when $\sigma(t) = +1$ and as "left movers" or in the "left-moving state" when $\sigma(t) = -1$.

The corresponding Fokker-Planck equation to Eq. (3.2) reads

$$\frac{\partial P_R^{[i]}(x,t)}{\partial t} = D\frac{\partial^2 P_R^{[i]}(x,t)}{\partial x^2} - \left(v - f - U'^{[i]}\right)\frac{\partial P_R^{[i]}(x,t)}{\partial x} - \gamma\left(P_R^{[i]}(x,t) - P_L^{[i]}(x,t)\right), \tag{3.3a}$$

$$\frac{\partial P_L^{[i]}(x,t)}{\partial t} = D\frac{\partial^2 P_L^{[i]}(x,t)}{\partial x^2} - \left(-v - f - U'^{[i]}\right)\frac{\partial P_L^{[i]}(x,t)}{\partial x} - \gamma\left(P_L^{[i]}(x,t) - P_R^{[i]}(x,t)\right), \tag{3.3b}$$

where $P_R^{[i]}(x,t)$ and $P_L^{[i]}(x,t)$ are the particle densities at position x and time t of right-moving and left-moving particles respectively. The superscript $[i]$ indicates the section of the ratchet on which the particle densities $P_{R,L}^{[i]}(x,t)$ are valid. For the uphill section (from the perspective of a right mover) $x \in [0,a)$, the densities are given by $P_{R,L}^{[1]}(x,t)$, and for the downhill section $x \in [a,\ell)$, the densities are given by $P_{R,L}^{[2]}(x,t)$. Hence, each $U'^{[i]}$ is in fact constant, specifically $U'^{[1]} = h/a$ and $U'^{[2]} = -h/(\ell - a)$, which has allowed the constants $(\pm v - f - U'^{[i]})$ to be brought in front of the $\partial_x P_{R,L}^{[i]}(x,t)$ in Eq. (3.3). As it is outlined in [63], it is possible for the derivative of the potential to be non-continuous. For there to be free motion across the discontinuity, we need the probability density and the current to be both continuous at the discontinuity.

Unless specified otherwise, the default parameter values used in the figures throughout this paper are $\ell = 1$, $a = 0.9$, $h = 4$, $D = 1$, $v = 1$, $\gamma = 1$ and $f = 0$, which corresponds to weakly persistent particles, characterised by small Péclet number, $\mathrm{Pe} = v^2/(D\gamma)$. Moreover, these parameters also correspond to the case where the particle is confined to the potential minimum $x = 0$ when $D = 0$, since $v - f < h/a$ and $v + f < h/(\ell - a)$ represent the conditions for right-moving and left-moving particles to be confined respectively. In this "confined" case, an overall current can be generated only by diffusive fluctuations that cross the potential barrier. We will focus on this confined case for much of this work because of its richer phase space and greater relevance, such as to the activated escape of particles via noise-induced transitions [175]. Finally, we have opted to keep the discussion of all results in terms of physically meaningful dimensionful parameters, rather than reducing the description of the system to 5 dimensionless parameters whose selection can be ambiguous.

3.3 Particle densities

The particle densities at stationarity $P_{R,L}^{[i]}(x) \equiv \lim_{t\to\infty} P_{R,L}^{[i]}(x,t)$ are derived from solving the coupled Fokker-Planck equations (3.3) with the left-hand sides set to zero, i.e. $\partial_t P_R^{[i]}(x) = \partial_t P_L^{[i]}(x) = 0$. For the specific case of $f = 0$, the steady-state solution to Eq. (3.3) was first derived in the context of Brownian/molecular motors [9], and was used principally to investigate how the steady-state current varies with the switching rate (equivalent to γ here) of the potential. However, this solution has never been

studied in the context of RnT motion and thus has remained relatively unknown to the active matter community. For instance, the current of an RnT particle moving on a piecewise linear potential has been studied for the less general case of $D = 0$ [6]. However, to the best of our knowledge, a detailed study of the more general $D > 0$ solution for RnT particles does not exist in the literature. Furthermore, we believe our subsequent derivations of the entropy production, power output, thermodynamic efficiency and first-passage properties, as well as the generalisation to $f \neq 0$, to all be novel results.

To obtain the steady-state particle density, we make the ansatz $P^{[i]}_{R,L}(x) = \mathcal{Z}^{[i]}_{R,L} \exp\left(\lambda^{[i]} x\right)$ [9]. Substituting this ansatz into Eq. (3.3) for $\partial_t P_{R,L}(x,t) = 0$ results in four linearly independent solutions for each of the particle species, right movers and left movers, in each section of the ratchet, $i = 1$ and $i = 2$, i.e. a total of 16 linearly independent solutions resulting from a quartic characteristic equation from each set of eigenvalues $\lambda^{[i]}$, $i \in \{1, 2\}$. One of the eigenvalues in each set vanishes and so the particle densities have the general solution

$$P^{[i]}_{R,L}(x) = \mathcal{A}^{[i]}_{R,L} e^{\lambda^{[i]}_{\mathcal{A}} x} + \mathcal{B}^{[i]}_{R,L} e^{\lambda^{[i]}_{\mathcal{B}} x} + \mathcal{C}^{[i]}_{R,L} e^{\lambda^{[i]}_{\mathcal{C}} x} + \mathcal{D}^{[i]}_{R,L}, \tag{3.4}$$

with the 16 coefficients $\mathcal{A}^{[1]}_R, \mathcal{A}^{[1]}_L, \mathcal{A}^{[2]}_R, \ldots, \mathcal{D}^{[2]}_L$ to be determined.

These coefficients are fixed by demanding each linearly independent term in Eq. (3.4) individually satisfies Eq. (3.3) in the steady state, i.e. the resulting prefactors after substitution of each $\exp\left(\lambda^{[i]} x\right)$ must be zero [9]. This fixes half of the 16 degrees of freedom in Eq. (3.4). The remaining half are fixed through continuity of the particle densities and currents for each species across $x = 0$ and $x = a$, as well as the normalisation condition $\int_0^\ell \mathrm{d}x\, P(x) = 1$, where $P(x) = P_R(x) + P_L(x)$ is the total particle density. Hence, in principle, the steady-state densities for RnT particles on a piecewise-linear ratchet can be obtained in closed form. However, solving 16 coupled equations unsurprisingly results in unwieldy expressions for the coefficients $\mathcal{A}^{[1]}_R, \mathcal{A}^{[1]}_L, \mathcal{A}^{[2]}_R, \ldots, \mathcal{D}^{[2]}_L$, so the bulk of the calculating was performed using Mathematica. The resulting solutions are too long to conveniently display as equations and so most of our results are displayed as graphs alongside descriptions of their qualitative behaviour in the main text. Nevertheless, we emphasise that all results presented in this paper originate from exact expressions. In fact, any observable that

can be written exclusively in terms of the system parameters and the coefficients $\mathcal{A}_R^{[1]}, \mathcal{A}_L^{[1]}, \mathcal{A}_R^{[2]}, \ldots, \mathcal{D}_L^{[2]}$, such as the steady-state current, Eq. (3.8), and the steady-state entropy production rate, Eq. (3.21), can be written in closed form. The full details of how the analytic expressions for the densities were obtained are left to Appendix 3.A.

The solutions for the steady-state particle densities, Eq. (3.4), are plotted in the top panel of Fig. 3.3. The solutions for the densities were verified by Monte Carlo simulations of the Langevin equation (3.2) by demonstrating the average density of many stochastic realisations converges to the theoretical steady-state density $P(x)$ as $t \to \infty$, Fig. 3.4.

It can be seen from the densities plotted in Fig. 3.3 that, for $h > 0$, particles are mostly aggregated around the minimum of the ratchet as it acts as a confining potential. For $a > \ell/2$, the overall motion of the particles is rectified in the $+x$ direction as right-moving particles penetrate further into the shallower slope of the potential than left-moving particles. Left-moving particles are more likely to be found close to $x = 0$ than right-moving particles as their preferred direction of motion is against the steeper slope of the potential resulting in greater confinement than for the right-moving particles.

The strength of the confinement can be adjusted by varying h. For $h \to 0$, the densities tend to uniform distributions $P_R(x) = P_L(x) = 1/(2\ell)$, since particles are unconfined. Uniform densities are similarly obtained for $v \to \infty$, $f \to \infty$ or $D \to \infty$ as these cases reflect the particle decoupling from the potential $U(x)$, Eq. (3.1). On the other hand, for $h \to \infty$ particles are confined to the point $x = 0$ and so $P_{R,L}(x) \to \delta(x)/2$ as $h \to \infty$. In the equilibrium limits, $f \to 0$ with either $v \to 0$ or $\gamma \to \infty$, the densities tend to Boltzmann distributions $P(x) \propto \exp(-V(x)/D)$. In the limit $\gamma \to 0$, right movers and left movers decouple and the solution reduces to that of two drift-diffusive species with drift speeds $w(t) \in [v - f, -(v + f)]$ on the piecewise linear ratchet potential $U(x)$, Eq. (3.1), i.e. $\lim_{\gamma \to 0} P_{R,L}^{[i]}(x) = A_{R,L}^{[i]} \exp\left(x/l_{R,L}^{[i]}\right) + B_{R,L}^{[i]}$, where $l_R^{[i]} = (v - f - U'^{[i]})/D$ and $l_L^{[i]} = (-v - f - U'^{[i]})/D$, and the (still complicated) expressions for the coefficients $A_R^{[1]}, A_L^{[1]}, \ldots, B_L^{[2]}$ are obtained by applying continuity and normalisation conditions as for the general particle densities, see Appendix 3.A. Finally, taking $D \to 0$ for $f = 0$ recovers the non-trivial case studied in Ref. [6].

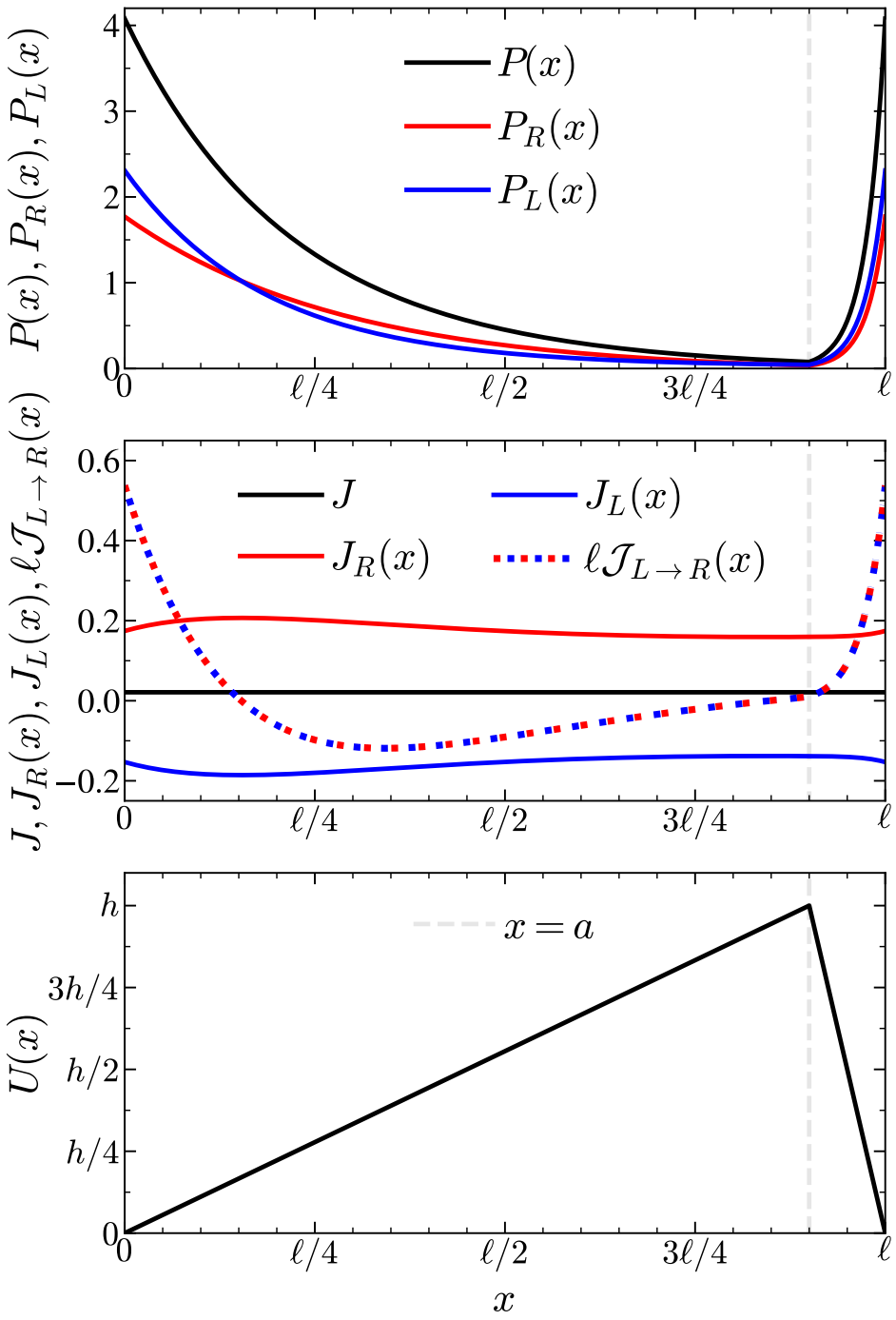


Figure 3.3: Steady-state particle densities $P(x), P_R(x), P_L(x)$, Eq. (3.4) (top), and particle currents $J, J_R(x), J_L(x), \mathcal{J}_{L\to R}(x)$, Eqs. (3.6)-(3.8) (middle), for a particular ratchet potential $U(x)$, Eq. (3.1), shown in the bottom panel. The vertical dashed lines indicate the position of the ratchet apex, x = a.

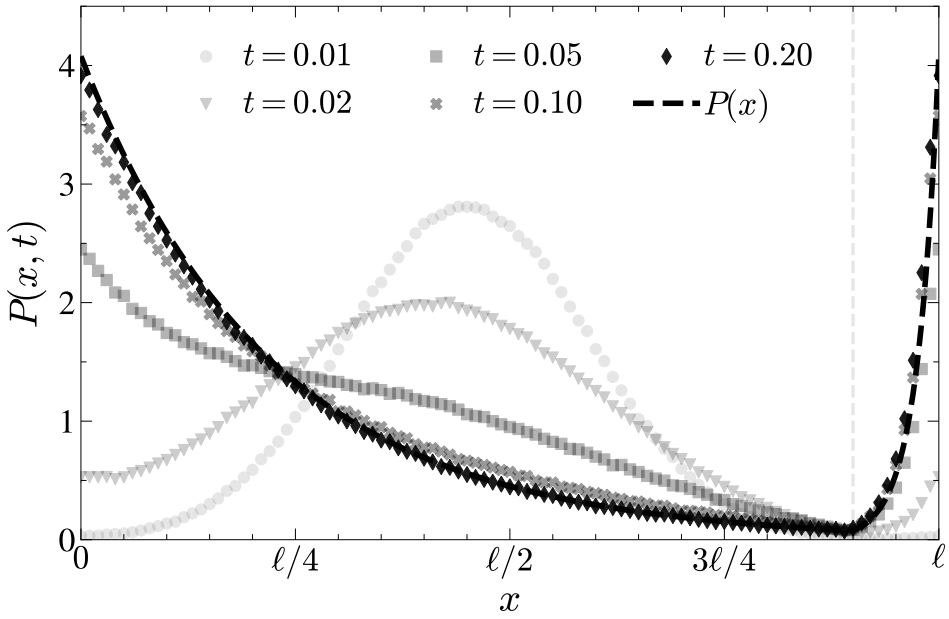


Figure 3.4: Time evolution of the overall particle density $P(x,t) = P_R(x,t) + P_L(x,t)$ obtained from averaging 10^6 stochastic trajectories of an RnT particle on a ratchet. In each realisation, a particle is initialised with equal probability of being a right mover or a left mover at $x = \ell/2$ and $t = 0$, i.e. $P_R(x,0) = P_L(x,0) = \delta(x - \ell/2)/2$, before it is evolved in time by numerically integrating Eq. (3.2) in timesteps of $\mathrm{d}t = 10^{-5}$. At large times $t \to \infty$, the simulated densities converge to the theoretical steady-state density $P(x) = P_R(x) + P_L(x)$, Eq. (3.4). We also numerically integrated Eq. (3.2) in timesteps of $\mathrm{d}t = 10^{-4}$ to check for convergence and obtained the same result.

The particle currents for the right-moving and left-moving particles are, respectively,

$$J_R^{[i]}(x,t) = \left(v - f - U'^{[i]}\right) P_R^{[i]}(x,t) - D\frac{\partial P_R^{[i]}(x,t)}{\partial x}, \tag{3.5a}$$

$$J_L^{[i]}(x,t) = \left(-v - f - U'^{[i]}\right) P_L^{[i]}(x,t) - D\frac{\partial P_L^{[i]}(x,t)}{\partial x}, \tag{3.5b}$$

where, again, the currents are defined separately over the different regions of the ratchet denoted by the superscript $[i]$ and we recall that the $U'^{[i]}$ are constant, see Sec. 3.2. The Fokker-Planck equation (3.3) can be rewritten as a continuity equation in terms of the currents defined in Eq. (3.5),

$$\frac{\partial P_R^{[i]}(x,t)}{\partial t} + \frac{\partial J_R^{[i]}(x,t)}{\partial x} - \mathcal{J}_{L\to R}^{[i]}(x,t) = 0, \tag{3.6a}$$

$$\frac{\partial P_L^{[i]}(x,t)}{\partial t} + \frac{\partial J_L^{[i]}(x,t)}{\partial x} + \mathcal{J}_{L\to R}^{[i]}(x,t) = 0, \tag{3.6b}$$

where we have also defined the flux density of transitions from the left-moving state to the right-moving state as

$$\mathcal{J}_{L\to R}^{[i]}(x,t) \equiv \gamma\left(P_L^{[i]}(x,t) - P_R^{[i]}(x,t)\right) = -\mathcal{J}_{R\to L}^{[i]}(x,t). \tag{3.7}$$

The overall particle current is given by $J(x,t) = J_R(x,t) + J_L(x,t)$. By summing Eqs. (3.6a) and (3.6b), it can be seen that the stationary condition $\partial_t P^{[i]}(x) = 0$ implies the overall current at stationarity is constant across space since $\partial_x J^{[i]} = 0$. Hence, J can be calculated from the particle densities across only a single section $[i]$ of the ratchet since the other section must have the same current. If we choose $i = 1$, corresponding to $x \in [0, a)$, then the resulting expression for $J = J_R^{[1]}(x) + J_L^{[1]}(x)$ can be simplified significantly by setting $x = 0$, yielding a closed expression in terms of the known coefficients $\mathcal{A}_R^{[1]}, \mathcal{A}_L^{[1]}, \mathcal{A}_R^{[2]}, \ldots, \mathcal{D}_L^{[2]}$ from Eq. (3.4),

$$J = \sum_{\mathcal{Z}=\mathcal{A}}^{\mathcal{C}} \left[v\mathcal{Z}_-^{[1]} - \left(f + \frac{h}{a} + D\lambda_{\mathcal{Z}}^{[1]}\right)\mathcal{Z}_+^{[1]}\right] - \left(f + \frac{h}{a}\right)\mathcal{D}^{[i]}, \tag{3.8}$$

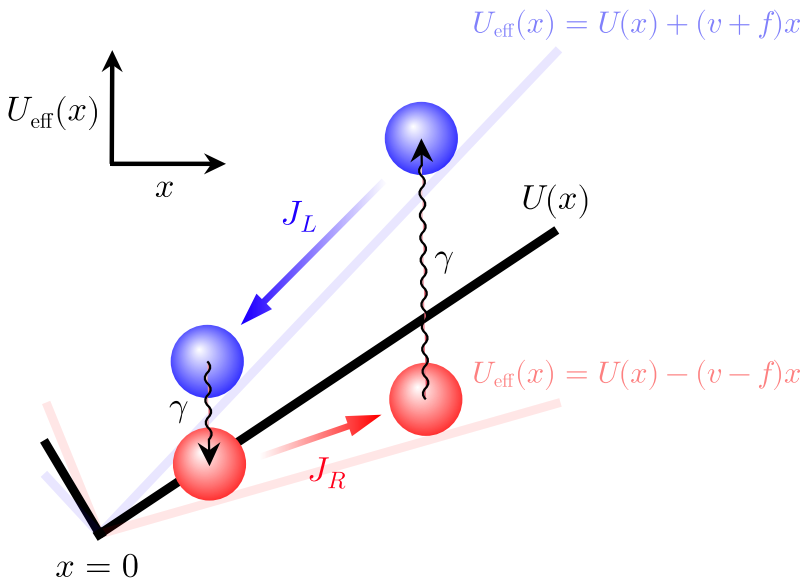


Figure 3.5: Mechanism through which the magnitude of the current of each species, i.e. $|J_R(x)|$ and $|J_L(x)|$, is greater close to the potential minimum $x = 0$ due to a "circulating" current effect from particles that tumble before overcoming the potential barrier. When in the right-moving state (red spheres), the particle experiences a smaller effective potential $U_{\text{eff}}(x) = U(x) - (v - f)x$ than when in the left-moving state (blue spheres) $U_{\text{eff}}(x) = U(x) + (v + f)x$. Even in the case where the self-propulsion v is suppressed by the force $U'(x)$ from the ratchet, i.e. $0 < v - f < U'^{[1]}$, the asymmetry in $U_{\text{eff}}(x)$ between species will result in, on average, a greater number of right movers diffusing up the slope that return back down the slope as left movers.

where we have defined $\mathcal{Z}_\pm \equiv \mathcal{Z}_R \pm \mathcal{Z}_L$ and have used that $\mathcal{D}_R^{[i]} = \mathcal{D}_L^{[i]} \equiv \mathcal{D}^{[i]}$, Appendix 3.A.

The particle currents, Eqs. (3.5) and (3.8), and flux density of transitions, Eq. (3.7), are plotted in Fig. 3.3 alongside the corresponding particle densities, Eq. (3.4). It can be seen that the currents for each species, $J_R(x)$ and $J_L(x)$, are greater in magnitude close to the potential minimum $x = 0$. This results from particles that tumble before crossing the potential barrier and so return to the bottom of the potential before attempting another crossing. Hence, one observes a "circulating" current of right movers moving part way up the slope $0 \leq x < a$ before tumbling and returning down the slope as left movers (and vice versa for particles on the opposite slope $a < x < \ell$). Importantly, this effect is still observed when particles are confined, e.g. a non-zero right-moving current $J_R(x)$ still exists on the uphill slope even in the case where $v - f < U'^{[1]}$. As shown in Fig. 3.5, 'circulating' currents still exist in

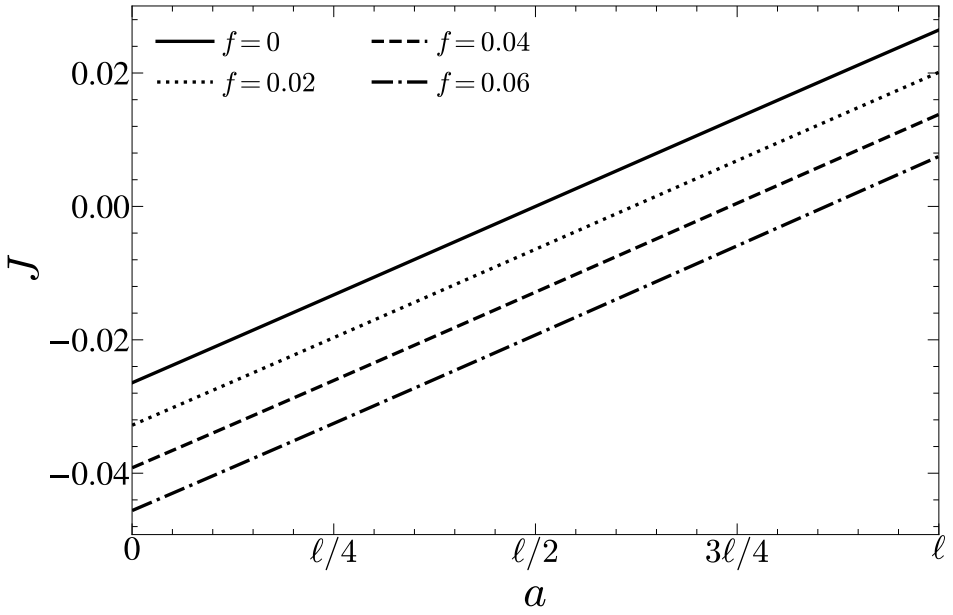


Figure 3.6: Particle current J, Eq. (3.8), as a function of the position of the ratchet apex a for various external forces f.

the confined case as particles can be considered to experience different effective potentials $U_{\text{eff}}(x)$ depending on the particle's internal state, see Sec. 3.2. Specifically, a right-mover can be considered as a Brownian particle moving on an effective potential $U_{\text{eff}}(x) = U(x) - (v - f)x$. Assuming $v - f > 0$, right-moving particles experience a smaller $U'^{[1]}_{\text{eff}}$ than left movers. This asymmetry means, on average, that a greater number of right movers than left movers will diffuse up the potential slope $U'^{[1]}$. When this surplus of right movers tumble, they will return back down the slope as left movers, just as in the unconfined case. As D is decreased, these local circulating currents become more localised and pronounced as the chance of a particle crossing the potential barrier for small D becomes increasingly unlikely [175].

Based on the mechanism described above, we expect each particle to contribute $\sim \gamma$ to the particle currents $J_{R,L}(x)$. As will become apparent for the entropy production in Sec. 3.5, a particularly relevant case is the form of the confined currents as $D \to 0$. In this case, particles follow the Arrhenius law $J \sim \exp(-h/D) \approx 0$, so we can assume they almost never overcome the potential barrier, and so can approximate the barrier height h to be effectively infinite. Then, since the largest contribution to the left-moving current at a position x will come from right-moving particles higher

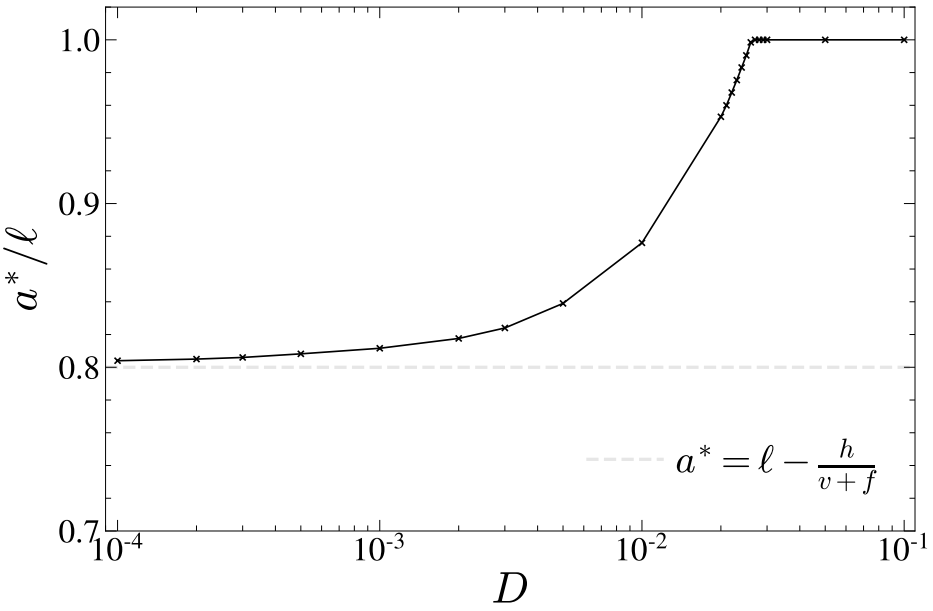


Figure 3.7: Position of the ratchet apex a^* resulting in maximum current J for various diffusion constants D and $h = 0.2$. Maximum current occurs for $a = \ell - h/(v + f)$ as $D \to 0$ and monotonically increases with D to $a \to \ell^-$.

up the slope, we have that $|J_L^{[1]}(x)| \approx \gamma \int_x^\infty \mathrm{d}x' \; P_R^{[1]}(x')$. Since the confined case is effectively equilibrium, then the right-moving particle density follows the Boltzmann distribution $P_R^{[1]}(x) \sim \exp\left(-x/l_D\right)/l_D$, assuming relaxation to the steady state occurs much faster than the transmutation between species, where $l_D = D/(U'^{[1]} - v + f)$ is the characteristic length scale of diffusive spreading on the slope $U'^{[1]}$. Hence, for $0 < v - f < U'^{[1]}$,

$$\lim_{D\to 0} |J_L^{[1]}(x)| \sim \gamma e^{-\frac{x}{l_D}}. \tag{3.9}$$

Since $J \to 0$ for $D \to 0$ in the confined case then $|J_R(x)| = |J_L(x)|$ and one can thus use Eq. (3.9) to also calculate $|J_R^{[1]}(x)|$ for $v - f < U'^{[1]}$. Similar arguments can be used to calculate the contributions $J_{R,L}^{[2]}(x)$ to the circulating currents $J_{R,L}(x)$ on the other slope of the ratchet $a < x < \ell$ for $D \to 0$.

In Fig. 3.6, it can be seen that motion is rectified to the right, $J > 0$, for $a > \ell/2$ when $f = 0$ and is rectified to the left, $J < 0$, for $a < \ell/2$. Contrary to that found for the $D = 0$ case in Ref. [6], where maximum positive current occurs for $a = \ell - h/(v + f)$, we find for the parameters used in Fig. 3.6 that maximum current is achieved for $a \to \ell^-$, i.e. when there is an infinitely steep slope $-U'^{[2]} \to \infty$ oppos-

ing the motion of left-moving particles. While taking $D \to 0$ in our model recovers the result of Ref. [6], we observe in Fig. 3.7 that the position a^* of the ratchet apex resulting in maximum current occurs at some non-trivial $\ell - h/(v+f) < a^* < \ell$ for finite $D > 0$. To see why, consider first a^* for the $D = 0$ case, which arises by choosing the exact a at which right-moving particles remain unconfined, i.e. $v - f > h/a$, while left-moving particles are *only just* confined by the potential, $v + f = h/(\ell - a)$, so as to not increase the distance right movers have to traverse the uphill section of the ratchet. However, when diffusion is switched on, $D > 0$, left-moving particles are once again able to overcome the barrier to the left. Hence, to achieve maximum current J, one must increase a to some $a > \ell - h/(v+f)$ to hinder the left movers' ability to overcome the barrier while also bearing in mind the same compromise that applies to the $D = 0$ case. As D is increased further, the point a^* at which maximum current occurs continues to increase up until the "best" one can do is to set $a \to \ell^-$ to minimise the left-moving current as much as possible.

The expression for the $D = 0$ current j cannot be obtained by simply setting $D = 0$ in our expression for the current J above, which is valid for $D > 0$. Hence, for completeness, we provide a detailed derivation of the $D = 0$ current j in Appendix 3.B, resulting in a closed-form expression that is simple enough to be written down. This derivation generalises the results of Ref. [6] to include an additional external force $f \neq 0$ or, equivalently, to allow for asymmetric self-propulsion speeds between right movers and left movers.

The effect of varying the ratchet height h on the current is plotted in Fig. 3.8. For vanishing height $h = 0$, equivalent to the absence of a potential $U(x)$, Eq. (3.1), the current is given by $J = -f/\ell$. As $h \to \infty$, the current vanishes as the particle is confined by an infinitely steep potential at both sides of $x = 0$. In between these extremes, J peaks at a finite value of h. This reflects that the potential $U(x)$ that optimises the current must be suitably strong to rectify the symmetric motion of the RnT particles but simultaneously must not confine them too strongly.

A similar nonmonotonic dependence was observed for varying the other parameters of the system, such as v, for which J peaks at some finite value for similar reasoning. For $v \to 0$, J tends to the current for a drift-diffusive particle with drift speed $-f$ on the ratchet potential $U(x)$, Eq. (3.1), which is generally $|J| < |-f/\ell|$, and as $v \to \infty$ the particle decouples from the potential such that $J \to -f/\ell$. The particle simi-

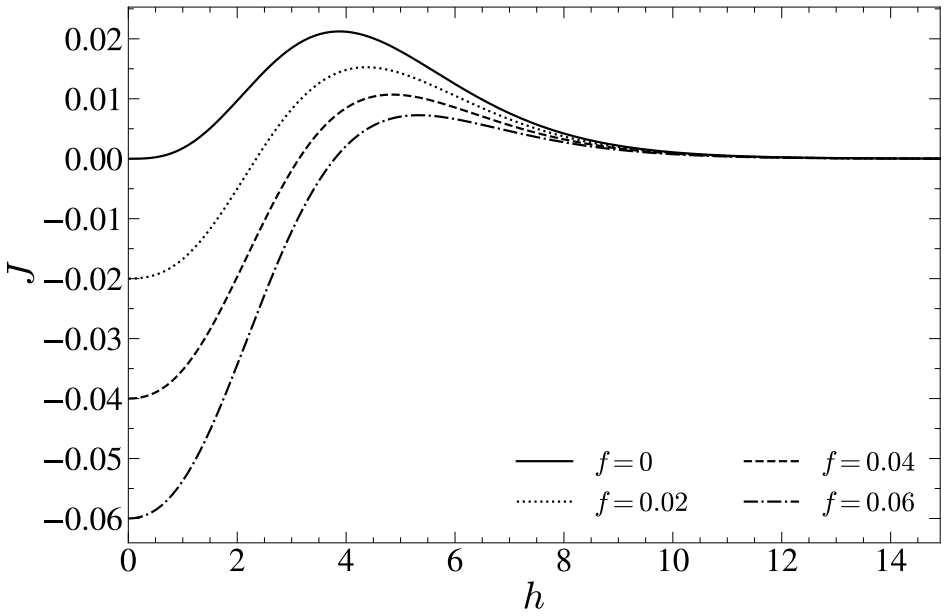


Figure 3.8: Particle current J, Eq. (3.8), as a function of the ratchet height h for various external forces f. For $h = 0$, the current is given by $J = -f/\ell$. The current vanishes for all f as $h \to \infty$, due to the confinement at $x = 0$ being infinitely strong. The peak in the current around $h \approx 4$ reflects a compromise between the degree to which particles are rectified while not being confined too strongly.

larly decouples from the potential for $D \to \infty$ and thus asymptotically approaches $J \to -f/\ell$. The behaviour of J for $D \to 0$ depends on whether or not the particle is confined, i.e. whether or not $v - f < U'^{[1]}$ and $v + f < U'^{[2]}$, see Sec. 3.2. If the particle's self-propulsive force is not large enough to penetrate the potential barrier, $v - f < U'^{[1]}$ and $v + f < U'^{[2]}$, then the particle is confined to the potential well at $x = 0$ and thus $J = 0$, Fig. 3.9. If the particle is unconfined $v - f > U'^{[1]}$ *or* $v + f > U'^{[2]}$ then there is a non-zero current as $D \to 0$. As for h and v, the current J has nonmonotonic dependence on D, Fig. 3.9.

As demonstrated in Ref. [9] for $f = 0$, J monotonically decreases with the tumble rate γ of particles with symmetric self propulsion. For $\gamma = 0$, the overall current $J = J_R(x) + J_L(x)$ is the sum of two maximally unidirectional currents for the two uncoupled drift-diffusive particles with opposing drift speeds. As $\gamma \to \infty$, the particle's self propulsion becomes effectively diffusive leaving only a drift contribution from the external force f. Hence, the current J tends to that of a drift-diffusive particle on a ratchet potential $U(x)$, Eq. (3.1) with drift speed $-f$ as $\gamma \to \infty$.

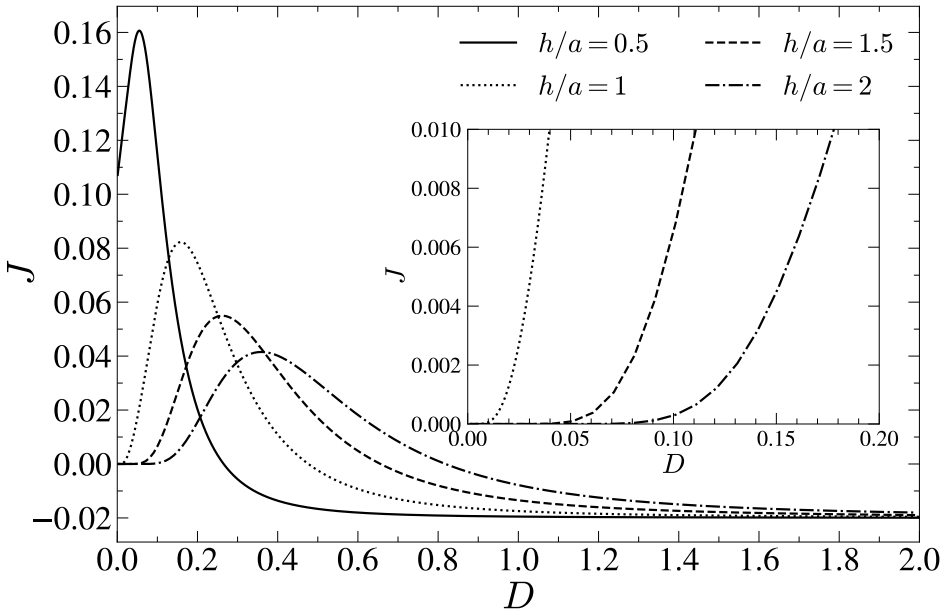


Figure 3.9: Particle current J, Eq. (3.8), as a function of diffusion D for various magnitudes of the slope $U'^{[1]} = h/a$ and for parameter values $a = 0.9$, $v = 1$ and $f = 0.02$. For $D \to \infty$, the current asymptotically approaches $J = -f/\ell$. As $D \to 0$, the value of J depends on whether $v - f < h/a$ and $v + f < h/(\ell - a)$, which are sufficient conditions for vanishing current since the resulting confining force is greater than the combined self-propulsive and external forces. For $v - f > h/a$, it is possible that $J > 0$, even for $D = 0$, as illustrated by the line for $h/a = 0.5$. The inset shows that for $v - f < h/a$, J picks up abruptly in D indicating transport is due to diffusive fluctuations.

Finally, we observe three regions of approximate piecewise linearity in the current's dependence on f. These come from the linear expansion around $f = 0$, i.e. $J \approx J_0 + f\partial_f J$, where J_0 is the current for $f = 0$, as well as the asymptotic behaviour as $|f| \to \infty$, for which the current is dominated by the external force, resulting in $J \approx -f/\ell$.

3.5 Entropy production

The entropy production rate $\dot{S}_{\text{int}}$ quantifies the degree to which time-reversal symmetry is broken and therefore distinguishes between non-equilibrium, $\dot{S}_{\text{int}} > 0$, and equilibrium, $\dot{S}_{\text{int}} = 0$, systems. In the present case, there are several sources of symmetry breaking, such as asymmetric overall drift speeds due to the external force f, and that particles tend to run faster down the sides of the ratchet potential $U(x)$ when the force due to the potential is aligned with the particle's own self-propulsion speed v, similarly to RnT particles in a harmonic potential [62]. Starting from the Gibbs-Shannon entropy [149], we can take a well-established approach to obtain an exact expression for the entropy production rate at stationarity [144, 2, 131].

The Gibbs-Shannon entropy for the present system is defined as

$$S(t) = -\sum_{k=R,L} \int_0^\ell \mathrm{d}x \; P_k(x,t) \log\left(\frac{P_k(x,t)}{\bar{P}}\right), \tag{3.10}$$

where $\bar{P}$, with $\left[\bar{P}\right] = 1/\ell$, is for dimensional consistency in the logarithm but will drop out of the final expression for $\dot{S}_{\text{int}}$. The time derivative of Eq. (3.10) is

$$\dot{S}(t) = -\sum_{k=R,L} \int_0^\ell \mathrm{d}x \; \frac{\partial P_k(x,t)}{\partial t} \left(\log\left(\frac{P_k(x,t)}{\bar{P}}\right) + 1\right). \tag{3.11}$$

After relating $\partial_t P_k(x,t)$ in Eq. (3.11) to the currents J_k and $\mathcal{J}_{L\to R}$ through the continuity equations, Eq. (3.6), integrating by parts, and dropping boundary terms due to

the periodic boundary conditions, we eventually obtain

$$\dot{S}(t) = -\int_0^\ell \mathrm{d}x \Bigg(\sum_{k=R,L} \frac{J_k(x,t)}{P_k(x,t)} \frac{\partial P_k(x,t)}{\partial x} + \mathcal{J}_{L\to R}(x,t) \log\left(\frac{P_R(x,t)}{P_L(x,t)}\right) \Bigg). \tag{3.12}$$

Using the definition of the currents, Eq. (3.5), $\partial_x P_k(x,t)$ in Eq. (3.12) can be rewritten to yield

$$\dot{S}(t) = \int_0^\ell \mathrm{d}x \Bigg[\sum_{k=R,L} \frac{J_k^2(x,t)}{D P_k(x,t)} + \frac{f + U'(x)}{D} J(x,t) - \frac{v}{D}\left(J_R(x,t) - J_L(x,t)\right) + \mathcal{J}_{L\to R}(x,t) \log\left(\frac{P_L(x,t)}{P_R(x,t)}\right) \Bigg], \tag{3.13}$$

where we have used that $J_R(x,t) + J_L(x,t) = J(x,t)$.

At this point, we separate the time derivative of the entropy into the contributions $\dot{S}(t) = \dot{S}_{\mathrm{int}}(t) - \dot{S}_{\mathrm{ext}}(t)$ and identify the positive-definite terms in Eq. (3.13) as those corresponding to the internal entropy production rate of the system $\dot{S}_{\mathrm{int}}(t)$ [30, 2, 131]. We thus have

$$\dot{S}_{\mathrm{int}}(t) = \dot{S}_R(t) + \dot{S}_L(t) + \dot{S}_{R\leftrightarrow L}(t) \tag{3.14}$$

where

$$\dot{S}_{R/L}(t) \equiv \int_0^\ell \mathrm{d}x \; \dot{s}_{R/L}(x,t) \equiv \int_0^\ell \mathrm{d}x \; \frac{J_{R/L}^2(x,t)}{D P_{R/L}(x,t)} \tag{3.15}$$

is the entropy production of right/left-moving particles and $\dot{s}_{R/L}(x,t) \equiv J_{R/L}^2(x,t)/D P_{R/L}(x,t)$ is the local entropy production *density* of right/left-moving particles at position x and time t [131, 62]. Similarly,

$$\begin{aligned} \dot{S}_{R\leftrightarrow L}(t) &\equiv \int_0^\ell \mathrm{d}x \; \dot{s}_{R\leftrightarrow L}(x,t) \\ &\equiv \int_0^\ell \mathrm{d}x \; \mathcal{J}_{L\to R}(x,t) \log\left(\frac{P_L(x,t)}{P_R(x,t)}\right) \end{aligned} \tag{3.16}$$

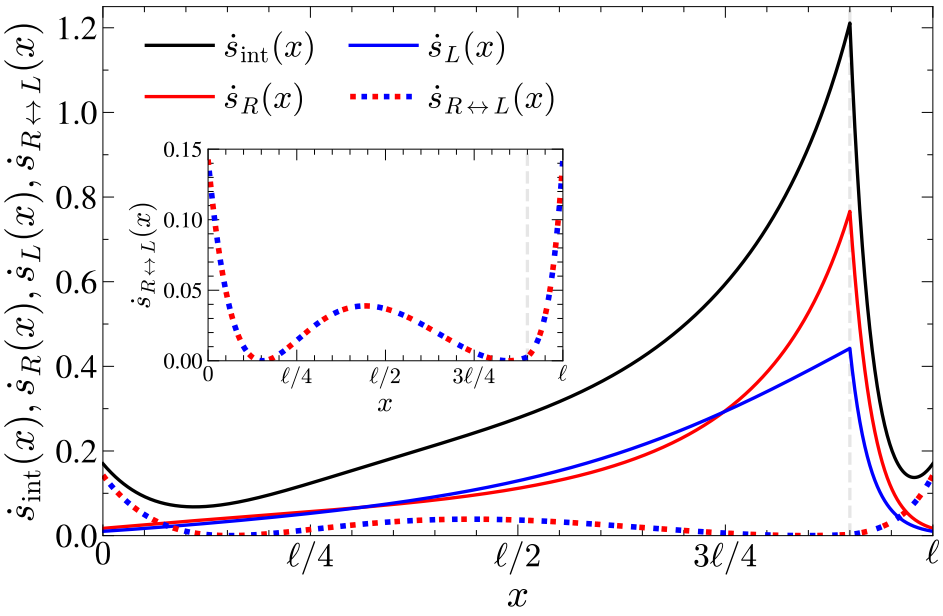


Figure 3.10: Steady-state entropy production density for right movers $\dot{s}_R(x)$, Eq. (3.15), left movers $\dot{s}_L(x)$, tumbling transitions between states $\dot{s}_{R\leftrightarrow L}(x)$, Eq. (3.16) (inset), and their sum $\dot{s}_{\rm int}(x) = \dot{s}_R(x) + \dot{s}_L(x) + \dot{s}_{R\leftrightarrow L}(x)$. The vertical dashed lines indicate the position of the ratchet apex, $x = a$.

is the entropy production due to transitions between right-moving and left-moving particles, with $\dot{s}_{R\leftrightarrow L}(x,t) = \mathcal{J}_{L\to R}(x,t)\log\left(P_L(x,t)/P_R(x,t)\right)$ being its local density.

The steady-state entropy production densities, as defined by $\lim_{t\to\infty} \dot{s}_R(x,t) \equiv \dot{s}_R(x)$ and $\lim_{t\to\infty} \dot{s}_{R\leftrightarrow L}(x,t) \equiv \dot{s}_{R\leftrightarrow L}(x)$ in Eqs. (3.15) and (3.16) respectively, are plotted in Fig. 3.10 for the same parameters as in Fig. 3.3. We find the overall contribution from right movers to the steady-state entropy production $\dot{s}_R(x)$ is larger than that from left movers $\dot{s}_L(x)$ in the case where motion is rectified to the right, i.e. $J > 0$ as a result of $a > \ell/2$. This is expected since left-moving particles are more confined than right-moving particles for $a > \ell/2$. The entropy production densities for both states, $s_R(x)$ and $s_L(x)$, are most concentrated around $x = a$, where the magnitude of the current per particle $J/P(x)$, i.e. the mean local velocity, is greatest. The total entropy production density $\dot{s}_{\rm int}(x)$ has another local maxima at $x = 0$ as a result of the entropy production from transitions between states $\dot{s}_{R\leftrightarrow L}(x)$, Eq. (3.16). The confinement due to the ratchet results in a higher concentration of particles around $x = 0$, Fig. 3.3, and thus a greater number of symmetry-breaking tumble events, which produces a local peak in the entropy production density. The density for tran-

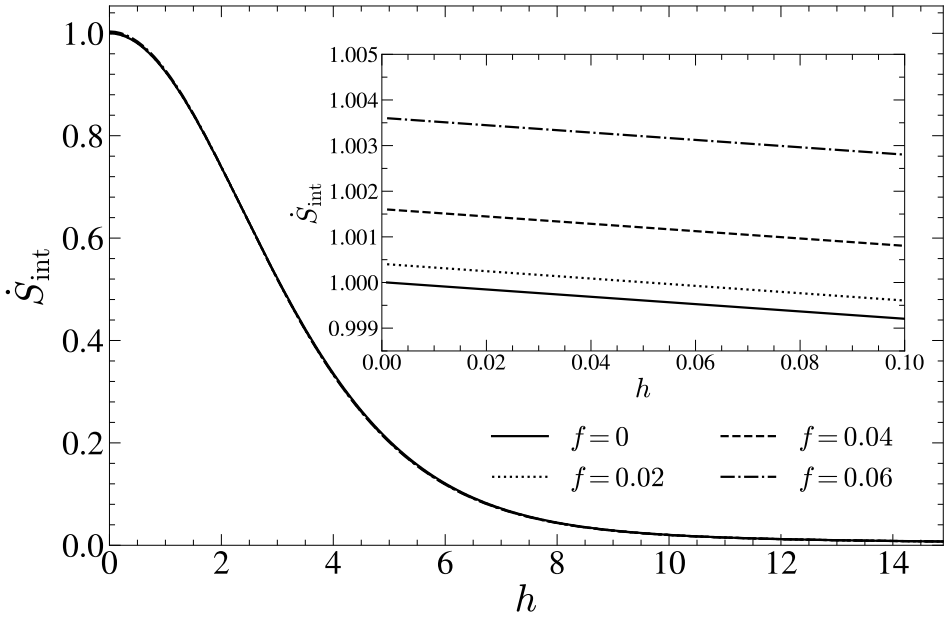


Figure 3.11: Steady-state entropy production rate $\dot{S}_{\rm int}$, Eq. (3.21), as a function of the ratchet height h for various external forces f. In the absence of a ratchet, $h = 0$, the entropy production is given by $\dot{S}_{\rm int} = (v^2 + f^2)/D$ (inset), whilst $\dot{S}_{\rm int} \to 0$ as $h \to \infty$ for all f.

sitions between states $\dot{s}_{R\leftrightarrow L}(x)$, essentially the Kullback-Leibler divergence of $P_R(x)$ and $P_L(x)$, itself has another local maxima in the bulk. In the case of the default parameters used in Fig. 3.10, this local maxima occurs between $x = \ell/4$ and $x = \ell/2$, coinciding with a large local difference in the particle densities, $P_R(x)$ and $P_L(x)$, as seen in Fig. 3.3.

After identifying the terms contributing to the internal entropy production rate $\dot{S}_{\rm int}(t)$, Eq. (3.14), the remaining terms in $\dot{S}(t)$, Eq. (3.13), are identified as the entropy flux lost from the system to the environment, i.e.

$$\dot{S}_{\rm ext}(t) = \frac{1}{D}\int_0^\ell \mathrm{d}x\, \big[v(J_R(x,t) - J_L(x,t)) - (f + U'(x))\, J(x,t)\big]. \tag{3.17}$$

At stationarity, $\dot{S} = 0$ implies $\dot{S}_{\rm int} = \dot{S}_{\rm ext}$, where $\dot{S} \equiv \lim_{t\to\infty} \dot{S}(t)$ etc. Thus, it is convenient to evaluate the steady-state entropy production $\dot{S}_{\rm int}$ through the simpler expres-

sion for the steady-state entropy flux $\dot{S}_{\text{ext}}$, Eq. (3.17), whence we obtain

$$\dot{S}_{\text{int}} = \frac{1}{D}\int_0^\ell \mathrm{d}x\ \left[v\left(J_R(x) - J_L(x)\right) - \left(f + U'(x)\right)J\right]. \tag{3.18}$$

After integrating by parts, and using the periodic boundary conditions $U(0) = U(\ell)$ for the ratchet potential, Eq. (3.1), as well as the flux balance condition $\partial_x J = 0$, the term $\propto U(x)$ vanishes. We can then use that J is constant across space, Eq. (3.8), to obtain

$$\dot{S}_{\text{int}} = \frac{v}{D}\int_0^\ell \mathrm{d}x\ \left(J_R(x) - J_L(x)\right) - \frac{f\ell J}{D}. \tag{3.19}$$

After reinserting the expressions for the individual currents $J_{R,L}(x)$ from Eq. (3.5), and applying the normalisation $\int_0^\ell \mathrm{d}x\ P(x) = 1$ and periodic boundary conditions $P_{R,L}(0) = P_{R,L}(\ell)$, Eq. (3.19) becomes

$$\dot{S}_{\text{int}} = \frac{v^2}{D} - \frac{f\ell J}{D} - \frac{v}{D}\int_0^\ell \mathrm{d}x\ U'(x)\left(P_R(x) - P_L(x)\right), \tag{3.20}$$

which, in the absence of an external counter force $f = 0$ and ratchet potential $U(x) = 0$, recovers the entropy production rate of a free particle v^2/D (in the case where its internal state is known) [30]. Finally, splitting the integral in Eq. (3.20) into separate contributions for each region of the ratchet and inserting the expressions for the particle densities, Eq. (3.4), we obtain an expression in terms of the known coefficients $\mathcal{A}_R^{[1]}, \mathcal{A}_L^{[1]}, \mathcal{A}_R^{[2]}, \ldots, \mathcal{D}_L^{[2]}$,

$$\begin{aligned}\dot{S}_{\text{int}} = \frac{v^2}{D} - \frac{f\ell J}{D} - \frac{v}{D}\sum_{\mathcal{Z}=\mathcal{A}}^{\mathcal{C}}\Bigg(&\frac{h}{a}\mathcal{Z}_-^{[1]}\frac{e^{\lambda_{\mathcal{Z}}^{[1]}a} - 1}{\lambda_{\mathcal{Z}}^{[1]}} \\ &- \frac{h}{\ell - a}\mathcal{Z}_-^{[2]}\frac{e^{\lambda_{\mathcal{Z}}^{[2]}\ell} - e^{\lambda_{\mathcal{Z}}^{[2]}a}}{\lambda_{\mathcal{Z}}^{[2]}}\Bigg),\end{aligned} \tag{3.21}$$

where we have used $\mathcal{D}_R^{[i]} = \mathcal{D}_L^{[i]}$, Appendix 3.A, and have adopted the same shorthand notation, i.e. $\mathcal{Z}_-^{[1]} \equiv \mathcal{Z}_R^{[1]} - \mathcal{Z}_L^{[1]}$, used in Eq. (3.8).

The entropy production $\dot{S}_{\text{int}}$, Eq. (3.21), is plotted in Fig. 3.11 against the height h of the ratchet. For $h = 0$, the entropy production reduces to $\dot{S}_{\text{int}} = (v^2 + f^2)/D$, which is that of a free RnT particle v^2/D plus a positive contribution f^2/D due to the asymmetry in the overall drift speeds breaking time-reversal symmetry. The en-

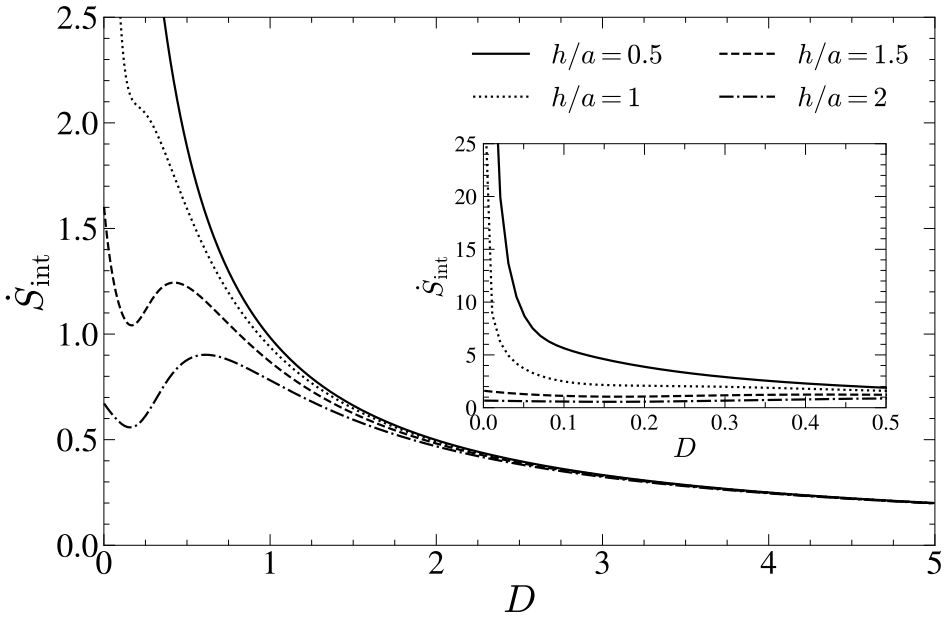


Figure 3.12: Steady-state entropy production rate $\dot{S}_{\rm int}$, Eq. (3.21), as a function of diffusion D for various magnitudes of the slope $U'^{[1]} = h/a$ and for parameter values $a = 0.9$, $v = 1$ and $f = 0$. The entropy production vanishes as $D \to \infty$. For $D \to 0$ (inset), $\dot{S}_{\rm int}$ diverges or remains finite depending on whether the particle is confined, i.e. whether $v - f < h/a$ and $v + f < h/(\ell - a)$.

tropy production monotonically decreases with h such that $\dot{S}_{\rm int} \to 0$ as $h \to \infty$ since the particles are confined to a single point $x = 0$ and therefore the system contains only stationary particles that are trivially at equilibrium.

As is typically the case for RnT particles, the entropy production $\dot{S}_{\rm int}$, Eq. (3.21), for the present system monotonically increases with v and diverges as $v \to \infty$ [131, 62]. For $D \to \infty$, the entropy production $\dot{S}_{\rm int} \to 0$, since any differences between the deterministic components of the forward and time-reversed trajectories of the RnT particle are washed out by diffusive noise. For $v \to 0$, $\dot{S}_{\rm int}$ tends to a positive value due to there still being a current from the remaining drift $-f$. However, the $D \to 0$ limit has surprisingly rich behaviour. Typically, one would expect $\dot{S}_{\rm int} \to \infty$ for $D \to 0$, as is the case for Refs. [131, 62], since the dynamics become more deterministic and it thus becomes easier to distinguish between forward and time-reversed trajectories. However, for certain parameter regimes, $\dot{S}_{\rm int}$ actually remains finite as $D \to 0$, Fig. 3.12. Similarly to the current J, Sec. 3.4, this is due to whether the particle is confined to $x = 0$ in the absence of diffusive fluctuations, i.e. whether $v - f < h/a$ and $v + f < h/(\ell - a)$ for $D = 0$. If these conditions are satisfied, then the confine-

ment imposed by the ratchet prevents $\dot{S}_{\text{int}}$ from diverging as $D \to 0$. That said, it is somewhat remarkable that the confining case results in $\dot{S}_{\text{int}} > 0$ for $D \to 0$, as well as a local minimum $\partial_D \dot{S}_{\text{int}} = 0$, since one may naïvely expect the entropy production to be $\dot{S}_{\text{int}} = 0$ for $D = 0$ if the particle is confined to $x = 0$. However, this result can be explained by the enhanced 'circulating' currents that appear when the particle is confined, Fig. 3.5. As argued in Sec. 3.4, we can expect the magnitude of the circulating currents to scale approximately as $|J^{[1]}_{R,L}(x)| \sim \gamma \exp(-x/l_D)$, Eq. (3.9), for $D \to 0$, where $l_D = D/(U'^{[1]} - v + f)$. Inserting Eq. (3.9) into Eq. (3.19), and using $J \to 0$ as $D \to 0$, we obtain for the entropy production in the confined case $v - f < U'^{[1]}$,

$$\begin{aligned} \lim_{D\to 0} \dot{S}_{\text{int}} &\sim \lim_{D\to 0} \gamma \, \frac{v}{D} \int_0^a \mathrm{d}x \; e^{-\frac{x}{l_D}} + \int_a^\ell \mathrm{d}x \; \dots \\ &\sim \gamma \, \frac{v}{U'^{[1]} - v + f} + \dots \, , \end{aligned} \tag{3.22}$$

where $\dots$ indicates additional non-diverging contributions from circulating currents on the $a < x < \ell$ section of the ratchet. Most importantly, Eq. (3.22) demonstrates there are no diverging terms but only non-vanishing contributions to the entropy production $\dot{S}_{\text{int}}$ as $D \to 0$ in the confined case. Furthermore, the dependence of $\dot{S}_{\text{int}}$ on D in Fig. 3.12 aligns with the dependence of J on D. In Fig. 3.9, it can be seen that $J \approx 0$ for $D \ll h$ in the confined case and picks up abruptly as D is increased. Thus, it is expected $\dot{S}_{\text{int}}$ should initially decrease with D in the confined case, since the dynamics become less deterministic with no significant gain in the overall current until the diffusion-mediated barrier crossings increase in frequency. As D is increased further, the onset of the rapid increase in J results in a similar increase in $\dot{S}_{\text{int}}$, as can be seen by comparing Figs. 3.9 and 3.12 where the onset of the increase in J coincides with the local minimum in $\dot{S}_{\text{int}}$. For $D \gg h$, $\dot{S}_{\text{int}}$ begins to monotonically decrease with D as the particle decouples from the potential and thus the entropy production decays as $\dot{S}_{\text{int}} \sim 1/D$ as for a free particle.

For $a < \ell/2$, $\dot{S}_{\text{int}}$ is a monotonically increasing function of f since the external force enhances the existing bias of the system to rectify motion to the left which, in turn, increases the degree to which time-reversal symmetry is broken. In the confined case, $v - f < U'^{[1]}$ and $v + f < U'^{[2]}$, for $a > \ell/2$, increasing the external force f initially decreases the overall bias $J > 0$ of the system, and so the entropy production $\dot{S}_{\text{int}}$ attains a global minimum at finite f before increasing with f again. As $|f| \to \infty$,

$\dot{S}_{\text{int}} \to f^2/D$ as the external force dominates over the ratchet force $U'(x)$ and the self-propulsion v.

For $\gamma \to 0$, the entropy production $\dot{S}_{\text{int}}$ is the average for that of drift-diffusive particles on a ratchet with drift speeds $w(t) \in [v - f, -v - f]$. The entropy production monotonically increases with γ and asymptotically approaches a value $\dot{S}_{\text{int}} \leq (v^2 + f^2)/D$ as $\gamma \to \infty$.

3.6 Power output and efficiency

By applying an external force $f > 0$, work W can be extracted from an RnT particle so long as $J > 0$. The average rate of work, i.e. power, that can be extracted from the particle in the steady state is

$$\dot{W} = J\ell f, \tag{3.23}$$

where $\dot{W} > 0$ indicates work is being done *by* the particle. The dependence of $\dot{W}$ on the system parameters is thus the same as for that of the current J, Eq. (3.8), for constant f and ℓ. Hence, much of the asymptotic behaviour of the extractable power, Eq. (3.23), can be readily obtained from that of the current J in Sec. 3.4, and we therefore omit this repetitive discussion. The only qualitatively different behaviour for $\dot{W}$ is obtained by varying the external force f, which is plotted in Fig. 3.13 alongside the thermodynamic efficiency $\eta \equiv \dot{W}/P_{\text{in}} = \dot{W}/(\dot{W} + D\dot{S}_{\text{int}})$ [124] for gradients $U'^{[1]} = h/a$ close to that achieving maximum extractable power for the default parameters defined in Sec. 3.2. For these particular parameters, the current $J \approx J_0(1 - f/f_{\text{stall}})$ for $f \neq 0$ and $J_0 \neq 0$, where f_{stall} is the stall force f at which the current $J = 0$, i.e. the point at which the force from the external load exactly cancels the current generated by the rectified motion. Hence, for these parameters where $J \approx J_0(1 - f/f_{\text{stall}})$ holds, the maximum extractable power $\dot{W}$, Eq. (3.23), and in turn the maximum efficiency η, occur for $f \approx f_{\text{stall}}/2$, as can be seen in Fig. 3.13. In the absence of an external force $f = 0$, no work W is produced and the efficiency of the power extraction is thus also $\eta = 0$. For $f < 0$, work is done *on* the particle and thus $\dot{W} < 0$ and $\eta < 0$. For $f = f_{\text{stall}}$, we have $\dot{W} = 0$ and $\eta = 0$ because of the absence of a current $J = 0$, and for forces greater than the stall force $f > f_{\text{stall}}$, work is done *on* the particle because the current generated by the force f outweighs that generated

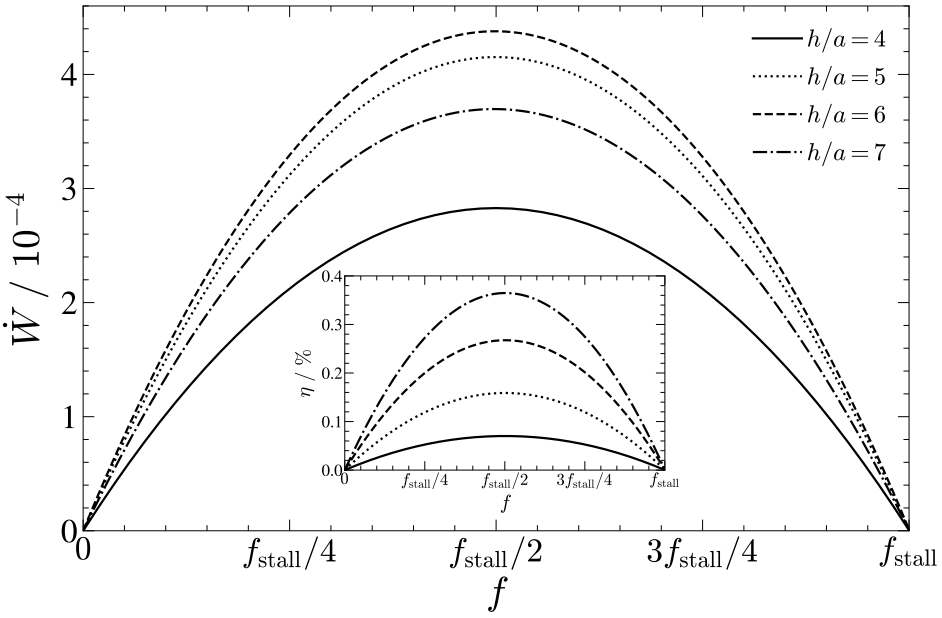


Figure 3.13: Steady-state power output $\dot{W}$, Eq. (3.23), as a function of the external force f for various magnitudes of the slope $U'^{[1]} = h/a$. Maximum power output is observed to occur for a slope around $U'^{[1]} \approx 6$ for the default parameters defined in Sec. 3.2. The power output $\dot{W}$ and thermodynamic efficiency η (inset) are non-zero for external forces $0 < f < f_{\mathrm{stall}}$. The stall forces in this case are $f_{\mathrm{stall}} \approx 0.054, 0.083, 0.112, 0.138$ for each $U'^{[1]} = 4, 5, 6, 7$ respectively.

by the rectification, causing the particle to be "dragged backwards". As $|f| \to \infty$, the power $\dot{W} \to -f^2$ and thus the efficiency $\eta \to -\infty$ since $D\dot{S}_{\mathrm{int}} \to f^2$, see Sec. 3.5.

As expected, the efficiency is small $\eta < 1\%$ for the default parameter values defined in Sec. 3.2 since an overall current J can be generated only by diffusive fluctuations that allow the particle to escape the confining potential well in the case $v - f < U'^{[1]}$ and $v + f < U'^{[2]}$. However, the efficiency η is vastly improved in the case where the particle is not confined by the potential for small diffusion D. This is illustrated in Fig. 3.14 for particle parameters $v = 10$, $\gamma = 1$, $D = 0.1$, corresponding to a Péclet number $\mathrm{Pe} = v^2/(D\gamma) = 1000$ comparable to that of an E. coli bacterium *. These parameters are seen to result in a much higher maximum efficiency of $\eta \approx 35\%$ for $h = 3$ and $f \approx 5$. However, these parameters are still by no means those that result

*The typical run speed and tumble rate of an *E. coli* are $v \approx 15\ \mu\mathrm{m\ s}^{-1}$ and $\gamma \approx 1\ \mathrm{s}^{-1}$ respectively [45, 111]. Meanwhile, the *thermal* diffusion constant D of an *E. coli* can be calculated from the Stokes-Einstein equation $D = k_B T/(6\pi\eta_{\mathrm{vis}} r)$. By approximating an *E. coli* as a sphere of radius $r = 1\ \mu$m immersed in water (of dynamic viscosity $\eta_{\mathrm{vis}} \approx 10^{-3}$ Pa s) this gives $D \approx 0.2\ \mu\mathrm{m}^2\ \mathrm{s}^{-1}$ at room temperature $T = 300$ K. Thus, the Péclet number of an *E. coli* is on the order of $\mathrm{Pe} \approx 1100$

in the maximum possible efficiency for this system, the finding of which would require a full exploration of the high-dimensional phase space. In the same figure, for $h = 4$, we observe a stretch of external forces f for which the efficiency is $\eta \approx 0$. This is due to forces $f_{\text{stall}} < f < h/(\ell - a) - v$ being larger than the mean velocity $J\ell$ induced by the ratchet in the absence of an external force but for which the combined external force f and self propulsion v is not large enough to overcome the potential barrier to the left. However, in this case of small but non-vanishing diffusion D, there is still an appreciable chance of the particle overcoming the barrier as a result of diffusive fluctuations and so the stretch of forces f for which $\eta \approx 0$ does not extend the *entire* way to $f = h/(\ell - a) - v$. As for the maximum power output $\dot{W}$, Eq. (3.23), that can be obtained from this system, it is known that in the case of $D = 0$ that maximum current j, and hence maximum power $\dot{W}$, is achieved by taking $h \to 0$ and $\ell \to 0$ for fixed $a = \ell - h/(v + f) > \ell/2$ [6], corresponding to an optimal ratchet on a ring of vanishing circumference that a particle circumnavigates an infinite number of times each second. However, this diverging $D = 0$ current j fails to take into account the finite size of the particles which would restrict the ratchet height h and length ℓ from becoming too small.

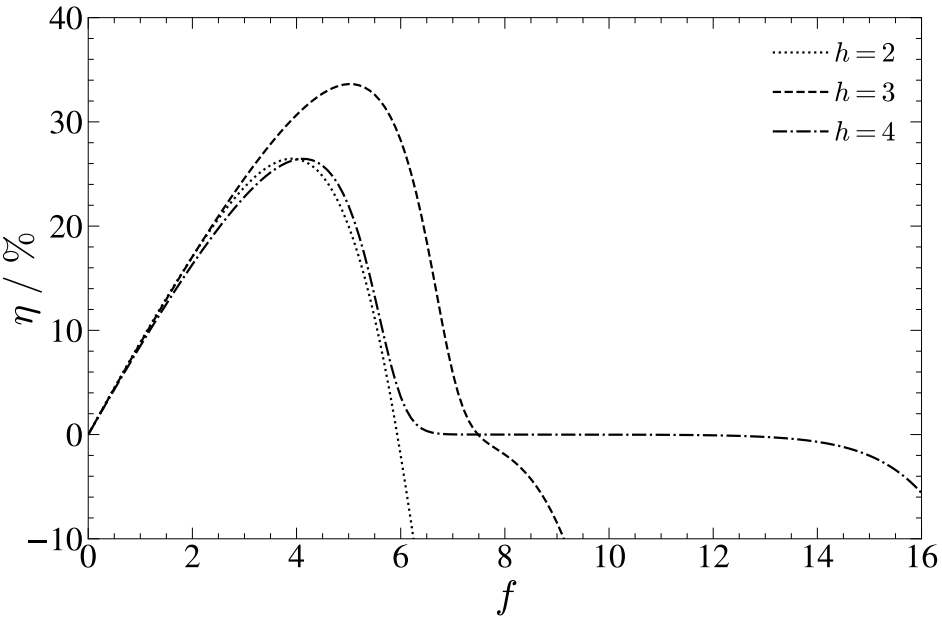


Figure 3.14: Steady-state efficiency η as a function of the external force f for various heights h of the ratchet.

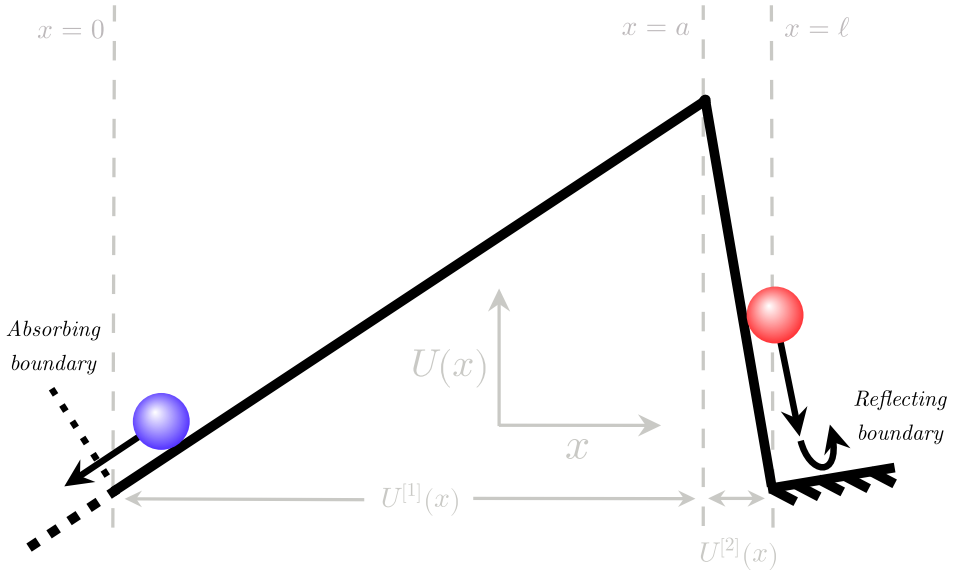


Figure 3.15: Schematic representation of configuration (ii) in Sec. 3.7, used to study the mean first-passage time of RnT particles on a ratchet with a reflecting boundary at $x = \ell$ and an absorbing boundary at $x = 0$. Configuration (i) is the same as configuration (ii) but with the reflecting boundary at $x = \ell$ replaced by an absorbing boundary.

3.7 First-passage properties

In this section we calculate the mean first-passage times $\tau_{R,L}(x)$ and splitting probabilities $\Pi_{R,L}(x)$ for an RnT particle in a ratchet potential $U(x)$, Eq. (3.1). Firstly, the mean first-passage times can be calculated for the cases of (i) two absorbing boundary conditions at $x = 0$ and $x = \ell$, and (ii) a single reflecting boundary at $x = \ell$ and an absorbing boundary at $x = 0$, Fig. 3.15. We define the mean first-passage time $\tau_{R/L}(x)$ as the average time it takes the RnT particle to be absorbed at a boundary, and thus leave the system, given the particle was initialised in the right/left-moving state at position $x \in [0, \ell]$. The mean first-passage times can be shown to satisfy the backward equations [166]

$$-1 = D\frac{\mathrm{d}^2\tau_R^{[i]}(x)}{\mathrm{d}x^2} + \left(v - f - U'^{[i]}\right)\frac{\mathrm{d}\tau_R^{[i]}(x)}{\mathrm{d}x} - \gamma\left(\tau_R^{[i]}(x) - \tau_L^{[i]}(x)\right), \tag{3.24a}$$

$$-1 = D\frac{\mathrm{d}^2\tau_L^{[i]}(x)}{\mathrm{d}x^2} + \left(-v - f - U'^{[i]}\right)\frac{\mathrm{d}\tau_L^{[i]}(x)}{\mathrm{d}x} - \gamma\left(\tau_L^{[i]}(x) - \tau_R^{[i]}(x)\right), \tag{3.24b}$$

with the separate boundary conditions (i) $\tau^{[1]}_{R,L}(0) = \tau^{[2]}_{R,L}(\ell) = 0$, and (ii) $\tau^{[1]}_{R,L}(0) = 0$ and $\partial_x \tau^{[2]}_{R,L}(x)|_{x=\ell} = 0$, for each system configuration. A derivation of Eq. (3.24a) and (3.24b) can be found in [87, ?].

The solutions for the mean first-passage time have the form

$$\tau^{[i]}_{R,L}(x) = \tilde{\mathcal{A}}^{[i]}_{R,L} e^{\tilde{\lambda}^{[i]}_{\mathcal{A}} x} + \tilde{\mathcal{B}}^{[i]}_{R,L} e^{\tilde{\lambda}^{[i]}_{\mathcal{B}} x} + \tilde{\mathcal{C}}^{[i]}_{R,L} e^{\tilde{\lambda}^{[i]}_{\mathcal{C}} x} + \tilde{\mathcal{D}}^{[i]}_{R,L} + \frac{x}{f + U'^{[i]}} \,, \tag{3.25}$$

where, compared to the general solution for the particle densities $P^{[i]}_{R,L}(x)$ in Eq. (3.4), an additional term that is linear in x arises from the particular solution to the non-homogeneous Eq. (3.24), see Appendix 3.C.1. Again, as for the particle densities $P^{[i]}_{R,L}(x)$ in Sec. 3.3, we fix the coefficients $\tilde{\mathcal{A}}^{[1]}_R, \tilde{\mathcal{A}}^{[1]}_L, \tilde{\mathcal{A}}^{[2]}_R, \ldots, \tilde{\mathcal{D}}^{[2]}_L$ by substituting each linearly independent term in Eq. (3.25) into Eq. (3.24), before applying boundary conditions and continuity conditions, see Appendix 3.C.1.

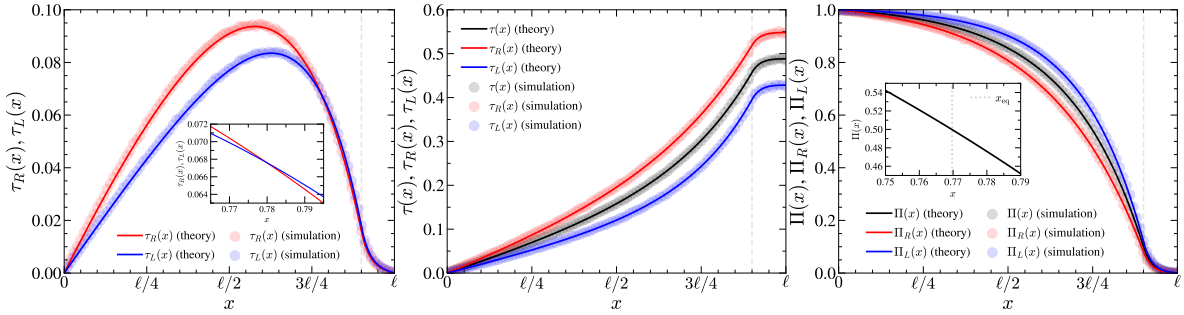
For configuration (i), the presence of two absorbing boundaries allows us to also calculate the splitting probabilities $\Pi_{R,L}(x)$ for the system. The splitting probabilities are the probabilities of a particle being absorbed at the left-hand boundary $x = 0$ (before being absorbed at $x = \ell$) given it was initialised as a right mover $\Pi_R(x)$ or as a left mover $\Pi_L(x)$ at position $x \in [0, \ell]$. The splitting probabilities at the opposite boundary $x = \ell$ are readily obtained from $1 - \Pi_{R,L}(x)$ and their discussion is therefore omitted. Similarly to the mean first-passage times, Eq. (3.24), the splitting probabilities obey the backward equations [166]

$$0 = D \frac{\mathrm{d}^2 \Pi^{[i]}_R(x)}{\mathrm{d}x^2} + \left(v - f - U'^{[i]}\right) \frac{\mathrm{d}\Pi^{[i]}_R(x)}{\mathrm{d}x} - \gamma \left(\Pi^{[i]}_R(x) - \Pi^{[i]}_L(x)\right), \tag{3.26a}$$

$$0 = D \frac{\mathrm{d}^2 \Pi^{[i]}_L(x)}{\mathrm{d}x^2} + \left(-v - f - U'^{[i]}\right) \frac{\mathrm{d}\Pi^{[i]}_L(x)}{\mathrm{d}x} - \gamma \left(\Pi^{[i]}_L(x) - \Pi^{[i]}_R(x)\right), \tag{3.26b}$$

which are homogeneous, meaning the solutions $\Pi^{[i]}_{R,L}(x)$ to Eq. (3.26) can be obtained in a similar manner to that of the homogeneous Eq. (3.3), see Appendix 3.C.2, by applying the boundary conditions $\Pi^{[1]}_{R,L}(0) = 1$ and $\Pi^{[2]}_{R,L}(\ell) = 0$, as well as analogous continuity conditions as for the mean first-passage times $\tau^{[i]}_{R,L}(x)$.

In Fig. 3.16a, we plot the mean first-passage times $\tau_{R,L}(x)$, Eq. (3.25), using our default parameter values, Sec. 3.2, for absorbing boundaries at $x = 0$ and $x = \ell$. Both

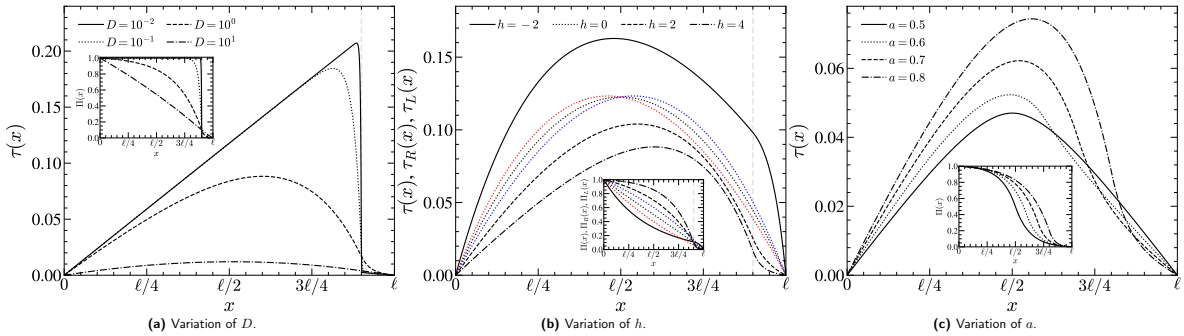


(a) Mean first-passage times $\tau_{R,L}(x)$, Eq. (3.25), for absorbing boundaries at $x = 0$ and $x = \ell$.

(b) Mean first-passage times $\tau_{R,L}(x)$, Eq. (3.25), for an absorbing boundary at $x = 0$ and a reflecting boundary at $x = \ell$.

(c) Splitting probabilities $\Pi_{R,L}(x)$, Eq. (3.26) for absorbing boundaries at $x = 0$ and $x = \ell$.

Figure 3.16: Comparison between simulations and theoretical results for mean first-passage times $\tau_{R/L}(x)$, Eq. (3.25), and splitting probabilities $\Pi_{R/L}(x)$, Eq. (3.26), for initialisation of an RnT particle as a right/left mover. As in Fig. 3.4, simulations were performed by numerically integrating the Langevin equation (3.2) in timesteps of $\mathrm{d}t = 10^{-5}$. The mean first-passage times and splitting probabilities were calculated from the average time it takes the particle to escape the interval, in the case of (a) and (b), and the proportion of times it escapes through $x = 0$, in the case of (c), for 10^5 realisations at each $x = 0, 0.01, \ldots, \ell = 1$. The vertical dashed lines indicate the position of the ratchet apex, $x = a$. The theoretical results are in good agreement with simulations. We also numerically integrated Eq. (3.2) in timesteps of $\mathrm{d}t = 10^{-4}$ to check for convergence and obtained the same result.



(a) Variation of D.

(b) Variation of h.

(c) Variation of a.

Figure 3.17: Mean first-passage times $\tau(x)$, Eq. (3.25), and corresponding splitting probabilities $\Pi(x)$ (insets), Eq. (3.26), for varying different parameters of the system in the case of absorbing boundaries at $x = 0$ and $x = \ell$. In (b), red (respectively, blue) lines indicate initialisation as a right mover (respectively, left mover) for $h = 0$, as studied in Ref. [105]. In (a) and (b), the vertical dashed lines indicate the position of the ratchet apex, $x = a$.

$\tau_R(x)$ and $\tau_L(x)$ are skewed to the right compared to a symmetric distribution (which is the case for a Brownian particle in free space), i.e. the maximum mean first-passage times both occur for $x > \ell/2$, due to the asymmetry $a > \ell/2$ of the system. This asymmetry becomes more exaggerated as the distance $|a - \ell/2|$ from the symmetric potential is increased, Fig. 3.17c. The ratchet breaks the symmetry in the mean first-passage times $\tau_{R,L}(x)$ of an RnT particle in a bounded interval without a potential, which satisfy $\tau_R(x) = \tau_L(\ell - x)$ [105], but is restored upon taking $h \to 0$, Fig. 3.17b. As a result of $a > \ell/2$, a particle initialised on the slope $U'^{[1]}$, i.e. at $x \in [0, a)$, experiences an average force to the left and thus has a higher chance to escape through the left-hand boundary $x = 0$ than for the free case. This is seen in the splitting probabilities $\Pi(x)$ plotted in Fig. 3.16c, where an equal chance of escaping through either boundary, i.e. $\Pi(x) = 0.5$, occurs at $x = x_{\text{eq}} \approx 3\ell/4$. This point x_{eq} also approximately coincides with the point where the mean first-passage times for right movers and left movers are the same, $\tau_R(x_{\text{eq}}) \approx \tau_L(x_{\text{eq}})$, Fig. 3.16a. There is thus a crossover regime where, for $x \lesssim x_{\text{eq}}$, a left-moving particle takes less time on average to exit the interval than a right-moving particle, $\tau_L(x \lesssim x_{\text{eq}}) < \tau_R(x \lesssim x_{\text{eq}})$, since both are more likely to exit at the left-hand boundary $x = 0$, whilst the opposite is true for $x \gtrsim x_{\text{eq}}$. As D is increased, the effect of the ratchet on the mean first-passage time is diminished, resulting in an average time to exit the interval that is symmetric about $x = \ell/2$, Fig. 3.17a. Similarly, the large diffusion limit results in the familiar form $\Pi(x) = 1 - x/\ell$ for the splitting probability, see inset of Fig. 3.17a.

The bounded interval also allows us to explore the first-passage properties for the case $h < 0$, which is no longer degenerate, as in Sec. 3.2, since the boundaries result in broken translational symmetry. The resulting inverted potential for $h < 0$ has the character of a confining potential well, rather than a potential barrier, similarly to the potential $U(x) \sim |x|$ considered in Ref. [39]. However, in the present case, our framework allows us to explore a more general asymmetric variation of the piecewise-linear potential well considered in that work. From Fig. 3.17b, $h < 0$ results in an overall increase in the mean first-passage time $\tau(x)$, as well as concave distributions in the region $a < x \leq \ell$ for both $\tau(x)$ and the splitting probability $\Pi(x)$, compared to the convex curves that occur in this region when $h > 0$ due to the favourable gradient towards the right-hand boundary.

For configuration (ii), where the absorbing boundary at $x = \ell$ is replaced with a re-

flecting boundary, the mean first-passage time of a right mover is trivially greater than that of a left mover for any initial position due to the initial self propulsion of a right mover always being directed away from the only available exit to the interval, Fig. 3.16b. This is also reflected in the splitting probabilities $\Pi_{R,L}(x)$ in Fig. 3.16c, where the probability for the particle to exit at the left-hand boundary at $x = 0$ is always greater for an initial left mover than an initial right mover.

For completeness, in Appendix 3.C.3, we derive the "conditional splitting probabilities" $\pi_{X|Y}(x_0)$ for a particle initialised in state $Y \in [R, L]$ at $x = x_0$ to leave through the left-hand boundary at $x = 0$ in the internal state $X \in [R, L]$, generalising what was first derived in Ref. [31] to incorporate piecewise linear potentials $U(x)$, Eq. (3.1). In the free case [31], conditional splitting probabilities allow for the study of particles that exit an interval via diffusive fluctuations even when the particle's self propulsion favours escape at the opposite boundary, e.g. a right-moving particle exiting through the left-hand boundary at $x = 0$. The derivation of the conditional splitting probabilities in this work allows for the study of the combined role of diffusion and a potential.

3.8 Conclusion

We have studied the motion of an RnT particle in a piecewise linear potential, Eq. (3.1), that is also subject to an external drift which we interpret as a counter force to extract useful work. We obtained the stationary particle densities, Fig. 3.3, for both right-moving and left-moving species and discussed their properties.

We then calculated the current J and analysed how it depends on the system parameters. It turns out for the application of a small force f, the current decreases linearly. When the piecewise potential is skewed to the right with $a > \ell/2$, as we increase the height of the potential h, the current first increases to a maximum and then decays to zero as $h \to \infty$. The current also displayed similar non-monotonic dependencies on the other system parameters.

From the current, we derived the steady-state entropy production $\dot{S}_{\text{int}}$ and the entropy production density $\dot{s}_{\text{int}}(x)$ following the formalism in Ref. [144]. The steady-state entropy production was found to decrease monotonically as the height h of the potential was increased. The most surprising result is there is a finite steady-state en-

tropy production in the limit $D \to 0$ when the particle is confined by the piecewise linear ratchet.

As the set-up can also be interpreted as an autonomous engine extracting work by placing an RnT particle in an external piecewise linear potential, we found an expression for the power extracted $\dot{W}$ and the thermodynamic efficiency η of the engine. The power output is maximised when the external force is approximately half of the stall force $f = f_{\text{stall}}/2$. Finally, we computed the mean first-passage time and splitting probability with different boundary conditions and discussed their implications.

A prevalent theme throughout this paper is that, for many of the derived observables, there is a compromise between choosing a ratchet potential $U(x)$, Eq. (3.1), that rectifies the motion of the RnT particles but without confining them too strongly. This has lead to many, often surprising, nonmonotonic dependencies on the system parameters. Perhaps the most striking of these is the dependence of the entropy production $\dot{S}_{\text{int}}$, Eq. (3.21) on the diffusion constant D which, as it generally would for other RnT systems [131, 62], does not diverge as $D \to 0$ if the particle is confined, i.e. if $v - f < h/a$ and $v + f > h/(\ell - a)$, as illustrated in Fig. 3.12. We would expect to see similar behaviour for the entropy production of RnT particles in confining potentials of the form $U_p(x) \sim |x|^p$, where $p \in \mathbb{R}^+$, considered in Ref. [39] for $D = 0$. Therefore, we believe solving the Fokker-Planck equation for RnT motion in the presence of confining potentials of the form $U_p(x)$ for $D \neq 0$ is an interesting avenue for further research.

Statement of contribution

Connor Roberts and Zigan Zhen contributed equally to this chapter.

Acknowledgement

I would like to thank my collaborators for their permission to present our joint work as a part of my PhD thesis. I have obtained their approval which is shown in Appendix A. We are grateful to Gunnar Pruessner, Thibault Bertrand, Ziluo Zhang, Jacob Knight, Luca Cocconi, Henry Alston, and Sinead O'Brien for useful discussions.

Appendix

3.A Derivation of steady-state particle densities $P_{R,L}^{[i]}(x)$

To solve the coupled Fokker-Planck equations, Eq. (3.3), for the steady-state particle densities $P_{R,L}^{[i]}(x)$, we rewrite Eq. (3.3) as a four-dimensional first-order ODE system for both $i = 1$ and $i = 2$. Introducing $\eta_{R,L}^{[i]}(x) \equiv P_{R,L}^{\prime[i]}(x)$, Eq. (3.3) can be rewritten as

$$\mathbf{y}'(x) = \mathsf{A}\mathbf{y}(x), \tag{3.27}$$

where

$$\mathbf{y}(x) = \begin{pmatrix} P_R^{[i]}(x) \\ \eta_R^{[i]}(x) \\ P_L^{[i]}(x) \\ \eta_L^{[i]}(x) \end{pmatrix} \quad \text{and} \quad \mathsf{A} = \begin{pmatrix} 0 & 1 & 0 & 0 \\ \frac{\gamma}{D} & \frac{v-f-U'^{[i]}}{D} & -\frac{\gamma}{D} & 0 \\ 0 & 0 & 0 & 1 \\ -\frac{\gamma}{D} & 0 & \frac{\gamma}{D} & \frac{-v-f-U'^{[i]}}{D} \end{pmatrix}. \tag{3.28}$$

As Eq. (3.27) is linear and homogeneous for both $i = 1$ and $i = 2$, we make the ansatz $P_{R,L}^{[i]}(x) = \mathcal{Z}_{R,L}^{[i]} \exp\left(\lambda^{[i]}x\right)$, where the $\lambda^{[i]}$ are the eigenvalues of A. After substituting this ansatz into Eq. (3.27), the eigenvalues $\lambda^{[i]}$ are found to satisfy a quartic characteristic equation (arising from two coupled quadratic equations),

$$D^2(\lambda^{[i]})^4+(\lambda^{[i]})^3\left(2Df+2DU'^{[i]}\right)+(\lambda^{[i]})^2\left(-2\gamma D+f^2+2fU'^{[i]}+\left(U'^{[i]}\right)^2-v^2\right)-\lambda^{[i]}\left(2\gamma f+2\gamma U'^{[i]}\right)= \tag{3.29}$$

The solutions $\lambda^{[i]}$ to Eq. (3.29) are too long to display conveniently as equations. However, one of the solutions to Eq. (3.29) is $\lambda^{[i]} = 0$ for both $i \in \{1, 2\}$, and so the general solution to the matrix differential equation (3.27) is

$$P_{R,L}^{[i]}(x) = \mathcal{A}_{R,L}^{[i]} e^{\lambda_{\mathcal{A}}^{[i]}x} + \mathcal{B}_{R,L}^{[i]} e^{\lambda_{\mathcal{B}}^{[i]}x} + \mathcal{C}_{R,L}^{[i]} e^{\lambda_{\mathcal{C}}^{[i]}x} + \mathcal{D}_{R,L}^{[i]}, \tag{3.30}$$

where $\lambda_{\mathcal{A}}^{[i]}, \lambda_{\mathcal{B}}^{[i]}, \lambda_{\mathcal{C}}^{[i]}$ are the other three nonzero solutions (for a given $[i]$) to the quartic equation (3.29).

It remains to calculate the 16 coefficients $\mathcal{A}_R^{[1]}, \mathcal{A}_L^{[1]}, \mathcal{A}_R^{[2]}, \ldots, \mathcal{D}_L^{[2]}$ in Eq. (3.30). First, the ratios of the coefficients $\mathcal{A}_R^{[i]}/\mathcal{A}_L^{[i]}$, representing half of the degrees of freedom, are fixed from substituting Eq. (3.30) into Eq. (3.27) and requiring the resulting prefactor of each linearly independent $\exp\left(\lambda^{[i]}x\right)$ term to vanish. This results in

$$\frac{\mathcal{Z}_R^{[i]}}{\mathcal{Z}_L^{[i]}} = \frac{\gamma}{\gamma + (v - f - U'^{[i]})\,\lambda_{\mathcal{Z}}^{[i]} - D(\lambda_{\mathcal{Z}}^{[i]})^2}, \quad \text{and} \quad \mathcal{D}_R^{[i]} = \mathcal{D}_L^{[i]}, \tag{3.31}$$

where $\mathcal{Z} \in \{\mathcal{A}, \mathcal{B}, \mathcal{C}\}$. The remaining eight degrees of freedom are fixed through normalisation as well as continuity of the particle densities $P_{R,L}^{[i]}(x)$ and currents $J_{R,L}^{[i]}(x)$, Eq. (3.5), for each species across $x = 0$ and $x = a$. Specifically, the continuity conditions require

$$P_{R,L}^{[1]}(0) = P_{R,L}^{[2]}(\ell), \tag{3.32a}$$
$$J_{R,L}^{[1]}(0) = J_{R,L}^{[2]}(\ell), \tag{3.32b}$$
$$P_{R,L}^{[1]}(a) = P_{R,L}^{[2]}(a), \tag{3.32c}$$
$$J_{R,L}^{[1]}(a) = J_{R,L}^{[2]}(a). \tag{3.32d}$$

Finally, we also have the normalisation condition

$$\int_0^a \mathrm{d}x \left(P_R^{[1]}(x) + P_L^{[1]}(x)\right) + \int_a^\ell \mathrm{d}x \left(P_R^{[2]}(x) + P_L^{[2]}(x)\right) = 1. \tag{3.33}$$

Only 15 of the resulting 16 equations from Eqs. (3.31) and (3.32) are linearly independent. After removing any one of these equations, the steady-state densities $P_{R,L}^{[i]}(x)$ for RnT particles on a piecewise-linear ratchet potential $U(x)$, Eq. (3.1), can be obtained in closed form by solving the remaining Eqs. (3.31), (3.32) and (3.33) for the coefficients $\mathcal{A}_R^{[1]}, \mathcal{A}_L^{[1]}, \mathcal{A}_R^{[2]}, \ldots, \mathcal{D}_L^{[2]}$.

3.B Derivation of $D = 0$ steady-state particle densities $p^{[i]}_{R,L}(x)$ and currents $j^{[i]}_{R,L}(x)$

Here, we derive the steady-state particle densities $p^{[i]}_{R,L}(x)$ and currents $j^{[i]}_{R,L}(x)$ for $D = 0$. We set $D = 0$ in Eq. (3.3) so that the coupled Fokker-Planck equations in the case of zero diffusion become

$$\frac{\partial p^{[i]}_R(x,t)}{\partial t} = -\left(v - f - U'^{[i]}\right)\frac{\partial p^{[i]}_R(x,t)}{\partial x} - \gamma\left(p^{[i]}_R(x,t) - p^{[i]}_L(x,t)\right), \tag{3.34a}$$

$$\frac{\partial p^{[i]}_L(x,t)}{\partial t} = -\left(-v - f - U'^{[i]}\right)\frac{\partial p^{[i]}_L(x,t)}{\partial x} - \gamma\left(p^{[i]}_L(x,t) - p^{[i]}_R(x,t)\right). \tag{3.34b}$$

The currents for the right-moving and left-moving particles then become, respectively,

$$j^{[i]}_R(x,t) = \left(v - f - U'^{[i]}\right)p^{[i]}_R(x,t), \tag{3.35a}$$

$$j^{[i]}_L(x,t) = \left(-v - f - U'^{[i]}\right)p^{[i]}_L(x,t). \tag{3.35b}$$

To solve the coupled Fokker-Planck equations (3.34) in the steady state, we again rewrite them in a matrix form as a two-dimensional system of first-order ODEs for both $i = 1$ and $i = 2$, i.e.

$$\hat{\mathbf{y}}'(x) = \hat{\mathsf{A}}\hat{\mathbf{y}}(x), \tag{3.36}$$

where

$$\hat{\mathbf{y}}(x) = \begin{pmatrix} p^{[i]}_R(x) \\ p^{[i]}_L(x) \end{pmatrix} \quad \text{and} \quad \hat{\mathsf{A}} = \begin{pmatrix} -\frac{\gamma}{v-f-U'^{[i]}(x)} & \frac{\gamma}{v-f-U'^{[i]}(x)} \\ \frac{\gamma}{-v-f-U'^{[i]}(x)} & -\frac{\gamma}{-v-f-U'^{[i]}(x)} \end{pmatrix}. \tag{3.37}$$

As Eq. (3.36) is homogenous, we again make the ansatz $p^{[i]}_{R,L}(x) = \hat{\mathcal{Z}}^{[i]}_{R,L}\exp\left(\hat{\lambda}^{[i]}x\right)$, where $\hat{\lambda}^{[i]}$ are the eigenvalues of $\hat{\mathsf{A}}$. The two eigenvalues are found to be

$$\hat{\lambda}^{[i]}_{\mathcal{A}} = \frac{2\gamma\,(f + U'^{[i]})}{(-v + f + U'^{[i]})(v + f + U'^{[i]})} \quad \text{and} \quad \hat{\lambda}^{[i]}_{\mathcal{B}} = 0. \tag{3.38}$$

The general solutions to the matrix ODE (3.36) are then

$$p^{[1]}_{R,L}(x) = \hat{\mathcal{A}}^{[1]}_{R,L} e^{\hat{\lambda}^{[1]}_{\mathcal{A}} x} + \hat{\mathcal{B}}^{[1]}_{R,L} + \hat{\mathcal{C}}_{R,L}\delta(x), \tag{3.39a}$$

$$p^{[2]}_{R,L}(x) = \hat{\mathcal{A}}^{[2]}_{R,L} e^{\hat{\lambda}^{[2]}_{\mathcal{A}} x} + \hat{\mathcal{B}}^{[2]}_{R,L}, \tag{3.39b}$$

where the $\delta(x)$ term is due to the possibility of particles becoming trapped at $x = 0$ in the absence of diffusion. There are 10 coeffiecients $\mathcal{A}^{[1]}_R, \mathcal{A}^{[1]}_L, \mathcal{A}^{[2]}_R, \ldots, \mathcal{B}^{[2]}_L, \mathcal{C}_R, \mathcal{C}_L$ in Eq. (3.39), but only 9 of these need to be fixed at any given time since $\mathcal{C}_R$ and $\mathcal{C}_L$ are both non-zero *only* in the case where the particle is completely confined, i.e. $v - f < U'^{[1]}$ *and* $v + f < |U'^{[2]}|$. In this case the solution is trivially given by $p_{R,L}(x) = \delta(x)/2$. Therefore, to fix the 9 coefficients that are non-zero, we first substitute Eq. (3.39) into the Fokker-Planck equation (3.34), and require the resulting prefactor of each linearly independent $\exp\left(\hat{\lambda}^{[i]} x\right)$ to vanish, resulting in

$$\frac{\hat{\mathcal{A}}^{[i]}_R}{\hat{\mathcal{A}}^{[i]}_L} = \frac{\gamma}{\gamma + (v - f - U'^{[i]}(x))\hat{\lambda}^{[i]}_{\mathcal{A}}} \quad \text{and} \quad \hat{\mathcal{B}}^{[i]}_R = \hat{\mathcal{B}}^{[i]}_L, \tag{3.40}$$

and leaving 5 degrees of freedom to fix.

Continuity in the densities $p^{[i]}_{R,L}(x)$ is no longer a viable condition to fix the degrees of freedom since the absence of diffusion ceases to smooth out the solutions to Eq. (3.36), resulting in the densities becoming discontinuous at $x = 0$ and $x = a$. The form of the solutions depends on the relations between the self-propulsion v and the slopes of the potential, $U'^{[1]} = h/a$ and $U'^{[2]} = -h/(\ell - a)$, in particular whether or not the particle is confined. For instance, the particle could climb over both slopes of the potential, i.e. $v - f > U'^{[1]}$ *and* $v + f > |U'^{[2]}|$, only one slope, $v - f > U'^{[1]}$ *or* $v + f > |U'^{[2]}|$, or be completely confined, $v - f < U'^{[1]}$ *and* $v + f < |U'^{[2]}|$. At $x = 0$, if the particle is confined by the barrier to the left, $v + f < |U'^{[2]}|$, then there is a $\delta(x)$ contribution to the left-moving density $p^{[1]}_L(x)$ with prefactor $\hat{\mathcal{C}}_L$. A tumbling event from a left mover to a right mover thus results in an instantaneous contribution $\gamma\hat{\mathcal{C}}_L$ to the right-moving current $j^{[1]}_R(x)$ at $x = 0$. Similarly, if the particle were instead confined to the right, $v - f < U'^{[1]}$, then there would be a $\delta(x)$ contribution to the right-moving density $p^{[1]}_R(x)$ with prefactor $\hat{\mathcal{C}}_R$, and therefore a contribution $-\gamma\hat{\mathcal{C}}_R$ to the left-moving current $j^{[1]}_L(x)$ at $x = 0$. Hence, in the case where the particle is confined only to the left, $v + f < |U'^{[2]}|$ *and* $v - f > U'^{[1]}$, the continuity conditions are

$$j_R^{[1]}(0) = j_R^{[2]}(\ell) + \gamma\hat{\mathcal{C}}_L, \tag{3.41a}$$
$$j_R^{[1]}(a) = j_R^{[2]}(a), \tag{3.41b}$$
$$p_L^{[1]}(a) = 0, \tag{3.41c}$$
$$p_L^{[2]}(a) = 0, \tag{3.41d}$$

where, since the particle cannot climb over the left barrier, there is no contribution to the left-moving particle density $p_L(x)$ at $x = a$. Similarly, in the case where the particle is instead confined only to the right, $v + f > |U'^{[2]}|$ *and* $v - f < U'^{[1]}$, the continuity conditions are

$$j_L^{[1]}(0) = j_L^{[2]}(\ell) - \gamma\hat{\mathcal{C}}_R, \tag{3.42a}$$
$$j_L^{[1]}(a) = j_L^{[2]}(a), \tag{3.42b}$$
$$p_R^{[1]}(a) = 0, \tag{3.42c}$$
$$p_R^{[2]}(a) = 0. \tag{3.42d}$$

Finally, if the particle can overcome both barriers, $v - f > U'^{[1]}$ *and* $v + f > |U'^{[2]}|$, then the continuity conditions are

$$j_{R,L}^{[1]}(0) = j_{R,L}^{[2]}(\ell), \tag{3.43a}$$
$$j_{R,L}^{[1]}(a) = j_{R,L}^{[2]}(a). \tag{3.43b}$$

The remaining degree of freedom is then fixed through the normalisation condition,

$$\int_0^a \mathrm{d}x \left(p_R^{[1]}(x) + p_L^{[1]}(x)\right) + \int_a^\ell \mathrm{d}x \left(p_R^{[2]}(x) + p_L^{[2]}(x)\right) = 1. \tag{3.44}$$

The overall particle current $j = j_R(x) + j_L(x)$ has a closed-form expression that is simple enough to be written down. In the case where the particle is unconfined and therefore able to climb over both barriers, $v + f > |U'^{[2]}|$ *and* $v - f > U'^{[1]}$, the current

is given by

$$j_{\leftrightarrow} = \frac{2\gamma(af+h)^2(af-f\ell+h)^2\left(e^{\kappa+\delta\ell}-e^{\delta a}\right)}{\theta_+ e^{\delta a}+\theta_- e^{\kappa+\delta\ell}+h^2\ell^2v^2(e^{\kappa}-1)(e^{\delta a}-e^{\delta\ell})}, \tag{3.45}$$

where

$$\delta = \frac{2\gamma(a-\ell)(af-f\ell+h)}{(af-f\ell+h)^2-v^2(a-\ell)^2}, \tag{3.46a}$$

$$\kappa = \frac{2\gamma a^2(af+h)}{(af+h)^2-a^2v^2}, \tag{3.46b}$$

$$\theta_\pm = \pm 2\gamma\ell(af+h)(af-f\ell+h)(a(af+2h)-\ell(af+h)). \tag{3.46c}$$

However, when the particle is confined only to the left, $v+f < |U'^{[2]}|$ *and* $v-f > U'^{[1]}$, the current is given by

$$j_{\not\leftarrow} = \frac{2\gamma(af+h)^2(af-f\ell+h)^2}{\tilde{\theta}_1 e^{-\kappa}+\tilde{\theta}_2 e^{\delta(\ell-a)}+\tilde{\theta}_3+\theta_-} \tag{3.47}$$

where

$$\tilde{\theta}_1 = (af-f\ell+h)^2(a(f+v)+h)^2, \tag{3.48a}$$

$$\tilde{\theta}_2 = -(af+h)^2(h+(a-\ell)(f+v))^2, \tag{3.48b}$$

$$\tilde{\theta}_3 = h\ell^2v^2(2af+h)-2h\ell v(af+h)(af+h-f\ell)-2h\ell av^2(af+h). \tag{3.48c}$$

Finally, the overall current $j_{\not\rightarrow}$ in the case where the particle is confined only to the right, $v+f > |U'^{[2]}|$ *and* $v-f < U'^{[1]}$, can be found by inverting the overall sign in Eq. (3.47) and replacing $a \to \ell - a$ in Eqs. (3.47) and (3.48) above.

Additionally, it is difficult to solve the dynamics Eq. (3.2) directly when the diffusion constant is 0 because of the existence of the RnT motion (the Poissonian noise).

3.C Derivation of first-passage properties

3.C.1 Mean first-passage times $\tau_{R,L}^{[i]}(x)$

As the coupled ODEs for the mean first-passage time $\tau_{R,L}^{[i]}(x)$, Eq. (3.24), are similar to the coupled Fokker-Planck equations (3.3) for the steady-state particle density $P_{R,L}^{[i]}(x)$, the procedure for solving Eq. (3.24) follows similarly as for solving Eq. (3.3) in Appendix 3.A. However, Eq. (3.24) is non-homogeneous and so we must also find a particular solution satisfying the equation. Again, Eq. (3.24) can be rewritten as a four-dimensional system of first-order ODEs for both $i = 1$ and $i = 2$. As before, introducing $\tilde{\eta}_{R,L}^{[i]}(x) = \tau_{R,L}'^{[i]}(x)$ allows Eq. (3.24) to be written as

$$\tilde{\mathbf{y}}'(x) = \tilde{\mathsf{A}}\tilde{\mathbf{y}}(x) + \tilde{\mathbf{b}} \tag{3.49}$$

where

$$\tilde{\mathbf{y}}(x) = \begin{pmatrix} \tau_R^{[i]}(x) \\ \tilde{\eta}_R^{[i]}(x) \\ \tau_L^{[i]}(x) \\ \tilde{\eta}_L^{[i]}(x) \end{pmatrix}, \quad \tilde{\mathsf{A}} = \begin{pmatrix} 0 & 1 & 0 & 0 \\ \frac{\gamma}{D} & \frac{-v+f+U'^{[i]}}{D} & -\frac{\gamma}{D} & 0 \\ 0 & 0 & 0 & 1 \\ -\frac{\gamma}{D} & 0 & \frac{\gamma}{D} & \frac{v+f+U'^{[i]}}{D} \end{pmatrix} \quad \text{and} \quad \tilde{\mathbf{b}} = \begin{pmatrix} -1 \\ 0 \\ -1 \\ 0 \end{pmatrix}. \tag{3.50}$$

First, the solution to the homogeneous equation is found by substituting the ansatz $\tau_{R,L}^{[i]}(x) = \tilde{\mathcal{Z}}_{R,L}^{[i]} \exp\left(\tilde{\lambda}^{[i]}x\right)$ into Eq. (3.49) to obtain a quartic equation for the eigenvalues $\tilde{\lambda}^{[i]}$,

$$\begin{aligned} &D^2(\tilde{\lambda}^{[i]})^4 - (\tilde{\lambda}^{[i]})^3\left(2Df + 2DU'^{[i]}\right) \\ &+(\tilde{\lambda}^{[i]})^2\left(-2\gamma D + f^2 + 2fU'^{[i]} + \left(U'^{[i]}\right)^2 - v^2\right) + \tilde{\lambda}^{[i]}\left(2\gamma f + 2\gamma U'^{[i]}\right) = 0, \end{aligned} \tag{3.51}$$

which differs to Eq. (3.29) only in the sign of the eigenvalues, i.e. $\lambda^{[i]} \to -\tilde{\lambda}^{[i]}$. As in Appendix 3.A, one eigenvalue for each of $i = 1$ and $i = 2$ vanishes and so the solution to the homogeneous part of Eq. (3.49) has the same form as for $P_{R,L}^{[i]}(x)$ in Eq. (3.30), i.e.

$$\tau_{R,L}^{[i]}\Big|_{\mathrm{H}}(x) = \tilde{\mathcal{A}}_{R,L}^{[i]}e^{\tilde{\lambda}_{\mathcal{A}}^{[i]}x} + \tilde{\mathcal{B}}_{R,L}^{[i]}e^{\tilde{\lambda}_{\mathcal{B}}^{[i]}x} + \tilde{\mathcal{C}}_{R,L}^{[i]}e^{\tilde{\lambda}_{\mathcal{C}}^{[i]}x} + \tilde{\mathcal{D}}_{R,L}^{[i]}. \tag{3.52}$$

Next, it is easily verified that the particular solution satisfies

$$\tau_{R,L}^{[i]}\Big|_{\mathrm{P}}(x) = \tilde{\mathcal{E}}_{R,L}^{[i]} x + \tilde{\mathcal{F}}_{R,L}^{[i]}, \tag{3.53}$$

and after substituting Eq. (3.53) into Eq. (3.49), we obtain

$$(v - f - U'^{[i]})\tilde{\mathcal{E}}_R^{[i]} - \gamma(\tilde{\mathcal{E}}_R^{[i]} x + \tilde{\mathcal{F}}_R^{[i]} - \tilde{\mathcal{E}}_L^{[i]} x - \tilde{\mathcal{F}}_L^{[i]}) = 0, \tag{3.54a}$$
$$(-v - f - U'^{[i]})\tilde{\mathcal{E}}_L^{[i]} - \gamma(\mathcal{E}_L^{[i]} x + \tilde{\mathcal{F}}_L^{[i]} - \tilde{\mathcal{E}}_R^{[i]} x - \tilde{\mathcal{F}}_R^{[i]}) = 0. \tag{3.54b}$$

As Eqs. (3.54a) and (3.54b) are true for all x, then we must have that

$$\tilde{\mathcal{E}}_R^{[i]} = \tilde{\mathcal{E}}_L^{[i]} \tag{3.55}$$

and

$$(v - f - U'^{[i]})\tilde{\mathcal{E}}_R^{[i]} - \gamma(\tilde{\mathcal{F}}_R^{[i]} - \tilde{\mathcal{F}}_L^{[i]}) = 0, \tag{3.56a}$$
$$(-v - f - U'^{[i]})\tilde{\mathcal{E}}_L^{[i]} - \gamma(\mathcal{F}_L^{[i]} - \tilde{\mathcal{F}}_R^{[i]}) = 0. \tag{3.56b}$$

Adding Eqs. (3.56a) and (3.56b), then combining with Eq. (3.55), yields

$$\tilde{\mathcal{E}}_R^{[i]} = \tilde{\mathcal{E}}_L^{[i]} = \frac{1}{f + U'^{[i]}}. \tag{3.57}$$

Absorbing the constant $\tilde{\mathcal{F}}_{R,L}^{[i]}$ into $\tilde{\mathcal{D}}_{R,L}^{[i]}$, the full solution to Eq. (3.49) is therefore

$$\tau_{R,L}^{[i]}(x) = \tau_{R,L}^{[i]}\Big|_{\mathrm{H}}(x) + \tau_{R,L}^{[i]}\Big|_{\mathrm{P}}(x) = \tilde{\mathcal{A}}_{R,L}^{[i]} e^{\tilde{\lambda}_{\mathcal{A}}^{[i]} x} + \tilde{\mathcal{B}}_{R,L}^{[i]} e^{\tilde{\lambda}_{\mathcal{B}}^{[i]} x} + \tilde{\mathcal{C}}_{R,L}^{[i]} e^{\tilde{\lambda}_{\mathcal{C}}^{[i]} x} + \tilde{\mathcal{D}}_{R,L}^{[i]} + \frac{x}{f + U'^{[i]}}. \tag{3.58}$$

As for the particle densities $P_{R,L}^{[i]}(x)$ in Appendix 3.A, the ratios $\tilde{\mathcal{Z}}_R^{[i]}/\tilde{\mathcal{Z}}_L^{[i]}$, where $\tilde{\mathcal{Z}} \in [\tilde{\mathcal{A}}, \tilde{\mathcal{B}}, \tilde{\mathcal{C}}, \tilde{\mathcal{D}}]$, are fixed by requiring each linearly independent term in Eq. (3.58) to satisfy Eq. (3.49), resulting in

$$\frac{\tilde{\mathcal{Z}}_R^{[i]}}{\tilde{\mathcal{Z}}_L^{[i]}} = \frac{\gamma}{\gamma - (v - f - U'^{[i]})\,\tilde{\lambda}_{\mathcal{Z}}^{[i]} - D(\tilde{\lambda}_{\mathcal{Z}}^{[i]})^2}, \quad \text{and} \quad \tilde{\mathcal{D}}_R^{[i]} = \tilde{\mathcal{D}}_L^{[i]}. \tag{3.59}$$

The remaining degrees of freedom are then fixed from the boundary conditions and

continuity conditions,

$$\tau^{[1]}_{R,L}(0) = 0, \tag{3.60a}$$

$$\tau^{[1]}_{R,L}(a) = \tau^{[2]}_{R,L}(a), \tag{3.60b}$$

$$\frac{\mathrm{d}\tau^{[1]}_{R,L}(x)}{\mathrm{d}x}\bigg|_{x=a} = \frac{\mathrm{d}\tau^{[2]}_{R,L}(x)}{\mathrm{d}x}\bigg|_{x=a}, \tag{3.60c}$$

and

$$\text{(i)} \quad \tau^{[2]}_{R,L}(\ell) = 0, \quad \text{or} \quad \text{(ii)} \quad \frac{\mathrm{d}\tau^{[2]}_{R,L}(x)}{\mathrm{d}x}\bigg|_{x=\ell} = 0, \tag{3.60d}$$

depending on whether the system has (i) an absorbing boundary or (ii) a reflecting boundary at $x = \ell$ (see, for instance, Ref. [1]).

3.C.2 Splitting probabilities $\Pi^{[i]}_{R,L}(x)$

To derive the splitting probabilities $\Pi^{[i]}_{R,L}(x)$, we define $\check{\eta}^{[i]}_{R,L}(x) = \Pi'^{[i]}_{R,L}(x)$ and $\check{\mathbf{y}}(x) = (\pi^{[i]}_R(x), \check{\eta}^{[i]}_R(x), \pi^{[i]}_L(x), \check{\eta}^{[i]}_L(x))$ such that the governing equations (3.26) for the splitting probabilities $\Pi^{[i]}_{R,L}(x)$ can be written as a four-dimensional system of first-order ODEs, $\check{\mathbf{y}}'(x) = \tilde{\mathsf{A}}\check{\mathbf{y}}(x)$, where $\tilde{\mathsf{A}}$ is the same operator acting on the mean first-passage times $\tau^{[i]}_{R,L}(x)$ above, Eq. (3.50). Thus, the splitting probabilities $\Pi^{[i]}_{R,L}(x)$ obey the same (backward) equations as for that of the mean first-passage times $\tau^{[i]}_{R,L}(x)$, Eqs. (3.49)-(3.50), aside from being homogeneous, i.e. $\tilde{\mathbf{b}} = \mathbf{0}$. Hence, the splitting probabilities have the same form of general solution as for the homogeneous part to the mean first-passage times, Eq. (3.52), but with different coefficients, i.e.

$$\Pi^{[i]}_{R,L}(x) = \check{\mathcal{A}}^{[i]}_{R,L} e^{\tilde{\lambda}^{[i]}_{\mathcal{A}} x} + \check{\mathcal{B}}^{[i]}_{R,L} e^{\tilde{\lambda}^{[i]}_{\mathcal{B}} x} + \check{\mathcal{C}}^{[i]}_{R,L} e^{\tilde{\lambda}^{[i]}_{\mathcal{C}} x} + \check{\mathcal{D}}^{[i]}_{R,L}, \tag{3.61}$$

where the eigenvalues $\tilde{\lambda}^{[i]}$ are the same as those obtained through solving Eq. (3.51) and the ratios $\check{\mathcal{Z}}^{[i]}_R / \check{\mathcal{Z}}^{[i]}_L$, where $\check{\mathcal{Z}} \in [\check{\mathcal{A}}, \check{\mathcal{B}}, \check{\mathcal{C}}, \check{\mathcal{D}}]$, also satisfy the analogous equations as for the mean first-passage times $\tau^{[i]}_{R,L}(x)$, i.e. Eq. (3.59). The remaining degrees of freedom in the general solution for the splitting probabilities $\Pi^{[i]}_{R,L}(x)$, Eq. (3.61), are

fixed from the boundary conditions and continuity conditions,

$$\Pi^{[1]}_{R,L}(0) = 1, \tag{3.62a}$$
$$\Pi^{[2]}_{R,L}(\ell) = 0, \tag{3.62b}$$
$$\Pi^{[1]}_{R,L}(a) = \Pi^{[2]}_{R,L}(a), \tag{3.62c}$$
$$\frac{\mathrm{d}\Pi^{[1]}_{R,L}(x)}{\mathrm{d}x}\Big|_{x=a} = \frac{\mathrm{d}\Pi^{[2]}_{R,L}(x)}{\mathrm{d}x}\Big|_{x=a}, \tag{3.62d}$$

recalling that we define $\Pi_{R/L}(x)$ to be the probabilities for a right/left mover to exit at the *left*-hand boundary of the system at $x = 0$.

3.C.3 Conditional splitting probabilities $\pi^{[i]}_{X|Y}(x)$

The splitting probabilities $\Pi^{[i]}_{R,L}(x)$ defined above can be generalised to be conditioned on the particle's self-propulsion state as it exits the interval. Following the calculation in Ref. [31], we define $\pi_{X|Y}(x_0)$ as the "conditional splitting probability" for a particle initialised in state $Y \in [R, L]$ at $x = x_0$ to leave through the left-hand boundary at $x = 0$ in the internal state $X \in [R, L]$. Hence, there are four conditional splitting probabilities that exist for each boundary, obtained from every possible permutation of $X, Y \in [R, L]$. Introducing $\breve{\eta}^{[i]}_{X|Y}(x) = \pi'^{[i]}_{X|Y}(x)$, the conditional splitting probabilities satisfy $\breve{\mathbf{y}}'_{R,L}(x) = \tilde{\mathsf{A}}\breve{\mathbf{y}}_{R,L}(x)$ where $\tilde{\mathsf{A}}$ is the same operator, defined in Eq. (3.50), acting on the "unconditional" splitting probabilities $\Pi^{[i]}_{R,L}(x)$ and mean first-passage times $\tau^{[i]}_{R,L}(x)$ above, and $\breve{\mathbf{y}}_{R,L}(x) = (\pi^{[i]}_{R,L|R}(x), \breve{\eta}^{[i]}_{R,L|R}(x), \pi^{[i]}_{R,L|L}(x), \breve{\eta}^{[i]}_{R,L|L}(x))$. Hence, the conditional splitting probabilities satisfy two different sets of coupled ODEs, one for each conditional exit state. As these ODEs are the same as for that of the unconditional splitting probabilities, Eq. (3.26), they thus have the same general solution given in Eq. (3.61), i.e.

$$\pi^{[i]}_{X|Y}(x) = \breve{\mathcal{A}}^{[i]}_{X|Y} e^{\tilde{\lambda}^{[i]}_{\mathcal{A}} x} + \breve{\mathcal{B}}^{[i]}_{X|Y} e^{\tilde{\lambda}^{[i]}_{\mathcal{B}} x} + \breve{\mathcal{C}}^{[i]}_{X|Y} e^{\tilde{\lambda}^{[i]}_{\mathcal{C}} x} + \breve{\mathcal{D}}^{[i]}_{X|Y}, \tag{3.63}$$

where $X, Y \in [R, L]$ and the eigenvalues $\tilde{\lambda}^{[i]}$ are found through solving Eq. (3.51). The coefficients $\breve{\mathcal{A}}^{[1]}_{X|Y}, \breve{\mathcal{A}}^{[2]}_{X|Y}, \ldots, \breve{\mathcal{D}}^{[2]}_{X|Y}$ are fixed in the same manner as for the mean first-passage times $\tau^{[i]}_{R,L}(x)$ and splitting probabilities $\Pi^{[i]}_{R,L}(x)$ above, by requiring each linearly independent term to satisfy the ODEs before applying boundary conditions

and continuity conditions. The boundary conditions of the ODEs are

$$\pi^{[1]}_{R|R}(0) = \pi^{[1]}_{L|L}(0) = 1, \tag{3.64a}$$
$$\pi^{[1]}_{R|L}(0) = \pi^{[1]}_{L|R}(0) = 0, \tag{3.64b}$$
$$\pi^{[2]}_{R|R}(\ell) = \pi^{[2]}_{L|L}(\ell) = 0, \tag{3.64c}$$
$$\pi^{[2]}_{R|L}(\ell) = \pi^{[2]}_{L|R}(\ell) = 0, \tag{3.64d}$$

and the continuity conditions are analogous to that of the unconditional splitting probabilities in Eq. (3.62), i.e.

$$\pi^{[1]}_{R,L|R}(a) = \pi^{[2]}_{R,L|R}(a), \tag{3.65a}$$
$$\pi^{[1]}_{R,L|L}(a) = \pi^{[2]}_{R,L|L}(a), \tag{3.65b}$$
$$\frac{\mathrm{d}\pi^{[1]}_{R,L|R}(x)}{\mathrm{d}x}\Big|_{x=a} = \frac{\mathrm{d}\pi^{[2]}_{R,L|R}(x)}{\mathrm{d}x}\Big|_{x=a}, \tag{3.65c}$$
$$\frac{\mathrm{d}\pi^{[1]}_{R,L|L}(x)}{\mathrm{d}x}\Big|_{x=a} = \frac{\mathrm{d}\pi^{[2]}_{R,L|L}(x)}{\mathrm{d}x}\Big|_{x=a}. \tag{3.65d}$$

4

Statistical Field Theories

Abstract

The following derivations and results in this Chapter are heavily based on J. Pausch's PhD thesis [119], G. Pruessner's lecture notes [128] and U. Täuber's book *Critical Dynamics: A Field Theory Approach to Equilibrium and Non-Equilibrium Scaling Behavior* [161].

Doi-Peliti field theory and response field theory are the main methods in Chapter 5 and 6. In this chapter, we first derive Doi-Peliti field theory starting from master equations and use the language of second quantisation to turn it into a path-integral. We then derive the fundamentals of response field theory starting from Langevin dynamics and cast it into a path-integral using the Onsager-Machlup framework and then introduce a response field. Both field theories enable us to calculate observables in non-equilibrium settings.

4.1 Doi-Peliti field theory

Recall that the Master equation Eq. (1.1) has the form

$$\frac{\partial P_n(t)}{\partial t} = \dot{P}_n(t) = \sum_m W(m \to n) P_m(t) - W(n \to m) P_n(t). \tag{4.1}$$

On a lattice, the microstates m, n are instead of the occupation number of each site $\{n\}$, which is a vector of all occupation numbers n_x at position x. The position space is discretised by a constant spacing Δx. In this setup, the master equation becomes

$$\frac{\partial P(\{n\},t)}{\partial t} = \sum_{\{n'\}\neq\{n\}} W(\{n'\}\to\{n\})P(\{n'\},t) - \sum_{\{n'\}\neq\{n\}} W(\{n\}\to\{n'\})P(\{n\},t) \tag{4.2}$$

where $W(\{n\} \to \{n'\})$ is the transition probability from state $\{n\}$ to state $\{n'\}$. Eq. (4.2) has a similar form to the Schrödinger equation that is linear in $P(\{n\}, t)$ and has a first order derivative in $\partial/\partial t$.

4.1.1 Operator and states

To turn Eq. (4.2) into a field theory, we follow a similar procedure in the second quantisation of quantum mechanics. Introducing a pure, normalised state vector $|\{n_x\}\rangle$ which describes a system with configuration $\{n_x\}$. These states satisfy the orthogonality condition

$$\langle\{n_x\}|\{m_x\}\rangle = \prod_x \delta_{n_x,m_x}. \tag{4.3}$$

The vacuum state is where every configuration takes value 0, in other words, $\forall x, n_x = 0$. We denote the left and the right vacuum as $\langle 0|$ and $|0\rangle$ respectively.

We introduce the creation operator $a(x)$ and annihilation operator $a^\dagger(x)$. Below, we use the notation $|n_x\rangle$ to denote that there are n particles at position x throughout. The creation and annihilation operators satisfy the relations

$$a^\dagger(x)\,|n_x\rangle = |n_x + 1\rangle \tag{4.4}$$

$$a(x)\,|n_x\rangle = n_x\,|n_x - 1\rangle\,. \tag{4.5}$$

The particle number operator is given by $a^\dagger(x)a(x)$ as

$$a^\dagger(x)a(x)\,|n_x\rangle = n_x\,|n_x\rangle\,. \tag{4.6}$$

It is important to note that the ladder operators do not commute

$$[a(x), a^\dagger(x)] := a(x)a^\dagger(x) - a^\dagger(x)a(x) = 1. \tag{4.7}$$

We are interested in the mixed state

$$|\Psi(t)\rangle = \sum_{\{n_x\}} P(\{n_x\}, t)\, |\{n_x\}\rangle \tag{4.8}$$

where we sum over the occupation numbers state $\{n_x\}$ weighted by its probability density. The function $\Psi(t)$ will act as a moment-generating function and a probability-generating function. For example, we can find out the probability distribution by taking the inner product

$$\langle\{n_x\}|\Psi(t)\rangle = P(\{n_x\}, t). \tag{4.9}$$

4.1.2 Deriving the field theory

We are now in a position to pivot into field theory. Using an operator $\mathcal{A}$ to describe the time evolution of the mixed state Eq. (4.8)

$$\frac{\mathrm{d}}{\mathrm{d}t}\,|\Psi(t)\rangle = \widehat{\mathcal{A}}\,|\psi(t)\rangle\,. \tag{4.10}$$

where $|\Psi(0)\rangle$ is the initial state. The formal solution to the time-evolution equation Eq. (4.10) is

$$|\Psi(t)\rangle = \exp\left(\widehat{\mathcal{A}}t\right)|\Psi(0)\rangle\,. \tag{4.11}$$

Defining the *abyss*

$$\langle\text{☼}| = \sum_{\{n_x\}} \langle\{n_x\}|\,, \tag{4.12}$$

the expectation of any observable $\widehat{\mathcal{O}}$ can be expressed as the inner product

$$\langle\widehat{\mathcal{O}}\rangle(t) = \langle\text{☼}|\,\widehat{\mathcal{O}}\exp\left(\widehat{\mathcal{A}}t\right)|\Psi(0)\rangle = \langle\text{☼}|\,\widehat{\mathcal{O}}\exp\left(\widehat{\mathcal{A}}t\right)J\,|0\rangle\,, \tag{4.13}$$

where J is an initialisation operator acting on the vacuum state $|0\rangle$ that generates $|\Psi(0)\rangle$. In the following, it is always assumed that the operator $\widehat{\mathcal{A}}$ is normal ordered.

For reaction-diffusion processes, it is always possible to write the operator $\widehat{\mathcal{A}}$

$$\widehat{\mathcal{A}} = \sum_{\gamma,\sigma} h_{\sigma,\gamma} a^{\dagger\gamma} a^{\sigma} \tag{4.14}$$

where $h_{\sigma,\gamma} \in \mathbb{R}$ and $\sigma, \gamma \in \mathbb{N}$.

In order to turn it into a field theory, we consider the coherent states which are the right and left eigenvectors of the operators $a^\dagger$ and a respectively,

$$|\phi\rangle := e^{\phi a^\dagger} |0\rangle \quad \left\langle \phi^\dagger \right| := \langle 0| e^{\phi^\dagger a} \tag{4.15}$$

such that

$$a |\phi\rangle = \phi |\phi\rangle \quad \left\langle \phi^\dagger \right| a^\dagger = \left\langle \phi^\dagger \right| \phi^\dagger \tag{4.16}$$

with eigenvalues $\phi, \phi^\dagger \in \mathbb{C}$.

The identity operator $\mathbb{I}$ can be rewritten using coherent states

$$\mathbb{I} = \int \frac{\mathrm{dRe}\phi \mathrm{dIm}\phi}{\pi} e^{-\phi^\dagger \phi} \left\langle \phi \middle| \phi^\dagger \right\rangle, \tag{4.17}$$

where $\mathrm{Re}\phi$ and $\mathrm{Im}\phi$ are the real and the imaginary parts of ϕ, and $\phi^\dagger$ is the complex conjugate of ϕ. The identity operator can be made time-dependent by demanding $\phi = \phi(t)$. The time-dependent identity operator is denoted by $\mathbb{I}_t$.

4.1.3 Path integral representation

The exponential in the formal solution to the time evolution Eq. (4.11) can be discretised as

$$\exp\left(\widehat{\mathcal{A}} t\right) = \lim_{\Delta t \to 0} (1 + \widehat{\mathcal{A}} \Delta t)^{t/\Delta t} = \lim_{\Delta t \to 0} \mathbb{I}_t \prod_{i=0}^{t/\Delta t - 1} (1 + \Delta t \widehat{\mathcal{A}}) \mathbb{I}_{i\Delta t} \tag{4.18}$$

where I have inserted the identity operator $\mathbb{I}$ between each factor of $(1 + \Delta t \widehat{\mathcal{A}})$.

Using the coherent-state representation of the identity operator, we can rewrite Eq. (4.18)

as

$$\exp\left(\widehat{\mathcal{A}}t\right) = \lim_{\Delta t\to 0}\int |\phi(t)\rangle \left(\prod_{i=0}^{t/\Delta t-1} \left\langle\phi^\dagger((i+1)\Delta t)\right| (1+\Delta t\widehat{\mathcal{A}}) \left|\phi(i\Delta t)\right\rangle\right) \left\langle\phi^\dagger(0)\right| \prod_{j=0}^{t/\Delta t}\left[\frac{\mathrm{dRe}\phi(j\Delta t)\mathrm{dIm}\phi(j\Delta t)}{\pi} e^{-\phi^\dagger(j\Delta t)\phi(j\Delta t)}\right]. \tag{4.19}$$

In order to evaluate Eq. (4.19), we first evaluate

$$\begin{aligned}
\left\langle\phi^\dagger((i+1)\Delta t)\middle|\phi(i\Delta t)\right\rangle &= \langle 0| e^{\phi^\dagger((i+1)\Delta t)a} |\phi(i\Delta t)\rangle && (4.20)\\
&= \langle 0| \sum_{k=0}^{\infty} \frac{\phi^{\dagger k}((i+1)\Delta t)}{k!} a^k |\phi(i\Delta t)\rangle && (4.21)\\
&= \langle 0| \sum_{k=0}^{\infty} \frac{\phi^{\dagger k}((i+1)\Delta t)}{k!} \phi^k(i\Delta t) |\phi(i\Delta t)\rangle && (4.22)\\
&= e^{\phi^\dagger((i+1)\Delta t)\phi(i\Delta t)}, && (4.23)
\end{aligned}$$

where we have used that $|\phi\rangle$ is an eigenvector of the annihilation operator a. We then consider the quantity

$$\begin{aligned}
\Xi(i\Delta t) :&= \left\langle\phi^\dagger((i+1)\Delta t)\right| (1+\Delta t\widehat{\mathcal{A}}) \left|\phi(i\Delta t)\right\rangle && (4.24)\\
&= \left\langle\phi^\dagger((i+1)\Delta t)\middle|\phi(i\Delta t)\right\rangle + \left\langle\phi^\dagger((i+1)\Delta t)\right| \Delta t \sum_{\gamma,\sigma} h_{\gamma,\sigma} a^{\dagger\gamma} a^\sigma |\phi(i\Delta t)\rangle && (4.25)\\
&= e^{\phi^\dagger((i+1)\Delta t)\phi(i\Delta t)} + \Delta t \sum_{\gamma,\sigma} h_{\gamma,\sigma} \phi^{\dagger\gamma}((i+1)\Delta t)\phi^\sigma(i\Delta t) e^{\phi^\dagger((i+1)\Delta t)\phi(i\Delta t)} && (4.26)\\
&= \left(1+\Delta t\widehat{\mathcal{A}}[\phi^\dagger((i+1)\Delta t), \phi(i\Delta t)]\right) e^{\phi^\dagger((i+1)\Delta t)\phi(i\Delta t)}, && (4.27)
\end{aligned}$$

where we have used that the coherent states are the eigenvectors of operators a and

$a^\dagger$. Substituting Eq. (4.27) into Eq. (4.19) yields

$$\exp\left(\widehat{\mathcal{A}}t\right) = \lim_{\Delta t\to 0}\int |\phi(t)\rangle \prod_{i=0}^{t/\Delta t-1} e^{\phi^\dagger((i+1)\Delta t)\phi(i\Delta t)}\left(1+\Delta t\widehat{\mathcal{A}}[\phi^\dagger((i+1)\Delta t),\phi(i\Delta t)]\right)\times$$
$$\left\langle\phi^\dagger(0)\right| \prod_{j=0}^{t/\Delta t}\left[\frac{\mathrm{dRe}\phi(j\Delta t)\mathrm{dIm}\phi(j\Delta t)}{\pi}e^{-\phi^\dagger(j\Delta t)\phi(j\Delta t)}\right] \tag{4.28}$$
$$= \lim_{\Delta\to 0}\int \prod_{j=0}^{t/\Delta t}\left[\frac{\mathrm{dRe}\phi(j\Delta t)\mathrm{dIm}\phi(j\Delta t)}{\pi}\right]\times$$
$$e^{-\phi^\dagger(t)\phi(t)+\sum_{j=0}^{t/\Delta t-1}\left(\phi^\dagger((j+1)\Delta t)-\phi^\dagger(j\Delta t)\right)\phi(j\Delta t)}\times$$
$$|\phi(t)\rangle \prod_{i=0}^{t/\Delta t-1}\left[1+\widehat{\mathcal{A}}[\phi^\dagger((i+1)\Delta t),\phi(i\Delta t)]e^{\phi^\dagger((i+1)\Delta t)\phi(i\Delta t)}\right]\left\langle\phi^\dagger(0)\right|. \tag{4.29}$$

Taking the continuous limit $\Delta t\to 0$

1. The product converges to an exponential

$$\lim_{\Delta t\to 0}\prod_{i=0}^{t/\Delta t-1}\left(1+\widehat{\mathcal{A}}[\phi^\dagger((i+1)\Delta t),\phi(i\Delta t)]e^{\phi^\dagger((i+1)\Delta t)\phi(i\Delta t)}\right)$$
$$\to e^{\int_0^t \mathrm{d}t'\mathcal{A}[\phi^\dagger(t'),\phi(t')]} \tag{4.30}$$

.

2. The integration measure becomes a path-integration measure

$$\lim_{\Delta t\to 0}\int\prod_{j=0}^{t/\Delta t}\frac{\mathrm{dRe}\phi(j\Delta t)\mathrm{dIm}\phi(j\Delta t)}{\pi}\to\int\mathcal{D}[\phi^\dagger,\phi] \tag{4.31}$$

3. The sum becomes a Riemann integral

$$\lim_{\Delta t\to 0}\sum_{j=0}^{t/\Delta t-1}\left(\phi^\dagger((j+1)\Delta t)-\phi^\dagger(j\Delta t)\right)\phi(j\Delta t)\to\int_0^t\mathrm{d}t'\left(\frac{d}{dt'}\phi^\dagger(t')\right). \tag{4.32}$$

Now, the exponential of the operator Eq. (4.10) reads

$$e^{\widehat{\mathcal{A}}t} = \int \mathcal{D}[\phi^\dagger, \phi] e^{-\phi^\dagger(t)\phi(t) + \int_0^t \mathrm{d}t' \left(\frac{d}{dt'}\phi^\dagger(t')\right)\phi(t') + \mathcal{A}[\phi^\dagger(t'), \phi(t')]} \left|\phi(t)\right\rangle \left\langle\phi^\dagger(0)\right| . \tag{4.33}$$

After integration by parts, Eq. (4.33) becomes

$$e^{\widehat{\mathcal{A}}t} = \int \mathcal{D}[\phi^\dagger, \phi] e^{-\phi^\dagger(0)\phi(0) + \int_0^t \mathrm{d}t' \phi^\dagger(t') \left(-\frac{d}{dt'}\phi(t')\right) + \mathcal{A}[\phi^\dagger(t'), \phi(t')]} \left|\phi(t)\right\rangle \left\langle\phi^\dagger(0)\right| \tag{4.34}$$

$$= \int \mathcal{D}[\phi^\dagger, \phi] e^{-\phi^\dagger(0)\phi(0) + \mathcal{A}'[\phi^\dagger, \phi]} \left|\phi(t)\right\rangle \left\langle\phi^\dagger(0)\right| , \tag{4.35}$$

where $\mathcal{A}'[\phi^\dagger, \phi]$ is the action functional. Notice that the $\phi(t)\phi(t)$ in the first line becomes $\phi^\dagger(0)\phi(0)$ in the second line due to boundary term from integration by parts.

Alternatively, we introduce the *Doi*-shift $\phi^\dagger = \tilde{\phi} + 1$, and the Doi-shifted operator $\tilde{\mathcal{A}}$, the exponential becomes

$$e^{\tilde{\mathcal{A}}t} = \int \mathcal{D}[\phi^\dagger, \phi] e^{-\phi(t) - \tilde{\phi}(0)\phi(0) + \int_0^t \mathrm{d}t' \phi^\dagger(t') \left(-\frac{d}{dt'}\phi(t')\right) + \tilde{\mathcal{A}}[\tilde{\phi}(t'), \phi(t')]} \left|\phi(t)\right\rangle \left\langle\phi^\dagger(0)\right| \tag{4.36}$$

$$= \int \mathcal{D}[\phi^\dagger, \phi] e^{-\phi(t) - \tilde{\phi}(0)\phi(0) + \mathcal{A}[\tilde{\phi}, \phi]} \left|\phi(t)\right\rangle \left\langle\phi^\dagger(0)\right| . \tag{4.37}$$

Both time evolution operators and $e^{\mathcal{A}t}$ and $e^{\tilde{\mathcal{A}}t}$ are the same physically but are simply written in different representations. The Doi-shifted action $\mathcal{A}$ will be used almost everywhere in literature, I will instead use the notation $\mathcal{A}$ instead of $\tilde{\mathcal{A}}$. The notation $\mathcal{A}'$ is employed to denote the non-Doi shifted action.

Observables and Doi-shift

The system is normally initialised by creating k particle using the creation operator at $t_0 = 0$, therefore the operator is $J = a^{\dagger k}$. To evaluate the observable (4.13), assuming it can be written in the form

$$\mathcal{O}(t) = \sum_{\alpha,\beta} a^{\dagger\alpha}(t) a^{\beta}(t). \tag{4.38}$$

Assuming the operator of the observable can be written using creation and annihilation operators:

$$\widehat{\mathcal{O}} = \sum_{\alpha,\beta} c_{\alpha,\beta} a^{\dagger\alpha} a^{\beta}, \tag{4.39}$$

using the Doi-shifted operator $\mathcal{A}$, the observable Eq. (4.13) becomes

$$\begin{aligned}
\langle \widehat{\mathcal{O}} \rangle(t) &= \langle \text{☼} | \, \widehat{\mathcal{O}} e^{At} a^{\dagger k} \, | 0 \rangle && (4.40)\\
&= \int \mathcal{D}[\phi^\dagger, \phi] \, \langle \text{☼} | \, \widehat{\mathcal{O}}(t) e^{-\phi(t) - \tilde{\phi}(0)\phi(0) + \mathcal{A}[\tilde{\phi},\phi]} \, | \phi(t) \rangle \, \langle \phi^\dagger(0) | k \rangle && (4.41)\\
&= \int \mathcal{D}[\phi^\dagger, \phi] \, \langle \text{☼} | \sum_{\alpha,\beta} c_{\alpha,\beta} a^{\dagger\alpha}(t) a^{\beta}(t) e^{-\phi(t) - \tilde{\phi}(0)\phi(0) + \mathcal{A}[\tilde{\phi},\phi]} \, | \phi(t) \rangle \, \langle \phi^\dagger(0) | k \rangle && (4.42)\\
&= \sum_{\alpha,\beta} c_{\alpha,\beta} \int \mathcal{D}[\phi^\dagger, \phi] \phi^{\beta}(t) e^{\mathcal{A}[\tilde{\phi},\phi]} \phi^{k}(0) && (4.43)\\
&=: \sum_{\alpha,\beta} c_{\alpha,\beta} \langle \phi^{\beta}(t) \phi^{\dagger k}(0) \rangle && (4.44)
\end{aligned}$$

where we have used the identity that

$$\langle \phi^\dagger(0) | k \rangle = \phi^{\dagger k}(0). \tag{4.45}$$

We see the advantage of using the Doi-shift: the factor $e^{\phi(t)}$ cancels out with the $e^{-\phi(t)}$ factor in the $e^{\tilde{A}t}$.

4.1.4 From Fokker-Planck equations to field theories

In the following section, we derive the Doi-Peliti field theory using the Langevin dynamics Eq. (1.3). We first derive a Master equation from the Langevin equation Eq. (1.3). In order to do so, we discretise the position space x by spacing Δx. Recall the Master equation

$$\frac{\partial P(\{n\}, t)}{\partial t} = \sum_{\{n'\} \neq \{n\}} W(\{n'\} \to \{n\}) P(\{n'\}, t) - \sum_{\{n'\} \neq \{n\}} W(\{n\} \to \{n'\}) P(\{n\}, t) \tag{4.46}$$

where $W(\{n\} \to \{n'\})$ is the transition probability from state $\{n\}$ to state $\{n'\}$. The transitions are Poisson processes that change the occupation number. As the

Langevin equation Eq. (1.3) describes a diffusive particle under an external potential, we use the transition probability $W_x(\{n\} \to \{n'\})$ to denote the change in the spatial process. The hopping rate in the position space x to the right and the left is respectively,

$$W_x(\{n\} \to \{n_x - 1, n_{x+\Delta x} + 1\}) = r(x)n_x \tag{4.47}$$
$$W_x(\{n\} \to \{n_{x-\Delta x} + 1, n_x - 1\}) = l(x)n_x. \tag{4.48}$$

When we take the continuous limit $\Delta x \to 0$, the conditions that

$$(\Delta x)^2(r(x) + l(x)) = 2D \quad \text{and} \quad \Delta x(r(x) - l(x)) = -V'(x) \tag{4.49}$$

are demanded. Solving $r(x)$ and $l(x)$ from the constrains yields

$$r(x) = \frac{D}{(\Delta x)^2} - \frac{V'(x)}{2\Delta x}. \tag{4.50}$$

However as the external potential $V'(x)$ is not a constant and could take any sign, the hopping rate $r(x)$ could be negative. To avoid such a situation, we make use of the Heaviside function $\Theta(x)$ and write the hopping rate to the right and the left, respectively, as

$$r(x) = \frac{D}{(\Delta x)^2} - \frac{V'(x)\Theta(-V'(x))}{2\Delta x} \tag{4.51}$$
$$l(x) = \frac{D}{(\Delta x)^2} + \frac{V'(x)\Theta(V'(x))}{2\Delta x} \tag{4.52}$$

which satisfies the constraints Eq. (4.49). Now, we introduce the creation operator $a_x^\dagger$ and the annihilation operator a_x to write the master equation in terms of ladder operators that satisfy

$$a_x^\dagger \left|\{n\}\right\rangle = \left|n_x + 1\right\rangle \quad \text{and} \quad a_x \left|\{n\}\right\rangle = n_x \left|n_x - 1\right\rangle. \tag{4.53}$$

We can then define the mixed-state vector

$$\langle\Psi(t)| = \sum_n P(\{n_x\}, t) \left|\{n\}\right\rangle \tag{4.54}$$

and the time evolution of the mixed state

$$\frac{\mathrm{d}}{\mathrm{d}t}\left|\Psi(t)\right\rangle = \widehat{\mathcal{A}}[a^\dagger, a]\left|\Psi(t)\right\rangle. \tag{4.55}$$

The Hamiltonian operator $\widehat{\mathcal{A}}[a, a^\dagger]$ needs to be determined from the master equation which in turn depends on the transition rates in Eq. (4.52). We find that

$$\widehat{\mathcal{A}}[a, a^\dagger] = \sum_x \left[\frac{D}{(\Delta x)^2} a_x^\dagger (a_{x+\Delta x} - 2a_x + a_{x-\Delta x}) - \frac{\Theta(-V'(x))V'(x)a_x^\dagger}{\Delta x}(a_{x-\Delta x} - a_x) + \frac{\Theta(V'(x))V'(x)a_x^\dagger}{\Delta x}(a_{x+\Delta x} - a_x)\right]. \tag{4.56}$$

As the Hamiltonian operator $\widehat{\mathcal{A}}$ is normal ordered, to turn it into a field theory, we can replace the creation and annihilation operators by fields $a_x^\dagger \to \phi^\dagger(x,t)$ and $a_x \to \phi(x,t)$ and then take the limit $\Delta x \to 0$. A Doi-shifted $\phi^\dagger(x,t) = \tilde{\phi}(x,t) + 1$ is then applied to arrive at the action

$$\mathcal{A}[\tilde{\phi}(x,t), \phi(x,t)] = \phi(\tilde{x}, t)\left[D\frac{\partial^2}{\partial x^2} + \frac{\partial}{\partial x}V'(x)\right]\phi(x,t). \tag{4.57}$$

4.1.5 Generating functions and correlation functions

In general, the action $\mathcal{A}$ can be split into the bilinear part $\mathcal{A}_{\text{lin}}$ which is both linear in ϕ and $\tilde{\phi}$, and the interaction part $\mathcal{A}_{\text{int}}$ which contains all other terms.

Supposing there are n particles in the system, represented by different fields with different indices ϕ_i and $\tilde{\phi}_i$. The bilinear part of the action can then be written by

$$\mathcal{A}_{\text{lin}} = \int \mathrm{d}t'\mathrm{d}x\,(\tilde{\phi}_1, \ldots, \tilde{\phi}_n)A\begin{pmatrix}\phi_1\\ \vdots \\ \phi_n\end{pmatrix} = \int \mathrm{d}t'\mathrm{d}x\,\tilde{\phi}^\top A\phi \tag{4.58}$$

where A is a matrix of differential operators.

To compute correlation functions, we introduce the generating functional

$$\mathcal{Z}[J,\tilde{J}] = \langle \exp\left(\int \mathrm{d}x\mathrm{d}t\, \tilde{J}(x,t)\tilde{\phi}(x,t) + J(x,t)\phi(x,t)\right)\rangle_0, \tag{4.59}$$

where the average $\langle\bullet\rangle_0$ denotes the path-integral

$$\langle\bullet\rangle_0 = \int \mathcal{D}[\phi,\tilde{\phi}]\bullet e^{\mathcal{A}_{\mathrm{lin}}}. \tag{4.60}$$

The correlation functions can be obtained by taking the functional derivative with respect to $J(x,t)$ and $\tilde{J}(x,t)$ and evaluated at 0:

$$\langle\phi(x,t)\tilde{\phi}(x',t')\rangle_0 = \frac{\delta}{\delta J(x,t)}\frac{\delta}{\delta\tilde{J}(x',t')}\mathcal{Z}[J,\tilde{J}]\Big|_{J=\tilde{J}=0}. \tag{4.61}$$

The action of an active field theory will normally also consist of both a bilinear part and an interaction part. To include the contribution of interactions, we usually perform a perturbative expansion around the bilinear term. The entire path-integral of an observable $\mathcal{O}$, incorporating the contribution from interactions, is

$$\langle\mathcal{O}\rangle = \int \mathcal{D}[\tilde{\phi},\phi]\mathcal{O}e^{\mathcal{A}} = \sum_{n=0}^{\infty}\int \mathcal{D}[\tilde{\phi},\phi]\mathcal{O}e^{\mathcal{A}_{\mathrm{lin}}}\frac{\mathcal{A}_{\mathrm{int}}^n}{n!}. \tag{4.62}$$

4.2 Response field theory

The response field theory is a class of field theories to formulate stochastic differential equations using path integrals. The response field theory is built on work by [110, 44].

Below, we outline the derivation for the Martin-Siggia-Rose-Janssen-De Dominicis path integral. For a Langevin equation of the coarse-grained stochastic field $\phi(x,t)$, of generic form

$$\frac{\partial\phi(x,t)}{\partial t} = F[\phi](x,t) + \eta(x,t) \tag{4.63}$$

where F is a deterministic functional of the field $\phi(x,t)$ and $\eta(x,t)$ is a noise with

arbitrary correlation function:

$$\langle \eta(x,t)\eta(x',t')\rangle = 2L\delta(x-x')\delta(t-t'). \tag{4.64}$$

The noise strength L in general can be an operator. The following path-integral construction can be employed for both equilibrium and non-equilibrium processes given suitable Langevin equations of motions and corresponding correlation functions or noise strength L.

Notice that the noise correlation (4.64) can be obtained from the probability distribution using the Onsager-Machlup formalism [116]

$$W[\xi] \propto \exp\left(-\frac{1}{4}\int \mathrm{d}x\mathrm{d}t\, \eta(x,t)[L^{-1}\eta(x,t)]\right). \tag{4.65}$$

Viewing the noise $\eta(x,t)$ as a functional of the field ψ and using the relation from the Langevin equation (4.63),

$$\eta(x,t) = \frac{\partial\phi(x,t)}{\partial t} - F[\phi](x,t), \tag{4.66}$$

we arrive at a probability distribution $P[\psi]$ as a functional of the field ψ

$$W[\eta]\mathcal{D}[\eta] = P[\psi]\mathcal{D}[\psi] \propto \exp(-\mathcal{A}[\psi])\mathcal{D}[\psi], \tag{4.67}$$

where $\mathcal{A}[\psi]$ is the Onsager-Machlup functional

$$\mathcal{A}[\psi] = \frac{1}{4}\int \mathrm{d}x\mathrm{d}t\, \left(\frac{\partial\phi(x,t)}{\partial t} - F[\phi](x,t)\right)\left[L^{-1}\left(\frac{\partial\phi(x,t)}{\partial t} - F[\phi](x,t)\right)\right] \tag{4.68}$$

which plays the equivalent role of a Hamiltonian in equilibrium statistical physics. As the probability distribution needs to be normalised,

$$\int \mathcal{D}[\eta]W[\eta] = 1, \tag{4.69}$$

the associated 'partition function' is always 1 and the corresponding free energy is always 0. Notice that, when we apply a Itô forward discretisation for the Langevin equation, the Jacobian for the change of measure is a constant, which can be ab-

sorbed into the integration measure $\mathcal{D}[\psi]$ [164]. A sketch of this proof is shown in Appendix 4.A.

4.2.1 Janssen–De Dominicis response functional

So far Eq. (4.67) and Eq. (4.68) already provide a field-theoretic formalism to represent both equilibrium and non-equilibrium Langevin dynamics. However, the existence of the inverse operator L^{-1} renders this approach difficult when it comes to the calculation of observables and correlation functions. It is therefore desirable to transfer the inverse operator L^{-1} to the numerator. To preserve the constraint that the fields are subject to the Langevin equations of motions (4.63), we insert a unity at each space-time point via a functional integral representation of the delta function with factors of 2π absorbed into the integration measure,

$$\begin{aligned} 1 &= \int \mathcal{D}[\phi] \prod_{(x,t)} \delta\left(\frac{\partial\phi(x,t)}{\partial t} - F[\phi](x,t) - \eta(x,t)\right) \\ &= \int \mathcal{D}[\mathring{i}\tilde{\phi}]\mathcal{D}[\phi]\exp\left[-\int \mathrm{d}x\mathrm{d}t\, \tilde{\phi}\left(\frac{\partial\phi(x,t)}{\partial t} - F[\phi](x,t) - \eta(x,t)\right)\right]. \end{aligned} \tag{4.70}$$

We have introduced a *Martin-Siggia-Rose* auxiliary field $\tilde{\phi}$, which is also known as the *response field*. By employing Eq. (4.70) as a proxy for 1, to calculate the observable $\langle\mathcal{O}[\psi]\rangle_\eta$, we have

$$\langle\mathcal{O}[\psi]\rangle_\eta \propto \int \mathcal{D}[\mathring{i}\tilde{\phi}]\mathcal{D}[\phi]\mathcal{D}[\eta]\exp\left[-\int \mathrm{d}x\mathrm{d}t\, \tilde{\phi}\left(\frac{\partial\phi(x,t)}{\partial t} - F[\phi](x,t)\right)\right] \tag{4.71}$$

$$\mathcal{O}[\phi]\exp\left(-\int \mathrm{d}x\mathrm{d}t\, \left[\frac{1}{4}\eta L^{-1}\eta - \phi\eta\right]\right). \tag{4.72}$$

By performing the path-integral via completing the square using

$$\int \mathrm{d}\eta\, e^{\tilde{\phi}\eta - \eta L^{-1}\eta/4} \propto e^{\tilde{\phi}L\tilde{\phi}} \tag{4.73}$$

to calculate the noise average, the probability distribution for the stochastic field satisfies

$$P[\phi] = \mathcal{Z}\int \mathcal{D}[\mathring{i}\phi]e^{-\mathcal{A}[\phi,\tilde{\phi}]} \tag{4.74}$$

with the action being the dynamic *Janssen-De Dominicis* response functional

$$\mathcal{A}[\tilde{\phi},\phi] = \int \mathrm{d}x\mathrm{d}t \left[\tilde{\psi}(x,t)\left(\frac{\partial\phi(x,t)}{\partial t} - F[\phi](x,t)\right) - \tilde{\phi}(x,t)L\tilde{\phi}(x,t)\right], \tag{4.75}$$

and the normalisation constant

$$\mathcal{Z} = \int \mathcal{D}[\mathring{\imath}\tilde{\phi}]\mathcal{D}[\phi]e^{-\mathcal{A}[\tilde{\phi},\phi]}. \tag{4.76}$$

When we explicitly perform the path-integral over the auxiliary fields $\tilde{\phi}$ in Eq. (4.74), we recover that Onsager-Matchlup function Eq. (4.68) because of the identity

$$\int e^{\mathring{\imath}(\mathring{\imath}\tilde{\phi}\eta[\phi])-(\mathring{\imath}\tilde{\phi})L(\mathring{\imath}\tilde{\phi})}\mathrm{d}(\mathring{\imath}\tilde{\phi}) = \int e^{-\bar{\phi}L\bar{\phi}}\mathrm{d}\bar{\phi}\, e^{-\eta[\psi]L^{-1}\eta[\phi]/4}, \tag{4.77}$$

where $\bar{\phi} = \mathring{\imath}\tilde{\phi} - \mathring{\imath}L^{-1}\eta/2$. The Jacobian is again a constant which is absorbed into the integration measure as we are using a forward Itô stochastic discretisation.

Notice that the integration over $\tilde{\phi}$ needs to be along the imaginary axis in order to ensure convergence.

In general, one may show that the contributions arising from the Jacobian precisely cancel these closed response loop diagrams, if a consistent discretisation is used. We may thus omit these Jacobian terms with the understanding that no Feynman diagrams containing closed response loops are to be permitted in the perturbation expansion to be constructed below. Note that in this manner, causality becomes implemented in our field theory representation for Langevin equations of the form Eq. (4.63).

Observables are generally expressed by taking the average over the statistical weight $e^{-\mathcal{A}[\phi,\tilde{\phi}]}$. For example, we have the two-point correlation function

$$\langle\phi(x,t)\phi(x',t')\rangle = \frac{\int \mathcal{D}[\mathring{\imath}\tilde{\phi}]\mathcal{D}[\phi]\phi(x,t)\phi(x',t')e^{-\mathcal{A}[\phi,\tilde{\phi}]}}{\int \mathcal{D}[\mathring{\imath}\tilde{\phi}]\mathcal{D}[\phi]e^{-\mathcal{A}[\phi,\tilde{\phi}]}}. \tag{4.78}$$

To compute correlation functions such as Eq. (4.78), we again introduce the generating functional

$$\mathcal{Z}[J,\tilde{J}] = \langle\exp\left(\int \mathrm{d}x\mathrm{d}t\, \tilde{J}(x,t)\tilde{\phi}(x,t) + J(x,t)\phi(x,t)\right)\rangle. \tag{4.79}$$

The correlation functions can be obtained by taking the functional derivative with respect to $J(x,t)$ and $\tilde{J}(x,t)$ and evaluated at 0:

$$\langle \phi(x,t)\phi(x',t')\rangle = \frac{\delta}{\delta J(x,t)}\frac{\delta}{\delta \tilde{J}(x',t')}\mathcal{Z}[J,\tilde{J}]\Big|_{J=\tilde{J}=0} \tag{4.80}$$

Similar to Doi-Peliti field theory, Sec. 4.1, the action $\mathcal{A}$ will normally consist of a bilinear part $\mathcal{A}_{\text{lin}}$ and an interactive part $\mathcal{A}_{\text{int}}$. We again perform a perturbative expansion around the bilinear terms. The expectation of an observable $\mathcal{O}$ is now

$$\langle \mathcal{O}\rangle = \frac{\langle \mathcal{O} e^{-\mathcal{A}_{\text{int}}}\rangle_0}{\langle e^{-\mathcal{A}_{\text{int}}}\rangle_0} \tag{4.81}$$

$$= \frac{\langle \mathcal{O}\sum_{n=0}^{\infty}(-\mathcal{A}_{\text{int}})^n/n!\rangle_0}{\langle \sum_{n=0}^{\infty}(-\mathcal{A}_{\text{int}})^n/n!\rangle_0} \tag{4.82}$$

where the average $\langle \bullet\rangle_0$ denotes the path-integral

$$\langle \bullet\rangle_0 = \int \mathcal{D}[\phi,\tilde{\phi}]\bullet e^{-\mathcal{A}_{\text{lin}}}. \tag{4.83}$$

Appendix

4.A Discretisation and Jacobian

In section 4.2, we used the Langevin equation Eq. (4.63) in order to perform a variable transformation to a probability distribution for the stochastic field ϕ and then again when we employed the set of delta function constraints in Eq. (4.70). This nonlinear variable transformation is accompanied by a functional determinant $\mathcal{D}[\eta]/\mathcal{D}[\phi]$. In order to compute this Jacobian, we discretise in time $t_l = t_0 + l\tau$, $t_M = t_f$ and set $\phi_l = \phi(t_l), \eta_l = \eta(t_l)$, whence the equation of motion Eq. (4.63) becomes a difference equation. For now, we choose an arbitrary linear splitting for the generalised force $F_l = F[\phi(t_l)]$ and namely with $0 \leq \kappa \leq 1$:

$$\frac{\phi_{l+1} - \phi_l}{\tau} = \kappa F_{l+1} + (1-\kappa)F_l + \eta_l. \tag{4.84}$$

With this choice, the functional determinant is this given by

$$\frac{1}{\tau^M}\left(1 - \kappa\tau\frac{\partial F_l}{\partial \phi_l}\right) \approx \frac{1}{\tau^M}\exp\left(-\kappa\sum_l \tau\frac{\partial F_l}{\partial \phi_l}\right). \tag{4.85}$$

The factor $1/\tau^M$ is then absorbed into the functional measure. Taking the limit $\tau \to 0$, we arrive at the additional term $\kappa\int \mathrm{d}x\mathrm{d}t\, \delta F[\phi]/\delta\phi$ both in the Onsager-Matchlup function Eq. (4.68) and in the Janssen-De Dominicis functional Eq. (4.75). Notice that the splitting in Eq. (4.85) corresponds to setting $\Theta(0) = \kappa$ for the Heaviside step function. The Itô for Langevin equations uses the forward discretisation $\kappa = 0$, where the Jacobian contribution to the action vanishes. The fact that $\Theta(0) = \kappa$ implies that the terms that contain closed response loops are exactly canceled by the contribution from the functional determinant. This ensures causality as one could construct acausal Feynmann diagrams if closed response loops were allowed.

5

Optimal Ratchet Potentials for Run-and-Tumble particles

Abstract

In this chapter, I presented a near-verbatim copy of the preprint

Z.Zhen and G.Pruessner. Optimal Ratchet Potentials for Run-and-Tumble particles [181].

I prepared in collaboration with G. Pruessner. G.P. conceived the project and supervised the project throughout. I did everything else, including the mathematical derivations, the diagrammatics, identifying symmetries and conservation laws. The writing of this manuscript was done jointly with G.P.

Run-and-Tumble particles, mimicking the behaviour of microorganisms like *E. coli*, are a paradigmatic model of active matter. Due to self-propulsion, their random and undirected motion can be rectified in a ratchet potential. Using perturbative field theory, we determine the shape of the potential that produces the maximum particle current as a function of the particles' parameters.

Active matter systems, operating away from equilibrium, are composed of agents that consume energy from the environment to exert mechanical work [106]. Even when their motion is isotropic in free space, they can break detailed-balance by producing a spontaneous and directional motion in asymmetric environments [42, 102, 9, 121, 59, 109, 6, 10, 8, 84] such as moving a ratchet wheel [40]. Such directed motion is known to control activated events in glassy systems [14], transport biological molecules [70, 97, 66, 23, 20, 175, 15, 170] and revert the Ostwald process in active fluids [162]. Compared to the many observational studies, relatively little theoretical progress has been made to quantify and optimise non-equilibrium transport from first principles [9, 8, 13].

In the present work, we find the periodic ratchet potential that optimises the steady-state current of one-dimensional Run-and-Tumble (RnT) particles [159]. These are diffusive particles that move ballistically by self-propulsion until they change direction instantaneously and spontaneously under a Poisson process [180], taking place symmetrically in both directions. Feynman famously used a ratchet to illustrate that useful work cannot be extracted from diffusive particles [52]. That the random motion of RnT particles can be rectified at all is somewhat counter-intuitive and possible only because the spatial scale of the external potential is commensurate with the particles' mean free path [29, 42, 102, 9].

Rectified unidirectional motion of RnT particles in an asymmetric sawtooth potential has been investigated both theoretically and experimentally in [40, 9, 6, 84]. The locomotion of *E. coli* can be rectified by means of microfluidic funnels, which were further studied through theoretical models and numerical simulations [66]. Such studies have illustrated the far-reaching technological implications of active particles for example for drug delivery or for separating particle species by activity. Despite the efforts made in experimental and numerical studies [15, 33], not a lot of light has been shed on the design principles of optimal transportation of active particles in ratchets. Extending well beyond existing work on RnT particles in specific potentials [9, 6], in the following we consider completely general potentials in a perturbative field theory, without making any approximations. While the perturbation theory can equally be implemented using classical methods, the field theory provides a systematic, diagrammatic framework to keep track of the contribution at every order. We subsequently use a numerical scheme to find the potential, such as Fig. 5.0.1, that maximises the

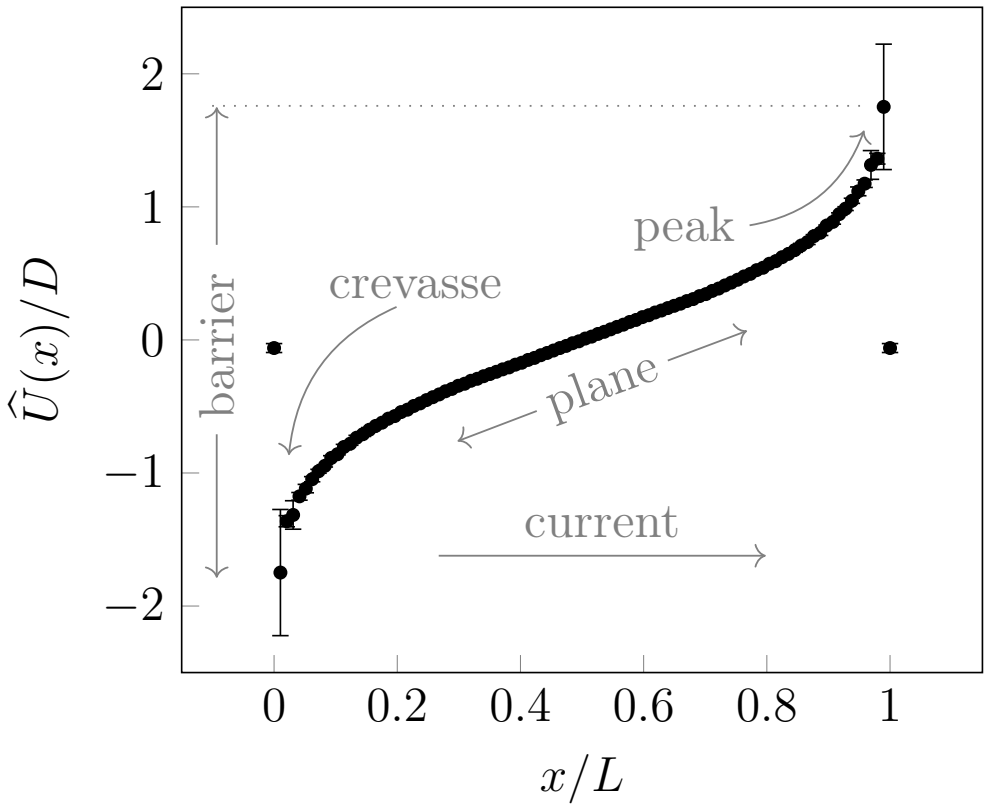


Figure 5.0.1: Optimal potential $\widehat{U}(x)/D$ for $f = 0, D = 1$, $w = 1$, $L = 1$ and $\gamma = 1$, so that $Pe = Qe = \kappa = 1$, resulting in the current $\widehat{J}L^2/D = 0.03789\ldots$ to the right and $\widehat{\nu^{<}_{\text{roc}}} = 1.167\ldots$. The details of the numerical scheme employed to produce the plot are discussed in Appendix. 5.A.2.

particle current.

Model and method. In this work, we study a single RnT particle with position $x(t) \in [0, L)$ in a potential $\Phi(x)$ with an drift on a ring with circumference L. The motion is governed by the Langevin equation

$$\dot{x}(t) = -\Phi'(x) + wu(t) - f + \sqrt{2D}\xi(t), \tag{5.1}$$

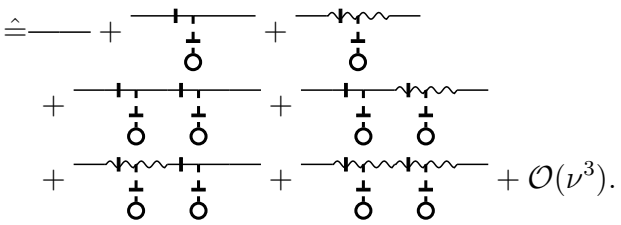
where $\Phi'(x)$ is the derivative of $\Phi(x)$, w is the particle's self-propulsion speed, f is the external drift $u(t)$ is a telegraphic noise switching between 1 and -1 with Poissonian rate γ and $\xi(t)$ is a unit Gaussian white noise with correlator $\langle \xi(t)\xi(t')\rangle = \delta(t - t')$ and diffusion constant D. The motion Eq. (5.1) is subject to periodic boundary con-

ditions with period L and $x \in [0, L)$, so that the process has a steady state and effectively $\Phi(x) = \Phi(x + L)$. By adding an external force to the RnT particles in the potential, the set-up is equivalent to an heat engine driven by a RnT particle in an external potential [118, 124]. Applying an external load f in the opposite direction of the particle movement, the engine extracts work by lifting the force f. Due to the self-propulsion and the external force, the system is driven out of equilibrium and its invariant measure is generically not of Boltzmann form $\rho(x) \propto e^{-\Phi(x)/D}$.

FIELD THEORY. In what follows, we calculate the steady-state density $\rho(x)$ of an RnT particle Eq. (5.1), as well as its steady-state current J in a perturbation theory in the coupling ν to the arbitrary potential $U(x)$, such that $\Phi(x) = \nu U(x)$. To this end, we cast the RnT dynamics in the language of a Doi-Peliti field theory [43, 123, 28, 164, 180, 129] as detailed in Appendix. 5.B. Observables are more conveniently expressed in frequencies ω instead of direct time t and discretised modes $k_a = 2\pi a/L$ instead of real space, Appendix. 5.B Eq. (5.24).

In the following, we express the propagator $\langle \phi(x,t)\phi(x_0,t_0)\rangle$ which is the probability density of locating a right-moving particle at position x and time t that has been initiated at position x_0 and time t_0. The propagators can then be written in a perturbation theory about $\nu = 0$. Using the potential vertices Appendix. 5.B Eq. (5.32), each propagator picks up 2^n contributions to order n in the perturbation theory, for example, in Fourier representation

$\left\langle \phi_a(\omega)\widetilde{\phi}_b(\omega')\right\rangle$



(5.2)

STEADY-STATE DENSITY AND CURRENT. In the present work we focus on the steady state, Appendix. 5.C. We write the steady-state density ρ_+ of right-moving particles

as a power series in ν^n with coefficients $\rho_+^{(n)}$,

$$\rho_+(x) = \sum_{n=0}^{\infty} \nu^n \rho_+^{(n)}(x) \tag{5.3}$$

$$= \lim_{t_0 \to -\infty} \left\langle \phi(x,t)\widetilde{\phi}(x_0,t_0) \right\rangle \tag{5.4}$$

and similarly for the density of left moving particles ρ_-, so that $\rho(x) = \rho_+(x) + \rho_-(x)$. For finite tumble rate γ, the steady-state densities $\rho_\pm$ are independent of the initial state. As discussed in Appendix. 5.C, the limit $t_0 \to -\infty$ effectively amputates the right, incoming leg in the diagrams, Eq. (5.2), so that they readily provide us with a diagrammatic expansion of the steady state density, order by order in ν.

Calculating the ath Fourier coefficient $\rho_a^{(n)}$ of the steady-state density ρ to order n in ν is now a matter of some well-organised algebra (Appendix. 5.C). To this end, we introduce the polarity $\mu(x) = \rho_+(x) - \rho_-(x)$ and establish a recurrence relation between each order in ν of the density $\rho(x)$ and the polarity $\mu(x)$. Starting from the zeroth order in ν for both the density and the polarity, the recurrence relation allows us to compute each order of the density $\rho^{(n)}(x)$ and the polarity $\mu^{(n)}(x)$. With both $\mu^{(n)}(x)$ in hand, we calculate the density and the polarity by summing the power series

$$\rho(x) = \sum_{n=0}^{\infty} \nu^n \rho^{(n)}(x) \tag{5.5}$$

$$\mu(x) = \sum_{n=0}^{\infty} \nu^n \mu^{(n)}(x). \tag{5.6}$$

We express the steady-state current as

$$J = w\mu(x) - (D\partial_x + f + \nu U'(x))\rho(x) \ . \tag{5.7}$$

Defining the matrix (Appendix. 5.C.2)

$$\underline{\underline{M_a}} = \frac{-k_a \mathcal{I}_a}{\Gamma_a^0 \Gamma_{-a}^0 - \gamma^2} \begin{pmatrix} Dk_a^2 + 2\gamma - \mathring{\imath} f k_a & -\mathring{\imath} w k_a \\ -\mathring{\imath} w k_a & Dk_a^2 - \mathring{\imath} f k_a \end{pmatrix} \tag{5.8}$$

with $\Gamma_a^0 = \Gamma_a(0;0) = Dk_a^2 - \mathring{\imath} w k_a - \mathring{\imath} f k_a + \gamma$, Appendix. 5.C Eq. (5.30), and $\mathcal{I}_a =$

$1-\delta_{a,0}$, Appendix. 5.C Eq. (5.41), the density and the polarity at order n in ν are the elements of the vector

$$\begin{pmatrix} \rho_{a_1}^{(n)} \\ \mu_{a_1}^{(n)} \end{pmatrix} = \sum_{a_2,\ldots,a_n} W_{a_1-a_2} W_{a_2-a_3} \ldots W_{a_{n-1}-a_n} W_{a_n} \underline{\underline{M_{a_1}}}\, \underline{\underline{M_{a_2}}} \ldots \underline{\underline{M_{a_n}}} \begin{pmatrix} 1 \\ 0 \end{pmatrix} \tag{5.9}$$

with $W_a = U_a k_a / L$. Using Eq. (5.7), the steady-state current at order n in ν is correspondingly

$$J^{(n)} = -\frac{\mathring{\imath}}{L} \sum_{a_1,\ldots,a_{n-1}} W_{-a_1} W_{a_1-a_2} W_{a_2-a_3} \ldots W_{a_{n-2}-a_{n-1}} W_{a_{n-1}} \begin{pmatrix} 1 \\ 0 \end{pmatrix}^{\top} \underline{\underline{M_{a_1}}}\, \underline{\underline{M_{a_2}}} \ldots \underline{\underline{M_{a_{n-1}}}} \begin{pmatrix} 1 \\ 0 \end{pmatrix} . \tag{5.10}$$

This concludes our derivation. Calculating the current is now a matter of performing the matrix multiplications and summation in Eq. (5.10) for a potential given in terms of its modes U_a and summing these contributions order by order in ν, so that

$$J = \sum_{n=0}^{\infty} \nu^n J^{(n)} \ . \tag{5.11}$$

In the case of $f = 0$, which represents just an RnT in an potential, from the symmetries of $\underline{\underline{M_a}}$, Eq. (5.8), and the form of Eq. (5.10), it follows that there is no current to first order in ν and generally no contributions to the steady-state current in even powers of ν, Appendix. 5.E.1. As a result, the current reverts if the potential is inverted, $U \to -U$. This is not a trivial insight, because the steady-state *density* of the inverted potential generally bears no resemblance to that of the original potential, Appendix. 5.C Fig. 5.E.1, which may have been overlooked [133]. Several other properties of the steady-state current J arising from Eq. (5.11) are discussed in detail in Appendix. 5.C. Firstly, in a potential even about x^*, *i.e.* $U(x^* + x) = U(x^* - x)$, the steady-state current, of course, vanishes, because the potential fails to provide even just a preferred direction [131], Appendix. 5.E.3. The steady-state current also vanishes if the potential $U(x)$ has only odd modes, *i.e.* $U_a = 0$ for all even a, which renders it "supersymmetric" [133], $U(x) = -U(x + L/2)$, Appendix. 5.E.2. It is important to note that with the presence of external drift f, the above result no longer holds as f breaks the symmetry of the RnT particle even when the potential $U(x)$ is symmetric or "supersymmetric".

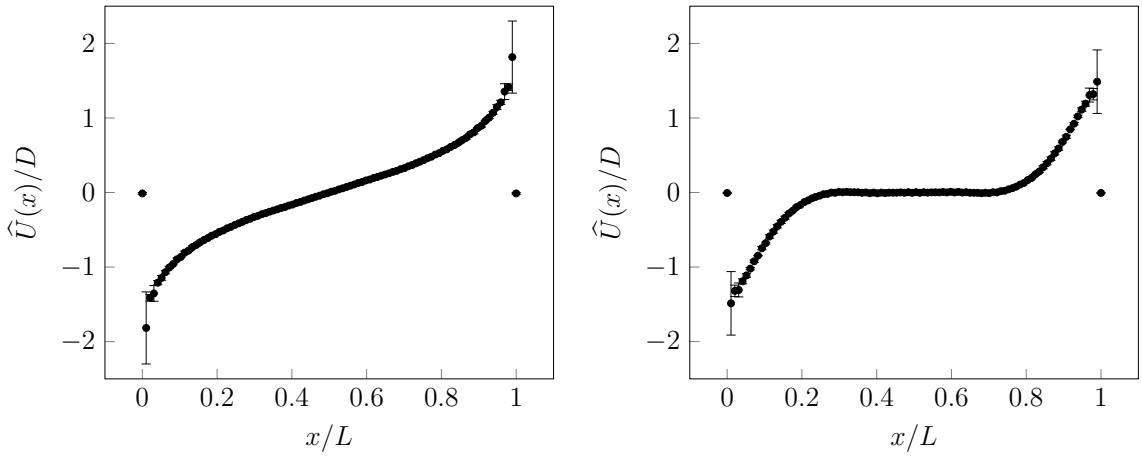
The steady-state current in any potential parameterised by U_a is given by Eqs. (5.10) and (5.11). Any numerical scheme can cope only with a finite number of modes, as the sums in Eq. (5.10) need to terminate, and similarly for the maximum order of ν entering in Eq. (5.11). Nevertheless, including hundreds of modes to calculate the current to hundreds of orders in ν, in principle poses little numerical difficulty. To confirm the correctness of our scheme, we calculate the current for a plain ratchet and compare to [9], which can be done to large extent in closed form, Appendix. 5.D, owing to the piece-wise linearity of the potential. Appendix. 5.D Fig. 5.D.2 demonstrates perfect agreement of the steady-state current calculated in both schemes for all $\nu < \nu_{\text{roc}}^{<}$. Beyond that point the power series Eq. (5.11) eventually diverges. In principle, the radius of convergence ν_{roc} is determined, say, through the root test on the odd terms of the series Eq. (5.11), $\nu_{\text{roc}} = 1/\limsup_{m\to\infty} |J^{(2m+1)}|^{1/(2m+1)}$, but in the present numerical procedures based on gradient descent, we used the more conservative estimate of the minimal radius of convergence of the derivative of Eq. (5.11),

$$\nu_{\text{roc}}^{<} = \min\left(\left|mJ^{(m)}\right|^{-\frac{1}{m-1}} : m = 3, 5, \ldots, n\right) \ , \tag{5.12}$$

with n the highest order calculated.

Optimising the potential. To find the best *shape* of the potential that maximises the current J, we remove the external drift by setting $f = 0$ and fix $\nu = 1$, rendering $\Phi(x)$ equal to $U(x)$ for the remainder of this section, and, leaving ν untouched, instead we find the modes U_a that maximise the steady-state current J, Eqs. (5.10) and (5.11). The detail of the procedure is found in Appendix. 5.A.1.

Further, we de-dimensionalise the problem, leaving only two parameters, the Péclet number $Pe = wL/D$ and $Qe = \gamma L^2/D$. In this parameterisation, length is measured in units of L, diffusion and the potential in units of D and time therefore in units of L^2/D. We think in the following of L and D as being fixed, so that Pe parameterises the self-propulsion velocity, Qe the tumbling rate and $\widehat{U}(D, w, L, \gamma; x) = D\widehat{U}(1, Pe, 1, Qe; x/L)$. While any particular choice of the underlying parameterisation should make no difference to the optimisation scheme, making different choices for D, w, L and γ for the same Pe and Qe gives us a way to overcome some practical, numerical limitations.



(a) $f = 0, D = 1$, $w = 2$, $L = 1$ and $\gamma = 200$, so that $Pe = 2$, $Qe = 200$, resulting in the current $\widehat{J}L^2/D = 0.01141\ldots$ and $\widehat{\nu^{<}_{\mathsf{roc}}} = 1.099\ldots$.

(b) $f = 0, D = 1$, $w = 2$, $L = 1$ and $\gamma = 0.02$, so that $Pe = 2$, $Qe = 0.02$, resulting in the current $\widehat{J}L^2/D = 0.16545\ldots$ and $\widehat{\nu^{<}_{\mathsf{roc}}} = 1.003\ldots$.

Figure 5.0.2: Shapes of potential maximising the steady-state current at the parameter values indicated. Technical details of the plots in Appendix. 5.A.2.

RESULTS. The resulting shape of the optimal potential is surprisingly stable across the range of Pe and Qe explored. Fig. 5.0.1 shows a typical shape, Fig. 5.0.2 shows two more for somewhat more extreme parameter values. The shape resembles that of the letter N, but it is not a simple, piece-wise linear ratchet. The resulting current in the figures above takes place from left to right. The deep crevasse towards $x = 0$ in Fig. 5.0.1, towards the left followed by a steep rise of the potential towards the left and over to the right by periodicity, traps particles and prevents them from moving left. There is always a shallower path towards the right, that terminates in a sharp peak towards $x = L$, rendering the whole shape inversion symmetric about $(L/2, 0)$. The presence of the sharp peak in Figure 5.A.2 is the result of an apparent discontinuity at $x = 0$ due to Gibbs phenomenon, Appendix. 5.A.2. To overcome the problem of convergence of the Gibbs phenomenon at $x = 0$, we have decreased the resolution of the graph by plotting the points sparsely. This is explained in more details in Appendix. 5.A.2. Despite the discontinuity at $x = 0$, the particle will still be able to get across the obstacle due to diffusion. To realise such a potential physically, we simply require a vertical drop in the potential at $x = 0$.

The Péclet-number Pe indicates whether *free* particle movement is dominated by dif-

fusion, $Pe < 1$, or ballistic motion, $Pe > 1$. The additional complications of tumbling and potential modify its rôle. On the large scale, diffusion is enhanced by $L\gamma^2$. On the small scale, diffusion D sets the scale of the maximum barrier height the particle can overcome. Without potential, ballistic transport dominates on the scale of the system, if $w/\gamma > L$, *i.e.* $\kappa = Pe/Qe > 1$.

To rectify the flow optimally, the basic design principles we derive from Figs. 5.0.1 and 5.0.2 are, firstly, the need for a deep crevasse, Fig. 5.0.1, to set a high hurdle to a RnT particle attempting to pass through the potential towards the left. Similarly, a sharp peak at around $x = L$ increases the barrier height. The rise of the potential required as a barrier grows linearly in D. The second design principle is the shallower incline of the potential towards the right, where the potential difference of the steep crevasse is spread out across the whole length L of the potential, making it much less of an obstacle for particle movement towards the right.

Apart from the deep crevasse and the sharp peak on either end of the shallow incline, the intermediate "plane", Fig. 5.0.1, may be expected to have a slope of around w, so that it is just about overcome by a right-moving RnT particle. However, for this long section to be passed *ballistically* within time $1/\gamma$, its slope would have to be less than $w - L\gamma$. This can be realised only when w is sufficiently large, as the slope is necessarily positive. If ballistic transport dominates over diffusion, $Pe > 1$, but ballistic transport itself is too slow to overcome any significant potential slope within the time available between tumbles, $\kappa = Pe/Qe = w/(L\gamma) \ll 1$, we expect a flat plane maximising the steady-state current. Together with the need of a high barrier around $x = 0$, $Pe > 1$ and $Qe \gg 1$ result in sharp crevasses and peaks, Fig. 5.0.2a.

If, on the other hand, ballistic transport is strong, $\kappa > 1$ and $Pe > 1$, the slope of the potential in the plane is not constrained by the ballistic transport but rather by the need to connect (only) between the bottom and the top of the barrier face, *i.e.* the slope will scale like D/L. In this case, $Pe > 1$ and $Qe \ll 1$, the intermediate slope is steeper and the crevasses widened, Fig. 5.0.2b, producing a relatively large current.

If transport is primarily diffusive, $Pe < 1$, large $Qe = \gamma L^2/D$ effectively enhances the diffusion on spatial scales greater than w/γ. Transport in this parameter region is typically poor.

In general, a high barrier helps rectify the steady-state current. The need for a high

barrier requires potential differences so large, that the slope of the potential $\propto D/L$ in the plane exceeds the self-propulsion velocity w. This phenomenon can be observed already in a piece-wise linear ratchet with the steady-state current J plotted in Appendix. 5.D Fig. 5.D.2, where the maximum current is attained when the slope of the long "plane" section is around 3.9/0.9, far exceeding the self-propulsion velocity of $w = 1$.

DISCUSSION. The optimal rectified current $\widehat{J}$ is generally small compared to the unidirectional current w/L. Only for $Pe \to \infty$ and $Qe \downarrow 0$ the particles whizz through the potential in one direction, getting stuck on any tiny snag of a conventional ratchet in the other, so that $\widehat{J} = (1/2)w/L$. A key question to address in future research is whether an external potential provides the best rectification or whether there are other passive devices that do a better job. What are the limits of rectification?

An experimental verification of our work requires a fine-tuned potential landscape. Microorganisms have been subjected to a potential well by optical trapping [176], bidirectional molecular motors by magnetic trapping [50], but simpler effective potential, due to boundary interaction [168, 151] and a transversal microfluidic flow may be equally feasible.

Typical values for *E. coli* are $D = 0.2\ \mu m^2/s$ for the *thermal* diffusion constant, $w = 40\ \mu m/s$ for the self-propulsion speed and $\gamma = 1s^{-1}$ for the tumble rate [150, 45], producing values between $Pe = 1000$ and $Qe = 125$ for $L = 5\ \mu m$ and $Pe = 2 \cdot 10^4$ and $Qe = 5 \cdot 10^4$ for $L = 100\ \mu m$. For these parameters we expect the optimal potential to be akin to Fig. 5.0.2a. Because the radius of convergence drops significantly with increasing Peclet number, we are not able to determine the shape directly.

The field theoretic formalism above can be extended: Firstly, it provides a route to the steady-state entropy production via Gaspard's [64, 30] approach, which, however, lies beyond the scope of the present work. While it is fairly straight-forward to calculate it for the full Markov process, determining it while ignoring the particle species is notoriously difficult [62]. One might expect, however, that maximised current coincides with maximised entropy production. Secondly, the lack of convergence as shown in Appendix. 5.D Fig. 5.D.2 for $\nu > \nu^{<}_{\text{roc}}$ is a challenge that needs to be overcome,

possibly with the help of renormalisation. Thirdly, although many experimental settings are well captured in one longitudinal and one transversal spatial dimension, extending the present framework to two dimension plus one transversal direction is an important generalisation.

This work determines the properties of the potential that optimally rectifies the steady-state current of RnT particles. We have shown that generally, the profile deviates significantly from an ordinary ratchet. Our quantitative and qualitative findings provide the design principles for rectification devices for microorganisms and for the cogs and wheels of an active engine [124].

Appendix

5.A Numerical optimisation and plotting procedure

In this section, we discuss the numerical procedures employed to determine the optimal shape $\widehat{U}(x)$ of the potential and to subsequently generate the plots of the potential $U(x)$ in Figs. 5.0.1 and 5.0.2. The optimisation scheme outlined in the main text results in the potential being characterised by its modes U_a and translating a finite number of them to a potential $U(x)$ in real space is marred by ambiguity. We will outline the process of generating the plots, the origin of the error bars, the Gibbs phenomenon and the resolution of troughs and peaks.

5.A.1 Optimisation procedure

In the following we outline the numerical procedure to determine the optimal potential $\widehat{U}(x)$, *i.e.* the potential that maximises the steady-state current J. The numerical scheme draws on Eqs. (5.10) and (5.11), which effectively produce the steady-state current J for any given, finite set of $2A+1$ modes of the potential U_a with $a = -A, -A+1, \ldots, A$. The numerical scheme is greatly improved by expressing the partial derivative of J with respect to any of the modes U_a. While tedious to determine, given the structure of Eq. (5.10), a closed-form expression is readily available.

While the finite number of modes, $2A+1$, limits the summation to be performed in Eq. (5.10), the order of ν needs to be limited to $\mathcal{N}_\nu$ in the sum Eq. (5.11).

As $U(x)$ is real, the modes U_a are complex conjugate pairs, $U_a^* = U_{-a}$. The 0-mode U_0 does not enter at all, so that for any given A the maximisation scheme determines A complex numbers, U_a with $a = 1, 2, \ldots, A$.

If $\widehat{U}(x)$ extremises the current, so does $\widehat{U}(L-x)$ and in fact any translation of the two, $\widehat{U}(x^* \pm x)$. To break symmetry, we demand U_1 be purely imaginary, leaving the

maximisation scheme with $2A-1$ degrees of freedom. We found that generally the maximisation scheme is not sensitive to the details of the initialisation. We have also verified that the maximum current is not obtained with periodically repeated potentials, "higher harmonics", where only modes are populated that are multiples of some a^*, *i.e.* U_{a^*}, U_{2a^*}, U_{3a^*} are non-zero and all other modes vanish.

We found numerically that the steady-state current is maximised if all U_a are purely imaginary up to a small numerical error. As a result the optimal potential obeys $\widehat{U}(L/2+x) = -\widehat{U}(L/2-x)$. Demanding this throughout the maximisation scheme reduces the degrees of freedom to A, without changing the optimal shape $\widehat{U}(x)$ or the optimal current $\widehat{J}$.

We used `frprmn` [127] to obtain the results reported in the present work. The following heuristic proved efficient:

0. Initialisation: $A = 50$, $\mathcal{N}_\nu = 75$ and U_a for $a = -50, -49, \ldots, 50$ are initialised with $U_a = \mathring{\imath}/(2\pi a)$, which are the Fourier coefficients of a piece-wise periodic linear ratchet $U(x) = x$ for $x \in [0, L)$.

1. Given the other parameters, D, w, L, γ, as well as Eqs. (5.10) and (5.11) with the sum running up to $\mathcal{N}_\nu$, the optimal $\widehat{U}_a$ are determined using `frprmn` [127].

2. The results are written into a file and A is increased by 50. These additional degrees of freedom are initialised with 0. Those determined so far serve as initial values for the optimisation with increased A. The procedure returns to step 1.

Throughout the optimisation procedure, we determine the apparent radius of convergence of the power series Eq. (5.11) as the value of $\left(J^{(n)}\right)^{-1/n}$ for the largest (odd) n that produces a finite numerical value. If the optimisation procedure strays into a parameter region where this radius of convergence drops below unity, the supposed current becomes numerically unreliable. In this case, the optimisation is considered unattainable within the present perturbative framework and the optimisation is abandoned, *i.e.* we do not pursue the optimsation for these parameter values further and no results are shown in the present work. If, on the other hand, an optimal potential $\widehat{U}(x)$ is eventually found, we also determine the radius of convergence $\widehat{\nu^<_{\mathrm{roc}}}$, Eq. (5.12), *a posteriori* to ensure that it is greater than unity.

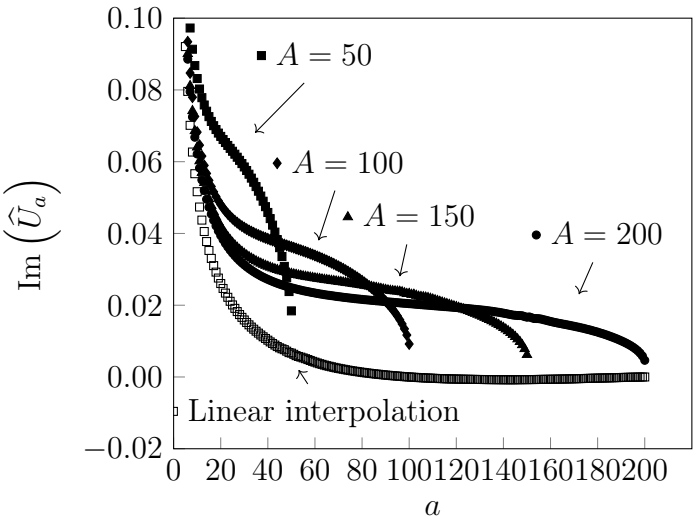


Figure 5.A.1: Imaginary part of the modes $\widehat{U}_a$ allowing for $A = 50, 100, 150, 200$ modes in the optimisation procedures (filled symbols) and, also, as extracted from the linear interpolation of the potential shown in Fig. 5.0.1 (open squares). Parameters are $D = 1$, $w = 1$, $L = 1$ and $\gamma = 1$, so that $Pe = Qe = \kappa = 1$.

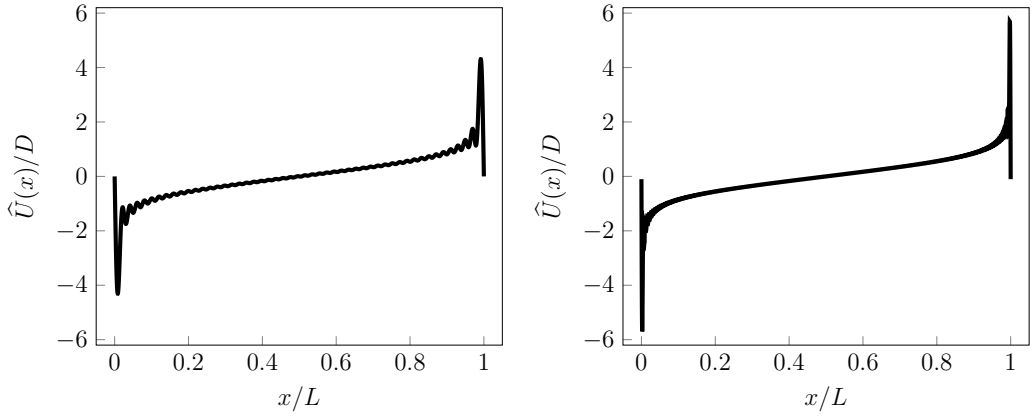
5.A.2 Plotting procedure

The plots Figs. 5.0.1 and 5.0.2 are generated as follows. With $\mathcal{N}_\nu = 75$ the modes $\widehat{U}_a$ are determined for $A = 100$, $A = 150$ and $A = 200$. Increasing A gives the optimisation procedure more degrees of freedom, which affects *all* modes, *e.g.* in general, $\widehat{U}_a$ determined with $A = 100$ differs from $\widehat{U}_a$ determined with $A = 150$ for all a, in particular at $a \leq 100$. Fig. 5.A.1 shows how $\widehat{U}_a$ changes with A, with the largest (relative) change visible for a close to A, whereas $\widehat{U}_a$ for smaller a suggest convergence.

Evaluating Eq. (5.25) in the form

$$\widehat{U}(x) = \frac{1}{L} \sum_{a=-A}^{A} \mathrm{e}^{\mathrm{i}k_a x} \widehat{U}_a \tag{5.13}$$

at numerically densely chosen positions x reveals an apparent undulation throughout and turning into some distinct peaks close to $x = 0$ and $x = L$ reminiscent of the Gibbs phenomenon [67], Fig. 5.A.2. The problem persists even at large A, although the undulations away from $x = 0, L$ become less noticeable.



(a) $A = 50$. **(b)** $A = 200$.

Figure 5.A.2: The optimal potential $\widehat{U}(x)$ of Fig. 5.0.1 shown with higher resolution of 2000 points and $A = 50, 200$ as indicated. The peaks around $x = 0$ and $x = L$ are likely to be artefacts, as discussed in the text.

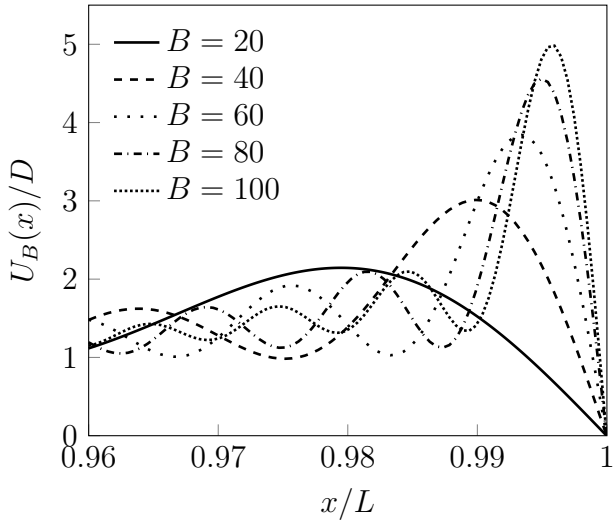


Figure 5.A.3: Detail of the potential $U_B(x)/D$ of Eq. (5.14) around the peak near $x/L = 1$ based on $A = 100$ modes using $B = 20, 40, 60, 80$ and 100 modes respectively in the sum. Parameters: $f = 0, D = 1$, $w = 1$, $L = 1$ and $\gamma = 1$, so that $Pe = Qe = \kappa = 1$.

This is confirmed in a modified sum,

$$U_B(x) = \frac{1}{L} \sum_{a=-B}^{B} \mathrm{e}^{\mathrm{i}k_a x} \widehat{U}_a \tag{5.14}$$

where the summation runs only over $B \leq A$ modes, *i.e.* it takes into account fewer modes in the plot than are available in the given numerical optimisation of the first A modes. As shown in Fig. 5.A.3, the resulting sharp peaks around $x = 0$ and $x = L$ are present even for moderate values of B, although they, of course, change shape. This suggests that their presence in Fig. 5.A.2 is not due to the relatively big error of $\widehat{U}_a$ at a around A, but due to the Gibbs phenomenon, which arises when a Fourier-sum of a discontinuous function is terminated after finitely many terms, even when the infinite sum is exact. In other words, some features around $x = 0$ and $x = L$ are not due to poor numerical estimates of $\widehat{U}_a$ as A is finite, but instead caused by the Gibbs phenomenon, *i.e.* using a finite number of modes to describe a discontinuous function.

The plots shown in Figs. 5.0.1 and 5.0.2 are designed to show what we know about the potential $\widehat{U}(x)$ and quantify its convergence. To achieve this, we determine the modes of the best potential for $A = 100$, $A = 150$ and $A = 200$ and evaluate Eq. (5.13) at values of x incommensurate with all L/A in an attempt to avoid "resonances" and with spacing greater than the largest L/A. In Figs. 5.0.1 and 5.0.2 we choose x at multiples of $L/97$. The error bars in these plots indicate the range of $\widehat{U}(x)$ for the different A at the corresponding x. This procedure avoids artefacts due to the Gibbs phenomenon at $x = 0$ and $x = L$ as well as the undulations throughout finite A. However, given the comparative sparseness of the points, sharp features are not well resolved, in particular those close to $x = 0$ and $x = L$.

One might be tempted to linearly interpolate the points in the resulting plots, say Fig. 5.0.1. However, as shown in Fig. 5.A.1, determining the resulting modes U_a by Fourier-transform of such a linear interpolation, shows that they are generally a very poor match with the modes that gave rise to the plot in the first place, even when their inverse Fourier transform reproduces Fig. 5.0.1 perfectly. Only the very low modes up to $|a| = 5$ agree within 10%. As a result, the current of 200 such modes produces only $JL^2/D = 0.01872...$, and is thus reduced by a factor 0.5 compared to

the optimal current obtained originally.

The plotting procedure used in the main text thus provides a useful representation of the potential in real space with suitable indication of how reliably we have determined certain features. The ambiguity arises because the optimisation procedure produces modes, as shown in Fig. 5.A.1 rather than an estimate of the shape in real space.

To clarify the nature of the optimal potential, we want to give the amplitude of all modes. By the nature of our setup, it is natural to start with a fewer number of modes and then incorporate the higher frequency modes. Using the parameters of Figure 5.0.1, a table is shown below to compare the current of the optimal potential with a different number of modes.

Number of modes	Optimal current
50	0.03694...
100	0.03757...
150	0.03778...
200	0.03789...

We should also note that, similar to the piecewise linear ratchet in Chapter 3, it is possible for the derivative of the potential to be non-continuous as long as the probability density and the current are both continuous at the discontinuity. Since we are adopting a Fourier series approach, the above conditions are satisfied.

5.B Field theory

In this section, we give a derivation of the path-integral formulation of RnT motion in a periodic potential using Doi-Peliti field theory. The coupled Fokker-Planck equations describing an RnT particle in a periodic potential $\nu U(x)$ are, similar to Eqs. (5.70),

$$\begin{aligned}\partial_t\rho_+(x,t) &= -\partial_x[(w-f-\nu U'(x))\rho_+(x,t)] - \gamma(\rho_+(x,t)-\rho_-(x,t)) + D\partial_x^2\rho_+(x,t)\\ \partial_t\rho_-(x,t) &= -\partial_x[(-w-f-\nu U'(x))\rho_-(x,t)] - \gamma(\rho_-(x,t)-\rho_+(x,t)) + D\partial_x^2\rho_-(x,t)\end{aligned} \tag{5.15a}$$

where $\rho_+(x,t)$ and $\rho_-(x,t)$ are the densities of right-moving and left-moving particles respectively, as a function of the position x and time t. The dashed potential $U'(x)$ denotes its derivative. We further introduce the total particle density $\rho(x,t) = \rho_+(x,t) + \rho_-(x,t)$ and the polarity $\mu(x,t) = \rho_+(x,t) - \rho_-(x,t)$, so that the particle current

$$J(x,t) = \big(w - f - \nu U'(x) - D\partial_x\big)\rho_+(x,t) + \big(-w - f - \nu U'(x) - D\partial_x\big)\rho_-(x,t) \quad (5.16)$$

can be re-written as

$$J(x,t) = w\mu(x,t) - \rho(x,t)(\nu U'(x) + f) - D\partial_x\rho(x,t) \quad (5.17)$$

and the Fokker-Planck equation as

$$\begin{aligned}\partial_t\rho(x,t) &= -\partial_x[w\mu(x,t) - \rho(x,t)(\nu U'(x) + f) - D\partial_x\rho(x,t)] = -\partial_x J(x,t)\\ \partial_t\mu(x,t) &= -\partial_x[w\rho(x,t) - \mu(x,t)(\nu U'(x) + f)] - 2\gamma\mu(x,t) + D\partial_x^2\mu(x,t)\ .\end{aligned} \quad (5.18)$$

The Fokker-Planck equation describes the evolution of a particle density. *A priori*, it does not enforce the particle entity of the constituent degrees of freedom, nor is it concerned with it — the *densities* $\rho_\pm$ above are completely unconstrained by being due to particles and could equally describe, say, a temperature profile. To cast it into a Doi-Peliti field theory, the Fokker-Planck equation is normally re-written as a master equation by discretising space and interpreting it as the evolution of the *probability (density)* of finding a *single particle* at a particular position, before generalising it to the evolution of *multiple, indistinguishable particles* and the probability of obtaining a particular *occupation number configuration*. In the canonical procedure [28, 161] the field-theoretic action is then obtained by expressing the evolution in terms of ladder operators, turning them into conjugate fields and taking the continuum limit. This procedure invariably reproduces the Fokker-Planck operator in the action $\mathcal{A}$ [129], which after rearranging can be expressed as the sum $\mathcal{A} = \mathcal{A}_0 + \mathcal{A}_1$ of

a harmonic part

$$\mathcal{A}_0 = \int_0^L \mathrm{d}x \int \mathrm{d}t\, \widetilde{\phi}(x,t)(\partial_t + w\partial_x - f\partial_x - D\partial_x^2 + r)\phi(x,t) + \\ \widetilde{\psi}(x,t)(\partial_t - w\partial_x - f\partial_x - D\partial_x^2 + r)\psi(x,t) + \gamma\big(\widetilde{\phi}(x,t) - \widetilde{\psi}(x,t)\big)\big(\phi(x,t) - \psi(x,t)\big) \tag{5.19}$$

and a perturbative part,

$$\mathcal{A}_1 = \int_0^L \mathrm{d}x \int \mathrm{d}t\, \nu\big(\partial_x\widetilde{\phi}(x,t)\big)U'(x)\phi(x,t) + \nu\big(\partial_x\widetilde{\psi}(x,t)\big)U'(x)\psi(x,t) \tag{5.20}$$

where $\phi(x,t)$ and $\psi(x,t)$ are the annihilation fields of a right-moving and a left-moving particle respectively and $\widetilde{\phi}(x,t)$ and $\widetilde{\psi}(x,t)$ are, correspondingly, the Doi-shifted [28] creation fields of a right-moving and a left-moving particle so that $\phi^\dagger = \tilde{\phi} + 1$ and $\psi^\dagger = \tilde{\psi} + 1$. We have included in the harmonic part a positive *mass* r as to regularise the infrared and restore causality. The mass is a mere technicality and will be taken to 0^+ whenever suitable. The perturbative part of the action $\mathcal{A}_1$ in Eq. (5.20) incorporates the perturbative parameter ν in front of the potential $U(x)$ to guide the perturbation theory that is to follow.

The expectation of an observable in terms of fields is taken via the path-integral [62]

$$\langle \bullet \rangle = \int \mathcal{D}[\phi, \tilde{\phi}, \psi, \tilde{\psi}] \bullet e^{-\mathcal{A}[\phi,\tilde{\phi},\psi,\tilde{\psi}]}. \tag{5.21}$$

Only at $\nu = 0$ this path integral can generally be taken in closed form,

$$\langle \bullet \rangle_0 = \int \mathcal{D}[\phi, \tilde{\phi}, \psi, \tilde{\psi}] \bullet e^{-\mathcal{A}_0[\phi,\tilde{\phi},\psi,\tilde{\psi}]} \tag{5.22}$$

about which the action in the perturbative part is expanded, so that

$$\langle \bullet \rangle = \sum_{n=0}^{\infty} \frac{1}{n!} \langle \bullet (-\mathcal{A}_1)^n \rangle_0 \ . \tag{5.23}$$

To make the action local in the fields, we introduce a Fourier representation in the

form

$$\phi(x,t) = \frac{1}{L}\sum_{a=-\infty}^{\infty} \mathrm{e}^{\mathring{\imath}k_a x} \int_{-\infty}^{\infty} \text{đ}\omega\, \mathrm{e}^{-\mathring{\imath}\omega t}\phi_a(\omega) \tag{5.24}$$

and correspondingly for all other fields and observables, with $\text{đ}\omega = \mathrm{d}\omega/(2\pi)$ and $k_a = 2\pi a/L$, which readily accommodates the periodic nature of x. For example the potential in real space is expressed as

$$U(x) = \frac{1}{L}\sum_{a=-\infty}^{\infty} \mathrm{e}^{\mathring{\imath}k_a x} U_a \quad \text{with} \quad U_a = \int_0^L \mathrm{d}x\, \mathrm{e}^{-\mathring{\imath}k_a x} U(x) \tag{5.25}$$

in terms of its *modes* or coefficients U_a.

The bare propagators are easily determined from Eq. (5.19) in the form

$$\mathcal{A}_0 = \frac{1}{L}\sum_a \int \text{đ}\omega \begin{pmatrix} \widetilde{\phi}_{-a}(-\omega) \\ \widetilde{\psi}_{-a}(-\omega) \end{pmatrix}^{\top} \underline{\underline{A}}_a(\omega) \begin{pmatrix} \widetilde{\phi}_a(\omega) \\ \widetilde{\psi}_a(\omega) \end{pmatrix} \tag{5.26}$$

with

$$\underline{\underline{A}}_a(\omega) = \begin{pmatrix} -\mathring{\imath}\omega + Dk_a^2 + \mathring{\imath}wk_a - \mathring{\imath}fk_a + r + \gamma & -\gamma \\ -\gamma & -\mathring{\imath}\omega + Dk_a^2 - \mathring{\imath}wk_a - \mathring{\imath}fk_a + r + \gamma \end{pmatrix} \tag{5.27}$$

by calculating the inverse

$$\Big(\underline{\underline{A}}_a(\omega)\Big)^{-1} \text{đ}(\omega+\omega')L\delta_{a+b,0} = \begin{pmatrix} \langle\phi_a(\omega)\phi_b(\omega')\rangle & \langle\phi_a(\omega)\psi_b(\omega')\rangle \\ \langle\psi_a(\omega)\psi_b(\omega')\rangle & \langle\psi_a(\omega)\phi_b(\omega')\rangle \end{pmatrix} \tag{5.28}$$

with the Kronecker δ-function denoted by $\delta_{a+b,0}$ and the Dirac δ-function by $\text{đ}(\omega) =$

$2\pi\delta(\omega)$. The propagators are then found to be

$$\left\langle \phi_a(\omega)\widetilde{\phi}_b(\omega')\right\rangle_0 = \frac{\Gamma_a(\omega;r)\delta(\omega+\omega')L\delta_{a+b,0}}{\Gamma_a(\omega;r)\Gamma_{-a}(\omega;r)-\gamma^2} \qquad \hat{=}\ \phi_a(\omega) \quad \tilde{\phi}_b(\omega') \tag{5.29a}$$

$$\left\langle \psi_a(\omega)\widetilde{\psi}_b(\omega')\right\rangle_0 = \frac{\Gamma_{-a}(\omega;r)\delta(\omega+\omega')L\delta_{a+b,0}}{\Gamma_a(\omega;r)\Gamma_{-a}(\omega;r)-\gamma^2} \qquad \hat{=}\ \psi_a(\omega) \quad \tilde{\psi}_b(\omega') \tag{5.29b}$$

$$\left\langle \phi_a(\omega)\widetilde{\psi}_b(\omega')\right\rangle_0 = \frac{\gamma\delta(\omega+\omega')L\delta_{a+b,0}}{\Gamma_a(\omega;r)\Gamma_{-a}(\omega;r)-\gamma^2} \qquad \hat{=}\ \phi_a(\omega) \quad \tilde{\psi}_b(\omega') \tag{5.29c}$$

$$\left\langle \psi_a(\omega)\widetilde{\phi}_b(\omega')\right\rangle_0 = \frac{\gamma\delta(\omega+\omega')L\delta_{a+b,0}}{\Gamma_a(\omega;r)\Gamma_{-a}(\omega;r)-\gamma^2} \qquad \hat{=}\ \psi_a(\omega) \quad \tilde{\phi}_b(\omega') \tag{5.29d}$$

where we have introduced

$$\Gamma_a(\omega;r) = -\mathring{\imath}\omega + Dk_a^2 - \mathring{\imath}wk_a - \mathring{\imath}fk_{|a|} + r + \gamma \tag{5.30}$$

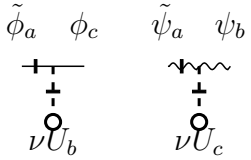
to ease notation.

After Fourier-transforming, the perturbative part of the action, Eq. (5.20) reads

$$\mathcal{A}_1 = -\frac{1}{L^3}\sum_{a,b,c} L\delta_{a+b+c,0}\int \mathrm{d}\omega\, \nu\big(k_a\widetilde{\phi}_a(\omega)\big)k_bU_b\phi_c(-\omega) + \nu\big(k_a\widetilde{\psi}_a(\omega)\big)k_bU_b\psi_c(-\omega) \tag{5.31}$$

which effectively destroys momentum conservation, as any mismatch $a+c\neq 0$ can be made up by the Fourier modes b of the potential, U_b. Each order in the perturbative expansion thus requires a summation over the momenta, similar to integrating a loop.

The ensuing diagrammatics significantly simplifies the bookkeeping. The external potential vertex may be written as



(5.32)

with the bauble representing the external potential, which supplies the missing momentum. The short, thick dashes across (amputated) propagators indicate diagrammatically the factors k_a and k_b, Eq. (5.31). Eq. (5.32) corrects the propagators as shown in Eq. (5.2). Unfortunately, the (Dyson) summation can generally not be per-

formed in closed form, but rather needs to be done order by order in the perturbative parameter ν. How this is done to determine steady-state expectations is described in the next section.

5.C Steady-state density and current

In the following, we present the details of the derivation of the steady-state particle densities

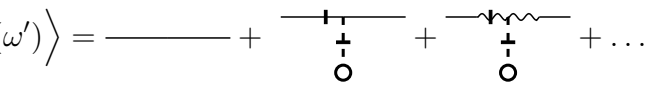
$$\rho_+(x) = \lim_{t_0\to-\infty} \left\langle \phi(x,t)\widetilde{\phi}(x_0,t_0)\right\rangle = \lim_{t_0\to-\infty} \left\langle \phi(x,t)\widetilde{\psi}(x_0,t_0)\right\rangle \tag{5.33a}$$

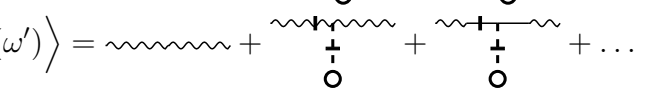
$$\rho_-(x) = \lim_{t_0\to-\infty} \left\langle \psi(x,t)\widetilde{\phi}(x_0,t_0)\right\rangle = \lim_{t_0\to-\infty} \left\langle \psi(x,t)\widetilde{\psi}(x_0,t_0)\right\rangle \ , \tag{5.33b}$$

independent of t and x_0 given the limit to the steady state and ergodicity due to the perturbation theory about vanishing potential at positive tumbling rate γ. We will firstly give a rather general argument about the effect of the limit $t_0 \to -\infty$ on diagrams, before focusing on the present field theory.

5.C.1 General arguments

The diagrammatic expansion of the propagators, Eq. (5.2) or

$\left\langle \phi_a(\omega)\widetilde{\phi}_b(\omega')\right\rangle =$  (5.34)

$\left\langle \psi_a(\omega)\widetilde{\psi}_b(\omega')\right\rangle =$  (5.35)

is most easily written in Fourier space, where the steady-state limit $t_0 \to -\infty$ has the effect of restricting any incoming frequency and momentum to $\omega' = 0$ and $b = 0$. We discuss this mechanism, which is very widely applicable, in the following.

Firstly, any tree-like contribution to, say, $\left\langle \phi_a(\omega)\widetilde{\phi}_b(\omega')\right\rangle$ has an incoming right bare propagator as well as a number of internal bare propagators, which each "carry" all of ω'. Given the pre-factor of $\delta(\omega+\omega')$ of each diagram, taking the Fourier transform

in t and t_0 of such a diagram amounts to identifying the poles p_i in ω' throughout, so that in direct time, the nth order contribution to the propagator generally has the structure

$$\left\langle \phi_a(t)\widetilde{\phi}_b(t_0)\mathcal{A}_1^n \right\rangle_0 = \sum_i \mathrm{e}^{\mathring{\imath}(t-t_0)p_i}\mathcal{F}_{ab}(p_i) \tag{5.36}$$

with some (complicated) $\mathcal{F}_{ab}(p_i)$ determined by the residues. By causality, all poles in ω' have positive imaginary part, provided the mass r is positive. Taking the limit $t_0 \to -\infty$ selects those poles that vanish in the limit $r \downarrow 0$. In tree diagrams, these poles are entirely given by the bare propagators, featuring as external or internal legs.

The poles of the bare propagators Eq. (5.29) are determined by

$$\begin{aligned} 0 &= \Gamma_a(\omega;r)\Gamma_{-a}(\omega;r) - \gamma^2 \\ &= \Big(\mathring{\imath}\omega' + Dk_b^2 + r + 2\gamma\Big)\Big(\mathring{\imath}\omega' + Dk_b^2 + r\Big) + 2\mathring{\imath}fk_b(\mathring{\imath}\omega' + Dk_b^2 + r + \gamma) + (wk_b)^2 - f^2k_b^2 \end{aligned} \tag{5.37}$$

using $b = -a$ from $\delta_{a+b,0}$ and $\omega' = -\omega$ from $\delta(\omega'+\omega)$ in the numerators of Eqs. (5.29). It is immediately clear that any $\mathring{\imath}\omega' + r$ that solves this equation cannot be arbitrarily small for any $\mathbb{Z} \ni b \neq 0$. This leaves us with requiring $b = 0$, which has one pole that vanishes at $r \downarrow 0$, namely $\omega' = \mathring{\imath}r$. Taking $t_0 \to -\infty$ after Fourier transforming and $r \downarrow 0$ therefore leaves only those propagators that have $a = -b = 0$.

Because of the structure of the vertex, Eq. (5.31), the perturbative contributions to the full propagators due to tree-level diagrams such as Eq. (5.2) all have dashed internal and outgoing propagators, *i.e.* they all, except the incoming leg, carry a prefactor k_a, so that they each vanish for vanishing momentum. Taking therefore the limit $t_0 \to -\infty$, leaves (of the many residues there might be), only those that do not carry such an extra factor $k_a = 0$ of a momentum. In the present field theory, the only such bare propagator is the incoming leg. We will next determine its value in the limit $t_0 \to -\infty$ and the effect that this limit has on the rest of the diagram. We can safely assume that this pole is simple, because if it was repeated by being equally the pole of another propagator, its residue must vanish, because any such other propagator is guaranteed to carry a factor of k_a.

At $a = 0$ the poles Eq. (5.37) are conveniently written as $(-\mathring{\imath}\omega + r + 2\gamma)(-\mathring{\imath}\omega + r) = 0$, leaving a factor of 2γ in the denominator as a residue. As far as the numer-

ators of the propagators are concerned, Eqs. (5.29a) and (5.29b) produce a factor of $\Gamma_0(-\mathring{\imath}r;r)\delta(\omega+\omega')L\delta_{a+b,0}$ and Eqs. (5.29c) and (5.29d) a factor of $\gamma\delta(\omega+\omega')L\delta_{a+b,0}$, which are in fact the same as $\Gamma_0(-\mathring{\imath}r;r)=\gamma$, Eq. (5.30).

This mechanism of taking the Fourier transform in ω' and ω and taking the limit $t_0\to-\infty$ after $r\downarrow 0$ thus has the effect of replacing any incoming bare propagator such as $\left\langle\phi_a(t)\widetilde{\phi}_b(t_0)\right\rangle_0$ by $\gamma L\delta_{a+b,0}\delta_{b,0}/(2\gamma)$, where $\delta_{b,0}$ enforces that only $b=0=-a$ ever contributes. Taking further the inverse Fourier-sum over b, Eq. (5.24), and transforming t back to ω then gives

$$\lim_{t_0\to-\infty}\lim_{r\downarrow 0}\left\langle\phi_a(\omega)\widetilde{\phi}(x_0,t_0)\right\rangle_0=\frac{1}{L}\sum_b \mathrm{e}^{\mathring{\imath}k_bx_0}\int\mathrm{d}t\,\mathrm{e}^{\mathring{\imath}\omega t}\lim_{t_0\to-\infty}\lim_{r\downarrow 0}\left\langle\phi_a(t)\widetilde{\phi}_b(t_0)\right\rangle_0=\frac{1}{2}\delta\!\!\!^{-}(\omega)\delta_{a,0} \tag{5.38}$$

which is identically the same for all bare propagators Eqs. (5.29). Within a diagram the effect of the limit $t_0\to-\infty$ is thus a pre-factor determined by the diagram and an amputation, as both ω and a are forced to vanish. Because the internal field $\phi_a(\omega)$ will feature in an integral $\int\mathrm{d}\!\!\!^{-}\omega$, the $\delta\!\!\!^{-}(\omega)$ will simply be integrated out, whereas the sum over the spatial modes, $L^{-1}\sum_a$ will leave behind a factor $1/L$. In summary, the limit $t_0\to-\infty$ in a bare propagator is given by Eq. (5.38) and in all the diagrams considered here, amounts to an amputation of the incoming leg and a multiplication by of the diagram by $1/(2L)$.

After the removal of the incoming leg and thus setting effectively $-\mathring{\imath}\omega+r=0$ throughout a diagram, some residues of the form

$$k_c^2\left(\Gamma_c(-\mathring{\imath}r;r)\Gamma_{-c}(-\mathring{\imath}r;r)-\gamma^2\right)^{-1}=\frac{k_c^2}{(Dk_c^2)^2+(w^2+2D\gamma)k_c^2-2\mathring{\imath}fk_c(Dk_c^2+r+\gamma)-f^2k_c^2} \tag{5.39}$$

feature with index c still to be summed over. At $k_c=0$ such residues are in fact repeated poles of ω', that are, however, bound to vanish as argued above. Cancelling k_c^2 in numerator and denominator for $c=0$ nevertheless ignores the fact that the term

that gives rise to it,

$$\begin{aligned}&k_c^2\left(\Gamma_c(\omega;r)\Gamma_{-c}(\omega;r)-\gamma^2\right)^{-1}\\ =&\frac{k_c^2}{\Big(-\mathring{\imath}\omega+Dk_c^2+r+2\gamma\Big)\Big(-\mathring{\imath}\omega+Dk_c^2+r\Big)+(wk_c)^2-2\mathring{\imath}fk_c(Dk_c^2+r+\gamma-f^2k_c^2)}\end{aligned} \tag{5.40}$$

strictly vanishes at $c = 0$. This is the reason for the introduction of the indicator function

$$\mathcal{I}_a = 1-\delta_{a,0} = \begin{cases} 0 & \text{for } a=0 \\ 1 & \text{otherwise} \end{cases}. \tag{5.41}$$

As $c \in \mathbb{Z}$, this is merely a matter of bookkeeping and algebra, not a matter of complex analysis or exchange of limits, as is illustrated by the example

$$\lim_{t_0\to-\infty}\lim_{r\downarrow 0}\int \text{đ}\omega'\,\mathrm{e}^{-\mathring{\imath}\omega' t_0}\frac{Dk_c^2}{\mathring{\imath}\omega'+Dk_c^2+r}\frac{1}{\mathring{\imath}\omega'+r} = \begin{cases} 0 & \text{for } c=0 \qquad (5.42a)\\ 1 & \text{otherwise} \qquad (5.42b)\end{cases}$$

for any $c \in \mathbb{Z}$.

5.C.2 Steady-state density of Run-and-Tumble particles in a periodic potential

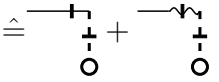
On the basis of the mechanism outlined above, we can write down a perturbative expansion Eq. (5.23) of the steady-state density, for example

$$\begin{aligned}\lim_{t_0\to-\infty}\left\langle\phi_a(t)\widetilde{\phi}(x_0,t_0)\right\rangle &= \lim_{t_0\to-\infty}\left\langle\phi_a(t)\widetilde{\psi}(x_0,t_0)\right\rangle\\ &= \lim_{t_0\to-\infty}\left\langle\phi_a(t)\widetilde{\phi}(x_0,t_0)\right\rangle_0 + \lim_{t_0\to-\infty}\left\langle\phi_a(t)\widetilde{\phi}(x_0,t_0)(-\mathcal{A}_1)\right\rangle_0+\ldots\end{aligned} \tag{5.43}$$

where we have trivially taken the inverse Fourier transform from ω to t. The limit $\lim_{t_0\to-\infty}\left\langle\phi_a(t)\widetilde{\phi}(x_0,t_0)\right\rangle_0 = \delta_{a,0}/2$ is given by Eq. (5.38), whereas the higher order terms are most easily calculated using the diagrammatics. The lowest order correc-

tions are of the form

$$\lim_{t_0\to-\infty}\left\langle\phi_a(t)\widetilde{\phi}(x_0,t_0)(-\mathcal{A}_1)\right\rangle_0 \hat{=} \tag{5.44a}$$



$$\hat{=}(-k_a\mathcal{I}_a)\frac{\Gamma^0_a}{\Gamma^0_a\Gamma^0_{-a}-\gamma^2}\Big(\nu k_a U_a\Big)\frac{1}{2L}+(-k_a\mathcal{I}_a)\frac{\gamma\mathcal{I}_a}{\Gamma^0_a\Gamma^0_{-a}-\gamma^2}\Big(\nu k_a U_a\Big)\frac{1}{2L} \tag{5.44b}$$

$$=-\frac{(Dk_a^2-\mathring{\imath}wk_a-\mathring{\imath}fk_a+2\gamma)k_a\mathcal{I}_a}{D^2k_a^3+2D\gamma k_a+w^2k_a-2\mathring{\imath}f(Dk_a^2+r+\gamma)-f^2k_a}\frac{\nu U_a}{2L} \tag{5.44c}$$

where, again, the Fourier transform in ω is easily taken as no ω flows through the diagrams Eq. (5.44a), reducing any $\Gamma_a(\omega;r)$ in Eq. (5.29) to $\Gamma_a(0;r)$ and further to $\Gamma^0_a=\Gamma_a(0;0)=Dk_a^2-\mathring{\imath}wk_a-\mathring{\imath}fk_a+\gamma$ as $r\downarrow 0$. To arrive at Eq. (5.44b), we have firstly inserted the dash on the outgoing propagator due to the perturbation, $(-k_a\mathcal{I}_a)$, with the indicator function due to the $t_0\to-\infty$ mechanism, secondly the propagators Eqs. (5.29a) and (5.29c) respectively, both evaluated at $\omega=0$ and $r\downarrow 0$, thirdly the derivative of the potential due to the perturbation and finally a factor $1/(2L)$ due to the $t_0\to-\infty$ mechanism. The final line Eq. (5.44c) is then a matter of algebra.

As all bare propagators will be evaluated at $\omega'=0$ and $r\downarrow 0$ in the following, we introduce $X_a=Y_a^*$ and Z_a to ease notation,

$$\left\langle\phi_a(\omega)\widetilde{\phi}_b(\omega'=0)\right\rangle_0 k_{-a}\mathcal{I}_a=X_a\delta(\omega)L\delta_{a+b,0}$$

$$=\frac{Dk_a^2-\mathring{\imath}wk_a-\mathring{\imath}fk_a+\gamma}{k_a^2(D^2k_a^2+2D\gamma+w^2)-2\mathring{\imath}fk_a(Dk_a^2+r+\gamma)-f^2k_a^2}\delta(\omega)L\delta_{a+b,0}k_{-a}\mathcal{I}_a \tag{5.45a}$$

$$\left\langle\psi_a(\omega)\widetilde{\psi}_b(\omega'=0)\right\rangle_0 k_{-a}\mathcal{I}_a=Y_a\delta(\omega)L\delta_{a+b,0}$$

$$=\frac{Dk_a^2+\mathring{\imath}wk_a-\mathring{\imath}fk_a+\gamma}{k_a^2(D^2k_a^2+2D\gamma+w^2)-2\mathring{\imath}fk_a(Dk_a^2+r+\gamma)-f^2k_a^2}\delta(\omega)L\delta_{a+b,0}k_{-a}\mathcal{I}_a \tag{5.45b}$$

$$\left\langle\phi_a(\omega)\widetilde{\psi}_b(\omega'=0)\right\rangle_0 k_{-a}\mathcal{I}_a=Z_a\delta(\omega)L\delta_{a+b,0}$$

$$=\frac{\gamma}{k_a^2(D^2k_a^2+2D\gamma+w^2)-2\mathring{\imath}fk_a(Dk_a^2+r+\gamma)-f^2k_a^2}\delta(\omega)L\delta_{a+b,0}k_{-a}\mathcal{I}_a \tag{5.45c}$$

$$\left\langle\psi_a(\omega)\widetilde{\phi}_b(\omega'=0)\right\rangle_0 k_{-a}\mathcal{I}_a=Z_a\delta(\omega)L\delta_{a+b,0}$$

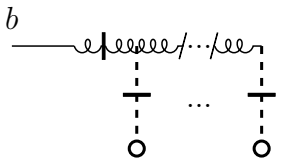
$$\frac{\gamma}{k_a^2(D^2k_a^2+2D\gamma+w^2)-2\mathring{\imath}fk_a(Dk_a^2+r+\gamma)-f^2k_a^2}\delta(\omega)L\delta_{a+b,0}k_{-a}\mathcal{I}_a \tag{5.45d}$$

where we have anticipated the factor $k_{-a}\mathcal{I}_a$ that each propagator will pick up.

Recurrence relation for density $\rho(x)$ and polarity $\mu(x)$

In the following, we obtain a recurrence relation of the orders in ν of $\rho(x)$ and $\mu(x)$ using their diagrammatic representation. To this end, we introduce a diagrammatic notation for the bth Fourier coefficient of the $(n-1)$th order steady-state density of right-moving particles

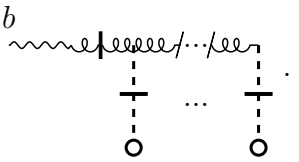
$$\nu^{n-1}\rho_{b+}^{(n-1)} = \lim_{t_0\to-\infty}\left\langle \phi_b(t)\widetilde{\phi}(x_0,t_0)\frac{(-\mathcal{A}_1)^{n-1}}{(n-1)!}\right\rangle_0 = \lim_{t_0\to-\infty}\left\langle \phi_b(t)\widetilde{\psi}(x_0,t_0)\frac{(-\mathcal{A}_1)^{n-1}}{(n-1)!}\right\rangle_0$$

$\hat{=}$ 

(5.46)

and the $(n-1)$th order steady-state density of left-moving particles

$$\nu^{n-1}\rho_{b-}^{(n-1)} = \lim_{t_0\to-\infty}\left\langle \phi_b(t)\widetilde{\phi}(x_0,t_0)\frac{(-\mathcal{A}_1)^{n-1}}{(n-1)!}\right\rangle_0 = \lim_{t_0\to-\infty}\left\langle \phi_b(t)\widetilde{\psi}(x_0,t_0)\frac{(-\mathcal{A}_1)^{n-1}}{(n-1)!}\right\rangle_0$$

$\hat{=}$ 

. (5.47)

As indicated by the dots, both diagrams, Eqs. (5.46) and (5.47), contain $n-1$ potential "baubles" and both are written in terms of "gluonic" propagators which we use to represent the sum over all possibilities of connecting the baubles to each other and finally to the external field. Much of what follows is about the bookkeeping of these diagrams. The lowest order is given by Eq. (5.38),

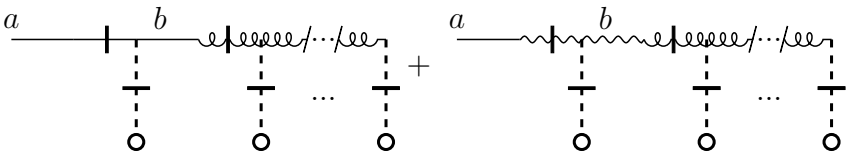
$$\rho_{a+}^{(0)} = \rho_{a-}^{(0)} = \frac{1}{2}\delta_{a,0}\ , \tag{5.48}$$

after the inverse Fourier transform that simply removes $\tilde{\delta}(\omega)$.

To construct the n order diagrams of both particle species we need to attach a potential bauble to the $n-1$th order diagrams. Any such potential term Eq. (5.31) comes with a summation over all three indices associated with its three terms, namely the potential, a creator field with a derivative and an annihilator field. By adding a fur-

ther perturbative term in this way, both $\rho_{a+}^{(n)}$ and $\rho_{a-}^{(n)}$ each acquire two contributions due to $\rho_{b+}^{(n-1)}$ and $\rho_{b-}^{(n-1)}$, both connecting to $\rho_{b+}^{(n)}$ and $\rho_{b-}^{(n)}$ using Eq. (5.32) and a suitable propagator Eq. (5.29). The resulting terms are

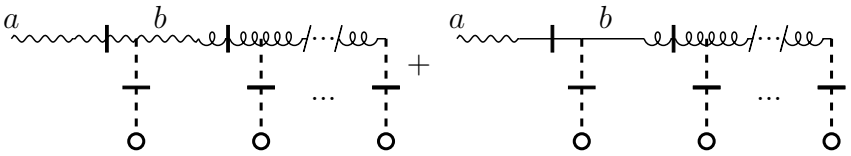
$$\nu^n \rho_{a+}^{(n)} \hat{=} \tag{5.49a}$$



$$\hat{=} \frac{1}{L} \sum_b k_{a-b} \nu U_{a-b} \Big(X_a \nu^{n-1} \rho_{b+}^{(n-1)} + Z_a \nu^{n-1} \rho_{b-}^{(n-1)} \Big) \tag{5.49b}$$

and

$$\nu^n \rho_{a-}^{(n)} \hat{=} \tag{5.50a}$$



$$\hat{=} \frac{1}{L} \sum_b k_{a-b} \nu U_{a-b} \Big(Z_a \nu^{n-1} \rho_{b+}^{(n-1)} + Y_a \nu^{n-1} \rho_{b-}^{(n-1)} \Big) \ . \tag{5.50b}$$

Using Eqs. (5.49) and (5.48) with $n = 1$ produces for example Eqs. (5.44),

$$\nu \rho_{a+}^{(1)} = \frac{1}{L} k_a \nu U_a (X_a + Z_a) \frac{1}{2} \tag{5.51}$$

with Eqs. (5.45a) and (5.45c).

In the following, it is more instructive to work with the density

$$\rho_a^{(n)} = \rho_{a+}^{(n)} + \rho_{a-}^{(n)} \quad \text{so that} \quad \rho(x) = \frac{1}{L} \sum_{a=-\infty}^{\infty} \mathrm{e}^{\mathrm{i} k_a x} \sum_{n=0}^{\infty} \nu^n \rho_a^{(n)} \tag{5.52a}$$

and the polarity

$$\mu_a^{(n)} = \rho_{a+}^{(n)} - \rho_{a-}^{(n)} \quad \text{so that} \quad \mu(x) = \frac{1}{L} \sum_{a=-\infty}^{\infty} \mathrm{e}^{\mathrm{i} k_a x} \sum_{n=0}^{\infty} \nu^n \mu_a^{(n)} \ , \tag{5.52b}$$

and write the convolutions Eqs. (5.49) and (5.50) in terms of a single matrix equation

$$\begin{pmatrix} \rho_a^{(n)} \\ \mu_a^{(n)} \end{pmatrix} = \underline{\underline{M_a}} \sum_{b=-\infty}^{\infty} W_{a-b} \begin{pmatrix} \rho_b^{(n-1)} \\ \mu_b^{(n-1)} \end{pmatrix} \tag{5.53}$$

with

$$W_{a-b} = \frac{k_{a-b} U_{a-b}}{L} \tag{5.54}$$

and the matrix

$$\begin{aligned} \underline{\underline{M_a}} &= \frac{1}{2} \begin{pmatrix} X_a + Y_a + 2Z_a & X_a - Y_a \\ X_a - Y_a & X_a + Y_a - 2Z_a \end{pmatrix} \\ &= \frac{(-k_a)\mathcal{I}_a}{k_a^2(D^2k_a^2 + 2D\gamma + w^2) - 2\mathring{\imath} f k_a (Dk_a^2 + \gamma) - f^2 k_a^2} \begin{pmatrix} Dk_a^2 + 2\gamma - \mathring{\imath} f k_a & -\mathring{\imath} w k_a \\ -\mathring{\imath} w k_a & Dk_a^2 - \mathring{\imath} f k_a \end{pmatrix}, \end{aligned} \tag{5.55}$$

as a function of the mode a, closely related to Eq. (5.28). Eqs. (5.53) and (5.55) are the main result of the present section as they determine density and polarity to arbitrary order in ν. As a sanity check, we may verify that both density $\rho(x)$ and polarity $\mu(x)$, Eqs. (5.52), are real, or equivalently that complex conjugates of the modes obey $\left(\rho_a^{(n)}\right)^* = \rho_{-a}^{(n)}$ and $\left(\mu_a^{(n)}\right)^* = \mu_{-a}^{(n)}$. This can be done by induction, assuming that $\left(\rho_a^{(n-1)}\right)^* = \rho_{-a}^{(n-1)}$ and $\left(\mu_a^{(n-1)}\right)^* = \mu_{-a}^{(n-1)}$, and further observing that $\left(\underline{\underline{M_a}}\right)^* = -\underline{\underline{M_{-a}}}$ from Eq. (5.55) and that a real external potential implies $\left(W_{a-b}\right)^* = -W_{b-a}$. From Eq. (5.48) we have

$$\begin{pmatrix} \rho_a^{(0)} \\ \mu_a^{(0)} \end{pmatrix} = \begin{pmatrix} 1 \\ 0 \end{pmatrix} \delta_{a,0} \tag{5.56}$$

as induction basis and, more importantly, as the staring point for the systematic calculation Eq. (5.53) of the modes of the density and polarity Eq. (5.52). With that established, we may write Eq. (5.9)

$$\begin{pmatrix} \rho_{a_1}^{(n)} \\ \mu_{a_1}^{(n)} \end{pmatrix} = \underline{\underline{M_{a_1}}} \sum_{a_2, a_3, \ldots, a_n = -\infty}^{\infty} W_{a_1 - a_2} \underline{\underline{M_{a_2}}} W_{a_2 - a_3} \underline{\underline{M_{a_3}}} \cdots W_{a_{n-1} - a_n} \underline{\underline{M_{a_n}}} W_{a_n} \begin{pmatrix} 1 \\ 0 \end{pmatrix}, \tag{5.57}$$

with each of the $n-1$ indeces running from $-\infty$ to ∞. We will now turn our atten-

tion to the steady-state current.

5.C.3 Steady-state current

From Fick's law of diffusion and the coupled Fokker-Planck equation, the steady-state probability current $J(x)$ reads

$$J(x) = w\mu(x) - (\nu U'(x) + f)\rho(x) - D\partial_x\rho(x) \ , \tag{5.58}$$

which in the steady state must in fact be constant in x. We will demonstrate this property perturbatively, order by order in ν. To this end, we introduce the inverse Fourier-transforms

$$\rho^{(n)}(x) = \frac{1}{L}\sum_{a=-\infty}^{\infty} \mathrm{e}^{\mathrm{i}k_a x}\rho_a^{(n)} \tag{5.59a}$$

$$\mu^{(n)}(x) = \frac{1}{L}\sum_{a=-\infty}^{\infty} \mathrm{e}^{\mathrm{i}k_a x}\mu_a^{(n)} \tag{5.59b}$$

of the nth order Fourier coefficients $\rho_a^{(n)}$ and $\mu_a^{(n)}$, similar to Eq. (5.52). The steady-state current $J(x)$ in Eq. (5.58) may then be written order by order in ν,

$$J(x) = \sum_{n=0}^{\infty} \nu^n J^{(n)}(x) \tag{5.60}$$

with $J^{(n)}(x)$ for $n > 0$ extracted from Eq. (5.58) by identifying terms of order n in ν,

$$J^{(n)}(x) = w\mu^{(n)}(x) - \rho^{(n-1)}(x)U'(x) - f\rho^{(n)}(x) - D\partial_x\rho^{(n)}(x) \ . \tag{5.61}$$

We will proceed by showing that $J^{(n)}(x)$ is constant in x and can easily be expressed in terms of the Fourier coefficients $\rho_a^{(n)}$ and $\mu_a^{(n)}$ using Eqs. (5.59) and (5.53),

$$J^{(n)}(x) = -\rho^{(n-1)}(x)U'(x)\frac{1}{L} + \sum_{a,b=-\infty}^{\infty} \mathrm{e}^{\mathrm{i}k_a x} \begin{pmatrix} -D\mathrm{i}k_a - f \\ w \end{pmatrix}^{\top} \underline{\underline{M_a}}\, W_{a-b} \begin{pmatrix} \rho_b^{(n-1)} \\ \mu_b^{(n-1)} \end{pmatrix} \ . \tag{5.62}$$

By direct calculation the linear algebra involving $\underline{\underline{M_a}}$, Eq. (5.55), simplifies drastically,

$$\begin{pmatrix} -D\mathring{\imath}k_a - f \\ w \end{pmatrix}^\top \underline{\underline{M_a}} = \mathring{\imath}\mathcal{I}_a \begin{pmatrix} 1 \\ 0 \end{pmatrix}^\top . \tag{5.63}$$

The first term in Eq. (5.62) can be written in modes as

$$\rho^{(n-1)}(x)U'(x) = \frac{1}{L^2}\sum_{a,b=-\infty}^{\infty} \mathrm{e}^{\mathring{\imath}k_a x}\mathrm{e}^{\mathring{\imath}k_b x}\rho_b^{(n-1)}\mathring{\imath}k_a U_a = \frac{\mathring{\imath}}{L}\sum_{a,b=-\infty}^{\infty} \mathrm{e}^{\mathring{\imath}k_a x}\rho_b^{(n-1)}W_{a-b} \tag{5.64}$$

with Eqs. (5.25) and (5.54) and using $k_{a-b} + k_b = k_a$ after shifting the dummy index a by $-b$, so that the final expression is the inverse Fourier-transform of a convolution. Using Eqs. (5.63) and (5.64) in Eq. (5.62) finally gives

$$J^{(n)}(x) = \frac{\mathring{\imath}}{L}\sum_{a,b=-\infty}^{\infty} \mathrm{e}^{\mathring{\imath}k_a x}\rho_b^{(n-1)}W_{a-b}(-1+\mathcal{I}_a) = -\frac{\mathring{\imath}}{L}\sum_{b=-\infty}^{\infty} \rho_b^{(n-1)}W_{-b} \tag{5.65}$$

using the definition of the indicator function, $\mathcal{I}_a = 1 - \delta_{a,0}$. Eq. (5.65) not only shows that every perturbative order of the steady-state current is independent of the position x, as it should be, but also expresses the current to order n in terms of the density to order $n-1$. The 0th order of current follows immediately from Eq. (5.58) as

$$J^{(0)}(x) = w\mu^{(0)}(x) - D\partial_x\rho^{(0)}(x) - f\rho^{(0)}(x) = -f/L \tag{5.66}$$

because $\mu^{(0)}(x) = 0$ and $\rho^{(0)}(x) = 1/L$ from the inverse Fourier transform of Eq. (5.56).

Eq. (5.65) is the main result of the present section. With Eq. (5.57) we can write it as Eq. (5.10),

$$\begin{aligned} J^{(n)}(x) = -\frac{\mathring{\imath}}{L}\sum_{a_1,a_2,\ldots,a_{n-1}=-\infty}^{\infty} & W_{-a_1}W_{a_1-a_2}\cdots W_{a_{n-2}-a_{n-1}}W_{a_{n-1}} \\ & \begin{pmatrix} 1 \\ 0 \end{pmatrix}^\top \underline{\underline{M_{a_1}}}\,\underline{\underline{M_{a_2}}}\cdots\underline{\underline{M_{a_{n-1}}}} \begin{pmatrix} 1 \\ 0 \end{pmatrix} \end{aligned} \tag{5.67}$$

which contains n factors of W and $n-1$ factors of the matrix $\underline{\underline{M_a}}$. It will prove useful to relabel the $n-1$ dummy variables a_i by n dummy variables $b_1 = -a_1$, $b_2 = a_1 - a_2$,

$b_3 = a_2 - a_3$, ..., $b_{n-1} = a_{n-2} - a_{n-1}$, $b_n = a_{n-1}$, imposing that $\sum_{i=1}^{n} b_i = 0$ by a Kronecker δ-function,

$$J^{(n)}(x) = -\frac{\mathring{\imath}}{L} \sum_{b_1,b_2,\ldots,b_n=-\infty}^{\infty} \delta_{b_1+b_2+\ldots+b_n,0} W_{b_1} W_{b_2} \cdots W_{b_{n-1}} W_{b_n} \times \begin{pmatrix} 1 \\ 0 \end{pmatrix}^{\top} \underline{\underline{M_{-b_1}}}\, \underline{\underline{M_{-(b_1+b_2)}}}\, \underline{\underline{M_{-(b_1+b_2+b_3)}}} \cdots \underline{\underline{M_{-(b_1+b_2+\ldots+b_{n-1})}}} \begin{pmatrix} 1 \\ 0 \end{pmatrix} . \quad (5.68)$$

In Appendix. 5.E we consider properties of the steady-state current generally and in relation to the potential.

5.D Comparison between the field theory and the exact result [9] for a piece-wise linear potential

In this section, we compare our field-theoretic result of the steady-state current J to the exact result [9]. We consider an RnT particle with no external drift in a periodic, piece-wise linear ratchet potential $U(x) = U(x + L)$ of the form

$$U(x) = \begin{cases} U_0 \frac{x}{\alpha L} & \text{for } x \in [0, \alpha L) \\ U_0 \frac{L-x}{(1-\alpha)L} & \text{for } x \in [\alpha L, L) \end{cases} \quad (5.69)$$

as shown in Fig. 5.D.1.

The Fokker-Planck equations for RnT particles in a piece-wise linear potential are most easily written down by distinguishing the two intervals $x \in [0, \alpha L)$, by, say, superscript $[i] = [1]$ and $x \in [\alpha L, L)$ by, say, superscript $[i] = [2]$, so that

$$\begin{aligned} \partial_t \rho_+^{[i]}(x,t) &= -\partial_x[(w - \nu U'^{[i]})\rho_+^{[i]}(x,t)] - \gamma(\rho_+^{[i]}(x,t) - \rho_-^{[i]}(x,t)) + D\partial_x^2 \rho_+^{[i]}(x,t) \\ \partial_t \rho_-^{[i]}(x,t) &= -\partial_x[(-w - \nu U'^{[i]})\rho_-^{[i]}(x,t)] - \gamma(\rho_-^{[i]}(x,t) - \rho_+^{[i]}(x,t)) + D\partial_x^2 \rho_-^{[i]}(x,t) \end{aligned} \quad (5.70a)$$

with constant slopes $U'^{[1]} = U_0/(\alpha L)$ and $U'^{[2]} = -U_0/((1-\alpha)L)$. Similar to the main text, the densities $\rho_+^{[i]}(x,t)$ and $\rho_-^{[i]}(x,t)$ refer to the right-moving and the left-moving particles respectively. Solving this system of equations is greatly facilitated by the

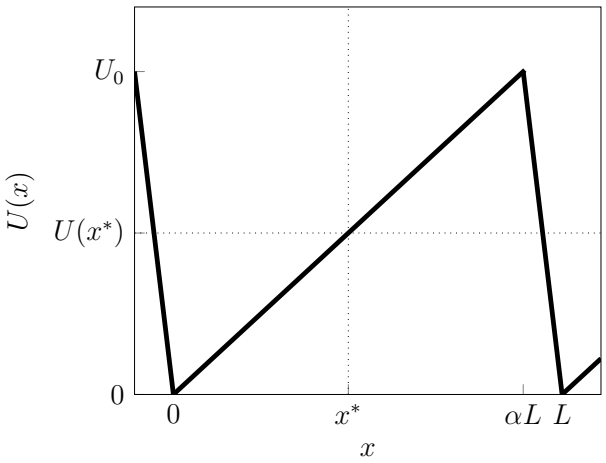


Figure 5.D.1: The periodic, piece-wise linear ratchet described by Eq. (5.69) with $\alpha = 0.9$. The ratchet has $U(0) = 0$ rises up to $U(\alpha L) = U_0$ and descends again to $U(L) = 0$. The point $x^* = \alpha L/2$ marks the point where $U(x^* + x) - U(x^*) = U(x^*) - U(x^* - x)$ with $U(x^*) = U_0/2$, Eq. (5.73), Appendix. 5.E.

slopes being piece-wise constant.

Following the procedure outlined in [9], the steady-state densities $\rho_{\pm}^{[i]}(x)$ are determined by making the ansatz $\rho_{\pm}^{[i]} = Z_{\pm}^{[i]} e^{\lambda^{[i]} x}$, to find 4 linearly independent solutions of Eqs. (5.70) for $i = 1, 2$ and both particle species $\rho_{\pm}$, and solving two coupled quadratic characteristic equations for the eigenvalues. One of those always vanishes, while the others can be relabelled as $\alpha^{[i]}$, $\beta^{[i]}$ and $\gamma^{[i]}$, producing the ansatz

$$\rho_{\pm}^{[i]}(x) = A_{\pm}^{[i]} e^{\alpha^{[i]} x} + B_{\pm}^{[i]} e^{\beta^{[i]} x} + C_{\pm}^{[i]} e^{\gamma^{[i]} x} + D_{\pm} \ , \tag{5.71}$$

which leaves 16 amplitudes to be determined: $A_{+}^{[1]}$, $A_{-}^{[1]}$, $A_{+}^{[2]}$, ..., $D_{-}^{[2]}$.

The 16 amplitudes are determined by substituting Eqs. (5.71) into Eqs. (5.70) at steady state, when the left hand side of the latter vanishes. As a result, the pre-factor of every linearly independent exponential on the right has to vanish, fixing the ratios $A_{+}^{[i]}/A_{-}^{[i]}$, $B_{+}^{[i]}/B_{-}^{[i]}$, $C_{+}^{[i]}/C_{-}^{[i]}$ and $D_{+}^{[i]}/D_{-}^{[i]}$ in terms of system parameters for both $i = 1, 2$, which amounts to 8 equations for 16 unknowns. A further 8 equations are obtained by matching conditions at the boundaries of intervals $i = 1$ and $i = 2$, more specifically for the density, $\rho_{\pm}^{[1]}(0) = \rho_{\pm}^{[2]}(L)$ and $\rho_{\pm}^{[1]}(\alpha L) = \rho_{\pm}^{[2]}(\alpha L)$, and correspondingly for the current $J_{\pm}^{[i]}(x) = (\pm w - \nu U'^{[i]} - \mathrm{d}/\mathrm{d}x)\rho_{\pm}^{[i]}(x)$. It turns out that only 15 of those 16 equations are linearly independent, as expected in a homogeneous, linear

system of equations. The final equation is in fact obtained by demanding in addition overall normalisation of the density. This procedure, best done in a computational algebra system [77], results in the density and the current being determined in closed form.

To compare to our field-theory, we choose the height of the piece-wise linear potential $U(x)$ in Eq. (5.69) by setting $U_0 = 1$ and vary the coupling ν in Eqs. (5.70). Density and current are then determined through the procedure outlined above.

The field-theoretic approach on the other hand is based on the Fourier coefficients of the potential Eq. (5.69). Taking the first 200 such modes,

$$U_a = \frac{U_0\,(1 - e^{-2i\pi a\alpha})}{4\pi^2 a^2 \alpha(\alpha - 1)}\ , \tag{5.72}$$

for $a = -200, -199, \cdots, 200$, we have calculated the steady-state current J to order 75 in ν. A comparison between this field-theoretic result and the exact result obtained above is shown in Fig. 5.D.2. It shows perfect agreement for ν up to the radius of convergence $\nu^{<}_{\text{roc}} = 4.272\ldots$ estimated via Eq. (5.12).

5.D.1 Radius of convergence in field theory

Given the issue of convergence in our field theory shown in Figure 5.D.2, we investigate in the following section what parameters the radius of convergence depends on. We use the conservative estimate of the radius of convergence shown in (5.12). The dimension of $\nu^{<}_{\text{roc}}$ is L^2/T which is consistent with the dimension of the diffusion constant D. We therefore fix all other parameters in our system and fix all the modes from the external potential and plot $\nu^{<}_{\text{roc}}$ against D. The plot is shown below. From the plot Figure 5.D.3, we see a linear relationship between $\nu^{<}_{\text{roc}}$ and D is linear. Therefore, when D is too small, the perturbative expansion Eq. (5.11) breaks down.

The dimensionless parameters in our system are $\nu^{<}_{\text{roc}}/D$, Pe and Qe. We therefore investigate the dependence of $\nu^{<}_{\text{roc}}/D$ on Pe and Qe. In the following, we plot the value of $\nu^{<}_{\text{roc}}/D$ against Pe and Qe with all other system parameters fixed. The result is shown in Fig. 5.D.4. As Pe increases, the radius of convergence first decreases and then increases. Regarding Qe, there is a linear relationship between the radius of con-

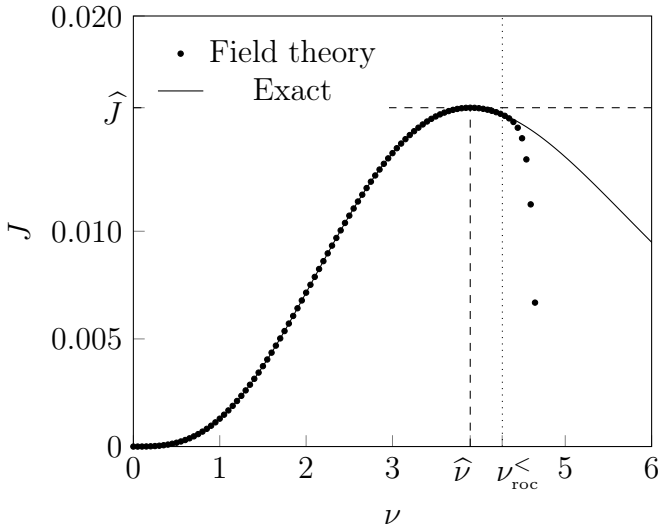


Figure 5.D.2: Comparison of the present field-theoretic result (filled circles) for the steady-state current and the exact solution [9] (solid line) for a piece-wise linear ratchet potential Eq. (5.69) with $\alpha = 0.9$ and $U_0 = 1$ as shown in Fig. 5.D.1. The other parameters are $f = 0, w = 1, \gamma = 5$, $D = 1$ and $L = 1$. The field theoretic results are based on 200 Fourier coefficients and up to 75 orders in ν. The agreement is perfect (deviation of less than 0.15% up until $\nu^{<}_{\rm roc} = 4.272\ldots$ the radius of convergence estimated via Eq. (5.12) and shown as a dotted vertical line Beyond that, the current due to the field theory diverges sharply. The coupling ν that produces the best current $\widehat{J} = 0.015739\ldots$ in this potential is $\widehat{\nu} = 3.90\ldots$, where even the shallow part of the potential has a slope greater than the self-propulsion speed, $\widehat{\nu} U_0/(\alpha L) = 3.9 \cdot 1/(0.9 \cdot 1) > w = 1$, indicating that transport is dominated by diffusion.

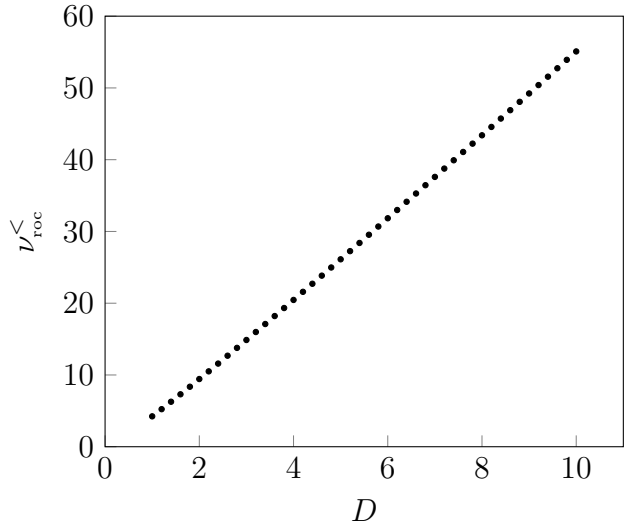


Figure 5.D.3: A plot of $\nu^{<}_{\text{roc}}$ against D with all other parameters using the first 200 modes of a piece-wise linear ratchet potential Eq. (5.69) with $\alpha = 0.9$ and $U_0 = 1$ as shown in Fig. 5.D.1. The other parameters are $f = 0, w = 1, \gamma = 1$, $D = 1$ and $L = 1$. The field theoretic results are based on 200 Fourier coefficients and up to 75 orders in ν. One can see there is a linear relationship between $\nu^{<}_{\text{roc}}$ and D.

vergence and Qe. At the same time, the increase in the radius convergence is small as Qe increases.

5.E Symmetry properties of the steady-state current with no external force

In the following we derive some general properties of the steady-state current when there is no external force, $f = 0$, on the basis of Eqs. (5.65) and (5.53), that hold to all orders of the perturbation theory. We may briefly consider an odd potential, $U(-x) = -U(x)$, or, given periodicity, more generally a potential with

$$U(x^* + x) - U(x^*) = U(x^*) - U(x^* - x) \tag{5.73}$$

allowing for some offset $U(x^*)$ and a more general point of inversion x^*. An example is shown in Fig. 5.D.1. If such a potential Eq. (5.73) sustains a finite current, it must revert if the coupling changes sign, $\nu \mapsto -\nu$ because by Eq. (5.73) this is equivalent to mirroring space $x^* + x \mapsto x^* - x$. We conclude that the expansion of the steady-

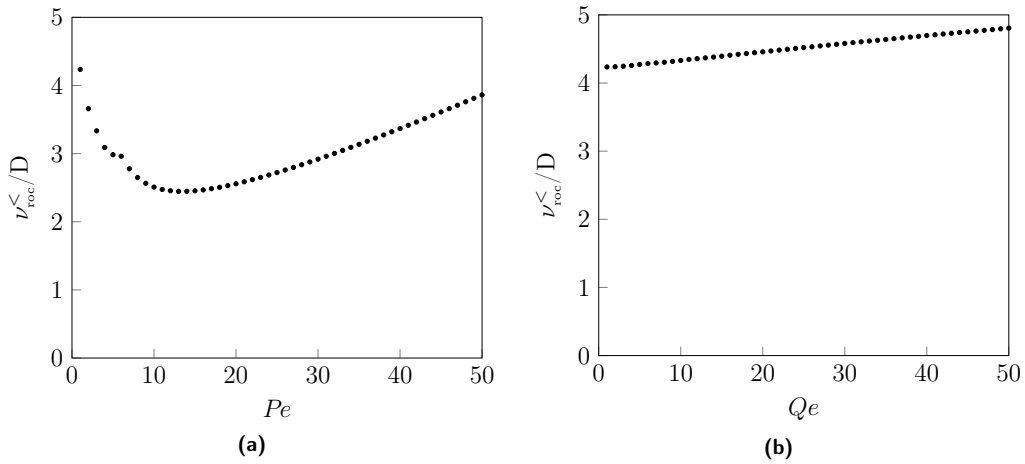


Figure 5.D.4: A plot of $\nu^{<}_{\mathrm{roc}}/D$ against Pe and Qe with all other parameters using the first 200 modes of a piece-wise linear ratchet potential Eq. (5.69) with $\alpha = 0.9$ and $U_0 = 1$ as shown in Fig. 5.D.1. The other parameters are $f = 0, \gamma = 1$, $D = 1$ and $L = 1$. The field theoretic results are based on 200 Fourier coefficients and up to 75 orders in ν.

state current Eq. (5.60) of RnT particles *in such a potential* Eq. (5.73) must be odd in ν, in other words, $J^{(2n)} = 0$ for $n \in \mathbb{N}$.

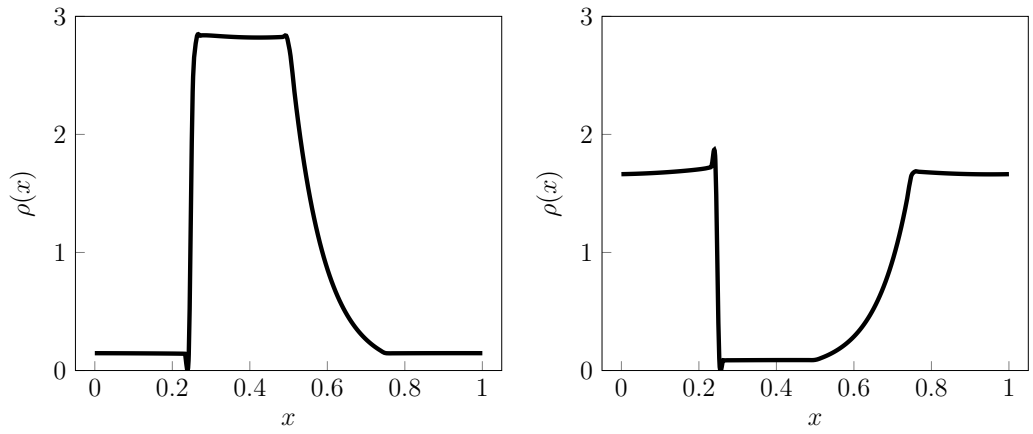
It is far from obvious why this should be the case for a general potential. In [133] an argument is sketched that time reversal $z(t) = x(T - t)$ of trajectories $x(t)$ obeying, say,

$$\dot{x} = -\nu U'(x) + \xi_x(t) \tag{5.74}$$

with white noise ξ_x are generally solutions of the Langevin equation

$$\dot{z} = \nu U'(z) + \xi_z(t) \tag{5.75}$$

with white noise ξ_z distributed identically to ξ_x. The time reversal from Eq. (5.74) to (5.75) apparently amounts to a change of sign of the coupling ν to $-\nu$ and clearly inverts the total displacement $z(T) - z(0) = -(x(T) - x(0))$. However, in order to conclude that time reversal reverts the *steady-state* current, one has to show that the probabilistic weight of trajectories is unchanged under time reversal. To put it more succinctly, one has to show that typical steady-state trajectories $x(t)$ of Eq. (5.74) are typical steady-state trajectories $z(t)$ of Eq. (5.75). That this is generally not the case can be seen in the counter example of a harmonic $U(x) = x^2/2$, where only one of the



(a) $\nu = 1,\ J = -0.001873\ldots$ **(b)** $\nu = -1,\ J = 0.001873\ldots$

Figure 5.E.1: Particle density $\rho(x)$ for an RnT particle in the periodic "hurdle" potential $U(x)$ Eq. (5.76) shown in Fig. 5.E.2, based on 100 modes calculated perturbatively to 75th order in ν. Even when the density profiles cannot be related by a simple geometrical transformation, the steady-state currents are simple the negative of each other. Parameters: $f = 0$, $D = 1$, $w = 1$, $L = 1$ and $\gamma = 1$, so that $Pe = Qe = \kappa = 1$.

two Eqs. (5.74) and (5.75) has a stationary state at all. We conclude that there is no such simple argument as to why the steady-state current is generally odd in ν.

To illustrate the subtleties further, we show in Fig. 5.E.1a the particle density $\rho(x)$ of RnT particles in the "hurdle" potential $U(x)$

$$U(x) = \begin{cases} 0 & x \in [0, \frac{L}{4}) \\ 3D & x \in [\frac{L}{4}, \frac{L}{2}) \\ (-12\frac{x}{L} + 9)D & x \in [\frac{L}{2}, \frac{3L}{4}) \\ 0 & x \in [\frac{3L}{4}, L) \end{cases} \tag{5.76}$$

shown in Fig. 5.E.2 for $\nu = 1$. This is contrasted by Fig. 5.E.1b, which shows the particle density for the inverted potential, *i.e.* for the potential Fig. 5.E.2 but with coupling $\nu = -1$. The two density profiles are clearly and obviously very distinct, even when they both seem to suffer slightly from the Gibbs phenomenon. While they share some features, there is also no simple geometrical transformation that maps one density profile to the other, and surely not one that is its own inverse as is $\nu \mapsto -\nu$. For example, both densities being convex from below for the sloped region $x \in$

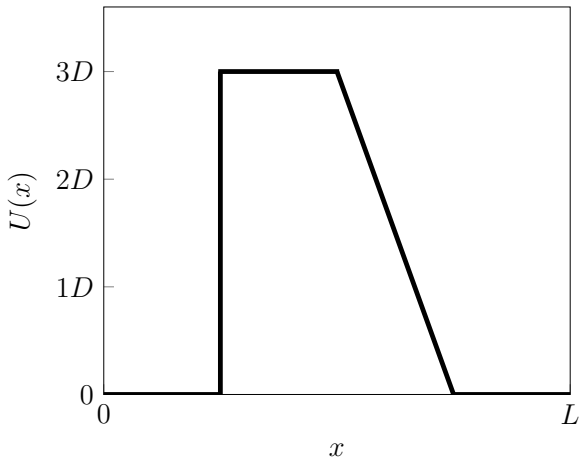


Figure 5.E.2: The "hurdle" potential Eq. (5.76), whose resulting RnT particle density is shown in Fig. 5.E.1a.

$[L/2, 3L/4)$ makes it impossible to, say, mirror and overlay the two. The steady-state trajectories in the potential $U(x)$ of Eq. (5.76) produce therefore demonstrably a very different density $\rho(x)$ compared to $-U(x)$. And yet, we find that the steady-state currents in the two setups are indeed simply the negative of each other. The following section derives this property perturbatively.

5.E.1 The steady-state current J is odd in ν

In the present section we show that changing the sign of ν of the potential simply reverses the steady-state current of RnT particles with no external drift, despite the density $\rho(x)$ showing none such simple relationship as outlined above. We will do so by showing $J^{(n)} = (-1)^n J^{(n)}$, *i.e.* $J^{(n)} = 0$ for all even n.

The starting point for the derivation is Eq. (5.68), where we will rearrange the products of $\underline{\underline{M_b}}$ to arrive at the desired expression. We set $f = 0$ in Eq. (5.55), so

$$\underline{\underline{M_a}} = \frac{(-k_a)\mathcal{I}_a}{k_a^2(D^2k_a^2 + 2D\gamma + w^2)} \begin{pmatrix} Dk_a^2 + 2\gamma & -\mathring{\imath}wk_a \\ -\mathring{\imath}wk_a & Dk_a^2 \end{pmatrix} . \tag{5.77}$$

The key observation is that the complex matrix Eq. (5.77) is symmetric (rather than Hermitian) when $f = 0$, with purely real entries along the diagonal and purely imagi-

nary off-diagonal elements. Firstly, the symmetry implies

$$\mathbf{d}^\top \underline{\underline{M_{c_1}}}\,\underline{\underline{M_{c_2}}} \cdots \underline{\underline{M_{c_{n-1}}}}\,\mathbf{e} = \mathbf{e}^\top \underline{\underline{M_{c_{n-1}}}}\,\underline{\underline{M_{c_{n-2}}}} \cdots \underline{\underline{M_{c_1}}}\,\mathbf{d}\ , \tag{5.78}$$

for arbitrary vectors $\mathbf{e}$ and $\mathbf{d}$, so that Eq. (5.68), that has $\mathbf{e} = \mathbf{d} = (1,0)^\top$, is invariant under the inversion of the sequence of Fourier-indices in the product of $\underline{\underline{M_b}}$.

Secondly, the make-up of the elements of $\underline{\underline{M_b}}$, namely purely real diagonal elements and purely imaginary off-diagonal elements, means that any product of $\underline{\underline{M_b}}$ has the same property, so that

$$\begin{pmatrix}1\\0\end{pmatrix}^\top \underline{\underline{M_{c_1}}}\,\underline{\underline{M_{c_2}}} \cdots \underline{\underline{M_{c_{n-1}}}} \begin{pmatrix}1\\0\end{pmatrix} \in \mathbb{R}\ . \tag{5.79}$$

Taking the complex conjugate of this expression thus leaves it unchanged. By the definition Eq. (5.77), the complex conjugate can be written as $(\underline{\underline{M_a}})^* = -\underline{\underline{M_{-a}}}$, so that

$$\begin{pmatrix}1\\0\end{pmatrix}^\top \underline{\underline{M_{c_1}}}\,\underline{\underline{M_{c_2}}} \cdots \underline{\underline{M_{c_{n-1}}}} \begin{pmatrix}1\\0\end{pmatrix} = (-1)^{n-1} \begin{pmatrix}1\\0\end{pmatrix}^\top \underline{\underline{M_{-c_1}}}\,\underline{\underline{M_{-c_2}}} \cdots \underline{\underline{M_{-c_{n-1}}}} \begin{pmatrix}1\\0\end{pmatrix}\ . \tag{5.80}$$

Applying then Eq. (5.78) followed by Eq. (5.80) to Eq. (5.68) gives

$$\begin{aligned} J^{(n)}(x) = -(-1)^{n-1}\frac{\mathring{i}}{L} \sum_{b_1,b_2,\ldots,b_n=-\infty} & \delta_{b_1+b_2+\ldots+b_n,0} W_{b_1} W_{b_2} \cdots W_{b_{n-1}} W_{b_n} \\ & \times \begin{pmatrix}1\\0\end{pmatrix}^\top \underline{\underline{M_{b_1+b_2+\ldots+b_{n-1}}}}\,\underline{\underline{M_{b_1+b_2+\ldots+b_{n-2}}}} \cdots \underline{\underline{M_{b_1+b_2}}}\,\underline{\underline{M_{b_1}}} \begin{pmatrix}1\\0\end{pmatrix}\ . \end{aligned} \tag{5.81}$$

Because $\sum_{i=1}^n b_i = 0$, each of the matrices on the right hand side of Eq. (5.81) may be indexed alternatively by $b_1 + b_2 + \ldots + b_{n-1} = -b_n$, $b_1 + b_2 + \ldots + b_{n-2} = -(b_n + b_{n-1})$,

$\ldots$, $b_1 + b_2 = -(b_n + b_{n-1} + \ldots + b_3)$ and $b_1 = -(b_n + b_{n-1} + \ldots + b_2)$, resulting in

$$J^{(n)}(x) = -(-1)^{n-1}\frac{\mathring{\imath}}{L}\sum_{b_1,b_2,\ldots,b_n=-\infty}\delta_{b_1+b_2+\ldots+b_n,0}W_{b_1}W_{b_2}\cdots W_{b_{n-1}}W_{b_n}$$
$$\times\begin{pmatrix}1\\0\end{pmatrix}^{\top}\underline{\underline{M_{-b_n}}}\,\underline{\underline{M_{-(b_n+b_{n-1})}}}\cdots\underline{\underline{M_{-(b_n+b_{n-1}+\ldots+b_3)}}}\,\underline{\underline{M_{-(b_n+b_{n-1}+\ldots+b_2)}}}\begin{pmatrix}1\\0\end{pmatrix}\ , \quad (5.82)$$

before "mirroring" the indices' indices, $c_i = b_{n+1-i}$, so that

$$J^{(n)}(x) = -(-1)^{n-1}\frac{\mathring{\imath}}{L}\sum_{c_1,c_2,\ldots,c_n=-\infty}\delta_{c_1+c_2+\ldots+c_n,0}W_{c_n}W_{c_{n-1}}\cdots W_{c_2}W_{c_1}$$
$$\times\begin{pmatrix}1\\0\end{pmatrix}^{\top}\underline{\underline{M_{-c_1}}}\,\underline{\underline{M_{-(c_1+c_2)}}}\cdots\underline{\underline{M_{-(c_1+b_2+\ldots+c_{n-2})}}}\,\underline{\underline{M_{-(c_1+b_2+\ldots+c_{n-1})}}}\begin{pmatrix}1\\0\end{pmatrix}\ . \quad (5.83)$$

As the factors W_{c_i} are scalars, Eq. (5.83) is identical to Eq. (5.68) up to a factor of $(-1)^{n-1}$, which produces the desired identity

$$J^{(n)}(x) = (-1)^{n-1}J^{(n)}(x)\ , \quad (5.84)$$

which implies that $J^{(n)}(x)$ vanishes for even n. This is the main result of the present section. It follows immediately, that J, Eq. (5.11), is odd in ν and thus changes sign when ν does. It is important to notice that the above is no longer generally correct for $f \neq 0$.

5.E.2 The steady-state current vanishes in potentials with only odd Fourier coefficients

We first show that potentials whose even Fourier coefficients all vanish obey

$$U(x) = -U(x + L/2) \quad (5.85)$$

and vice versa and are thus identical to those that have been dubbed "supersymmetric" [133]. A schematic representation of a "supersymmetric" potential is shown in Figure 5.E.3.

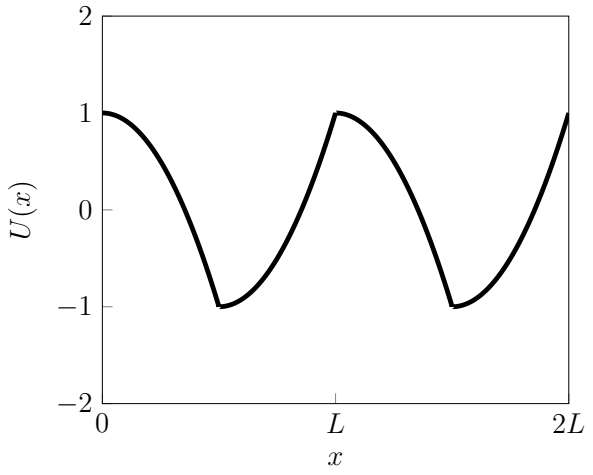


Figure 5.E.3: A schematic representation of a "supersymmetric" ratchet.

Firstly, if $U_a = 0$ for all even a, then Eq. (5.25) gives

$$U(x + L/2) = \frac{1}{L} \sum_{a=-\infty}^{\infty} \mathrm{e}^{\mathring{\imath} k_a (x+L/2)} U_a = -U(x) \tag{5.86}$$

using that $\exp(\mathring{\imath} k_a (x + L/2)) = (-1)^a \exp(\mathring{\imath} k_a x)$ and only odd a enters.

Secondly, if $U(x) = U(x + L/2)$, then Eq. (5.25) gives

$$U_a = -\int_0^L \mathrm{d}x\, \mathrm{e}^{-\mathring{\imath} k_a x} U(x + L/2) = -(-1)^a \int_{L/2}^{3L/2} \mathrm{d}x\, \mathrm{e}^{-\mathring{\imath} k_a x} U(x) = -(-1)^a U_a \ , \tag{5.87}$$

which means that U_a must vanish for even a.

In the following we demonstrate that the steady-state current vanishes if $U_a = 0$ for all even a.

The potential enters into the perturbative expansion Eq. (5.68) of the steady-state current only via W_a Eq. (5.54). It features in Eq. (5.68) as a product involving all n indices $b_1, b_2, \ldots, b_n$. If W_a vanishes for all even a, then all indices $b_1, b_2, \ldots, b_n$ need to be odd in order for the product $W_{b_1} W_{b_1} \ldots W_{b_n}$ to be non-zero. However, if all indices b_i are odd, then the sum of an odd number of them cannot possible vanish, $\sum_{i=1}^{n} b_i \neq 0$, so that $\delta_{b_1+b_2+\ldots+b_n} = 0$ for odd n. It follows that $J^{(n)}$ vanishes for all odd n if U_a vanishes for all even a.

In Appendix. 5.E.1 we have demonstrated that $J^{(n)}$ vanishes generally for even n. If $J^{(n)}$ also vanishes for all odd n, then it must vanish overall. In summary, if U_a vanishes for all even a, which is equivalent to saying that the potential is supersymmetric, then J vanishes.

5.E.3 The steady-state current vanishes in potentials even about some x^*

The steady-state current of RnT particles in a potential even about x^*,

$$U(x^* + x) = U(x^* - x) \tag{5.88}$$

vanishes trivially because there is no preferred direction. In the following, we rederive this property perturbatively from the expression for the current Eq. (5.68).

From Eq. (5.88), we derive for the Fourier coefficients using Eq. (5.25),

$$\begin{aligned} \mathrm{e}^{\mathrm{i}k_a x^*} U_a = \mathrm{e}^{\mathrm{i}k_a x^*} \int_0^L \mathrm{d}x\, \mathrm{e}^{-\mathrm{i}k_a(x+x^*)} U(x^* + x) = \int_0^L \mathrm{d}x\, \mathrm{e}^{-\mathrm{i}k_a x} U(x^* - x) \\ = \mathrm{e}^{-\mathrm{i}k_a x^*} \int_0^L \mathrm{d}x\, \mathrm{e}^{\mathrm{i}k_a(x^*-x)} U(x^* - x) = \mathrm{e}^{-\mathrm{i}k_a x^*} U_{-a} \ . \end{aligned} \tag{5.89}$$

Considering now the product of W_b, Eq. (5.54), in Eq. (5.68), it generally has the property

$$\begin{aligned} \left(W_{b_1} W_{b_2} \cdots W_{b_n}\right) + \left(W_{-b_1} W_{-b_2} \cdots W_{-b_n}\right) \\ = L^{-n} k_{b_1} k_{b_2} \cdots k_{b_n} \Big(U_{b_1} U_{b_2} \cdots U_{b_n} + (-1)^n U_{-b_1} U_{-b_2} \cdots U_{-b_n} \Big) \ , \end{aligned} \tag{5.90}$$

With Eq. (5.89), the product of modes of the potential obeys

$$U_{b_1} U_{b_2} \cdots U_{b_n} = \mathrm{e}^{-2\mathrm{i}\sum_{a=1}^n k_a x^*} U_{-b_1} U_{-b_2} \cdots U_{-b_n} = U_{-b_1} U_{-b_2} \cdots U_{-b_n} \ , \tag{5.91}$$

provided $\sum_{i=1}^n k_{b_i} = (2\pi/L) \sum_{i=1}^n b_i = 0$, as is enforced by the Kronecker δ-function in

Eq. (5.68). For a potential even about some x^*, we thus have

$$\delta_{b_1+b_2+\ldots+b_n,0}\big(W_{b_1}W_{b_2}\cdots W_{b_n}+W_{-b_1}W_{-b_2}\cdots W_{-b_n}\big)$$
$$=\delta_{b_1+b_2+\ldots+b_n,0}L^{-n}k_{b_1}k_{b_2}\ldots k_{b_n}\times\begin{cases}2U_{b_1}U_{b_2}\ldots U_{b_n} & \text{for } n \text{ even}\\ 0 & \text{for } n \text{ odd}\,.\end{cases} \tag{5.92}$$

This identity can be used in the expression for the steady-state current Eq. (5.68) once it has been suitably rewritten. To this end, we double up all terms in Eq. (5.68),

$$2J^{(n)}(x)=-\frac{\mathring{\imath}}{L}\sum_{b_1,b_2,\ldots,b_n=-\infty}^{\infty}\delta_{b_1+b_2+\ldots+b_n,0} \tag{5.93}$$
$$\times\Big\{W_{b_1}W_{b_2}\cdots W_{b_{n-1}}W_{b_n}\begin{pmatrix}1\\0\end{pmatrix}^{\top}\underline{\underline{M_{-b_1}}}\,\underline{\underline{M_{-(b_1+b_2)}}}\cdots\underline{\underline{M_{-(b_1+b_2+\ldots+b_{n-1})}}}\begin{pmatrix}1\\0\end{pmatrix}$$
$$+W_{-b_1}W_{-b_2}\cdots W_{-b_{n-1}}W_{-b_n}(-1)^{n-1}\begin{pmatrix}1\\0\end{pmatrix}^{\top}\underline{\underline{M_{b_1}}}\,\underline{\underline{M_{b_1+b_2}}}\cdots\underline{\underline{M_{b_1+b_2+\ldots+b_{n-1}}}}\begin{pmatrix}1\\0\end{pmatrix}\Big\}\,,$$

which by means of Eq. (5.80) simplifies to

$$2J^{(n)}(x)=-\frac{\mathring{\imath}}{L}\sum_{b_1,b_2,\ldots,b_n=-\infty}^{\infty}\delta_{b_1+b_2+\ldots+b_n,0}\begin{pmatrix}1\\0\end{pmatrix}^{\top}\underline{\underline{M_{-b_1}}}\,\underline{\underline{M_{-(b_1+b_2)}}}\cdots\underline{\underline{M_{-(b_1+b_2+\ldots+b_{n-1})}}}\begin{pmatrix}1\\0\end{pmatrix} \tag{5.94}$$
$$\times\big\{W_{b_1}W_{b_2}\cdots W_{b_{n-1}}W_{b_n}+(-1)^{n-1}W_{-b_1}W_{-b_2}\cdots W_{-b_{n-1}}W_{-b_n}\big\}\,.$$

If the potential is even, then Eq. (5.92) can be used on the right hand side for odd n, where $(-1)^{n-1}=1$, so that

$$2J^{(n)}(x)=0\quad\text{for odd } n \text{ if the potential is even, Eq. (5.88)}\quad. \tag{5.95}$$

As $J^{(n)}(x)=0$ for all even n, it implies that the steady-state current vanishes altogether. In other words, even potentials, Eq. (5.88), have no steady-state current, $J(x)=0$.

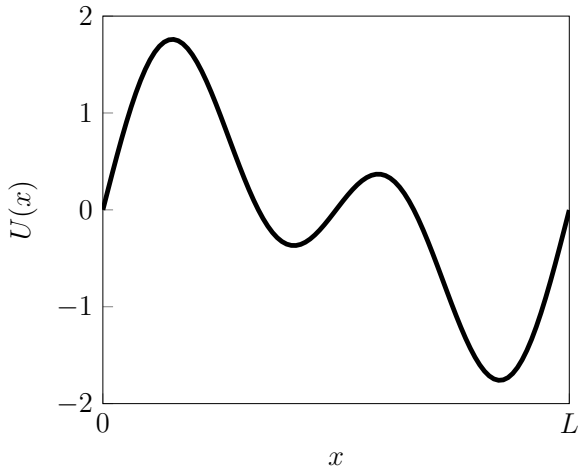


Figure 5.F.1: The 2-mode potential from Eq. (5.96).

5.F Current for more different ratchet profiles

In this section, we compare the optimal current $\widehat{J}$ produced by the best potential in Fig. 5.0.1 with other types of ratchet potentials [109].

First, we compare the current produced by the 2-mode potential

$$U(x) = \sin(2\pi x/L) + \sin(4\pi x/L) \quad x \in [0, L) \tag{5.96}$$

shown in Fig. 5.F.1.

We plot the current produced by the potential in Eq. (5.96) against the coupling ν. The result is shown in Fig. 5.F.2. We also compare the current produced by the potential

$$U(x) = -\frac{\sin(2\pi x/L)}{1.09 - 0.6\cos(2\pi x/L)} \quad x \in [0, L) \tag{5.97}$$

shown in Fig. 5.F.3

We plot the current produced by the potential in Eq. (5.97) against the coupling ν. The result is shown in Fig. 5.F.4.

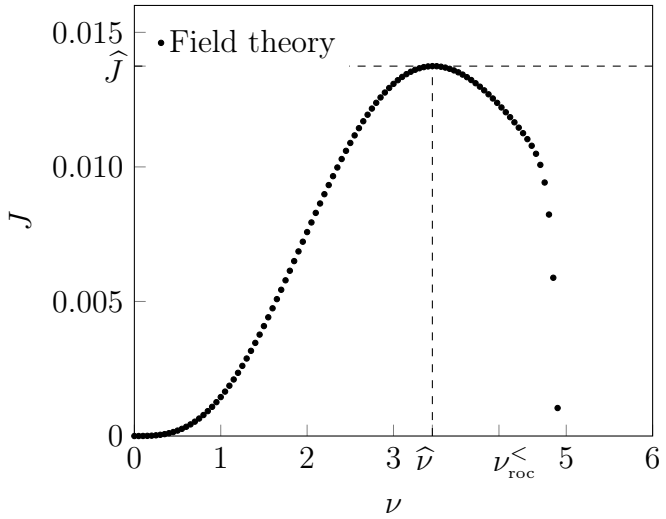


Figure 5.F.2: Current produced by the ratchet potential Eq. (5.96) against the coupling parameter ν. The system parameters are $w = 1, \gamma = 1$, $D = 1$ and $L = 1$. The field theoretic results are up to 75 orders in ν. The radius of convergence $\nu^{<}_{\rm roc} = 4.221\ldots$ estimated via Eq. (5.12) is shown as a dotted vertical line Beyond that, the current due to the field theory diverges sharply. The coupling ν that produces the best current $\widehat{J} = 0.013735\ldots$ in this potential is $\widehat{\nu} = 3.45\ldots$. The optimal current produced by Eq. (5.96) is about 64% smaller versus the optimal current in Fig. 5.0.1.

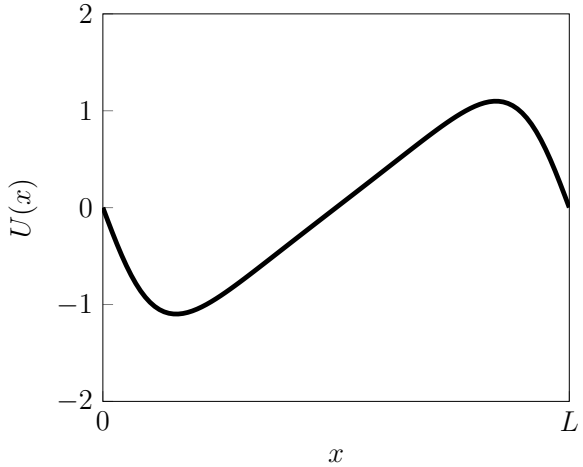


Figure 5.F.3: The ratchet potential profile in Eq. (5.97).

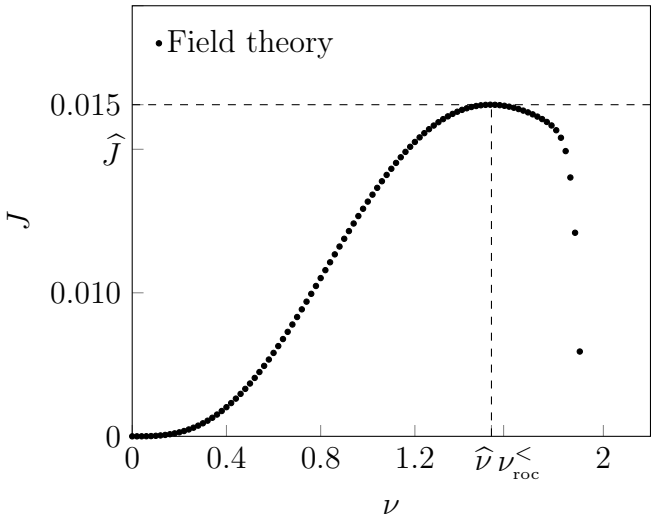


Figure 5.F.4: Current produced by the ratchet potential Eq. (5.97) against the coupling parameter ν. The system parameters are $w = 1, \gamma = 1$, $D = 1$ and $L = 1$. The field theoretic results are up to 75 orders in ν. The radius of convergence $\nu^{<}_{\text{roc}} = 1.5767\ldots$ estimated via Eq. (5.12) is shown as a dotted vertical line Beyond that, the current due to the field theory diverges sharply. The coupling ν that produces the best current $\widehat{J} = 0.011553\ldots$ in this potential is $\widehat{\nu} = 1.525\ldots$. The optimal current produced by Eq. (5.97) is about 69% smaller versus the optimal current in Fig. 5.0.1.

5.G Current with an external force

So far, we have only been studying the effect of the current J when the external force f is zero. We now investigate the effect of non-zero force. We again use the piece-wise linear potential shown in Eq. (5.69) with $U_0 = 3$ and $\nu = 1$. As the particle has a net current to the right due to the potential, when the external force f, which is acting to the left of the particle, is small, with other parameters unchanged, we expect a roughly linear relationship between the current and the external force f. A plot of J against f with small f is shown below. However, it is interesting to see that with small f, the impact on the current J from the external force is linear but the gradient is not -1. When the external force is large, we expect the effect of the current to be dominated by the external force f, as the impact on the current solely from the RnT particle interacting with the potential is negligible, implying the gradient will be -1. Below, we plot the current J against f for large f confirms our hypothesis. One can see the current first has a flatter gradient for small f and soon becomes steeper so the gradient 'catches up' to be -1.

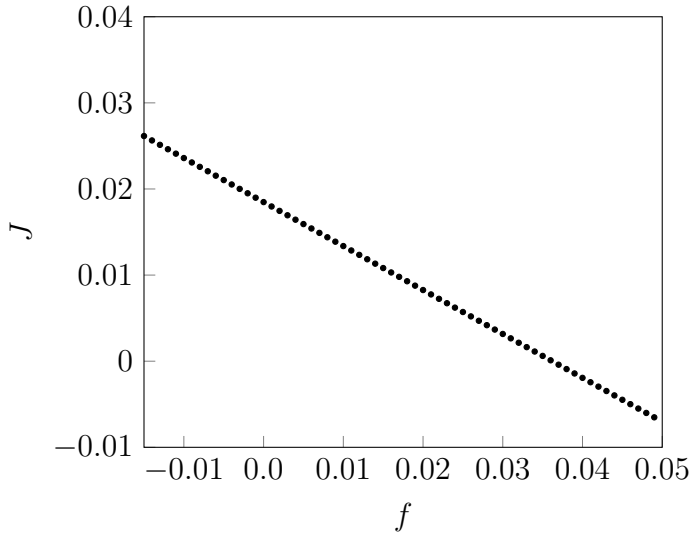


Figure 5.G.1: Current produced by piece-wise linear ratchet potential Eq. (5.69) against the force f using the perturbative expansion arising from Eq. (5.11). The system parameters are $w = 1, \gamma = 1$, $D = 1$ and $L = 1$. For the piece-wise linear ratchet potential Eq. (5.69), we used $\alpha = 0.9$ and 200 modes. The field theoretic results are up to 75 orders in ν.

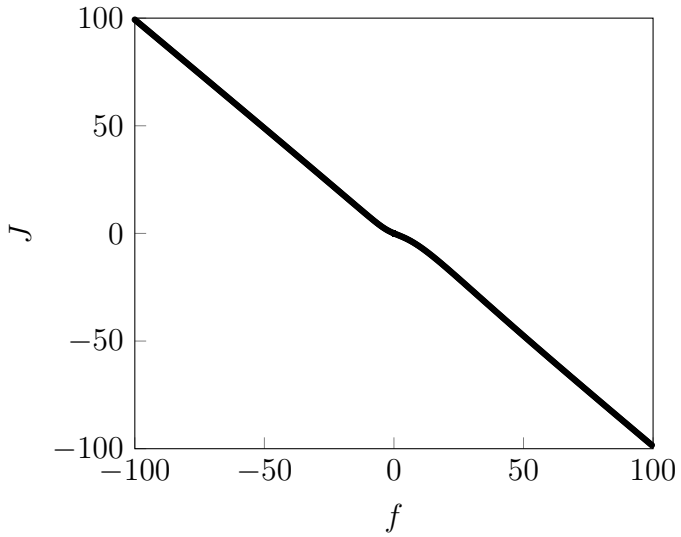


Figure 5.G.2: Current produced by piece-wise linear ratchet potential Eq. (5.69) against the force f using the perturbative expansion arising from Eq. (5.11). The system parameters are $w = 1, \gamma = 1$, $D = 1$ and $L = 1$. For the piece-wise linear ratchet potential Eq. (5.69), we used $\alpha = 0.9$ and 200 modes. The field theoretic results are up to 75 orders in ν.

5.H Entropy production

In this section, we compute the steady-state entropy production rate $\mathcal{S}$ of our set-up in Eq. (5.74) using the framework shown in [131]. At stationarity, the total entropy production rate $\mathcal{S}$ can be expressed as

$$\mathcal{S} = \frac{w}{D}\int_0^L \mathrm{d}x\, J_+(x) - J_-(x) - \frac{fLJ}{D} \tag{5.98}$$

where

$$J_+(x) = (w - f - \nu U'(x))\rho_+(x,t) - D\partial_x\rho_+(x,t) \tag{5.99}$$

is the right-moving current and

$$J_-(x) = (-w - f - \nu U'(x))\rho_-(x,t) - D\partial_x\rho_-(x,t) \tag{5.100}$$

is the left-moving current. Inserting Eq. (5.99) and Eq. (5.100) into Eq. (5.98) yields

$$\mathcal{S} = \frac{w^2}{D} - \frac{w}{D}\int_0^L \mathrm{d}x\, \nu U'(x)\mu(x) - \frac{wf}{D}\int_0^L \mathrm{d}x\, \mu(x) - \frac{fLJ}{D}. \tag{5.101}$$

We also compute the entropy production rate $\mathcal{S}$ using the formalism outlined in [64]. The entropy production rate reads

$$\mathcal{S} = \sum_{A,B\in\{+,-\}} \int_0^L dxdy P_A \dot{W}(x \to y, A \to B) \lim_{\tau\to 0}\left(\frac{W(x \to y, A \to B;\tau)}{W(y \to x, B \to A;\tau)}\right).. \tag{5.102}$$

Below, we analyse which terms contribute to the entropy production Eq. (5.106). As the short-time transition probability for both displacement and a transmutation satisfy

$$W(x \to y, + \to -;\tau) = W(x \to y, + \to -;\tau) = \frac{1}{\sqrt{4\pi D\tau}}\left(\gamma\tau + \mathcal{O}(\tau^2)\right). \tag{5.103}$$

For dynamics involving transmutations between left-moving particles and right-moving particles, as the logarithm in Eq. (5.106) vanishes, there is no contribution to the entropy production. The short-time transition probability for right/left-moving particles

reads

$$W(x \to y, \pm \to \pm; \tau) = \frac{1}{\sqrt{4\pi D\tau}} e^{-\frac{(y-x-\tau(\pm w - \nu U'(x)))^2}{4D\tau}} \left(1 + \mathcal{O}(\tau)\right). \tag{5.104}$$

Using the kernel

$$\dot{W}(x \to y, \pm \to \pm; \tau) = (\nu U''(y) - \gamma)\delta(y-x) - (\pm w - \nu U'(y))\delta'(y-x) + D\delta''(y-x) \tag{5.105}$$

Using Eq. (5.104) and Eq. (5.105),the total entropy production rate reads

$$\mathcal{S} = \frac{w^2}{D} + \frac{f^2}{D} + \int_0^L \mathrm{d}x \, \frac{\rho(x)\left(-D\nu U''(x) + 2f\nu U'(x) + \nu^2 U'(x)^2\right) - 2w\mu(x)\left(f + \nu U'(x)\right)}{D}. \tag{5.106}$$

At the moment, the entropy production rate from Eq. (5.106) looks different from Eq. (5.101). Using the steady-state Fokker-Planck equation to substitute the $-2w\mu(x)/D$ term in the integrand of Eq. (5.106), the entropy production rate reads

$$\begin{aligned}
\mathcal{S} =& \frac{w^2}{D} + \frac{f^2}{D} + \int_0^L \mathrm{d}x \, \frac{\rho(x)\left(-D\nu U''(x) + 2f\nu U'(x) + \nu^2 U'(x)^2\right) - w\mu(x)\left(f + \nu U'(x)\right)}{D} \\
& - \int_0^L \mathrm{d}x \, \frac{J(f + \nu U'(x)) - \rho(x)(\nu U'(x) + f)^2 - D\partial_x \rho(x)(f + \nu U'(x))}{D} \qquad (5.107) \\
=& \frac{w^2}{D} + \int_0^L \mathrm{d}x \, \frac{-w\mu(x)\left(f + \nu U'(x)\right) - \rho(x) D\nu U''(x) - D\partial_x \rho(x)\nu U'(x)}{D} - \frac{fLJ}{D} \qquad (5.108) \\
=& \frac{w^2}{D} - \frac{w}{D}\int_0^L \mathrm{d}x \, \nu U'(x)\mu(x) - \frac{wf}{D}\int_0^L \mathrm{d}x \, \mu(x) - \frac{fLJ}{D} \qquad (5.109)
\end{aligned}$$

which is now consistent with Eq. (5.101). In the above derivation, we have used the periodicity of $U(x)$ and $\rho(x)$ and integration by parts.

5.I Active engine efficiency

In the following we discuss the properties of the active heat engine driven by a RnT particle. As there is a force term acting in the opposite in the Langevin dynamics

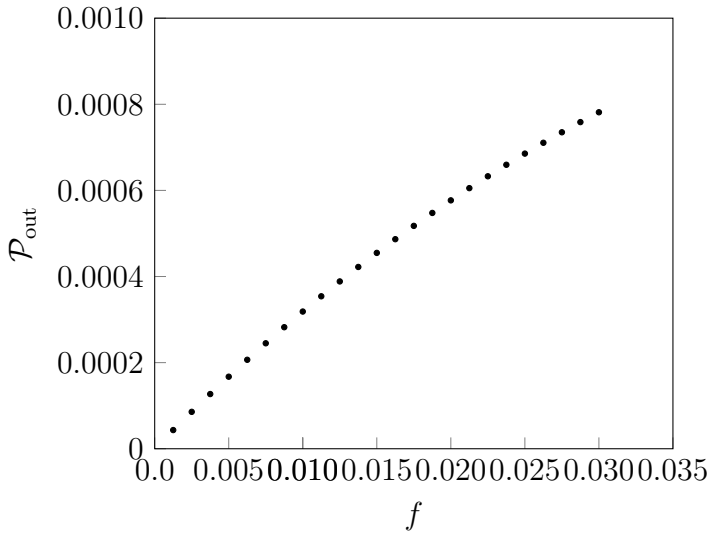


Figure 5.I.1: Optimal power output $\mathcal{P}_{\text{out}}$ against the force f. The system parameters are $w = 1, \gamma = 1$, $D = 1$ and $L = 1$. We used 20 modes and the field theoretic results are up to 75 orders in ν.

Eq. (5.1), one can view this as a RnT particle extracting work by lifting the load with force f. The power output $\mathcal{P}_{\text{out}}$ by the particle extracting work is given by the expression

$$\mathcal{P}_{\text{out}} \equiv fJL. \tag{5.110}$$

Intuitively, the work is given by the product of the force f and the effective velocity JL. Now with the expression of the power output at hand and the mechanism to calculate the current, we follow the same framework as in Sec. 5.A.1 to find the best shape of the potential $U(x)$ to optimise the J for different forces f for fixed L so that we try to work out the optimal power extracted $\mathcal{P}_{\text{out}}$. Below, we plot the optimal $\mathcal{P}_{\text{out}}$ against different f. Unfortunately, for $f > 0.03$, our optimisation procedure is no longer able to find the best $\mathcal{P}_{\text{out}}$ with the best f due to divergence issue of our field theory.

For the heat engine described by the Langevin dyanmics Eq. (5.1), the power input is given by

$$\mathcal{P}_{\text{in}} \equiv D\mathcal{S} + \mathcal{P}_{\text{out}}. \tag{5.111}$$

Therefore, the efficiency of the heat engine is

$$\eta \equiv \frac{\mathcal{P}_{\text{out}}}{\mathcal{P}_{\text{in}}}. \tag{5.112}$$

Acknowledgement

I would like to thank my collaborators very much for their permission to present our joint work as a part of my PhD thesis. I have obtained their approval which is shown in Appendix A.

We thank Martin Bier for helpful discussions and acknowledge communications with Peter Reimann. We thank Martin Bier for helpful discussions and acknowledge communications with Peter Reimann. Z.Z. thanks Huiyao Zheng for technical support.

6

Particle Entity in the Doi-Peliti and Response Field Formalisms

Abstract

In this chapter, I presented a near-verbatim copy of the preprint

M.Bothe, L.Cocconi, Z.Zhen and G.Pruessner. Particle Entity in the Doi-Peliti and Response Field Formalisms [18].

The research project was in collaboration with M.Bothe, L.Cocconi and G.Pruessner. My contribution to the project consisted of the construction and the derivation of the field theory. I also contributed to the example of two-point correlation functions and proving the particle entity in the Doi-Peliti framework.

We introduce a procedure to test a theory for point particle entity, that is, whether said theory takes into account the discrete nature of the constituents of the system. We then identify the mechanism whereby particle entity is enforced in the context of two field-theoretic frameworks designed to incorporate the particle nature of the degrees of freedom, namely the Doi-Peliti field theory and the response field field theory that derives from Dean's equation. While the Doi-Peliti field theory encodes the particle nature at a very fundamental level that is easily revealed, demonstrating the same for Dean's equation is more involved and

results in a number of surprising diagrammatic identities. We derive those and discuss their implications. These results are particularly pertinent in the context of active matter, whose surprising and often counterintuitive phenomenology rests wholly on the particle nature of the agents and their degrees of freedom as particles.

6.1 Introduction

The mathematical description of non-equilibrium many-particle systems typically requires a choice of scale at which their behaviour is resolved. When the focus is on the collective dynamics of a large ensemble of particles, it can be convenient to disregard some of the microscopic information and to rely on a coarse-grained description in terms of densities $\rho(x,t)$, which are continuous in space. What is generally lost upon such coarse-graining is "particle entity", namely the familiar attribute of classical point particles whose initial property of being localised at one point only is preserved under the dynamics, in other words that individual particles can only exist at one position in space at any given time. The distinction between effective and microscopically resolved theories has recently been debated in the context of active matter and, more specifically, entropy production [113, 30, 62, 24], where different levels of description grant access to different types of information about the degree of irreversibility of a stochastic process [53]. More generally, the study of sparse collections of interacting particles [68, 156, 152] can make it necessary to equip theories with a notion of "granularity" of their constituents. Field theories have traditionally been the most successful approach to capture the physics and mathematics of phenomena emerging from the interaction of many degrees of freedom [92, 73, 164]. The Doi-Peliti formalism, which has a discrete number-state master equation as its starting point, is perhaps the best known example of a path-integral approach that preserves particle entity [27, 128]. Another, less familiar example is the response field or Martin-Siggia-Rose-Janssen-De Dominicis [110, 78, 44] field theory [72] that derives from Dean's equation [37, 65, 167]. While it is generally accepted that these theories correctly describe the behaviour of physical point particles by construction and that they are, in fact, equivalent [95], the precise mechanism whereby this property is enforced, as well as a general procedure to determine whether a given field theory possesses particle entity, have not been identified. We fill this gap in the following

by introducing a signature of particle entity, Eq. (6.63), that draws solely on the moments of the integrated number density in a patch Ω of space. These moments can be computed by standard Feynman diagrammatic techniques.

This work is organised as follows. In Section 6.2, we set the scene by introducing the Doi-Peliti field theory and the response field formalism. As an illustrative example, we compute the two-point correlation function of the number density of n_0 non-interacting diffusive particles, thus highlighting some of the key similarities and differences between the two approaches. In Section 6.3 we formalise the concept of single-particle entity and derive different observables to probe it. This signature of particle entity is then applied to the Doi-Peliti field theory (Section 6.4) and the response field formalism of Dean's equation without interaction (Section 6.5), confirming that both are indeed valid descriptions of physical point particles. In this last section we also discuss the role of integer particle numbers and relate some of the results to a more intuitive probabilistic picture. Finally, in Section 6.6, we summarise our findings and highlight some open questions. Some of the technical details are relegated to the appendices.

6.2 Setting up the formalisms

6.2.1 Doi-Peliti field theory

A Doi-Peliti field theory, sometimes referred to as a coherent-state path integral, is a standard procedure to cast the discrete-state, continuous-time master equation of reaction-diffusion processes in a second quantised form that is amenable to a perturbative treatment [27, 128, 161]. Its derivation starts from the master equation for the probability $P(\{n_i\}, t)$ to find the system in state $\{n_i\} = \{n_0, n_1, ...\}$, that is to find precisely n_i particles at each site i, which is then written in a second quantised form by introducing a Fock space vector $|\{n_i\}\rangle$, together with the ladder operators $a_i^\dagger$ and a_i for creation and annihilation on each lattice site i. The operators satisfy the commutation relations

$$[a_i, a_j^\dagger] = \delta_{ij}, \quad [a_i, a_j] = [a_i^\dagger, a_j^\dagger] = 0 \tag{6.1}$$

and act on $|\{n_i\}\rangle$ according to

$$a_j|\{n_i\}\rangle = n_j|\{n_j - 1\}\rangle, \quad a_j^\dagger|\{n_i\}\rangle = |\{n_j + 1\}\rangle \ , \tag{6.2}$$

so that $a_i^\dagger a_i$ is the number operator counting the number of particles at site i. The notation $\{n_j + 1\}$ and similar is a suggestive shorthand to indicate that this is the same particle number state as $\{n_i\}$ except that the count at site j is increased by one. The state of the system is thus described by the mixed state

$$|\Psi(t)\rangle = \sum_{\{n_i\}} P(\{n_i\}, t)|\{n_j\}\rangle \ , \tag{6.3}$$

which evolves in time according to an imaginary-time Schrödinger equation of the form [27, 128]

$$\partial_t|\Psi(t)\rangle = \hat{A}(a, a^\dagger)|\Psi(t)\rangle \ . \tag{6.4}$$

For a simple diffusive process on a one-dimensional lattice with homogeneous hopping rate h and extinction rate r, the operator $\hat{A}$ reads

$$\hat{A}(a, a^\dagger) = \sum_i h(a_{i+1}^\dagger + a_{i-1}^\dagger - 2a_i^\dagger)a_i - r(a_i^\dagger - 1)a_i \ . \tag{6.5}$$

The formal solution of Eq. (6.4), $|\Psi(t)\rangle = e^{\hat{A}t}|\Psi(0)\rangle$, can then be cast into path-integral form, whereby the creation and annihilation operators are converted to time-dependent fields, denoted $\psi_i^\dagger(t)$ and $\psi_i(t)$, respectively. For technical reasons discussed extensively elsewhere [27, 128], it is convenient at this stage to introduce the so-called Doi-shifted creation field, $\tilde{\psi}_i(t)$, according to the convention $\psi_i^\dagger(t) = 1+\tilde{\psi}_i(t)$. For the case of simple diffusion, Eq. (6.5), generalised to d dimensions, the action functional of the resulting field theory reads, upon taking the continuum limit,

$$A[\tilde{\psi}(\mathbf{x}, t), \psi(\mathbf{x}, t)] = \int \mathrm{d}^d x \mathrm{d}t \, \tilde{\psi}(\mathbf{x}, t)(\partial_t - D\Delta + r)\psi(\mathbf{x}, t) \tag{6.6}$$

and is fully bilinear. In the continuum limit, the hopping rate h and the diffusion constant D satisfy $D = \lim_{l\to 0} hl^2$ where l is the lattice spacing. In momentum and

frequency space it reads

$$A[\tilde{\psi}(\mathbf{k},\omega),\psi(\mathbf{k},\omega)] = \int \text{đ}^d k\, \text{đ}\omega\, \tilde{\psi}(\mathbf{k},\omega)(-\mathring{\imath}\omega + D\mathbf{k}^2 + r)\psi(-\mathbf{k},-\omega) \tag{6.7}$$

where we have used the convention

$$\psi(\mathbf{x},t) = \int \text{đ}^d k\, \text{đ}\omega\ e^{\mathring{\imath}\mathbf{k}\cdot\mathbf{x}} e^{-\mathring{\imath}\omega t}\psi(\mathbf{k},\omega) \quad \text{and} \quad \psi(\mathbf{k},\omega) = \int \text{d}^d x \text{d}t\ e^{-\mathring{\imath}\mathbf{k}\cdot\mathbf{x}} e^{\mathring{\imath}\omega t}\psi(\mathbf{x},t)\,, \tag{6.8}$$

with $\text{đ}^d k = \text{d}^d k/(2\pi)^d$ and $\text{đ}\omega = \text{d}^d\omega/(2\pi)$ (similarly for $\tilde{\psi}$). We will change freely between different representations.

The diffusive propagator can be obtained by Gaussian integration and reads in k,ω

$$\langle \psi(\mathbf{k},\omega)\tilde{\psi}(\mathbf{k}',\omega')\rangle = \frac{\bar{\delta}(\omega+\omega')\bar{\delta}(\mathbf{k}+\mathbf{k}')}{-\mathring{\imath}\omega + D\mathbf{k}^2 + r} \tag{6.9}$$

with $\bar{\delta}(\mathbf{k}) = (2\pi)\delta(\mathbf{k})$ and $\bar{\delta}(\omega) = (2\pi)\delta(\omega)$. Diagrammatically, the propagator is represented by the Feynman diagram [161]

$$\frac{\bar{\delta}(\omega+\omega')\bar{\delta}(\mathbf{k}+\mathbf{k}')}{-\mathring{\imath}\omega + D\mathbf{k}^2 + r} \hat{=} \quad \mathbf{k},\omega \quad \underline{\qquad} \quad \mathbf{k}',\omega' \quad . \tag{6.10}$$

Henceforth we will use the symbol $\hat{=}$ to indicate equivalence between diagrams and other mathematical expressions. In all diagrams the arrow of time runs from right to left. Expressing fields in x,t, the propagator reads

$$\langle \psi(\mathbf{x},t)\tilde{\psi}(\mathbf{x}',t')\rangle = \theta(t-t')\left(\frac{1}{4\pi D(t-t')}\right)^{d/2} \exp\left(-\frac{(\mathbf{x}-\mathbf{x}')^2}{4D(t-t')}\right)\ , \tag{6.11}$$

for $r \to 0^+$, with the Heaviside theta function $\theta(t)$ enforcing causality. The extinction rate r has solely the role to establish causality, as it generates the Heavyside theta function, and regularize the large t behavior, as it guarantees that any density vanishes in the large t limit. In the following, we may take the limit $r \to 0^+$ whenever convenient. For completeness, the propagator in mixed momentum-time representation reads

$$\langle \psi(\mathbf{k},t)\tilde{\psi}(\mathbf{k}',t')\rangle = \theta(t-t')\bar{\delta}(\mathbf{k}+\mathbf{k}')e^{-Dk^2(t-t')}\ . \tag{6.12}$$

A general observable in the Fock space system is given as a function of occupation numbers $\mathcal{O}(\{n_i\})$. In the Doi-Peliti formalism this corresponds to an operator $\hat{\mathcal{O}}'(\{a_i^\dagger a_i\})$, which is defined by acting on the pure state $|\{n_i\}\rangle$ according to $\hat{\mathcal{O}}'(\{a_i^\dagger a_i\})|\{n_i\}\rangle = \mathcal{O}(\{n_i\})|\{n_i\}\rangle$. We can use the commutation relation (6.1) to normal-order $\hat{\mathcal{O}}'(\{a_i^\dagger a_i\})$ such that all annihilation operators are on the right and all creation operators are on the left. We define the normal ordered operator that acts identical to $\hat{\mathcal{O}}'(\{a_i^\dagger a_i\})$ as $\hat{\mathcal{O}}(\{a_i^\dagger\},\{a_i\})$. Its expectation translates into a path integral according to the following procedure [119]

$$\langle\mathcal{O}\rangle = \sum_{\{n_i\}} \mathcal{O}(\{n_i\})P(\{n_i\},t)|\{n_j\}\rangle \tag{6.13}$$

$$= \langle\text{☼}|\hat{\mathcal{O}}(\{a_i^\dagger\},\{a_i\})e^{\tilde{A}t}|\Psi(0)\rangle \tag{6.14}$$

$$= \int \mathcal{D}\psi\mathcal{D}\tilde{\psi}\ \hat{\mathcal{O}}(\{\tilde{\psi}_i(t)+1\},\{\psi_i(t)\})\ e^{A[\tilde{\psi},\psi]}\mathbb{I}(\tilde{\psi}(0)+1) \tag{6.15}$$

where we have introduced the coherent state,

$$\langle\text{☼}| = \sum_{\{n_i\}}\langle\{n_i\}| \tag{6.16}$$

with $\sum_{\{n_i\}}\langle\{n_i\}|$ summing over all n-particle occupation number states, as well as the initialisation operator $\mathbb{I}(a_i^\dagger)$, which satisfies $\mathbb{I}(a_i^\dagger)|0\rangle = |\Psi(0)\rangle$, with $|0\rangle$ the vacuum state. Going to (6.15) the normal ordering of the operator $\hat{\mathcal{O}}(\{a_i\},\{a_i^\dagger\})$ allowed us to replace annihilation and creation operators by the right and left eigenvalues of the coherent states Ψ_i and $\tilde{\Psi}_i + 1$ respectively.

For an initial condition where m_i particles are placed at each site i at time $t = 0$, the initialisation appears within the path integral Eq. (6.15) as

$$\mathbb{I}(\tilde{\psi}(0)+1) = \prod_i(\tilde{\psi}_i(0)+1)^{m_i} = \prod_i\sum_{k=0}^{m_i}\binom{m_i}{k}\tilde{\psi}_i^k(0) \tag{6.17}$$

after the Doi shift. The process can also be initialised in a statistical mixture of occupation number states, e.g. where the occupation number at each site is drawn from a

Poisson distribution with mean q,

$$\mathbb{I}_{\text{Poiss}}(\tilde{\psi}(0)+1) = \prod_i \left[\sum_{k=0}^{\infty} \left(\frac{e^{-q} q^k}{k!} \right) (\tilde{\psi}_i(0)+1)^k \right] = \prod_i e^{q\tilde{\psi}_i(0)} \ . \tag{6.18}$$

6.2.2 Dean's equation in the response field formalism

Dean's equation [37] is a stochastic differential equation of the Itô type obeyed by the number density function $\rho(\mathbf{x},t)$ for a system of Langevin processes interacting via a pairwise potential. It is an exact mapping of, and thus contains the same information as, the full set of Langevin equations for the individual "single particle" processes. It reads

$$\partial_t \rho(\mathbf{x},t) = \nabla \cdot \left(\rho \nabla \left. \frac{\delta F[\rho]}{\delta \rho} \right|_{\rho(\mathbf{x},t)} \right) + \nabla \cdot (\rho^{1/2} \boldsymbol{\eta}(\mathbf{x},t)) + \sum_i n_i \delta(t-t_i)\delta(\mathbf{x}-\mathbf{x}_i) \tag{6.19}$$

where $F[\rho]$ denotes the free energy functional, defined as

$$F[\rho(\mathbf{x})] = \int \mathrm{d}^d x \, \rho(\mathbf{x}) \left(V(\mathbf{x}) + D \log(\rho(\mathbf{x})) + \frac{1}{2} \int \mathrm{d}^d y \, U(\mathbf{x}-\mathbf{y}) \rho(y) \right) \ , \tag{6.20}$$

with $V(\mathbf{x})$ a general single-particle potential and $U(\mathbf{x}-\mathbf{y})$ a translationally invariant pairwise interaction potential. The term $D\log(\rho)$in Eq. (6.20) is the additional second derivative from Ito's lemma rewritten as an entropic contribution to the free energy. The last term on the right-hand side of Eq. (6.19) describes the initialisation of $n_i \in \mathbb{Z}$ particles in state $\mathbf{x}_i$ at time t_i so that $\lim_{t\to-\infty} \rho(\mathbf{x},t) = 0$. The vector-valued noise $\boldsymbol{\eta}(\mathbf{x},t) \in \mathbb{R}^d$ is an uncorrelated white noise with covariance

$$\langle \eta_\mu(\mathbf{x},t)\eta_\nu(\mathbf{x}',t')\rangle = 2D\delta_{\mu\nu}\delta(t-t')\delta(\mathbf{x}-\mathbf{x}') \ , \tag{6.21}$$

for $\mu,\nu = 1,2,...,d$. The unique feature of Dean's formalism is the nature of the noise term in Eq. (6.19), $\nabla\cdot(\rho^{1/2}\boldsymbol{\eta})$, which is both conservative and Itô-multiplicative, thus conserving the total particle number while preventing fluctuations from producing regions of negative density. Following the standard procedure [72, 164], which requires special attention due to the multiplicative nature of the noise [74, 167], Dean's equation (6.19) for the time and space dependent field $\rho(\mathbf{x},t)$ can be cast as a response

field, or Martin-Siggia-Rose-Janssen-De Dominicis, field theory with action

$$A[\rho,\tilde{\rho}] = \int \mathrm{d}^d x \mathrm{d}t\, \tilde{\rho}\left(\partial_t \rho - \nabla\cdot\rho\nabla\left.\frac{\delta F[\rho]}{\delta\rho}\right|_{\rho(\mathbf{x},t)}\right) - \rho D(\nabla\tilde{\rho})^2 - \tilde{\rho}\sum_i n_i\delta(t-t_i)\delta(\mathbf{x}-\mathbf{x}_i)\ , \tag{6.22}$$

which simplifies to

$$A[\rho,\tilde{\rho}] = \int \mathrm{d}^d x \mathrm{d}t\, \tilde{\rho}(\mathbf{x},t)\left(\partial_t\rho(\mathbf{x},t) - D\Delta\rho(\mathbf{x},t)\right) - \tilde{\rho}\sum_i n_i\delta(t-t_i)\delta(\mathbf{x}-\mathbf{x}_i) - \rho D(\nabla\tilde{\rho})^2 \tag{6.23}$$

$$\begin{aligned} &= \int \text{đ}^d k\, \text{đ}\omega\, \tilde{\rho}(-\mathbf{k},-\omega)(-\mathring{\imath}\omega + D\mathbf{k}^2)\rho(\mathbf{k},\omega) - \tilde{\rho}(\mathbf{k},\omega)\sum_i n_i e^{\mathring{\imath}\mathbf{k}\cdot\mathbf{x}_i} e^{-\mathring{\imath}\omega t_i} \\ &\quad + \int \text{đ}^d k \text{đ}^d k'\, \text{đ}\omega\, \text{đ}\omega'\, D(\mathbf{k}\cdot\mathbf{k}')\tilde{\rho}(\mathbf{k},\omega)\tilde{\rho}(\mathbf{k}',\omega')\rho(-(\mathbf{k}+\mathbf{k}'),-(\omega+\omega')) \end{aligned} \tag{6.24}$$

in the case of non-interacting particles undergoing simple diffusion without external potential. Unlike the Doi-Peliti path integral, Eq. (6.15), the initialisation here shows up as a term in the action. In a diagrammatic perturbation theory, these n_i particles starting from positions $\mathbf{x}_i$ will be shown as a small, filled circle acting as a source:

 . (6.25)

We will make the simplifying assumption of having only a single non-zero n_i, namely n_0, and generalise our result in Appendix 6.B. The presence of the source spoils translational invariance and as a result, the hallmark δ-function as it normally multiplies any correlation function, say $\delta(\mathbf{k}_0+\mathbf{k}_1+\ldots+\mathbf{k}_n)$ will be replaced by

$$\int \text{đ}^d k_0\, \mathrm{e}^{\mathring{\imath}\mathbf{k}_0\cdot\mathbf{x}_0}\delta(\mathbf{k}_0+\mathbf{k}_1+\ldots+\mathbf{k}_n) = \mathrm{e}^{-\mathring{\imath}(\mathbf{k}_1+\ldots+\mathbf{k}_n)\cdot\mathbf{x}_0}\ . \tag{6.26}$$

Where readability is improved by it, we will retain the integral.

The expectation value of a field-dependent observable $\mathcal{O}[\rho]$ can then be computed via the path integral

$$\langle\mathcal{O}[\rho]\rangle = \int \mathcal{D}\rho\mathcal{D}\tilde{\rho}\ \mathcal{O}[\rho]\mathrm{e}^{-A[\rho,\tilde{\rho}]} \tag{6.27}$$

where $\tilde{\rho}$ is the purely imaginary response field. The normalisation is chosen such that

$\langle 1 \rangle = 1$. The action A is then split into a bilinear and an interacting part, denoted A_0 and A_{int} respectively, according to

$$A_0[\rho, \tilde{\rho}] = \int \mathrm{d}^d x \mathrm{d}t \, \tilde{\rho} \left(\partial_t \rho - D \Delta \rho \right) \tag{6.28}$$

and

$$\begin{aligned} A_{\text{int}}[\rho, \tilde{\rho}] = - \int \mathrm{d}^d x \mathrm{d}t \Bigg\{ & \rho(\mathbf{x}, t) D (\nabla \tilde{\rho}(\mathbf{x}, t))^2 \\ & + \tilde{\rho}(\mathbf{x}, t) \nabla_{\mathbf{x}} \cdot \left(\rho(\mathbf{x}, t) \nabla_{\mathbf{x}} \left[V(\mathbf{x}) + \int \mathrm{d}^d y \ \frac{1}{2} U(\mathbf{x} - \mathbf{y}) \rho(\mathbf{y}, t) \right] \right) \\ & + \tilde{\rho}(\mathbf{x}, t) \sum_i n_i \delta(\mathbf{x} - \mathbf{x}_i) \delta(t - t_i) \Bigg\} \end{aligned} \tag{6.29}$$

$$\begin{aligned} = & \int \text{đ}^d k_{1,2,3} \ \text{đ}\omega_{1,2,3} \, \delta(\mathbf{k}_1 + \mathbf{k}_2 + \mathbf{k}_3) \delta(\omega_1 + \omega_2 + \omega_3) \\ & \Bigg\{ \rho(\mathbf{k}_1, \omega_1) D (\mathbf{k}_2 \cdot \mathbf{k}_3) \tilde{\rho}(\mathbf{k}_2, \omega_2) \tilde{\rho}(\mathbf{k}_3, \omega_3) \\ & \quad + \tilde{\rho}(\mathbf{k}_1, \omega_1) ((\mathbf{k}_2 + \mathbf{k}_3) \cdot \mathbf{k}_3) \rho(\mathbf{k}_2, \omega_2) \left[V(\mathbf{k}_3) \delta(\omega_3) + \frac{1}{2} U(\mathbf{k}_3) \rho(\mathbf{k}_3, \omega_3) \right] \Bigg\} \\ & - \int \text{đ}^d k \ \text{đ}\omega \, \tilde{\rho}(\mathbf{k}, \omega) \sum_i n_i \mathrm{e}^{\mathrm{i} \mathbf{k} \cdot \mathbf{x}_i} \mathrm{e}^{-\mathrm{i} \omega t_i} \end{aligned} \tag{6.30}$$

Finally, expectations are computed in a perturbation theory about the bilinear theory using

$$\langle \mathcal{O}[\rho] \rangle = \sum_{n=0}^{\infty} \left\langle \frac{(-A_{\text{int}}[\rho, \tilde{\rho}])^n}{n!} \mathcal{O}[\rho] \right\rangle_0 , \tag{6.31}$$

where

$$\langle \bullet \rangle_0 = \int \mathcal{D}\rho \, \mathcal{D}\tilde{\rho} \ \bullet \ \mathrm{e}^{-A_0[\rho, \tilde{\rho}]} \tag{6.32}$$

denotes expectation with respect to the bilinear action, Eq. (6.28). The right hand side of Eq. (6.31) involves products of fields and the Wick-Isserlis theorem [92] can be

invoked to express these in terms of the bare propagator,

$$G(\mathbf{x}-\mathbf{x}',t-t') = \langle \rho(\mathbf{x},t)\tilde{\rho}(\mathbf{x}',t')\rangle_0 \mathrel{\hat{=}} \quad \mathbf{x},t \quad \mathbf{x}',t' \quad , \tag{6.33}$$

obtained from the bilinear action. In d dimensions, the bare propagator reads

$$G(\mathbf{x}-\mathbf{x}',t-t') = \theta(t-t')\left(\frac{1}{4\pi D(t-t')}\right)^{d/2} \exp\left(-\frac{(\mathbf{x}-\mathbf{x}')^2}{4D(t-t')}\right) \ , \tag{6.34}$$

with the Heaviside theta function $\theta(t)$ enforcing causality. This propagator is identical to that of the corresponding Doi-Peliti field theory, Eq. (6.11). For later use, we recall the form of the propagator in momentum-frequency representation,

$$\langle \rho(\mathbf{k},\omega)\tilde{\rho}(\mathbf{k}',\omega')\rangle_0 = \frac{\delta(\mathbf{k}+\mathbf{k}')\delta(\omega+\omega')}{-\mathring{\imath}\omega + D\mathbf{k}^2 + r} \ , \tag{6.35}$$

which we have amended by the extinction rate $r \to 0^+$ to enforce causality, as Eq. (6.9). Further, we introduce the mixed momentum-time representation,

$$\langle \rho(\mathbf{k},t)\tilde{\rho}(\mathbf{k}',t')\rangle_0 = \theta(t-t')\delta(\mathbf{k}+\mathbf{k}')\mathrm{e}^{-D(t-t')\mathbf{k}^2} \ , \tag{6.36}$$

see Eq. (6.12). For non-interacting particles in a flat potential, $\nabla V(\mathbf{x}) = 0$, $\nabla U(\mathbf{x}) = 0$, the bare propagator equals the full propagator,

$$\langle \rho(\mathbf{k},t)\tilde{\rho}(\mathbf{k}',t')\rangle = \langle \rho(\mathbf{k},t)\tilde{\rho}(\mathbf{k}',t')\rangle_0 \tag{6.37}$$

as the only non-linear term in the action is the amputated three-point vertex

$$-\rho D(\nabla\tilde{\rho})^2 \mathrel{\hat{=}} \tag{6.38}$$



with the dashes on the propagators denoting spatial derivatives acting on the response fields and the dotted line the scalar product of these derivatives. The presence of such a vertex in the free particle case is a non-trivial feature of Dean's equation and clashes somewhat with the notion of 'interaction' associated with terms of order higher than bilinear [164]. As we will demonstrate below, Eq. (6.38), which we will refer to interchangeably as *Dean's vertex* or a *virtual branching* vertex, is the term that implements the particle nature of the degrees of freedom within the Dean

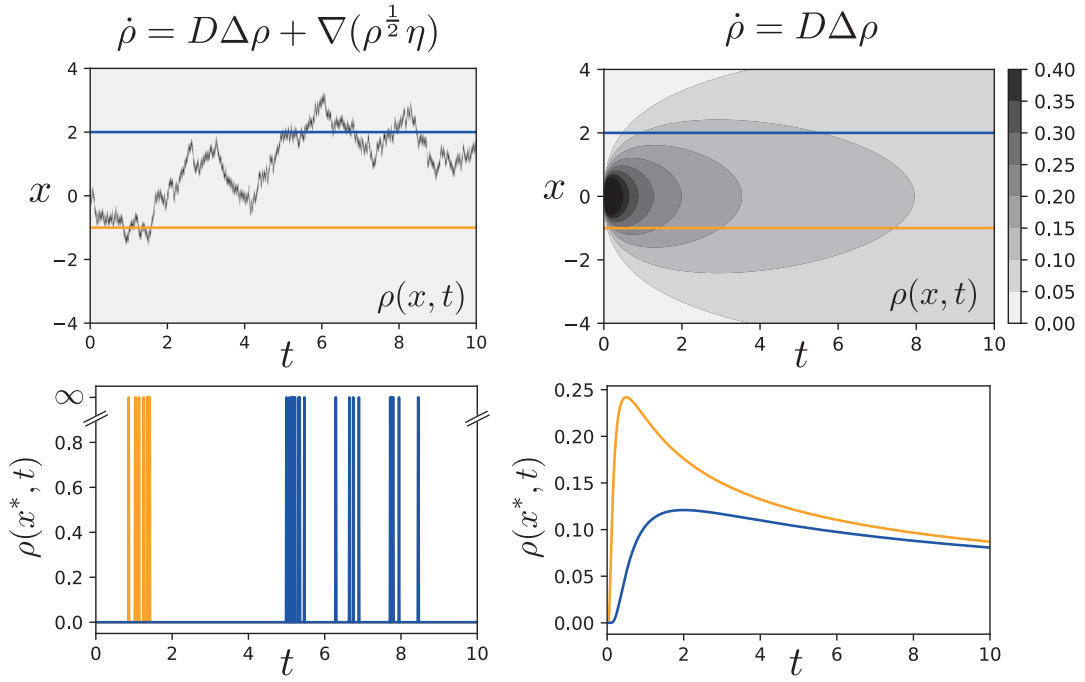


Figure 6.2.1: The time-dependent number density $\rho(x,t)$ for a physical point particle undergoing diffusion is expected to remain localised under the dynamics, indicating that the particle can only occupy one position in space at any given time. While this property is preserved under Dean's dynamics (left column), it is generally lost when resorting to effective descriptions, such as the classical diffusion equation (right column). This difference is most obvious when measuring the instantaneous particle number density at two points a finite distance away from each other (bottom row).

framework. In contrast to Doi-Peliti, particle entity in the response field formalism of Dean's equation is a perturbative feature. The effect of Dean's vertex is illustrated in Fig. 6.2.1 by comparison with the standard diffusion equation, which lacks particle entity. To generate Fig. 6.2.1, we do not solve the Deans equation Eq. (6.19) numerically. For the random walk in the top left plot of Fig. 6.2.1, we implement a finite difference numerical integration on the Langevin equation for a purely diffusive particle. To generate the bottom left plot of Fig. 6.2.1, we simply select some positions x from the Brownian trajectory and plot a peak at those positions to simply illustrate the meaning of particle entity.

The Doi-Peliti field theory and the response field field theory derived from Dean's equation can be mapped onto each other by means of a Cole-Hopf transformation of

the fields [95],

$$\psi^\dagger \to e^{\tilde{\rho}}, \quad \psi \to \rho e^{-\tilde{\rho}} \; . \tag{6.39}$$

This equivalence implies that the two formalisms should be equally capable of capturing particle entity. The precise mechanisms by which each does so, however, turn out to be very different, as we will see in detail in Section 6.4 and 6.5.

6.2.3 Example: the two-point density correlation function

To illustrate the similarities and differences between the two formalisms introduced above, we now calculate the two-point correlation function of the particle number density for n_0 non-interacting diffusive particles in a flat potential, $\nabla V(\mathbf{x}) = 0$ and $\nabla U(\mathbf{x}) = 0$, all initialised at the same position x_0 and time t_0, first in the Doi-Peliti scheme and then using Dean's equation. While the result of this detailed calculation is somewhat trivial and can be derived by straightforward probabilistic arguments, its derivation elucidates certain formalism-specific cancellation mechanisms that will play an important role in the remainder of this work. The reader interested in the generic definition of particle entity but not in the details of the field theoretic approach can skip directly to Section 6.3.

We first use the parameterisation of the field theories in $\mathbf{k}$ and ω, which is very commonly used in field theories. In real-space and time, the two-point correlation function $C(\mathbf{x}_1, \mathbf{x}_2, t_1, t_2)$ in the Doi-Peliti framework is the observable [164, 27]

$$C(\mathbf{x}_1, \mathbf{x}_2, t_1, t_2) = \left\langle \left(\psi^\dagger(\mathbf{x}_2, t_2)\psi(\mathbf{x}_2, t_2)\right)\left(\psi^\dagger(\mathbf{x}_1, t_1)\psi(\mathbf{x}_1, t_1)\right)\psi^{\dagger n_0}(\mathbf{x}_0, t_0)\right\rangle \tag{6.40}$$

$$\begin{aligned} &= \binom{n_0}{1}\left\langle \psi(\mathbf{x}_2, t_2)\widetilde{\psi}(\mathbf{x}_1, t_1)\right\rangle\left\langle \psi(\mathbf{x}_1, t_1)\widetilde{\psi}(\mathbf{x}_0, t_0)\right\rangle \\ &\quad + \binom{n_0}{1}\left\langle \psi(\mathbf{x}_1, t_1)\widetilde{\psi}(\mathbf{x}_2, t_2)\right\rangle\left\langle \psi(\mathbf{x}_2, t_2)\widetilde{\psi}(\mathbf{x}_0, t_0)\right\rangle \\ &\quad + 2\binom{n_0}{2}\left\langle \psi(\mathbf{x}_2, t_2)\widetilde{\psi}(\mathbf{x}_0, t_0)\right\rangle\left\langle \psi(\mathbf{x}_1, t_1)\widetilde{\psi}(\mathbf{x}_0, t_0)\right\rangle \end{aligned} \tag{6.41}$$

$$\hat{=} \binom{n_0}{1} \quad \mathbf{x}_2, t_2 \;\; \mathbf{x}_1, t_1 \;\; \mathbf{x}_0, t_0 \quad + \quad \binom{n_0}{1} \quad \mathbf{x}_1, t_1 \;\; \mathbf{x}_2, t_2 \;\; \mathbf{x}_0, t_0 \quad + \quad 2\binom{n_0}{2} \quad \begin{matrix} \mathbf{x}_1, t_1 & \mathbf{x}_0, t_0 \\ \mathbf{x}_2, t_2 & \mathbf{x}_0, t_0 \end{matrix} \tag{6.42}$$

where we assume $\mathbf{x}_1 \neq \mathbf{x}_2$ to avoid the special case of non-commutation of the operators. The high number of terms in Eq. (6.40) is due to the Doi-shift, which splits each daggered creator field in two terms, $\psi^\dagger = 1 + \widetilde{\psi}$. This turns the contribution of the initial particles into $\psi^{\dagger n_0} = \sum_k^{n_0} \binom{n_0}{k} \widetilde{\psi}^{n_0}$. The vertices made from a crossed circle in Eq. (6.42) are meant to indicate an annihilation field at the indicated position and time with immediate re-creation. Eq. (6.40) has the generic form of a two-point correlation function in the Doi-Peliti framework without interaction.

Eq. (6.41) is still expressed in real space and direct time and needs to be Fourier-transformed to write it in the common $\mathbf{k}, \omega$ parameterisation. Each of the three terms in Eq. (6.41) requires four integrals in $\mathbf{k}$ and four in ω, for example

$$n_0 \quad \mathbf{x}_2, t_2 \quad \mathbf{x}_1, t_1 \quad \mathbf{x}_0, t_0 \tag{6.43}$$

$$\hat{=} n_0 \int \text{đ}^d k_2 \text{đ}^d k_1' \text{đ}^d k_1 \text{đ}^d k_0 \, \text{đ}\omega_2 \, \text{đ}\omega_1' \, \text{đ}\omega_1 \, \text{đ}\omega_0 \, \frac{\delta(\mathbf{k}_2 + \mathbf{k}_1')\delta(\omega_2 + \omega_1')}{-\mathring{\imath}\omega_2 + D\mathbf{k}_2^2 + r} \frac{\delta(\mathbf{k}_1 + \mathbf{k}_0)\delta(\omega_1 + \omega_0)}{-\mathring{\imath}\omega_1 + D\mathbf{k}_1^2 + r} \tag{6.44}$$

$$\times \, \mathrm{e}^{\mathring{\imath}(\mathbf{k}_2 \cdot \mathbf{x}_2 + \mathbf{k}_1' \cdot \mathbf{x}_1 + \mathbf{k}_1 \cdot \mathbf{x}_1 + \mathbf{k}_0 \cdot \mathbf{x}_0)} \mathrm{e}^{-\mathring{\imath}(\omega_2 t_2 + \omega_1' t_1 + \omega_1 t_1 + \omega_0 t_0)}$$

drawing on the propagator introduced in Eq. (6.9). Using the δ-functions, the integrals in each term are immediately reduced to only two, all differing solely in the arguments of the exponentials:

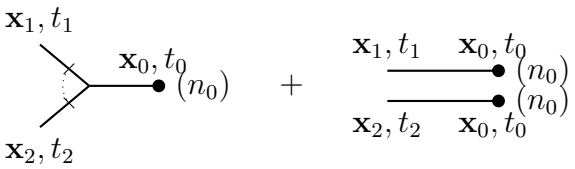
$$\begin{aligned} C(\mathbf{x}_1, \mathbf{x}_2, t_1, t_2) = \int \text{đ}^d k_2 \text{đ}^d k_1 \, \text{đ}\omega_2 \, \text{đ}\omega_1 \, \frac{1}{-\mathring{\imath}\omega_2 + D\mathbf{k}_2^2 + r} \frac{1}{-\mathring{\imath}\omega_1 + D\mathbf{k}_1^2 + r} \\ \times \Big\{ n_0 \mathrm{e}^{\mathring{\imath}(\mathbf{k}_2 \cdot (\mathbf{x}_2 - \mathbf{x}_1) + \mathbf{k}_1 \cdot (\mathbf{x}_1 - \mathbf{x}_0))} \mathrm{e}^{-\mathring{\imath}(\omega_2 (t_2 - t_1) + \omega_1 (t_1 - t_0))} \\ + n_0 \mathrm{e}^{\mathring{\imath}(\mathbf{k}_2 \cdot (\mathbf{x}_2 - \mathbf{x}_0) + \mathbf{k}_1 \cdot (\mathbf{x}_1 - \mathbf{x}_2))} \mathrm{e}^{-\mathring{\imath}(\omega_2 (t_2 - t_0) + \omega_1 (t_1 - t_2))} \\ + n_0 (n_0 - 1) \mathrm{e}^{\mathring{\imath}(\mathbf{k}_2 \cdot (\mathbf{x}_2 - \mathbf{x}_0) + \mathbf{k}_1 \cdot (\mathbf{x}_1 - \mathbf{x}_0))} \mathrm{e}^{-\mathring{\imath}(\omega_2 (t_2 - t_0) + \omega_1 (t_1 - t_0))} \Big\} \end{aligned} \tag{6.45}$$

with $r \to 0^+$ still to be taken. The first of the three terms in the integrand describes the propagation of any of n_0 particles from $\mathbf{x}_0$ at t_0 to $\mathbf{x}_1$ at t_1 and from there to $\mathbf{x}_2$ at t_2. This term will contribute only if $t_2 \geq t_1 \geq t_0$. The second term describes a similar process, from $\mathbf{x}_0$ at t_0 to $\mathbf{x}_2$ at t_2 and from there to $\mathbf{x}_1$ at t_1, contributing only if $t_1 \geq t_2 \geq t_0$. The last term describes the propagation of two independent particles from $\mathbf{x}_0$ at t_0 to $\mathbf{x}_1$ at t_1 and another one from $\mathbf{x}_0$ at t_0 to $\mathbf{x}_2$ at t_2. There are $n_0(n_0 -$

1) such pairs. If $n_0 \leq 1$, the last term vanishes, leaving only the first two terms, both of which vanish if $t_1 = t_2$ and $\mathbf{x}_1 \neq \mathbf{x}_2$ as we will show below, because a *particle* cannot possibly be found at two different places simultaneously. Eq. (6.45) completes the derivation of the correlation function in the Doi-Peliti framework.

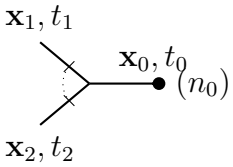
To derive the correlation function in Dean's framework, we use the action as stated in Eq. (6.23) with both the interaction and the source treated perturbatively. The role of the creator fields in the field theory of Dean's equation is very different from Doi-Peliti. In the Dean framework, the two-point correlation function is

$$C(\mathbf{x}_1, \mathbf{x}_2, t_1, t_2) = \langle \rho(\mathbf{x}_2, t_2)\rho(\mathbf{x}_1, t_1)\rangle \mathrel{\hat{=}}$$



(6.46)

as every field $\rho(\mathbf{x}, t)$ can be matched with a creator field from the perturbative part of the action, shown as a small filled circle at the right end of the incoming propagators. Each such creator field appears with a *coupling* n_0, which we have highlighted by writing it in brackets behind each source in the diagram. While the second term in Eq. (6.46) is structurally identical to the last term in Eq. (6.42) and indeed captures the same process, the pre-factors of the two differ by n_0. The first two terms in Eq. (6.42) on the other hand seem to be absent from Eq. (6.46). In turn, the first diagram of Eq. (6.46), is solely due to the Dean-vertex Eq. (6.38) and therefore absent in Doi-Peliti, Eq. (6.42). Writing this term in $\mathbf{k}, \omega$ gives

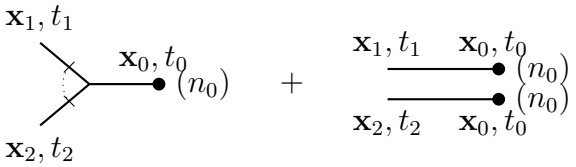


$$\mathrel{\hat{=}} \int \text{đ}^d k_2 \text{đ}^d k_1 \, \text{đ}\omega_2 \, \text{đ}\omega_1 \, \mathrm{e}^{\mathring{\imath}(\mathbf{k}_2\cdot(\mathbf{x}_2-\mathbf{x}_0)+\mathbf{k}_1\cdot(\mathbf{x}_1-\mathbf{x}_0))} \mathrm{e}^{-\mathring{\imath}(\omega_2(t_2-t_0)+\omega_1(t_1-t_0))}$$
$$\times (-2n_0 D\mathbf{k}_1\cdot\mathbf{k}_2) \frac{1}{-\mathring{\imath}\omega_2 + D\mathbf{k}_2^2 + r} \frac{1}{-\mathring{\imath}\omega_1 + D\mathbf{k}_1^2 + r} \frac{1}{-\mathring{\imath}(\omega_1+\omega_2) + D(\mathbf{k}_1+\mathbf{k}_2)^2 + r} \tag{6.47}$$

using Eq. (6.35) for the propagator and where the factor $(-2n_0 D\mathbf{k}_1 \cdot \mathbf{k}_2)$ is due to

the sign of the interaction term in the action Eq. (6.23), including a factor 2 from symmetry.

The second term in Eq. (6.46) can be read off from Eqs. (6.42) and (6.45). Its prefactor of n_0^2 has to be split into $n_0^2 = n_0(n_0-1)+n_0$ to reveal the cancellation mechanism,



(6.48)

$$\hat{=} \int \mathrm{đ}^d k_2 \mathrm{đ}^d k_1 \, \mathrm{đ}\omega_2 \, \mathrm{đ}\omega_1 \, \mathrm{e}^{\mathring{\imath}(\mathbf{k}_2\cdot(\mathbf{x}_2-\mathbf{x}_0)+\mathbf{k}_1\cdot(\mathbf{x}_1-\mathbf{x}_0))} \mathrm{e}^{-\mathring{\imath}(\omega_2(t_2-t_0)+\omega_1(t_1-t_0))} \times$$
$$\frac{1}{-\mathring{\imath}\omega_2 + D\mathbf{k}_2^2 + r} \frac{1}{-\mathring{\imath}\omega_1 + D\mathbf{k}_1^2 + r} \left(\frac{-2n_0 D\mathbf{k}_1\cdot\mathbf{k}_2}{-\mathring{\imath}(\omega_1+\omega_2) + D(\mathbf{k}_1+\mathbf{k}_2)^2 + r} + n_0 + n_0(n_0-1) \right) \tag{6.49}$$

$$= \int \mathrm{đ}^d k_2 \mathrm{đ}^d k_1 \, \mathrm{đ}\omega_2 \, \mathrm{đ}\omega_1 \, \mathrm{e}^{\mathring{\imath}(\mathbf{k}_2\cdot(\mathbf{x}_2-\mathbf{x}_0)+\mathbf{k}_1\cdot(\mathbf{x}_1-\mathbf{x}_0))} \mathrm{e}^{-\mathring{\imath}(\omega_2(t_2-t_0)+\omega_1(t_1-t_0))}$$
$$\times \Big\{ n_0 \frac{1}{-\mathring{\imath}(\omega_1+\omega_2) + D(\mathbf{k}_1+\mathbf{k}_2)^2 + r} \tag{6.50}$$
$$\times \left(\frac{1}{-\mathring{\imath}\omega_2 + D\mathbf{k}_2^2 + r} + \frac{1}{-\mathring{\imath}\omega_1 + D\mathbf{k}_1^2 + r} - \frac{r}{(-\mathring{\imath}\omega_1 + D\mathbf{k}_1^2 + r)(-\mathring{\imath}\omega_2 + D\mathbf{k}_2^2 + r)} \right)$$
$$+ n_0(n_0-1) \frac{1}{-\mathring{\imath}\omega_2 + D\mathbf{k}_2^2 + r} \frac{1}{-\mathring{\imath}\omega_1 + D\mathbf{k}_1^2 + r} \Big\} .$$

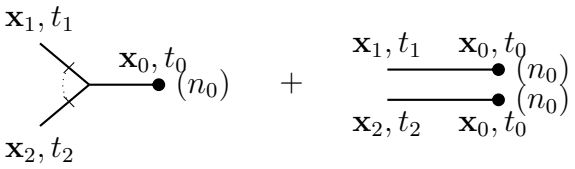
The term proportional to r in the numerator eventually vanishes when $r \to 0$. To see now that Eq. (6.50) is in fact identical to the first two terms in Eqs. (6.42) and (6.45) requires a simple substitution of the dummy variables, for example $\mathbf{k}_1 + \mathbf{k}_2$ becoming

$\mathbf{k}_1$,

$$\int \text{đ}^d k_2 \text{đ}^d k_1 \, \text{đ}\omega_2 \, \text{đ}\omega_1 \, \text{e}^{i(\mathbf{k}_2\cdot(\mathbf{x}_2-\mathbf{x}_0)+\mathbf{k}_1\cdot(\mathbf{x}_1-\mathbf{x}_0))}\text{e}^{-i(\omega_2(t_2-t_0)+\omega_1(t_1-t_0))}$$
$$\times \frac{1}{-i(\omega_1+\omega_2)+D(\mathbf{k}_1+\mathbf{k}_2)^2+r}\frac{1}{-i\omega_2+D\mathbf{k}_2^2+r} \tag{6.51}$$
$$= \int \text{đ}^d k_2 \text{đ}^d k_1 \, \text{đ}\omega_2 \, \text{đ}\omega_1 \, \text{e}^{i(\mathbf{k}_2\cdot(\mathbf{x}_2-\mathbf{x}_1)+\mathbf{k}_1\cdot(\mathbf{x}_1-\mathbf{x}_0))}\text{e}^{-i(\omega_2(t_2-t_1)+\omega_1(t_1-t_0))}$$
$$\times \frac{1}{-i\omega_1+D\mathbf{k}_1^2+r}\frac{1}{-i\omega_2+D\mathbf{k}_2^2+r} \, . \tag{6.52}$$

In summary, after pairing in Eq. (6.50) the interaction term of Dean's equation with the two independent propagators, the field theory of Dean's equation reproduces the two-point correlation function as the Doi-Peliti framework, Eq. (6.45), except for a term proportional to r which vanishes in the limit of $r \to 0$:

$$C(\mathbf{x}_1,\mathbf{x}_2,t_1,t_2) = \langle \rho(\mathbf{x}_2,t_2)\rho(\mathbf{x}_1,t_1)\rangle \mathrel{\hat{=}}$$



(6.53)

$$\mathrel{\hat{=}} \int \text{đ}^d k_2 \text{đ}^d k_1 \, \text{đ}\omega_2 \, \text{đ}\omega_1 \, \frac{1}{-i\omega_2+D\mathbf{k}_2^2+r}\frac{1}{-i\omega_1+D\mathbf{k}_1^2+r} \tag{6.54}$$
$$\times \Big\{ n_0 \text{e}^{i(\mathbf{k}_2\cdot(\mathbf{x}_2-\mathbf{x}_1)+\mathbf{k}_1\cdot(\mathbf{x}_1-\mathbf{x}_0))}\text{e}^{-i(\omega_2(t_2-t_1)+\omega_1(t_1-t_0))}$$
$$+ n_0 \text{e}^{i(\mathbf{k}_2\cdot(\mathbf{x}_2-\mathbf{x}_0)+\mathbf{k}_1\cdot(\mathbf{x}_1-\mathbf{x}_2))}\text{e}^{-i(\omega_2(t_2-t_0)+\omega_1(t_1-t_2))}$$
$$- n_0 \frac{r}{-i(\omega_1+\omega_2)+D(\mathbf{k}_1+\mathbf{k}_2)^2+r}$$
$$\times \text{e}^{i(\mathbf{k}_2\cdot(\mathbf{x}_2-\mathbf{x}_0)+\mathbf{k}_1\cdot(\mathbf{x}_1-\mathbf{x}_0))}\text{e}^{-i(\omega_2(t_2-t_0)+\omega_2(t_1-t_0))}$$
$$+ n_0(n_0-1)\text{e}^{i(\mathbf{k}_2\cdot(\mathbf{x}_2-\mathbf{x}_0)+\mathbf{k}_1\cdot(\mathbf{x}_1-\mathbf{x}_0))}\text{e}^{-i(\omega_2(t_2-t_0)+\omega_1(t_1-t_0))} \Big\} \, .$$

This concludes the demonstration that the Doi-Peliti framework and Dean's equation produce identical results for the two-point correlation function. Eq. (6.50) illustrates the central cancellation mechanism, which we generalise to the relevant observables below, in particular Appendix 6.A. As Eq. (6.38) is a perturbative term, the resulting branching diagrams in Eq. (6.53) *discount* contributions due to independent parti-

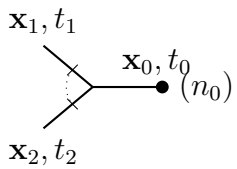
cle movement, shown as two parallel propagators in Eq. (6.53), of which there are n_0^2 rather than $n_0(n_0-1)$.

Performing the calculation above immediately in direct time and real space is most easily done assuming a particular time ordering, say $t_2 > t_1 > t_0$. In that case, Doi-Peliti produces

$$\begin{aligned} C(\mathbf{x}_1,\mathbf{x}_2,t_1,t_2) = n_0 \frac{e^{-\frac{(\mathbf{x}_2-\mathbf{x}_1)^2}{4D(t_2-t_1)}}}{(4\pi D(t_2-t_1))^{d/2}} \frac{e^{-\frac{(\mathbf{x}_1-\mathbf{x}_0)^2}{4D(t_1-t_0)}}}{(4\pi D(t_1-t_0))^{d/2}} \\ + n_0(n_0-1) \frac{e^{-\frac{(\mathbf{x}_1-\mathbf{x}_0)^2}{4D(t_1-t_0)}}}{(4\pi D(t_1-t_0))^{d/2}} \frac{e^{-\frac{(\mathbf{x}_2-\mathbf{x}_0)^2}{4D(t_2-t_0)}}}{(4\pi D(t_2-t_0))^{d/2}} \end{aligned} \tag{6.55}$$

directly from Eq. (6.42) using the propagator Eq. (6.11). As $t_2 > t_1$, only the first and the last diagrams of Eq. (6.42) contribute, the first due to a particle travelling from $\mathbf{x}_0$ to $\mathbf{x}_1$ and then to $\mathbf{x}_2$ and the last due to two particles travelling independently. In the limit of $t_2 \downarrow t_1$ the first term, proportional to n_0, becomes $n_0\delta(\mathbf{x}_2 - \mathbf{x}_1)(4\pi D(t_1-t_0))^{-d/2}\exp\left(-(\mathbf{x}_1-\mathbf{x}_0)^2/(4\pi D(t_1-t_0))\right)$, vanishing if $\mathbf{x}_1 \neq \mathbf{x}_2$ as the same particle cannot be at two different places simultaneously. Fig. 6.2.1 provides a visual illustration of this property.

Although this approach no longer requires regularisation by the extinction rate r, it is somewhat more demanding to perform the calculation of the correlation function within Dean's equation in direct time and real space using Eq. (6.34), because the Dean-vertex requires a convolution over the time and the position where the virtual branching takes place,



$$\hat{=} 2n_0 \int \mathrm{d}^d x' \mathrm{d}t' \left(\nabla_{\mathbf{x}'} G(\mathbf{x}_2 - \mathbf{x}', t_2 - t')\right) \cdot \left(\nabla_{\mathbf{x}'} G(\mathbf{x}_1 - \mathbf{x}', t_1 - t')\right) G(\mathbf{x}' - \mathbf{x}_0, t' - t_0) \ . \tag{6.56}$$

After some algebra, Dean's equation produces of course the same correlation function Eq. (6.55) as Doi-Peliti.

In explicit calculations below, notably Appendix 6.A, we will make use of a mixed

momentum-time, k, t, parameterisation, for which we briefly outline the cancellation mechanism in the following. In Doi-Peliti, the diagrams Eq. (6.42) can immediately be written as

$$\begin{aligned} C(\mathbf{x}_1, \mathbf{x}_2, t_1, t_2) = & \int \text{đ}^d k_2 \text{đ}^d k_1 \\ & \times \Big\{ n_0 \mathrm{e}^{i(\mathbf{k}_2\cdot(\mathbf{x}_2-\mathbf{x}_1)+\mathbf{k}_1\cdot(\mathbf{x}_1-\mathbf{x}_0))} \theta(t_2-t_1)\theta(t_1-t_0) \mathrm{e}^{-D\mathbf{k}_2^2(t_2-t_1)-D\mathbf{k}_1^2(t_1-t_0))} \\ & \quad + n_0 \mathrm{e}^{i(\mathbf{k}_2\cdot(\mathbf{x}_2-\mathbf{x}_0)+\mathbf{k}_1\cdot(\mathbf{x}_1-\mathbf{x}_2))} \theta(t_1-t_2)\theta(t_2-t_0) \mathrm{e}^{-D\mathbf{k}_1^2(t_1-t_2)-D\mathbf{k}_2^2(t_2-t_0))} \\ & + n_0(n_0-1) \mathrm{e}^{i(\mathbf{k}_2\cdot(\mathbf{x}_2-\mathbf{x}_0)+\mathbf{k}_1\cdot(\mathbf{x}_1-\mathbf{x}_0))} \theta(t_2-t_0)\theta(t_1-t_0) \mathrm{e}^{-D\mathbf{k}_2^2(t_2-t_0)-D\mathbf{k}_1^2(t_1-t_0))} \Big\} \end{aligned} \tag{6.57}$$

by replacing each of the bare propagators of Eq. (6.41) by Eq. (6.12) and making use of the δ-functions on the momenta, or by direct interpretation of the diagrams.

Dean's equation, Eq. (6.46), on the other hand, produces

$$\begin{aligned} C(\mathbf{x}_1, \mathbf{x}_2, t_1, t_2) = & \int \text{đ}^d k_2 \text{đ}^d k_1 \text{đ}^d k_0 \, \mathrm{e}^{i\mathbf{k}_2\cdot\mathbf{x}_2} \mathrm{e}^{i\mathbf{k}_1\cdot\mathbf{x}_1} \mathrm{e}^{i\mathbf{k}_0\cdot\mathbf{x}_0} \delta(\mathbf{k}_2+\mathbf{k}_1+\mathbf{k}_0) \\ & \times \Big\{ (-2n_0 D\mathbf{k}_1\cdot\mathbf{k}_2) \int_{-\infty}^{\infty} \mathrm{d}t' \, \theta(t_2-t') \mathrm{e}^{-D\mathbf{k}_2^2(t_2-t')} \theta(t_1-t') \mathrm{e}^{-D\mathbf{k}_1^2(t_1-t')} \theta(t'-t_0) \mathrm{e}^{-D\mathbf{k}_0^2(t'-t_0)} \Big\} \\ & + \int \text{đ}^d k_2 \text{đ}^d k_1 \, \mathrm{e}^{i\mathbf{k}_2\cdot(\mathbf{x}_2-\mathbf{x}_0)} \mathrm{e}^{i\mathbf{k}_1\cdot(\mathbf{x}_1-\mathbf{x}_0)} \\ & \qquad \times \Big\{ n_0^2 \theta(t_2-t_0) \mathrm{e}^{-D\mathbf{k}_2^2(t_2-t_0)} \theta(t_1-t_0) \mathrm{e}^{-D\mathbf{k}_1^2(t_1-t_0)} \Big\} \, , \end{aligned} \tag{6.58}$$

with the convolution over t', the time of the virtual branching in the first diagram. While the lower limit of this integral is fixed to t_0 by $\theta(t'-t_0)$, the upper limit is $t_{\min} = \min(t_1, t_2)$ via the product of two Heaviside θ-functions. Its two possible values generate two terms as in Eq. (6.42), conditioned by θ-functions. Using the δ-function in the first line of Eq. (6.58) to eliminate the integral over $\mathbf{k}_0$, the n_0 branching terms each produce

$$\begin{aligned} & \int_{t_0}^{t_{\min}} \mathrm{d}t' \, \mathrm{e}^{-D\mathbf{k}_2^2(t_2-t')} \mathrm{e}^{-D\mathbf{k}_1^2(t_1-t')} \mathrm{e}^{-D(\mathbf{k}_1+\mathbf{k}_2)^2(t'-t_0)} \\ & \qquad = \mathrm{e}^{-D\mathbf{k}_2^2(t_2-t_0)} \mathrm{e}^{-D\mathbf{k}_1^2(t_1-t_0)} \left(1 - \mathrm{e}^{-2D\mathbf{k}_1\cdot\mathbf{k}_2(t_{\min}-t_0)}\right) \frac{1}{2D\mathbf{k}_1\cdot\mathbf{k}_2} \, . \end{aligned} \tag{6.59}$$

The 1-term in the bracket is independent of $t_{\min}$ and cancels with n_0 of the n_0^2 discon-

nected terms. The remaining terms can be simplified using for example

$$\mathrm{e}^{-D\mathbf{k}_1^2(t_1-t_0)}\mathrm{e}^{-2D\mathbf{k}_1\cdot\mathbf{k}_2(t_1-t_0)} = \mathrm{e}^{-D(\mathbf{k}_1+\mathbf{k}_2)^2(t_1-t_0)}\mathrm{e}^{D\mathbf{k}_2^2(t_1-t_0)} \tag{6.60}$$

in the case of $t_{\min} = t_1$ and, after a shift in $\mathbf{k}_i$, such as $\mathbf{k}_1 + \mathbf{k}_2 \to \mathbf{k}_1$ in the example above, reproduce the result from Doi-Peliti, Eq. (6.57). This concludes the illustration.

To summarise this section, the correlation function of the particle position of n_0 non-interacting particles is not a single term, as it needs to capture multiple scenarios of particles moving, while keeping track of the particle nature of the constituent degrees of freedom. Both frameworks result in the same expressions, such Eqs. (6.45), (6.54), (6.55) and (6.57). A cancellation mechanism such as Eq. (6.49) in the $\mathbf{k}, \omega$ parameterisation and the convolution in Eq. (6.59) for $\mathbf{k}, t$, connects Doi-Peliti and Dean, revealing that the perturbative, virtual branching in Dean's framework is in fact a sum of sequential propagation of a single particle and independent propagation of two distinct ones.

The calculation in this preliminary section suggests that the interaction vertex Eq. (6.38) in Dean's formalism, a vertex that would be missing in a naive response field theory of the corresponding Fokker-Planck equation, contains the same information as the commutation relation of the Doi-Peliti ladder operators. The importance of this observation will become evident in Section 6.4 and 6.5, where we analyse the particle nature in greater detail.

6.3 Probing for particle entity

Within the Dean framework $\rho(\mathbf{x}, t)$ denotes the instantaneous particle number density in state $\mathbf{x}$ at time t. We define particle entity as a property of the evolution equation for $\rho(\mathbf{x}, t)$ whereby this time-dependent random variable can be written as a finite sum of "single particle densities" with integer coefficients. In the case of a discrete phase space, the single-particle density for a particle in state $\bar{\mathbf{x}}$ is the Kronecker-delta with unit prefactor, $\delta_{\mathbf{x},\bar{\mathbf{x}}}$. For continuous degrees of freedom, the single-particle density for a particle in state $\bar{\mathbf{x}}$ is the Dirac-delta distribution normalised to unity,

$\delta(\mathbf{x} - \bar{\mathbf{x}})$. Correspondingly,

$$\rho(\mathbf{x}, t) = \begin{cases} \sum_i n_i(t)\delta_{\mathbf{x},\bar{\mathbf{x}}_i}, & \text{for discrete states} \\ \sum_i n_i(t)\delta(\mathbf{x} - \bar{\mathbf{x}}_i), & \text{for continuous states} \end{cases} \tag{6.61}$$

where $n_i(t) \in \mathbb{N}$. It follows from this requirement that the integral of the particle number density $\rho(\mathbf{x}, t)$ over any (sub-)volume Ω of the space is an integer-valued random variable,

$$\forall \Omega \subset \mathbb{R}^d : \begin{cases} \sum_{i \in \Omega} \rho(\mathbf{x_i}, \mathbf{t}) \in \mathbb{N}, & \text{for discrete states} \\ \int_\Omega d^d x \rho(\mathbf{x}, \mathbf{t}) \in \mathbb{N}, & \text{for continuous states} \end{cases} , \tag{6.62}$$

where integrals are performed in the Dirac measure, rather than by expressing the Dirac-delta distribution as the limit of a series of bump functions under a Lebesgue integral.

For discrete states, Eq. (6.62) also implies Eq. (6.61), i.e. there can be no densities satisfying Eq. (6.62) that are not a sum of Kronecker deltas with integer coefficient. We leave the proof that this equivalence also holds in the continuum for future work. Such a proof will surely draw on the arbitrariness of Ω, which can be used to include or exclude from the integral in Eq. (6.62) any part of $\rho(\mathbf{x}, t)$. In the case of stochastic dynamics, it is convenient to re-express the condition Eq. (6.62) in terms of an expectation value as

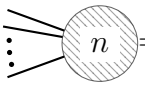
$$\left\langle \exp\left(2\pi \mathring{i} \int_\Omega \mathrm{d^d x}\, \rho(\mathbf{x}, \mathrm{t})\right) \right\rangle = 1 \ , \tag{6.63}$$

which needs to be satisfied for any volume Ω and all times t. Eq. (6.63) will play the role of a signature of particle entity in the following.

Obviously, Eq. (6.62) implies Eq. (6.63). Yet, expressing the particle entity condition as an expectation might appear less stringent than demanding it at the level of individual trajectories. However, rewriting Eq. (6.63) as $\langle \cos(2\pi \int \mathrm{d}^d x\, \rho(\mathbf{x}, t)) \rangle = 1$ on the basis of $\rho(\mathbf{x}, t)$ being real, shows that the integral must be integer valued almost surely, because $\mathbb{R} \ni \cos(x) \leq 1$ for $x \in \mathbb{R}$.

A mathematical definition for particle entity is for Eq. (6.62) to hold. To probe for particle entity, we use Eq. (6.63) as a test.

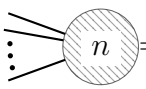
In order to ease the calculation of the left-hand side of Eq. (6.63) for a particular field theory of interest, we can expand the complex exponential as a Taylor series and invoke linearity of the expectation to obtain the particle entity signature,

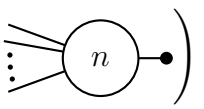
$$\sum_{n=0}^{\infty} \frac{(2\pi\mathring{\imath})^n}{n!}$$  $$\hat{=} \sum_{n=0}^{\infty} \frac{(2\pi\mathring{\imath})^n}{n!} \left\langle \left(\int_\Omega \mathrm{d}^d x \, \rho(\mathbf{x}, t) \right)^n \right\rangle$$

$$= \left\langle \exp\left(2\pi\mathring{\imath} \int_\Omega \mathrm{d^d x} \, \rho(\mathbf{x}, \mathrm{t}) \right) \right\rangle = 1 \ , \tag{6.64}$$

where the left-hand side is now a function of the nth full moment of the integrated particle number density, $\left\langle \left(\int_\Omega \mathrm{d}^d x \, \rho(\mathbf{x}, t) \right)^n \right\rangle$. In Eq. (6.64) we have also introduced the diagrammatic notation for the nth full moment of the *integrated* particle number density. The hatched vertex henceforth indicates generally a sum of possibly disconnected diagrams involving an arbitrary amount of sources. More specifically, here it is the n-fold spatial integral of a sum of products of connected diagrams. An example for such a sum is Eq. (6.46). These moments are perfectly suited for being calculated in both Doi-Peliti and response field field theories, as done in the following.

An alternative form of our particle entity signature can be obtained by recognising that the left hand side of Eq. (6.63) is also the moment-generating function $\langle \exp(zX) \rangle$ of the random variable $X = \int_\Omega \mathrm{d}\mathbf{x} \, \rho(\mathbf{x}, t)$ evaluated at $z = 2\pi\mathring{\imath}$. It is a well-known result from the field-theoretic literature on equilibrium critical phenomena [92, 16] that the generating function of the full moments $\langle X^n \rangle$ can be expressed as the exponential of the generating function of the so-called connected moments, denoted $\langle X^n \rangle_c$. Outside the field-theoretic literature, connected moments are usually referred to as cumulants [166]. While one would normally expect source fields $j(\mathbf{x}, t)$ to be introduced corresponding to a conjugate variable z at each point in space and time, in the present context a single variable suffices, as in Eq. (6.64) every field $\rho(\mathbf{x}, t)$ is integrated over the same volume Ω. Diagrammatically,

$$\sum_{n=0}^{\infty} \frac{z^n}{n!}$$  $$\hat{=} \sum_{n=0}^{\infty} \frac{z^n}{n!} \left\langle \left(\int_\Omega \mathrm{d}^d x \, \rho(\mathbf{x}, t) \right)^n \right\rangle = \left\langle \exp\left(z \int_\Omega \mathrm{d}^d x \, \rho(\mathbf{x}, t) \right) \right\rangle$$

$$= \exp\left(\sum_{n=1}^{\infty} \frac{z^n}{n!} \left\langle \left(\int_\Omega \mathrm{d}^d x \, \rho(\mathbf{x}, t) \right)^n \right\rangle_c \right) = \exp\left(\sum_{n=1}^{\infty} \frac{z^n}{n!}$$  $$\right) \ , \tag{6.65}$$

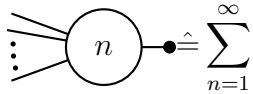
where we have introduced the notation for the nth *connected* moment of the integrated particle number density, shown as a circular vertex on the right, which differs from that of the corresponding full moment also by the presence of an explicit, single, ingoing propagator emerging from a single source, shown as a filled circle, the only possible form of a connected diagram contributing to moments of the density. In equilibrium statistical mechanics, this relationship provides the connection between the partition function and the Helmholtz free energy [92, 16]. Generating functions of observables such as n-point correlation functions of $\rho(\mathbf{x}, t)$ can be reduced to those of connected diagrams as long as the observables can be written as (functional) derivatives of an exponential and provided that each resulting diagram can be written as a product of connected diagrams. Under these conditions, Eq. (6.65) does all the right accounting.

Evaluating Eq. (6.65) at $z = 2\pi\mathring{\imath}$, according to Eq. (6.64) one can write

$$\exp\left(\sum_{\mathrm{n}=1}^{\infty}\frac{(2\pi\mathring{i})^{\mathrm{n}}}{\mathrm{n}!}\left\langle\left(\int_{\Omega}\mathrm{d}^{\mathrm{d}}\mathrm{x}\,\rho(\mathbf{x},\mathrm{t})\right)^{\mathrm{n}}\right\rangle_{\mathrm{c}}\right)=1\ , \tag{6.66}$$

or, equivalently,

$$\sum_{n=1}^{\infty}\frac{(2\pi\mathring{i})^{n}}{n!}\ \hat{=}\ \sum_{n=1}^{\infty}\frac{(2\pi\mathring{i})^{n}}{n!}\left\langle\left(\int_{\Omega}\mathrm{d}^{d}x\,\rho(\mathbf{x},t)\right)^{n}\right\rangle_{c}=2\pi\mathring{\imath}\ell \tag{6.67}$$



for some integer $\ell \in \mathbb{Z}$, on the basis of the connected moments of the particle number, to be compared to the particle signature on the basis of the full moments, Eq. (6.64).

6.4 Particle entity in Doi-Peliti

Doi-Peliti field theories are designed to respect particle entity and they do indeed do so on a rather fundamental level. To probe for particle entity, we want to use Eq. (6.63) with $\rho(\mathbf{x}, t)$ replaced by an object suitable for a Doi-Peliti field theory. In such a field theory, the instantaneous particle number at any position $\mathbf{x}$ is probed by the number operator $\hat{n}(\mathbf{x}) = a^{\dagger}(\mathbf{x})a(\mathbf{x})$. The expected particle number at position $\mathbf{x}$

and time t is therefore

$$\langle n(\mathbf{x},t)\rangle = \langle \text{☼}|\, a^\dagger(\mathbf{x})a(\mathbf{x})\,|\Psi(t)\rangle \ , \tag{6.68}$$

using a continuum version of the notation introduced in Section 6.2, in particular Eq. (6.3). While this expectation might be any non-negative real, the instantaneous $a^\dagger(\mathbf{x})a(\mathbf{x})$ is an integer. As already discussed in Section 6.3, Eq. (6.63), we therefore expect

$$\langle \text{☼}|\, \exp\big(2\pi\mathring{\imath} a^\dagger(\mathbf{x})a(\mathbf{x})\big)\,|\Psi(t)\rangle = 1 \tag{6.69}$$

to hold for every $\mathbf{x}$, as $\exp(2\pi\mathring{\imath} n) = 1$ for any $n \in \mathbb{Z}$. If this holds for every point $\mathbf{x}$, it also holds for every patch Ω, since

$$\langle \text{☼}|\, \exp\left(2\pi\mathring{\imath}\sum_{\mathbf{x}\in\Omega} a^\dagger(\mathbf{x})a(\mathbf{x})\right)|\Psi(t)\rangle = \langle \text{☼}|\prod_{\mathbf{x}\in\Omega}\exp\big(2\pi\mathring{\imath} a^\dagger(\mathbf{x})a(\mathbf{x})\big)\,|\Psi(t)\rangle \ , \tag{6.70}$$

where we have used that operators at different $\mathbf{x}$ commute. In the continuum, one might argue that the particle number at $\mathbf{x}$ can only ever be 0 or 1, possibly leading to some simplifications, but on the lattice occupation is not bound to be sparse in this sense.

To show that Eq. (6.69) is indeed satisfied in general Doi-Peliti field theories, we recall that the state $|\Psi(t)\rangle$ can be written as a statistical superposition of integer occupation number states on the lattice, Eq. (6.3), which are eigenstates of the number operator $a^\dagger(\mathbf{x})a(\mathbf{x})$ with integer eigenvalue $n_\mathbf{x} \in \mathbb{N}$. The left hand side of Eq. (6.69) thus immediately simplifies to the desired result,

$$\sum_{\{n_i\}} P(\{n_i\},t)\exp(2\pi\mathring{\imath} n_\mathbf{x})\,\langle \text{☼}|\,\{n_i\}\rangle = \sum_{\{n_i\}} P(\{n_i\},t) = 1 \ . \tag{6.71}$$

To see more clearly which features of the formalism are responsible for this particular property of the state $|\Psi(t)\rangle$ being preserved under the dynamics, and to see this at the level of fields, we can alternatively follow the standard procedure, outlined in Eq. (6.15), to express the operator $\exp\big(2\pi\mathring{\imath} a^\dagger(\mathbf{x})a(\mathbf{x})\big)$ in terms of scalar fields $\psi(\mathbf{x},t)$ and $\psi^\dagger(\mathbf{x},t)$. The simple mapping of operator to field applies as soon as the operators

are normal ordered,

$$\exp\big(za^\dagger(\mathbf{x})a(\mathbf{x})\big) = \sum_{n=0}^{\infty} \frac{1}{n!} z^n \left(a^\dagger(\mathbf{x})a(\mathbf{x})\right)^n \tag{6.72}$$

$$= \sum_{n=0}^{\infty} \frac{1}{n!} z^n \sum_{k=0}^{n} \left\{ {n \atop k} \right\} \left(a^\dagger(\mathbf{x})\right)^k a(\mathbf{x})^k \tag{6.73}$$

where we have replaced $2\pi\mathring{\imath}$ by z to improve readability and used [119] to normal order $\left(a^\dagger(\mathbf{x})a(\mathbf{x})\right)^n$. In terms of fields, the observable Eq. (6.70) is thus

$$\mathcal{O} = \langle \text{☼} | \exp\left(z \sum_{x\in\Omega} \left(a^\dagger(\mathbf{x})\right)^k a(\mathbf{x})^k \right) |\Psi(\mathbf{x},t)\rangle \tag{6.74}$$

$$= \langle \text{☼} | \prod_{x\in\Omega} \sum_{n=0}^{\infty} \frac{1}{n!} z^n \sum_{k=0}^{n} \left\{ {n \atop k} \right\} \left(a^\dagger(\mathbf{x})\right)^k a(\mathbf{x})^k |\Psi(\mathbf{x},t)\rangle \tag{6.75}$$

$$= \left\langle \prod_{x\in\Omega} \sum_{n=0}^{\infty} \frac{1}{n!} z^n \sum_{k=0}^{n} \left\{ {n \atop k} \right\} \psi^k(\mathbf{x},t)\, \mathbb{I}(\tilde{\psi}(0)+1) \right\rangle \tag{6.76}$$

$$= \left\langle \exp\left(\sum_{x\in\Omega} \psi(\mathbf{x},t)(e^z-1) \right) \mathbb{I}(\tilde{\psi}(0)+1) \right\rangle \tag{6.77}$$

as $\langle \text{☼} | \left(a^\dagger(\mathbf{x})\right)^k = \langle \text{☼} |$ [128] and using (6.17) for the initialisation $\mathbb{I}(\tilde{\psi}(0)+1)$. From Eq. (6.76) to (6.77), we draw on the the mixed bivariate generating function for the Stirling numbers of the second kind [32],

$$\sum_{n=0}^{\infty} \sum_{k=0}^{n} \left\{ {n \atop k} \right\} \frac{1}{n!} z^n y^k = \exp(y(\mathrm{e}^z - 1)) \ . \tag{6.78}$$

For $z = 2\pi\mathring{\imath}$, and any integer multiple thereof, Eq. (6.77) indeed produces $\mathcal{O} = \left\langle \mathbb{I}(\tilde{\psi}(0)+1) \right\rangle = 1$ as required by Eq. (6.63). Because this calculation never draws on any particular action, but rather on the fundamentals of normal ordering, Doi-Peliti field theories respect particle entity universally in the presence of any interactions and potentials.

Demonstrating that the response field theory derived from Dean's equation possesses particle entity turns out to be a much more challenging task, which requires us to compute explicitly the connected moments of the integrated particle number density to arbitrary order. This calculation draws on the specific action Eq. (6.23) and (6.24) as we perform it here for the case of non-interacting diffusive particles without external potential. This is done most conveniently by first computing the connected moments of the density in the mixed momentum-time representation, where Dean's action reads

$$A[\rho,\tilde{\rho}] = \int \mathrm{đ}^d k \mathrm{d}t\, \tilde{\rho}(\mathbf{k},t)(\partial_t + D\mathbf{k}^2)\rho(-\mathbf{k},t) - \tilde{\rho}(\mathbf{k},t)\sum_i n_i e^{\mathrm{i}\mathbf{k}\cdot\mathbf{x}_i}\delta(t-t_i)$$
$$+ \int \mathrm{đ}^d k \mathrm{đ}^d k' \mathrm{d}t\, D(\mathbf{k}\cdot\mathbf{k}')\tilde{\rho}(\mathbf{k},t)\tilde{\rho}(\mathbf{k}',t)\rho(-(\mathbf{k}+\mathbf{k}'),t). \tag{6.79}$$

In this parametrisation, we find (Appendix 6.A, Eq. (6.132))

$$\langle\rho(\mathbf{k}_1,t)...\rho(\mathbf{k}_n,t)\rangle_c = n_0\theta(t-t_0)\mathrm{e}^{-\mathrm{i}(\mathbf{k}_1+...\mathbf{k}_n)\cdot\mathbf{x}_0}\sum_{m=1}^{n}(-1)^{m-1}(m-1)! \tag{6.80}$$
$$\times \sum_{\{\mathbb{P}_1,...,\mathbb{P}_m\}\in\mathcal{P}(\{1,...,n\},m)} \mathrm{e}^{-T(t-t_0)\sum_{i=1}^m \mathbf{K}(\mathbb{P}_i)^2}.$$

with $\mathcal{P}(\{1,\ldots,n\},m)$ the set of all partitions of the set $\{1,\ldots,n\}$ into m non-empty, distinct subsets $\mathbb{P}_i$ with $i = 1,...,m$, *i.e.* $\cup_{i=1}^m \mathbb{P}_i = \{1,2,\ldots,n\}$ and $\mathbb{P}_i \cap \mathbb{P}_j = \emptyset$ for $i \neq j$. The sum thus runs over all possible partitions of {1,2,...,n} into m non-empty sets. There is one partition for $m = n$ and n for $m = 1$. The vector featuring in the right-most exponential of Eq. (6.80)

$$\mathbf{K}(\mathbb{P}_i) = \sum_{p\in\mathbb{P}_i}\mathbf{k}_p \tag{6.81}$$

is the total momentum given by the indices in the subset $\mathbb{P}_i$, *i.e.* it is the total momentum of the subset $\mathbb{P}_i$, and by linearity, $\mathbf{K}(\mathbb{A}) + \mathbf{K}(\mathbb{B}) = \mathbf{K}(\mathbb{A}\cup\mathbb{B})$. For example, one partition into two of $\{1,2,3,4\}$ is $\{\mathbb{P}_1 = \{1,2,4\}, \mathbb{P}_2 = \{3\}\}$, which is one of 7 elements of $\mathcal{P}(\{1,2,3,4\},2)$. In this example, the momenta of the subsets are

$\mathbf{K}(\mathbb{P}_1) = \mathbf{k}_1 + \mathbf{k}_2 + \mathbf{k}_4$ and $\mathbf{K}(\mathbb{P}_2) = \mathbf{k}_3$. Diagrammatically, the right-hand side of Eq. (6.80) is obtained by summing over all connected, topologically distinct diagrams with a single incoming propagator and n outgoing propagators labelled by the external momenta $\mathbf{k}_i$ $(i = 1, ..., n)$, where we need to account for all non-equivalent permutations of the latter.

The connected moments of the integrated particle number density in a patch Ω are then obtained by Fourier back-transforming Eq. (6.80) into position-time representation and integrating over the probing locations $\mathbf{x}_i \in \Omega$,

$$\left\langle \int_\Omega \mathrm{d}^d x_1 \, ... \, \mathrm{d}^d x_n \, \rho(\mathbf{x}_1, t) ... \rho(\mathbf{x}_n, t) \right\rangle_c \tag{6.82}$$

$$= \int_\Omega \prod_{i=1}^n \mathrm{d}^d x_i \int \prod_{j=0}^n \text{đ}^d k_j \, \exp\left(-\mathring{\imath} \sum_{\ell=1}^n \mathbf{k}_\ell \cdot \mathbf{x}_\ell \right) \langle \rho(\mathbf{k}_1, t) ... \rho(\mathbf{k}_n, t) \rangle_c \tag{6.83}$$

$$= \int_\Omega \prod_{i=1}^n \mathrm{d}^d x_i \int \prod_{j=1}^n \text{đ}^d k_j \, \exp\left(-\mathring{\imath} \sum_{\ell=1}^n \mathbf{k}_\ell \cdot (\mathbf{x}_\ell - \mathbf{x}_0) \right) \tag{6.84}$$

$$\times \, n_0 \theta(t - t_0) \sum_{m=1}^n (-1)^{m-1} (m-1)! \sum_{\{\mathbb{P}_1, ..., \mathbb{P}_m\} \in \mathcal{P}(\{1,...,n\}, m)} \mathrm{e}^{-D(t-t_0) \sum_{p=1}^m \mathbf{K}(\mathbb{P}_p)^2} \, .$$

The integrals in Eq. (6.84) can be carried out partition by partition, by taking the integration inside the summation over $m = 1, \ldots, n$ and the partitions $\{\mathbb{P}_1, \ldots\} \in \mathcal{P}(\{1, \ldots, n\}, m)$. As $\mathbf{x}_i$ and $\mathbf{k}_j$ are both dummy variables, we may think of subset $\mathbb{P}_p$ containing indices $1, \ldots, a$ with $a = |\mathbb{P}_p|$, so that the integrals to be carried out for each $p = 1, \ldots, m$ are

$$J_p = \int_\Omega \prod_{i=1}^a \mathrm{d}^d x_i \int \prod_{j=1}^a \text{đ}^d k_j \, \exp\left(-\mathring{\imath} \sum_{\ell=1}^a \mathbf{k}_\ell \cdot (\mathbf{x}_\ell - \mathbf{x}_0) \right) \mathrm{e}^{-D(t-t_0) \mathbf{K}(\mathbb{P}_p)^2} \, . \tag{6.85}$$

In this indexing we have $\mathbf{K}(\mathbb{P}_p) = \mathbf{k}_1 + \cdots + \mathbf{k}_a$ which simplifies to $\tilde{\mathbf{k}}_1$ after suitable

shifting of the origin in the integration over $\mathbf{k}_1 = \tilde{\mathbf{k}}_1 - (\mathbf{k}_2 + \cdots + \mathbf{k}_a)$, so that

$$J_p = \int_\Omega \prod_{i=1}^{a} \mathrm{d}^d x_i \int \mathrm{đ}^d \tilde{k}_1 \, \mathrm{e}^{-\mathring{\imath}\tilde{\mathbf{k}}_1\cdot(\mathbf{x}_1-\mathbf{x}_0)} \mathrm{e}^{-D(t-t_0)\tilde{\mathbf{k}}_1^2} \tag{6.86a}$$

$$\times \int \prod_{j=2}^{a} \mathrm{đ}^d k_j \, \exp\left(-\mathring{\imath} \sum_{\ell=2}^{a} \mathbf{k}_\ell \cdot (\mathbf{x}_\ell - \mathbf{x}_1) \right)$$

$$= \int_\Omega \prod_{i=1}^{a} \mathrm{d}^d x_i \, G(\mathbf{x}_1 - \mathbf{x}_0, t - t_0) \delta(\mathbf{x}_2 - \mathbf{x}_1) ... \delta(\mathbf{x}_a - \mathbf{x}_1) \tag{6.86b}$$

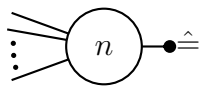
$$= I_\Omega(t - t_0) \tag{6.86c}$$

where we have used Eqs. (6.34) and (6.36) in Eq. (6.86b) and introduced

$$I_\Omega(t - t_0) = \int_\Omega \mathrm{d}^d x \, G(\mathbf{x} - \mathbf{x}_0, t - t_0) \ , \tag{6.87}$$

in Eq. (6.86c), which is the probability to find a particle at time t within the volume Ω that had at time t_0 been placed at $\mathbf{x}_0$. We may drop the time-dependence of I_Ω where that improves readability.

As J_p is independent of the specific partition, the sum over partitions $\{\mathbb{P}_1, \ldots, \mathbb{P}_m\} \in \mathcal{P}(\{1, \ldots, n\}, m)$ in Eq. (6.84) amounts to multiplying a product of m such integrals by the number of partitions, given by the Stirling numbers of the second kind. Overall,

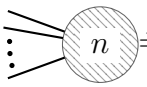


$$\hat{=} \left\langle \left(\int_\Omega \mathrm{d}^d x \, \rho(\mathbf{x}, t) \right)^n \right\rangle_c = -n_0 \theta(t - t_0) \sum_{m=1}^{n} \left(-I_\Omega \right)^m \left\{ {n \atop m} \right\} (m-1)! \ , \tag{6.88}$$

which provides us with the information we need to probe the theory for particle entity. It is a key result of the present work. Its derivation is generalised to distinct initial positions in Appendix 6.B.

Using the particle entity signature based on connected diagrams, Eq. (6.67), confronts us with some undesirable hurdles due to convergence. We therefore turn our attention to the full moments, which can be constructed from the connected moments via

Eq. (6.65), so that for $t > t_0$,



$$\hat{=} \left\langle \left(\int_\Omega \mathrm{d}^d x\, \rho(\mathbf{x},t) \right)^n \right\rangle \tag{6.89}$$

$$= \left. \frac{d^n}{dz^n} \right|_{z=0} \exp\left(\sum_{m=1}^{\infty} \frac{z^m}{m!} \left\langle \left(\int_\Omega \mathrm{d}^d x\, \rho(\mathbf{x},t) \right)^m \right\rangle_c \right) \tag{6.90}$$

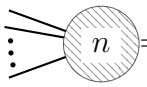
$$= \left. \frac{d^n}{dz^n} \right|_{z=0} \exp\left(\sum_{m=1}^{\infty} \frac{z^m}{m!} (-n_0) \sum_{\ell=1}^{m} (-I_\Omega)^\ell \left\{ {m \atop \ell} \right\} (\ell-1)! \right) \tag{6.91}$$

$$= \left. \frac{d^n}{dz^n} \right|_{z=0} \exp\left(-n_0 \sum_{\ell=1}^{\infty} (-I_\Omega)^\ell (\ell-1)! \sum_{m=\ell}^{\infty} \frac{z^m}{m!} \left\{ {m \atop \ell} \right\} \right) , \tag{6.92}$$

where we have changed the order of summation in the exponential to arrive at the final equality. This step deserves further scrutiny below. Using in Eq. (6.92) the generating function of the Stirling numbers [32] in the form

$$\sum_{m=\ell}^{\infty} \frac{z^m}{m!} \left\{ {m \atop \ell} \right\} = \frac{(e^z-1)^\ell}{\ell!} , \tag{6.93}$$

as used previously in the Doi-Peliti field theory, Eq. (6.78), leads to



$$\hat{=} \left. \frac{d^n}{dz^n} \right|_{z=0} \exp\left(-n_0 \sum_{\ell=1}^{\infty} (-I_\Omega)^\ell \frac{(e^z-1)^\ell}{\ell} \right) . \tag{6.94}$$

We briefly return to the change of the order of summation from Eq. (6.91) to (6.92). To justify this, we require *absolute* convergence

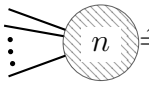
$$\sum_{\ell=1}^{\infty} \sum_{m=\ell}^{\infty} \frac{|z|^m}{m!} I_\Omega^\ell \left\{ {m \atop \ell} \right\} (\ell-1)! < \infty \tag{6.95}$$

for $I_\Omega \in [0,1]$ and z within a finite vicinity around the origin, given the repeated differentiation in Eq. (6.94). As Eq. (6.93) holds for all $z \in \mathbb{C}$, we require $\sum_{\ell=1}^{\infty} I_\Omega^\ell (\exp(|z|) - 1)^\ell / \ell < \infty$ and thus $|z| < \ln(2)$ by the ratio test.

Rewriting the exponent in Eq. (6.94) for any $|z| < \ln(2)$ as a logarithm,

$$\sum_{l=1}^{\infty} \frac{(-x)^l}{l} = -\log(1+x)\,, \tag{6.96}$$

we have



$$\hat{=} \left.\frac{d^n}{dz^n}\right|_{z=0} (1 + (e^z - 1)I_\Omega)^{n_0} \tag{6.97}$$

$$= \left.\frac{d^n}{dz^n}\right|_{z=0} \sum_{k=0}^{n_0} \binom{n_0}{k} (e^z - 1)^k I_\Omega^k \tag{6.98}$$

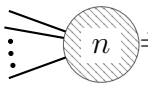
$$= \sum_{k=0}^{n_0} \binom{n_0}{k} I_\Omega^k \left.\frac{d^n}{dz^n}\right|_{z=0} \sum_{j=0}^{k} \binom{k}{j} (-1)^j e^{z(k-j)} \tag{6.99}$$

$$= \sum_{k=0}^{n_0} \binom{n_0}{k} I_\Omega^k \sum_{j=0}^{k} \binom{k}{j} (-1)^j (k-j)^n\,, \tag{6.100}$$

and using the definition of the Stirling numbers of the second kind [32]

$$\sum_{g=0}^{k} \binom{k}{g} (-1)^g (k-g)^n = k! \left\{ {n \atop k} \right\}, \tag{6.101}$$

we finally arrive at



$$\hat{=} \sum_{k=0}^{n_0} \binom{n_0}{k} I_\Omega^k k! \left\{ {n \atop k} \right\}. \tag{6.102}$$

This is the first central result of the present section. The derivation above implicitly used that n_0 is integer. This requirement turns out to also be important for the physical interpretation of the result, which we discuss in detail in Appendix 6.C.

We now derive a different form of Eq. (6.102), which offers a more immediate physical interpretation. To this end, we draw on the identity

$$\sum_{k=0}^{n_0} \binom{n_0}{k} (1-x)^{n_0-k} x^k k^n = \sum_{\ell=0}^{n_0} \binom{n_0}{\ell} x^\ell \ell! \left\{ {n \atop \ell} \right\} \tag{6.103}$$

which can be obtained by resolving the binomial $(1-x)^{n_0-k}$ on the left into a sum, collecting terms of order x^ℓ and then using $\binom{n_0}{k}\binom{n_0-k}{\ell-k} = \binom{n_0}{\ell}\binom{\ell}{k}$ to arrive at an expression that simplifies to the final sum by means of Eq. (6.101).

Using Eq. (6.103) in Eq. (6.102) gives

$$\left\langle \left(\int_\Omega \mathrm{d}^d x\, \rho(\mathbf{x},t) \right)^n \right\rangle = \sum_{k=0}^{n_0} \binom{n_0}{k} \Big(1 - I_\Omega(t-t_0)\Big)^{n_0-k} \Big(I_\Omega(t-t_0)\Big)^k k^n \ , \tag{6.104}$$

which has a rather simple physical interpretation: of the (integer) n_0 particles, k can be found in the volume Ω, each independently with probability I_Ω, so that the probability of such a configuration is that of a repeated Bernoulli trial, $\binom{n_0}{k}(1-I_\Omega)^{n_0-k} I_\Omega^k$. As k particles are in the relevant volume, the contribution to the nth particle number moment is k^n.

In the form Eq. (6.104), the particle number moments can be used in our particle entity signature Eq. (6.64),

$$\sum_{n=0}^{\infty} \frac{(2\pi\mathring{i})^n}{n!} \Big\{ \overset{n}{\cdots} = \sum_{n=0}^{\infty} \frac{(2\pi\mathring{i})^n}{n!} \sum_{k=0}^{n_0} \binom{n_0}{k} (1-I_\Omega)^{n_0-k} I_\Omega^k k^n \tag{6.105}$$

$$= \sum_{k=0}^{n_0} \binom{n_0}{k} (1-I_\Omega)^{n_0-k} I_\Omega^k \left(\sum_{n=0}^{\infty} \frac{(2\pi\mathring{i})^n}{n!} k^n \right) = 1 \ , \tag{6.106}$$

where we have used $e^{2\pi i k} = 1$ for $k \in \mathbb{Z}$ in the last bracket and the normalisation of a binomial distribution. To change the order of summation going from Eq. (6.105) to (6.106) we draw on the absolute convergence of the last line Eq. (6.106). This concludes the proof of particle entity on the basis of Eq. (6.64) in the Dean formalism, the second central result of this section. As already hinted at in Section 6.2.3, we have seen that the precise form of Dean's vertex Eq. (6.38) plays a fundamental role in generating the diagrammatic structure responsible for the enforcement of particle entity in its field theory. We expect that perturbative treatments affecting the vertex form, the extreme case being its complete removal and subsequent treatment of Dean's equation as a classical diffusion equation, results in the breakdown of particle entity under the dynamics (Fig. 6.2.1).

6.6 Conclusion

To the best of our knowledge, this paper presents the first formalisation and systematic study of the concept of particle entity in the context of statistical field theory. Focusing on two well-known field theoretic formalisms applied to the study of stochastic processes, namely the Doi-Peliti [164] and the Martin-Siggia-Rose-Janssen-De Dominicis [110, 78, 44] response field theories, we have demonstrated that particle entity is enforced in a formalism-specific way. In Doi-Peliti field theories, particle entity is built into its foundation, namely in the commutation relation of the ladder operators, Eq. (6.1). In the response field field theory derived from Dean's equation, particle entity is a perturbative feature that relies on the precise form of the interaction vertex, Eq. (6.38). This "Dean vertex" originates from the Itô-multiplicative noise term in the original Langevin equation Eq. (6.19). It compensates for some overcounting that occurs in the bilinear part of the field theory Eq. (6.28), a mechanism that was already identified in an earlier work on the statistics of the non-interacting Brownian gas [167]. As a result, one is faced with more complicated branching diagrams in the response field formalism equipped with particle entity via Dean's equation compared to the Doi-Peliti formalism, *cf.* Eqs. (6.40) and (6.46) or Eqs. (6.55) and (6.56).

To test for particle entity, we introduced the condition Eq. (6.63), that we rewrote in terms of particle number moments, Eq. (6.64), and, on the basis of the identity Eq. (6.65), in terms of connected moments, Eq. (6.67).

In Section 6.4, we were able to show in a few lines that particle entity according to Eq. (6.64) generally holds in Doi-Peliti field theories, Eq. (6.77). This finding is independent of the specifics of the action. To demonstrate particle entity for non-interacting, diffusive field theories on the basis of Dean's equation, we used in Section 6.5 our key result on the connected particle number moments, Eq. (6.88), before constructing the main result Eq. (6.106) on the basis of the full moments, with some of the more cumbersome calculations relegated to Appendix 6.A.

It is interesting to speculate whether our derivation simplifies further by exploiting the well-known identity [92] relating the Legendre transform of the generating function of the connected moments and the effective action, which only depends on the one-particle irreducible (1PI) diagrams. Since 1PIs represent a relatively small sub-

set of all connected diagrams, a particle entity signature of this type might be more easily applicable to theories involving pair interactions, which are beyond the scope of the present analysis.

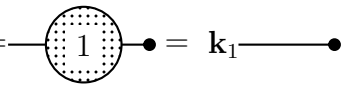
Appendix

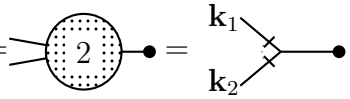
6.A Induction over connected diagrams

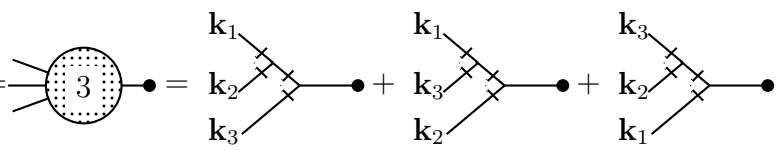
We want to prove that the connected moments of the particle number density in the response field field theory derived from Dean's equation obey Eq. (6.80) to all orders of n, restated here for convenience:

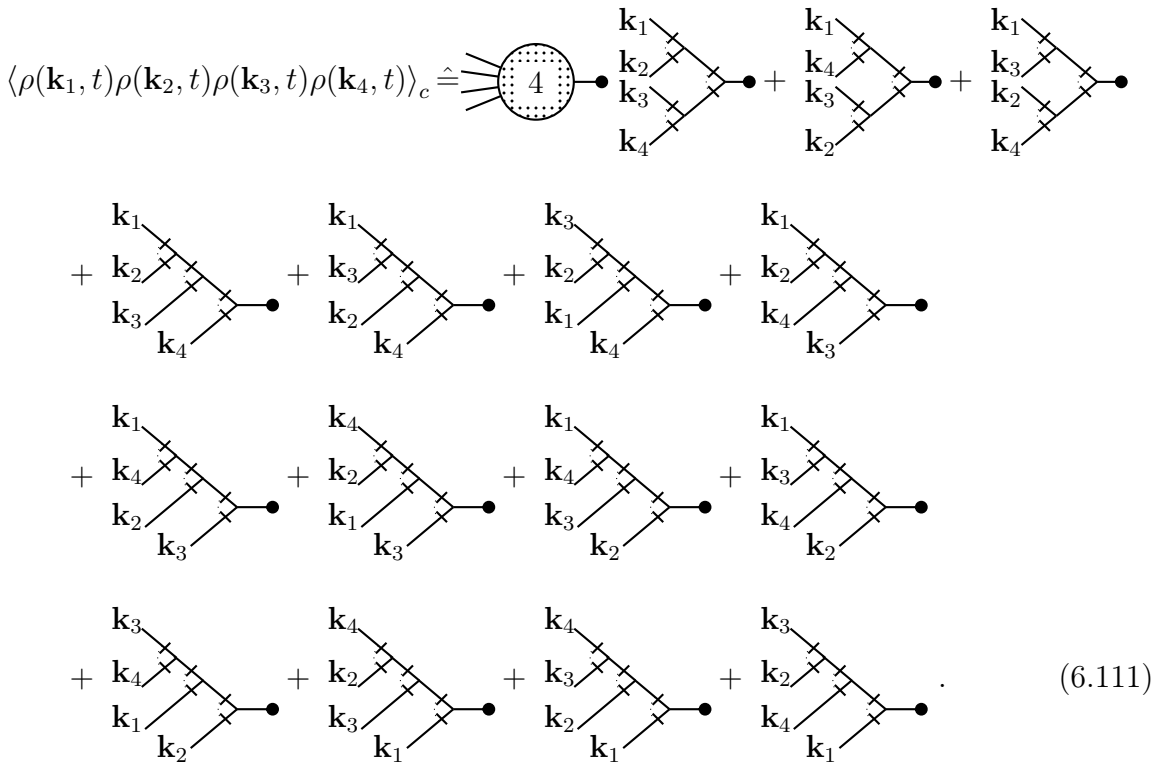
$$\langle \rho(\mathbf{k}_1,t)...\rho(\mathbf{k}_n,t)\rangle_c = n_0\theta(t-t_0)\mathrm{e}^{-i(\mathbf{k}_1+...\mathbf{k}_n)\cdot\mathbf{x}_0}\sum_{m=1}^{n}(-1)^{m-1}(m-1)! \tag{6.107}$$
$$\times \sum_{\{\mathbb{P}_1,...,\mathbb{P}_m\}\in\mathcal{P}(\{1,...,n\},m)} \mathrm{e}^{-D(t-t_0)\sum_{i=1}^{m}\mathbf{K}(\mathbb{P}_i)^2}.$$

For this we have to consider all diagrams with a single incoming leg and an arbitrary number n of outgoing legs, the first four orders of which are depicted in Eqs. (6.108), (6.109), (6.110) and (6.111).

$\langle \rho(\mathbf{k}_1,t)\rangle_c \mathrel{\hat{=}}$  (6.108)

$\langle \rho(\mathbf{k}_1,t)\rho(\mathbf{k}_2,t)\rangle_c \mathrel{\hat{=}}$  (6.109)

$\langle \rho(\mathbf{k}_1,t)\rho(\mathbf{k}_2,t)\rho(\mathbf{k}_3,t)\rangle_c \mathrel{\hat{=}}$  (6.110)

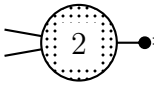


. (6.111)

The shading of the circular vertices above is meant as a visual reminder that we are now dealing with connected moments of the local number *density*, which depend on an unordered set of n external momenta $\mathbf{k}_1, ..., \mathbf{k}_n$, as opposed to connected moments of the *integrated* number density in a patch Ω (cf. Eq. (6.80) and Eq. (6.84)). The shaded diagrams are by construction invariant under permutations of the momenta $\mathbf{k}_1, ..., \mathbf{k}_n$.

We proceed by determining some of the shaded diagrams. The trivial case, $n = 1$ shown in Eq. (6.108), is given by the propagator Eq. (6.36) and the perturbative contribution from the source Eq. (6.24) with coupling n_0. Through direct computation in the mixed momentum-time representation, see Eq. (6.79), we find for the $n = 2$ case

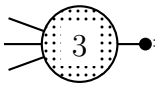
Eq. (6.109):



$$\hat{=} n_0\Theta(t-t_0)\mathrm{e}^{-i(\mathbf{k}_1+\mathbf{k}_2)\cdot\mathbf{x}_0}\int_{t_0}^{t}\mathrm{d}t'\,(-2D\mathbf{k}_1\cdot\mathbf{k}_2)\mathrm{e}^{-D(t-t')\mathbf{k}_1^2}\mathrm{e}^{-D(t-t')\mathbf{k}_2^2}\mathrm{e}^{-D(t'-t_0)\mathbf{k}_0^2} \tag{6.112}$$

$$= n_0\mathrm{e}^{-i(\mathbf{k}_1+\mathbf{k}_2)\cdot\mathbf{x}_0}\left[\mathrm{e}^{-D(t-t_0)(\mathbf{k}_1+\mathbf{k}_2)^2}-\mathrm{e}^{-D(t-t_0)(\mathbf{k}_1^2+\mathbf{k}_2^2)}\right]\,, \tag{6.113}$$

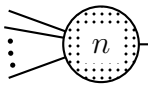
where the integral over t arises from representing the Dean vertex Eq. (6.38) in k-t-space. Each Dean vertex comes with a symmetry factor of 2. A factor of $(-2\mathbf{k}_1\cdot\mathbf{k}_2)^{-1}$ that arises in the t integration precisely cancels with the vertex prefactor $-2D\mathbf{k}_1\cdot\mathbf{k}_2$, which simplifies the result Eq. (6.113) considerably. A similar calculation for the $n=3$ case Eq. (6.110) yields



$$\hat{=} n_0\Theta(t-t_0)\mathrm{e}^{-i(\mathbf{k}_3+\mathbf{k}_2+\mathbf{k}_1)\cdot\mathbf{x}_0}\Big[\mathrm{e}^{-D(t-t_0)(\mathbf{k}_1+\mathbf{k}_2+\mathbf{k}_3)^2}-\mathrm{e}^{-D(t-t_0)((\mathbf{k}_1+\mathbf{k}_2)^2+\mathbf{k}_3^2)}$$
$$-\mathrm{e}^{-D(t-t_0)((\mathbf{k}_1+\mathbf{k}_3)^2+\mathbf{k}_2^2)}-\mathrm{e}^{-D(t-t_0)((\mathbf{k}_3+\mathbf{k}_2)^2+\mathbf{k}_1^2)}+2\mathrm{e}^{-D(t-t_0)(\mathbf{k}_1^2+\mathbf{k}_2^2+\mathbf{k}_3^2)}\Big]\,. \tag{6.114}$$

The left-hand side of Eq. (6.114) contains the sum over all distinct ways to assign the external momenta to the outgoing legs, as shown in (6.110). The whole sum of the terms is necessary for the coefficients of the Dean vertices to cancel with the k-dependent factor coming down from the t-integrations. We will see that this mechanism is instrumental in performing the induction later on.

Based on Eq. (6.113) and (6.114) we conjecture and indeed show below that a general connected moment has the form Eq. (6.80),



$$\hat{=}\langle\rho(\mathbf{k}_1,t)\rho(\mathbf{k}_1,t)\ldots\rho(\mathbf{k}_n,t)\rangle = n_0\theta(t-t_0)\mathrm{e}^{-i(\mathbf{k}_1+\ldots)\cdot\mathbf{x}_0}\sum_{m=1}^{n}(-1)^{m-1}(m-1)! \tag{6.115}$$

$$\times\sum_{\{\mathbb{P}_1,\ldots,\mathbb{P}_m\}\in\mathcal{P}(\{1,\ldots,n\},m)}\mathrm{e}^{-D(t-t_0)\sum_{i=1}^{m}\mathbf{K}(\mathbb{P}_i)^2}\,,$$

with $\mathcal{P}(\{1,\ldots,n\},m)$ the set of all partitions of the set $\{1,\ldots,n\}$ into m non-empty, distinct subsets $\mathbb{P}_i$ with $i=1,2,\ldots,m$ so that $\cup_{i=1}^{m}\mathbb{P}_i=\{1,2,\ldots,n\}$, as introduced

after Eq. (6.80). The second sum $\sum_{\{\mathbb{P}_1,\ldots,\mathbb{P}_m\}\in\mathcal{P}(\{1,\ldots,n\},m)}$ in Eq. (6.115) thus runs over all distinct partitions of $\{1,2,\ldots,n\}$ into m subsets $\mathbb{P}_1,\ldots,\mathbb{P}_m$. There is no order to the subsets, so that the partition $\{\{1\},\{2\}\}$ of $\{1,2\}$ is identical to $\{\{2\},\{1\}\}$ and thus considered the same in $\mathcal{P}(\{1,2\},2)$. We use $\mathbf{K}(\mathbb{P})$ to denote sums over momenta given by the indices in set $\mathbb{P}$, Eq. (6.81), $\mathbf{K}(\mathbb{P}) = \sum_{p\in\mathbb{P}} \mathbf{k}_p$. Eq. (6.115) is a function of the *set* of momenta $\{\mathbf{k}_1,\ldots,\mathbf{k}_n\}$, or simply the indices $\{1,\ldots,n\}$ alone, and invariant under their permutation.

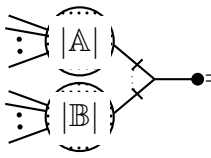
Eq. (6.115) will be our induction hypothesis, with the induction to be taken in n, the number of outgoing legs. The base cases $n = 1$, $n = 2$ and $n = 3$ are immediately verified, as $\mathcal{P}(\{1\},1) = \{\{\{1\}\}\}$ reduces Eq. (6.115) trivially to Eq. (6.36), $\mathcal{P}(\{1,2\},1) = \{\{\{1,2\}\}\}$ and $\mathcal{P}(\{1,2\},2) = \{\{\{1\},\{2\}\}\}$ to Eq. (6.113) and $\mathcal{P}(\{1,2,3\},1) = \{\{\{1,2,3\}\}\}$, $\mathcal{P}(\{1,2,3\},2) = \{\{\{1\},\{2,3\}\},\{\{2\},\{3,1\}\},\{\{3\},\{1,2\}\}\}$ and $\mathcal{P}(\{1,2,3\},3) = \{\{\{\{1\},\{2\},\{3\}\}\}\}$ to Eq. (6.114).

We want to show that if Eq. (6.115) holds for all strictly positive $n \leq m-1$ then it also holds for $n = m$. To this end we consider two distinct subsets of indices $\mathbb{A}$ and $\mathbb{B}$ with cardinality $|\mathbb{A}| > 0$ and $|\mathbb{B}| > 0$ respectively, so that $\mathbb{A}\cap\mathbb{B} = \emptyset$, $\mathbb{A}\cup\mathbb{B} = \{1,\ldots,n\}$ and thus $|\mathbb{A}| + |\mathbb{B}| = n$. Each of these sets enters as the argument of diagrams



that have $|\mathbb{A}|$ and $|\mathbb{B}|$ external legs respectively, each parameterised by the momenta given by the subsets, $\{\mathbf{k}_q | q\in\mathbb{A}\}$ and $\{\mathbf{k}_q | q\in\mathbb{B}\}$ respectively. These diagrams can be

"stitched together" via the Dean vertex, Eq. (6.38), so that



$$
\begin{aligned}
\hat{=} & n_0\theta(t-t_0)\mathrm{e}^{-i(\mathbf{k}_1+\ldots+\mathbf{k}_n)\cdot\mathbf{x}_0}\int_{t_0}^{t}\mathrm{d}t'\ (-2D\mathbf{K}(\mathbb{A})\cdot\mathbf{K}(\mathbb{B}))e^{-D(t'-t_0)(\mathbf{k}_1+\ldots+\mathbf{k}_n)^2} \\
& \times\left[\sum_{a=1}^{|\mathbb{A}|}(-1)^{a-1}(a-1)!\sum_{\{\mathbb{P}_1,\ldots,\mathbb{P}_a\}\in\mathcal{P}(\mathbb{A},a)}\mathrm{e}^{-D(t-t')\sum_{i=1}^{a}\mathbf{K}(\mathbb{P}_i)^2}\right] \qquad (6.116) \\
& \times\left[\sum_{b=1}^{|\mathbb{B}|}(-1)^{b-1}(b-1)!\sum_{\{\mathbb{Q}_1,\ldots,\mathbb{Q}_b\}\in\mathcal{P}(\mathbb{B},b)}\mathrm{e}^{-D(t-t')\sum_{j=1}^{b}\mathbf{K}(\mathbb{Q}_j)^2}\right] \\
= & n_0\theta(t-t_0)\mathrm{e}^{-i(\mathbf{k}_1+\ldots+\mathbf{k}_n)\cdot\mathbf{x}_0}\sum_{a=1}^{|\mathbb{A}|}\sum_{b=1}^{|\mathbb{B}|}(-1)^{a+b}(a-1)!(b-1)!(-2D\mathbf{K}(\mathbb{A})\cdot\mathbf{K}(\mathbb{B})) \\
& \times\sum_{\{\mathbb{P}_1,\ldots\}\in\mathcal{P}(\mathbb{A},a)}\sum_{\{\mathbb{Q}_1,\ldots\}\in\mathcal{P}(\mathbb{B},b)}\mathrm{e}^{D(\mathbf{k}_1+\ldots+\mathbf{k}_n)^2t_0}\mathrm{e}^{-Dt\sum_{i=1}^{a}\mathbf{K}(\mathbb{P}_i)^2}\mathrm{e}^{-Dt\sum_{j=1}^{b}\mathbf{K}(\mathbb{Q}_j)^2} \\
& \times\int_{t_0}^{t}\mathrm{d}t'\ \exp\left[Dt'\left(\sum_{i=1}^{a}\mathbf{K}(\mathbb{P}_i)^2+\sum_{j=1}^{b}\mathbf{K}(\mathbb{Q}_j)^2-(\mathbf{k}_1+\cdots+\mathbf{k}_n)^2\right)\right]\ .
\end{aligned}
$$

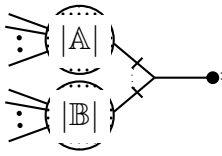
On the left is a diagram with $|\mathbb{A}|+|\mathbb{B}|$ legs and on the right we use Eq. (6.115) for diagrams with fewer legs, because neither $\mathbb{A}$ nor $\mathbb{B}$ can be empty. If we can show that the sum of all diagrams on the left obeys Eq. (6.115), then the induction step is completed.

Since $\cup_{i=1}^{a}\mathbb{P}_i=\mathbb{A}$, we have from Eq. (6.81) that $\sum_{i=1}^{a}\mathbf{K}(\mathbb{P}_i)=\mathbf{K}(\mathbb{A})$ and similarly $\sum_{j=1}^{b}\mathbf{K}(\mathbb{Q}_j)=\mathbf{K}(\mathbb{B})$ and further $\mathbf{K}(\mathbb{A})+\mathbf{K}(\mathbb{B})=\mathbf{K}(\{1,\ldots,n\})=\mathbf{k}_1+\ldots\mathbf{k}_n$, so that the exponent in square brackets appearing within the t' integral in the last line of Eq. (6.116) can be rearranged as follows:

$$
\begin{aligned}
& \sum_{i=1}^{a}\mathbf{K}(\mathbb{P}_i)^2+\sum_{j=1}^{b}\mathbf{K}(\mathbb{Q}_j)^2-(\mathbf{k}_1+\cdots+\mathbf{k}_n)^2 \\
& =-2\left(\mathbf{K}(\mathbb{A})\cdot\mathbf{K}(\mathbb{B})+\sum_{i=1}^{a}\sum_{e=i+1}^{a}\mathbf{K}(\mathbb{P}_i)\cdot\mathbf{K}(\mathbb{P}_e)+\sum_{j=1}^{b}\sum_{f=j+1}^{b}\mathbf{K}(\mathbb{Q}_j)\cdot\mathbf{K}(\mathbb{Q}_f)\right)\ , \qquad (6.117)
\end{aligned}
$$

with the nested double summations generating all cross-terms once. In fact, the bracket

on the right hand side of Eq. (6.117) is the sum of the vector products of all $ab+a(a-1)/2+b(b-1)/2 = (a+b)(a+b-1)/2$ distinct pairs of vectors generated with Eq. (6.81) from the $a+b$ sets $\{\mathbb{P}_1,\ldots,\mathbb{P}_a,\mathbb{Q}_1,\ldots,\mathbb{Q}_b\}$. With Eq. (6.117) we arrive at

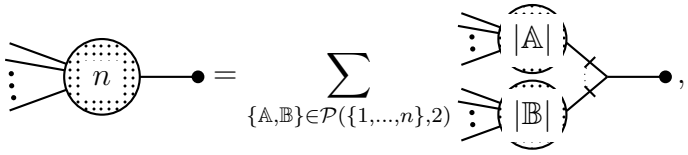


$$\hat{=} n_0\theta(t-t_0)\mathrm{e}^{-i(\mathbf{k}_1+\ldots+\mathbf{k}_n)\cdot\mathbf{x}_0}\sum_{a=1}^{|\mathbb{A}|}\sum_{b=1}^{|\mathbb{B}|}(-1)^{a+b}(a-1)!(b-1)!$$

$$\times\sum_{\{\mathbb{P}_1,\ldots\}\in\mathcal{P}(\mathbb{A},a)}\ \sum_{\{\mathbb{Q}_1,\ldots\}\in\mathcal{P}(\mathbb{B},b)}\frac{\mathbf{K}(\mathbb{A})\cdot\mathbf{K}(\mathbb{B})}{\mathbf{K}(\mathbb{A})\cdot\mathbf{K}(\mathbb{B})+\sum_{i=1}^{a}\sum_{e=i+1}^{a}\mathbf{K}(\mathbb{P}_i)\cdot\mathbf{K}(\mathbb{P}_e)+\sum_{j=1}^{b}\sum_{f=j+1}^{b}\mathbf{K}(\mathbb{Q}_j)\cdot\mathbf{K}(\mathbb{Q}_f)} \tag{6.118}$$

$$\times\left[e^{-D(t-t_0)(\mathbf{k}_1+\ldots+\mathbf{k}_n)^2}-e^{-D(t-t_0)\left(\sum_{i=1}^{a}\mathbf{K}(\mathbb{P}_i)^2+\sum_{j=1}^{b}\mathbf{K}(\mathbb{Q}_j)^2\right)}\right].$$

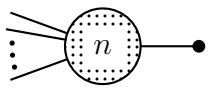
The main obstacle to simplify Eq. (6.118) further at this point is the fraction of scalar products of $\mathbf{K}(\cdot)$'s. Similar to the 3-point case, Eq. (6.114), this will simplify only once we consider the sum over all diagrams with non-equivalent permutations of the external momenta. Since the expressions inserted for sub-diagrams already take care of permutations within each subdiagram we need to consider only different partitionings of the indices $1,\ldots,n$ into subsets $\mathbb{A}$ and $\mathbb{B}$. Diagrammatically, for $n\geq 2$,



(6.119)

where $\mathbb{A}$ and $\mathbb{B}$ are again the sets of indices of the momenta associated with each part of the partition. The external fields of the sub-diagram labelled $|\mathbb{A}|$ have momenta $\mathbf{k}_a$ with $a\in\mathbb{A}$ and correspondingly for the other sub-diagram. The cardinality $|\mathbb{A}|$ of the non-empty partition $\mathbb{A}$, ranges from 1 to $n-1$. The cardinality of the non-empty partition $\mathbb{B}$ is then given by $|\mathbb{B}| = n-|\mathbb{A}|$. Using Eq. (6.118) for the diagrams summed over in Eq. (6.119), we re-organise the partitioning, as explained below, and rewrite it

as



$$\hat{=} \sum_{\{\mathbb{A},\mathbb{B}\}\in\mathcal{P}(\{1,\ldots,n\},2)} \sum_{a=1}^{|\mathbb{A}|} \sum_{\{\mathbb{P}_1,\ldots\}\in\mathcal{P}(\mathbb{A},a)} \sum_{b=1}^{|\mathbb{B}|} \sum_{\{\mathbb{Q}_1,\ldots\}\in\mathcal{P}(\mathbb{B},b)} \mathcal{F}(\{\mathbb{P}_1,\ldots,\mathbb{P}_a\},\{\mathbb{Q}_1,\ldots,\mathbb{Q}_b\}) \tag{6.120a}$$

$$= \sum_{m=2}^{n} \sum_{\{\mathbb{W}_1,\ldots,\mathbb{W}_m\}\in\mathcal{P}(\{1,\ldots,n\},m)} \left[\sum_{\{\mathbb{T}_A,\mathbb{T}_B\}\in\mathcal{P}(\{1,\ldots,m\},2)} \mathcal{F}\left(\bigcup_{t\in\mathbb{T}_A} \{\mathbb{W}_t\}, \bigcup_{t\in\mathbb{T}_B} \{\mathbb{W}_t\} \right) \right] , \tag{6.120b}$$

where $\mathcal{F}$ is given by

$$\begin{aligned} &\mathcal{F}(\{\mathbb{P}_1,\ldots,\mathbb{P}_a\},\{\mathbb{Q}_1,\ldots,\mathbb{Q}_b\}) \\ &= \frac{n_0\theta(t-t_0)\exp\left(-\mathring{\imath}(\mathbf{k}_1+\ldots+\mathbf{k}_n)\cdot\mathbf{x}_0\right)(-1)^{a+b}(a-1)!\,(b-1)!\,\mathbf{K}\left(\bigcup_{i=1}^{a}\mathbb{P}_i\right)\cdot\mathbf{K}\left(\bigcup_{i=1}^{b}\mathbb{Q}_i\right)}{\mathbf{K}\left(\bigcup_{i=1}^{a}\mathbb{P}_i\right)\cdot\mathbf{K}\left(\bigcup_{i=1}^{b}\mathbb{Q}_i\right)+\sum_{i=1}^{a}\sum_{e=i+1}^{a}\mathbf{K}(\mathbb{P}_i)\cdot\mathbf{K}(\mathbb{P}_e)+\sum_{j=1}^{b}\sum_{f=j+1}^{b}\mathbf{K}(\mathbb{Q}_j)\cdot\mathbf{K}(\mathbb{Q}_f)} \\ &\qquad\times\left[e^{-D(t-t_0)(\mathbf{k}_1+\ldots+\mathbf{k}_n)^2}-e^{-D(t-t_0)\left(\sum_{i=1}^{a}\mathbf{K}(\mathbb{P}_i)^2+\sum_{j=1}^{b}\mathbf{K}(\mathbb{Q}_j)^2\right)}\right]. \end{aligned} \tag{6.121}$$

The parameters a and b are the cardinalities of the first and the second partition in the argument of $\mathcal{F}$. This function depends on two partitions of two sets, $\mathbb{A}$ and $\mathbb{B}$, and it is invariant under exchange of its two arguments, which are sets of sets. On the basis of the partitions and the globally known $\mathbf{k}_1,\ldots,\mathbf{k}_n$, all the vectors on the right of Eq. (6.121) can be constructed, so that $\mathcal{F}$ is solely a function of the two partitions.

Both sides of Eq. (6.120) are performing the same summation, based on the five sums from Eqs. (6.118) and (6.119). Both summations generate all possible ways of partitioning the n external legs into two or more subsets. In fact there is a one-to-one correspondence between every term in the two sums, as we will demonstrate below. The first sum in Eq. (6.120a) considers all partitions $\mathcal{P}(\{1,\ldots,n\},2)$ of the full set of indices $\{1,\ldots,n\}$ into two sets, $\mathbb{A}$ and $\mathbb{B}$. These indicate the momenta the two subdiagrams shown in Eqs. (6.118) and (6.119) depend on. To calculate these two subdiagrams all partitions of $\mathbb{A}$ and $\mathbb{B}$ need to be summed over, which is done in

the remaining four sums. The right-hand side Eq. (6.120b) of Eq. (6.120) performs the same summation, but first produces all partitions of all $\{1,\dots,n\}$ into $m = 2,\dots,n$ non-empty subsets $\{\mathbb{W}_1,\dots,\mathbb{W}_m\}$. In the rightmost sum, these subsets are distributed among the upper and the lower subdiagram by perfoming a partition into two subsets $\mathbb{T}_A$ and $\mathbb{T}_B$ on the indexing $\{1,\dots,m\}$ of the subsets $\mathbb{W}_t$. These selections of subsets enter into the function $\mathcal{F}$, with, for example, the upper diagram being parameterised by the collection of sets

$$\bigcup_{t\in\mathbb{T}_A}\{\mathbb{W}_t\} = \{\mathbb{W}_{t_1},\mathbb{W}_{t_2},\dots\} \neq \bigcup_{t\in\mathbb{T}_A}\mathbb{W}_t \quad \text{for} \quad \mathbb{T}_A = \{t_1,t_2,\dots\}\,. \tag{6.122}$$

Both summations of Eq. (6.120) generate all partitions of the indices and their division into an upper and a lower subdiagram. Any term appearing on the left can be found on the right and vice versa. A set of parameters $\{\mathbb{P}_1,\dots,\mathbb{P}_a\}$ and $\{\mathbb{Q}_1,\dots,\mathbb{Q}_b\}$ on the left is found on the right when $m = a+b$ and $\{\mathbb{W}_1,\dots,\mathbb{W}_m\} = \{\mathbb{P}_1,\dots,\mathbb{P}_a\}\cup\{\mathbb{Q}_1,\dots,\mathbb{Q}_b\}$ are the same partition of $\{1,\dots,n\}$, with exactly one of the partitions $\mathbb{T}_A,\mathbb{T}_B$ of the elements of $\{\mathbb{W}_1,\dots\}$ such that $\cup_{t\in\mathbb{T}_A}\{\mathbb{W}_t\} = \{\mathbb{P}_1,\dots,\mathbb{P}_a\}$ and $\cup_{t\in\mathbb{T}_B}\{\mathbb{W}_t\} = \{\mathbb{Q}_1,\dots,\mathbb{Q}_b\}$ or equivalenty $\cup_{t\in\mathbb{T}_A}\{\mathbb{W}_t\} = \{\mathbb{Q}_1,\dots,\mathbb{Q}_b\}$ and $\cup_{t\in\mathbb{T}_B}\{\mathbb{W}_t\} = \{\mathbb{P}_1,\dots,\mathbb{P}_a\}$. Similarly, the term generated by the partition $\cup_{t\in\mathbb{T}_A}\{\mathbb{W}_t\},\cup_{t\in\mathbb{T}_B}\{\mathbb{W}_t\}$ on the right, can be identified on the left, as the one where $\mathbb{A} = \cup_{t\in\mathbb{T}_A}\mathbb{W}_t$ and $\mathbb{B} = \cup_{t\in\mathbb{T}_B}\mathbb{W}_t$ or vice versa, which are both sets, not partitions. They need to be partitioned subsequently, for example $\mathbb{A}$ into $\{\mathbb{P}_1,\dots,\mathbb{P}_a\} = \cup_{t\in\mathbb{T}_A}\mathbb{W}_t$ and $\mathbb{B}$ into $\{\mathbb{P}_1,\dots,\mathbb{P}_b\} = \cup_{t\in\mathbb{T}_B}\mathbb{W}_t$ or equally $\mathbb{A}$ into $\{\mathbb{P}_1,\dots,\mathbb{P}_a\} = \cup_{t\in\mathbb{T}_B}\mathbb{W}_t$ and $\mathbb{B}$ into $\{\mathbb{P}_1,\dots,\mathbb{P}_b\} = \cup_{t\in\mathbb{T}_A}\mathbb{W}_t$.

Writing $\mathbb{T}_A = \{\alpha_1,\alpha_2,\dots,\alpha_a\}$ and $\mathbb{T}_B = \{\beta_1,\beta_2,\dots,\beta_b\}$, the parameterisation of the right-hand side of Eq. (6.120) allows us to express the denominator of $\mathcal{F}$, Eq. (6.121), succinctly in terms of the new partition $\{\mathbb{W}_1,\dots,\mathbb{W}_m\}$,

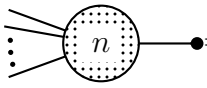
$$\begin{aligned}\mathbf{K}(\cup_{t\in\mathbb{T}_A}\{\mathbb{W}_t\})\cdot\mathbf{K}(\cup_{t\in\mathbb{T}_B}\{\mathbb{W}_t\}) + \sum_{i=1}^{a}\sum_{e=i+1}^{a}\mathbf{K}(\mathbb{W}_{\alpha_i})\cdot\mathbf{K}(\mathbb{W}_{\alpha_e}) + \sum_{j=1}^{b}\sum_{f=j+1}^{b}\mathbf{K}\big(\mathbb{W}_{\beta_j}\big)\cdot\mathbf{K}\big(\mathbb{W}_{\beta_f}\big)& \\ = \sum_{u=1}^{m}\sum_{v=u+1}^{m}\mathbf{K}(\mathbb{W}_u)\cdot\mathbf{K}(\mathbb{W}_v)&\end{aligned} \tag{6.123}$$

as this is the sum of all cross-terms in the square of $\sum_{t=1}^{m}\mathbf{K}(\mathbb{W}_t)$, as alluded to after Eq. (6.117). Further, the sum of the squares in the exponent of the right-most expo-

nential in Eq. (6.121) can be written as

$$\sum_{i=1}^{a} \mathbf{K}(\mathbb{W}_{\alpha_i})^2 + \sum_{j=1}^{b} \mathbf{K}\big(\mathbb{W}_{\beta_j}\big)^2 = \sum_{u=1}^{m} \mathbf{K}(\mathbb{W}_u)^2 \tag{6.124}$$

as $\mathbb{T}_A \cup \mathbb{T}_B = \{1, \ldots, m\}$. Because the right-hand sides of Eqs. (6.123) and (6.124) are independent of the partitioning of $\{\mathbb{W}_1, \ldots, \mathbb{W}_m\}$ via $\mathbb{T}_A$ and $\mathbb{T}_B$, they can be taken outside the sum over these partitions together with $(-1)^{|\mathbb{T}_A|+|\mathbb{T}_B|} = (-1)^m$,



$$\hat{=} n_0 \theta(t - t_0) \mathrm{e}^{-i(\mathbf{k}_1+\ldots+\mathbf{k}_n)\cdot\mathbf{x}_0} \tag{6.125}$$
$$\times \sum_{m=2}^{n} (-1)^m \sum_{\{\mathbb{W}_1,\ldots,\mathbb{W}_m\}\in\mathcal{P}(\{1,\ldots,n\},m)} \frac{e^{-D(t-t_0)(\mathbf{k}_1+\ldots+\mathbf{k}_n)^2} - e^{-D(t-t_0)\left(\sum_{u=1}^{m}\mathbf{K}(\mathbb{W}_u)^2\right)}}{\sum_{u=1}^{m}\sum_{v=u+1}^{m}\mathbf{K}(\mathbb{W}_u)\cdot\mathbf{K}(\mathbb{W}_v)}$$
$$\times \left[\sum_{\{\mathbb{T}_A,\mathbb{T}_B\}\in\mathcal{P}(\{1,\ldots,m\},2)} (|\mathbb{T}_A|-1)!\,(|\mathbb{T}_B|-1)!\,\bar{\mathbf{K}}_A\cdot\bar{\mathbf{K}}_B \right] ,$$

where we use the shorthands

$$\bar{\mathbf{K}}_A = \mathbf{K}\left(\bigcup_{t\in\mathbb{T}_A}\{\mathbb{W}_t\}\right) = \sum_{t\in\mathbb{T}_A}\mathbf{K}(\mathbb{W}_t) \tag{6.126a}$$

$$\bar{\mathbf{K}}_B = \mathbf{K}\left(\bigcup_{t\in\mathbb{T}_B}\{\mathbb{W}_t\}\right) = \sum_{t\in\mathbb{T}_B}\mathbf{K}(\mathbb{W}_t)\ . \tag{6.126b}$$

Next we want to simplify the sum in square brackets in Eq. (6.125). Since it is over all ways to partition $\{1, \ldots, m\}$ into the two distinct sets that define $\bar{\mathbf{K}}_A$ and $\bar{\mathbf{K}}_B$, we know that the sum over the products $\bar{\mathbf{K}}_A \cdots \bar{\mathbf{K}}_B$ will involve every cross-term $\mathbf{K}(\mathbb{W}_u)\cdot\mathbf{K}(\mathbb{W}_v)$ with $u \neq v$ at least once and by symmetry equally often. The sum will therefore cancel with the denominator up to a pre-factor. In order to determine it, we pick a particular scalar product, $\mathbf{K}(\mathbb{W}_u)\cdot\mathbf{K}(\mathbb{W}_v)$ for some fixed $u \neq v$ and

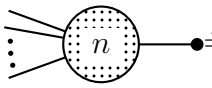
consider those terms in the sum that contain $\mathbf{K}(\mathbb{W}_u)\cdot\mathbf{K}(\mathbb{W}_v)$:

$$C_{u,v} = \mathbf{K}(\mathbb{W}_u)\cdot\mathbf{K}(\mathbb{W}_v)$$
$$\times \sum_{\{\mathbb{T}_A,\mathbb{T}_B\}\in\mathcal{P}(\{1,\ldots,m\},2)} \mathcal{I}\Big((u\in\mathbb{T}_A\wedge v\in\mathbb{T}_B)\vee(u\in\mathbb{T}_B\wedge v\in\mathbb{T}_A)\Big)\,(|\mathbb{T}_A|-1)!\,(|\mathbb{T}_B|-1)!\;, \tag{6.127}$$

where $\mathcal{I}(\ldots)$ is an indicator function that is 1 only if indices u and v are in different subsets and 0 otherwise, so that the square bracket in Eq. (6.125) becomes $\sum_{u=1}^{m}\sum_{v=u+1}^{m} C_{u,v}$. We may therefore simply sum over all partitions where u and v indeed *are* in different subsets, for example u in $\mathbb{T}_A$ and v in $\mathbb{T}_B$ — there is no need to separately consider the case $u\in\mathbb{T}_B$ and $v\in\mathbb{T}_A$, as the resulting partitions are identical. The make-up of the subsets enters only in as far as their cardinalities are concerned, which feature in the factorial. If $n_A = |\mathbb{T}_A| > 0$ is the cardinality of $\mathbb{T}_A$, that leaves $n_B = m - n_A > 0$ elements for $\mathbb{T}_B$. With one "seat" in $\mathbb{T}_A$ given to u, there are $n_A - 1$ further elements to be chosen from the $m-2$ elements in $\{1,\ldots,m\}\setminus\{u,v\}$,

$$\begin{aligned} C_{u,v} &= \mathbf{K}(\mathbb{W}_u)\cdot\mathbf{K}(\mathbb{W}_v)\sum_{n_A=1}^{m-1}\binom{m-2}{n_A-1}(n_A-1)!\,(m-n_A-1)! \\ &= \mathbf{K}(\mathbb{W}_u)\cdot\mathbf{K}(\mathbb{W}_v)\sum_{n_A=1}^{m-1}(m-2)! = (m-1)!\,\mathbf{K}(\mathbb{W}_u)\cdot\mathbf{K}(\mathbb{W}_v)\;, \end{aligned} \tag{6.128}$$

which means that the square bracket in Eq. (6.125) cancels with the denominator in the preceding fraction up to a factor $(m-1)!$, which can be taken outside the second sum,



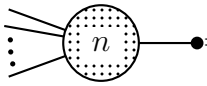
$$\hat{=} n_0\theta(t-t_0)\mathrm{e}^{-i(\mathbf{k}_1+\ldots+\mathbf{k}_n)\cdot\mathbf{x}_0} \tag{6.129}$$
$$\times\sum_{m=2}^{n}(-1)^m\,(m-1)!\sum_{\{\mathbb{W}_1,\ldots,\mathbb{W}_m\}\in\mathcal{P}(\{1,\ldots,n\},m)}\Big(e^{-D(t-t_0)(\mathbf{k}_1+\ldots+\mathbf{k}_n)^2} - e^{-D(t-t_0)\left(\sum_{u=1}^{m}\mathbf{K}(\mathbb{W}_u)^2\right)}\Big)\;.$$

The first exponential in the final bracket is independent of the partition, so that the sum degenerates into the count of the ways a set of n elements can be partitioned into m non-empty sets, given by the Stirling number of the second kind, $\left\{{n \atop m}\right\}$. We

find with the help of [69, 9.745.1]

$$\sum_{m=2}^{n}(-1)^m\,(m-1)!\sum_{\{\mathbb{W}_1,\ldots,\mathbb{W}_m\}\in\mathcal{P}(\{1,\ldots,n\},m)}1=\sum_{m=2}^{n}(-1)^m\,(m-1)!\left\{{n\atop m}\right\}=1\;. \tag{6.130}$$

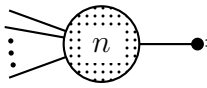
With that in place, we rewrite Eq. (6.129) as



$$\hat{=}n_0\theta(t-t_0)\mathrm{e}^{-i(\mathbf{k}_1+\ldots+\mathbf{k}_n)\cdot\mathbf{x}_0}\times \tag{6.131}$$

$$\left\{e^{-D(t-t_0)(\mathbf{k}_1+\ldots+\mathbf{k}_n)^2}+\sum_{m=2}^{n}(-1)^{m-1}\,(m-1)!\sum_{\{\mathbb{W}_1,\ldots,\mathbb{W}_m\}\in\mathcal{P}(\{1,\ldots,n\},m)}e^{-D(t-t_0)\left(\sum_{u=1}^{m}\mathbf{K}(\mathbb{W}_u)^2\right)}\right\}.$$

The exponential of $-D(t-t_0)(\mathbf{k}_1+\ldots+\mathbf{k}_n)^2$ in the curly brackets is the summand of the subsequent sum running over $m\geq 2$ evaluated for $m=1$, because the only partition of $\{1,\ldots,n\}$ into $m=1$ subsets is $\mathbb{W}_1=\{1,\ldots,n\}$ which produces the vector $\mathbf{K}(\mathbb{W}_1)=\mathbf{k}_1+\ldots+\mathbf{k}_n$. It follows that



$$\hat{=}n_0\theta(t-t_0)\mathrm{e}^{-i(\mathbf{k}_1+\ldots+\mathbf{k}_n)\cdot\mathbf{x}_0} \tag{6.132}$$

$$\times\sum_{m=1}^{n}(-1)^{m-1}\,(m-1)!\sum_{\{\mathbb{W}_1,\ldots,\mathbb{W}_m\}\in\mathcal{P}(\{1,\ldots,n\},m)}\left(e^{-D(t-t_0)\left(\sum_{u=1}^{m}\mathbf{K}(\mathbb{W}_u)^2\right)}\right)\;,$$

which is Eq. (6.115). We have thus demonstrated that if Eq. (6.115) holds for all diagrams with fewer than $n\geq 2$ legs, as they enter into Eq. (6.116), then Eq. (6.115) also holds for the diagrams with n legs. This concludes the induction step and together with the base case $n=1$ proves Eqs. (6.115) and (6.80) for all $n\geq 1$.

6.B Multiple starting points

We generalise our calculation of the connected and full moments of the integrated particle number density in Dean's formalism, Section 6.5, to the case where a total of n_0 particles are initialised at $H\leq n_0$ distinct sites. We upgrade the previous derivation by replacing in the action Eqs. (6.24) and (6.79) and correspondingly in

Eqs. (6.26) and (6.80)

$$n_0 \mathrm{e}^{i\mathbf{k}_0\mathbf{x}_0} \qquad \text{by} \qquad \sum_{h=1}^{H} n_{0,h} \mathrm{e}^{i\mathbf{k}_0\mathbf{x}_{0,h}} \tag{6.133}$$

where $x_{0,h}$ for $h = 1, ..., H$ denote the $n_{0,h} \in \mathbb{N}$ particles' initial positions such that

$$\sum_{h=1}^{H} n_{0,h} = n_0 \ . \tag{6.134}$$

In Section 6.5 and Appendix 6.A we were entirely concerned with connected diagrams, where $n_0 \exp\left(\mathring{\imath}\mathbf{x}_0 \cdot \mathbf{k}_0\right)$ only ever enters linearly. Replacing it according to Eq. (6.133) renders each such diagram a sum over the H distinct locations, each such sum still to be considered a single *connected* diagram. This equally applies to the central result Eq. (6.88), which now reads

$$\sum_{h=1}^{H} \quad n \quad n_{0,h} \quad = -\sum_{h=1}^{H} n_{0,h}\theta(t-t_0) \sum_{m=1}^{n} \left(I_{\Omega,h}(t-t_0)\right)^m (m-1)! \left\{ {n \atop m} \right\} \tag{6.135}$$

where $I_{\Omega,h}(t-t_0)$ denotes the transition probability from the starting point $x_{0,h}$ into the set Ω.

The full moments of the integrated particle number density for distinct starting points can also be derived straighforwardly following the calculation in Eqs. (6.90)–(6.100). Using Eq. (6.135) for the associated connected moments, we arrive at

$$n \quad \hat{=} \left. \frac{d^n}{dz^n} \right|_{z=0} \prod_{h=1}^{H} \left[1 + (e^z - 1) I_{\Omega,h})\right]^{n_{0,h}} \tag{6.136}$$

$$= \sum_{j_1+...+j_H=n} \binom{n}{j_1, ..., j_H} \prod_{h=1}^{H} \left. \frac{d^{j_h}}{dz^{j_h}} \right|_{z=0} \left[1 + (e^z - 1) I_{\Omega,h}\right]^{n_{0,h}} \tag{6.137}$$

$$= \sum_{j_1+...+j_H=n} \binom{n}{j_1, ..., j_H} \prod_{h=1}^{H} \sum_{k_h=0}^{n_{0,h}} \binom{n_{0,h}}{k_h} \left(I_{\Omega,h}\right)^{k_h} k_h! \left\{ {j_h \atop k_h} \right\} \ , \tag{6.138}$$

where we have used the generalised product rule to go from Eq. (6.136) to Eq. (6.137) by swapping the differential operator into the product, as well as the intermediate

result Eqs. (6.97)–(6.102) for the last step. One can easily verify that Eq. (6.138) reduces to Eq. (6.102) when $H = 1$, *i.e.* when all particles are initialised at the same point.

To show particle entity we use a similar procedure as in the single source case from Eq. (6.102) to (6.106),

$$\sum_{n=0}^{\infty} \frac{(2\pi\mathring{\imath})^n}{n!} \;\; n \;\; \hat{=} \sum_{n=0}^{\infty} \sum_{j_1+\ldots+j_H=n} \frac{(2\pi\mathring{\imath})^n}{j_1!\ldots j_H!} \prod_{h=1}^{H} \sum_{k_h=0}^{n_{0,h}} \binom{n_{0,h}}{k_h} (I_{\Omega,h})^{k_h} \, k_h! \left\{ {j_h \atop k_h} \right\} , \tag{6.139}$$

where the second sum on the right runs over all non-negative integers $j_1, j_2, \ldots, j_H$ which sum to n. We now use that $\sum_{n=0}^{\infty} \sum_{j_1+\ldots+j_H=n} = \sum_{j_1=0}^{\infty} \ldots \sum_{j_H=0}^{\infty}$ as the sums converge individually and absolutely, and Eq. (6.103) to obtain

$$\sum_{n=0}^{\infty} \frac{(2\pi\mathring{\imath})^n}{n!} \;\; n \;\; \hat{=} \sum_{j_1=0}^{\infty} \ldots \sum_{j_H=0}^{\infty} \frac{(2\pi\mathring{\imath})^{j_1+\ldots+j_H}}{j_1!\ldots j_H!} \prod_{h=1}^{H} \sum_{k_h=0}^{n_{0,h}} \binom{n_{0,h}}{k_h} (1 - I_{\Omega,h})^{n_{0,h}-k_h} (I_{\Omega,h})^{k_h} k_h^{j_h} \tag{6.140}$$

$$= \prod_{h=1}^{H} \left(\sum_{j_h=0}^{\infty} \sum_{k_h=0}^{n_{0,h}} \binom{n_{0,h}}{k_h} (1 - I_{\Omega,h})^{n_{0,h}-k_h} (I_{\Omega,h})^{k_h} \frac{(2\pi\mathring{\imath}k_h)^{j_h}}{j_h!} \right) \tag{6.141}$$

$$= \prod_{h=1}^{H} \left(\sum_{k_h=0}^{n_{0,h}} \binom{n_{0,h}}{k_h} (1 - I_{\Omega,h})^{n_{0,h}-k_h} (I_{\Omega,h})^{k_h} e^{2\pi\mathring{\imath}k_h} \right) \tag{6.142}$$

$$= \prod_{h=1}^{H} (1) \tag{6.143}$$

$$= 1 \, . \tag{6.144}$$

This completes the derivation of particle entity according to the criterion Eqs. (6.64) for particles initialised as multiple origins, *cf.* Eq. (6.106).

The nth full moment, in the form of the right hand side Eq. (6.102), has an instructive physical interpretation drawing on n_0 being integer. To see this, we write the nth moment of the particle number as

$$\left\langle \left(\int_\Omega \mathrm{d}^d x\, \rho(\mathbf{x},t) \right)^n \right\rangle = \int_\Omega \mathrm{d}^d x_1' \mathrm{d}^d x_2' \ldots \mathrm{d}^d x_n' \, \langle \rho(\mathbf{x}_1',t)\rho(\mathbf{x}_2',t)\ldots\rho(\mathbf{x}_n',t)\rangle \tag{6.145}$$

with each density $\rho(\mathbf{x}_i',t)$ considered a random variable as a function of the positions $x_j(t)$ of n_0 particles indexed by $j = 1,2,\ldots,n_0$

$$\rho(\mathbf{x}_i',t) = \sum_{j=1}^{n_0} \delta(\mathbf{x}_i' - \mathbf{x}_j(t)) \;, \tag{6.146}$$

generating n_0^n terms of products of δ-functions in Eq. (6.145). To calculate the right-hand side of Eq. (6.145) on the basis of Eq. (6.146) using Eq. (6.87) in the form

$$\int_\Omega \mathrm{d}^d x' \, \langle \delta(\mathbf{x}' - \mathbf{x}_j(t)\rangle = I_\Omega(t - t_0) \tag{6.147}$$

requires careful bookkeeping of how often each particle coordinate $\mathbf{x}_j(t)$ is repeated. For example

$$\int_\Omega \mathrm{d}^d x_1' \mathrm{d}^d x_2' \, \langle \delta(\mathbf{x}_1' - \mathbf{x}_1(t))\delta(\mathbf{x}_2' - \mathbf{x}_2(t))\rangle = I_\Omega^2 \tag{6.148a}$$

$$\int_\Omega \mathrm{d}^d x_1' \mathrm{d}^d x_2' \, \langle \delta(\mathbf{x}_1' - \mathbf{x}_1(t))\delta(\mathbf{x}_2' - \mathbf{x}_1(t))\rangle = I_\Omega \tag{6.148b}$$

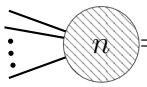
as particle coordinates are independent in Eq. (6.148a), but not in Eq. (6.148b), where in fact $\delta(\mathbf{x}_1' - \mathbf{x}_1(t))\delta(\mathbf{x}_2' - \mathbf{x}_1(t)) = \delta(\mathbf{x}_1' - \mathbf{x}_1(t))\delta(\mathbf{x}_2' - \mathbf{x}_1')$. To calculate the right-hand side of Eq. (6.145) thus is a matter of allowing for $k = 1,2,\ldots,n$ distinct particle coordinates $x_j(t)$ from each of the n sums Eq. (6.146). There are $n_0(n_0-1)\cdot\ldots\cdot(n_0-k+1) = \binom{n_0}{k}k!$ such choices. As each of the $\rho(\mathbf{x}_i',t)$ is a function of a different dummy variable, they have to be distributed among the k distinct particle coordinates. There are $\left\{ {n \atop k} \right\}$ choices for that. The integration produces I_Ω^k depending on the number k of distinct particle coordinates following the reasoning for Eq. (6.148). In summary, we

arrive at

$$\left\langle \left(\int_\Omega \mathrm{d}^d x \, \rho(\mathbf{x}, t) \right)^n \right\rangle = \sum_{k=0}^{n} \binom{n_0}{k} I_\Omega^k k! \left\{ {n \atop k} \right\} , \tag{6.149}$$

including $k = 0$ in the summation to cover the special case of $n = 0$. Eq. (6.149) is subtly different from Eq. (6.102), as the upper limit of the sum in Eq. (6.102) is n_0, while it is n in Eq. (6.149). However, $\left\{ {n \atop k} \right\}$ in Eq. (6.102) vanishes if k exceeds n and $\binom{n_0}{k}$ in Eq. (6.102) vanishes if *integer* k exceeds *integer* n_0, *i.e.* in both sums the upper limit may be replaced by $\min(n, n_0)$, provided only n_0 is integer. We conclude that the full moment Eq. (6.102) has a sensible interpretation in terms of particle numbers only if n_0 is integer.

The key ingredient here are the falling factorials $\binom{n_0}{k} k! = n_0(n_0 - 1) \cdot \ldots \cdot (n_0 - k + 1)$. We have seen how they emerge in Dean's theory by computing the connected moments, Eq. (6.102) and also Eq. (6.149), explicitly. This structure is another signature of particle entity, in the sense that it highlights the special role played by the integer nature of the initial particle number n_0. Unsurprisingly, it similarly emerges in Doi-Peliti. In particular, the full moments of the particle number at position $\mathbf{x}$ are given by



$$\hat{=} \langle ☼ | \left(a^\dagger(\mathbf{x}) a(\mathbf{x}) \right)^n \mathrm{e}^{\hat{A}(t-t_0)} \left(a^\dagger(\mathbf{x}_0) \right)^{n_0} |0\rangle \ , \tag{6.150}$$

where $\hat{A}$ denotes the time evolution operator of Eq. (6.4). We then use

$$\left(a^\dagger(\mathbf{x}_0) \right)^{n_0} = \left(\tilde{a}(\mathbf{x}_0) + 1 \right)^{n_0} = \sum_{k=0}^{n_0} \binom{n_0}{k} \left(\tilde{a}(\mathbf{x}_0) \right)^k \tag{6.151}$$

together with [61]

$$\langle ☼ | \left(a^\dagger(\mathbf{x}) a(\mathbf{x}) \right)^n = \sum_{\ell=0}^{n} \left\{ {n \atop \ell} \right\} \langle ☼ | \left(a(\mathbf{x}) \right)^\ell \tag{6.152}$$

to rewrite the right-hand side of Eq. (6.150) as

$$\langle \text{☼}| \left(a^\dagger(\mathbf{x})a(\mathbf{x})\right)^n \mathrm{e}^{\hat{A}(t-t_0)} \left(a^\dagger(\mathbf{x}_0)\right)^{n_0} |0\rangle = \sum_{\ell=0}^{n} \left\{ {n \atop \ell} \right\} \sum_{k=0}^{n_0} \binom{n_0}{k} \langle \text{☼}| \left(a(\mathbf{x})\right)^\ell \mathrm{e}^{\hat{A}(t-t_0)} \left(\tilde{a}(\mathbf{x}_0)\right)^k |0\rangle \tag{6.153}$$

$$= \sum_{\ell=0}^{n_0} \left\{ {n \atop \ell} \right\} \binom{n_0}{\ell} \ell! \, \langle \text{☼}| \, a(\mathbf{x}) \mathrm{e}^{\hat{A}(t-t_0)} \tilde{a}(\mathbf{x}_0) \, |0\rangle^\ell \tag{6.154}$$

where we have used $\langle \text{☼}| \left(a(\mathbf{x})\right)^\ell \exp \hat{A}(t-t_0)) (\tilde{a}(\mathbf{x}_0))^k \, |0\rangle = \delta_{k\ell} \ell! \, \langle \text{☼}| \, a(\mathbf{x}) \exp \hat{A}(t-t_0)) \tilde{a}(\mathbf{x}_0) \, |0\rangle^\ell$ in the absence of interactions. The final expression corresponds to the one we found via the Dean route, Eq. (6.102), with $I_\Omega(t-t_0)$ replaced by the Doi-Peliti propagator $\langle \text{☼}| \, a(\mathbf{x}) \exp A(t-t_0)) \tilde{a}(\mathbf{x}_0) \, |0\rangle$.

Acknowledgement

I would like to thank my collaborators very much for their permission to present our joint work as a part of my PhD thesis. I have obtained their approval which is shown in Appendix A.

7

Conclusion

Active matter is a wide field of which four topics are presented in this thesis. Exactly solvable models and their entropy productions are calculated in Chapter 2. In the next chapter, RnT particles in a piecewise linear ratchet are studied (Chapter 3). Using field theoretic methods, results for RnT particles in general external potentials are presented (Chapter 5). In Chapter 6, the mechanism for particle entity under the Doi-Peliti field theory and the response field theory derived by Dean's equation is then demonstrated.

Methods from stochastic processes and statistical field theories are versatile toolboxes for studying active matter. In the first half of the thesis, I mainly concentrated on presenting the results employing techniques from stochastic processes. In Chapter 2, I presented a review of entropy production and calculated it for models including random walks, multi-state Markov processes, driven Brownian motions in potentials and RnT particles on a ring. In Chapter 3, I calculated the exact steady-state probability distribution, current, entropy production, power extraction and first passage properties of a RnT in an asymmetric piecewise ratchet. In the second part of the thesis, field-theoretic approaches were utilised. Using Doi-Peliti field theory, I solved the steady-state probability distribution of a RnT particle in a general external potential $U(x)$ and found that the optimal potential that maximises the current of RnT

has a deep crevasse then a flat plane in the middle and then a sharp peak (Chapter 5). In Chapter 6, I demonstrated the particle entity of focusing on two well-known statistical field theories, namely the Doi-Peliti field theory and the response field theory.

There are a few questions that I believe can be addressed as future research direction related to Chapter 3, 5 and 6:

- What is the effect of the piecewise ratchet on the effective diffusion constant of the RnT particle and does it also cause the giant acceleration [134]?
- Can we solve the steady-state distribution exactly, therefore the entropy production, work extraction and first-passage properties for an active Ornstein-Uhlenbeck particle [55], where the noise is driven by an Ornstein-Uhlenbeck process, in a piecewise ratchet?
- To resolve the issue of the radius of convergence in the perturbative expansion of the Doi-Peliti field theory for a RnT particle in a periodic potential using renormalisation groups. Is there a way to find the analytical form of the optimal potential that maximises the particle current?
- Introduce a formalism to probe particle entity when there is an interacting potential between particles under the two field-theoretic frameworks.

Active matter is a fascinating field where more novel results continue to be discovered. Overall, this thesis develops and addresses topics and viewpoints that will support future scientific research. I have considered a wide range of questions addressing problems in active matter using techniques from stochastic processes and field theories. I hope to continue to contribute to the development of the field in the future.

Bibliography

[1] S. Ahmad, K. Rijal, and D. Das. First passage in the presence of stochastic resetting and a potential barrier. *Phys. Rev. E* **105** (4):044134, 2022. Cited on p. 139.

[2] H. Alston, L. Cocconi, and T. Bertrand. Non-equilibrium thermodynamics of diffusion in fluctuating potentials. *J. Phys. A: Math. Theor.* **55** (27):274004, 2022. Cited on p. 114 and 115.

[3] D. Andrieux, P. Gaspard, S. Ciliberto, N. Garnier, S. Joubaud, and A. Petrosyan. Thermodynamic time asymmetry in non-equilibrium fluctuations. *J. Stat. Mech.: Theory Exp.* **2008** (01):01002, 2008. Cited on p. 80.

[4] L. Angelani. Run-and-tumble particles, telegrapher's equation and absorption problems with partially reflecting boundaries. *J. Phys. A: Math. Theor.* **48** (49):495003, 2015. Cited on p. 97.

[5] L. Angelani. Confined run-and-tumble swimmers in one dimension. *J. Phys. A: Math. Theor.* **50** (32):325601, 2017. Cited on p. 96 and 97.

[6] L. Angelani, A. Costanzo, and R. Di Leonardo. Active ratchets. *Europhys. Lett.* **96** (6):68002, 2011. Cited on p. 96, 103, 104, 110, 111, 123, and 162.

[7] L. Angelani, R. Di Leonardo, and M. Paoluzzi. First-passage time of run-and-tumble particles. *Eur. Phys. J. E* **37** (7):1, 2014. Cited on p. 97.

[8] L. Angelani, R. Di Leonardo, and G. Ruocco. Self-Starting Micromotors in a Bacterial Bath. *Phys. Rev. Lett.* **102** (4):048104, 2009. Cited on p. 96 and 162.

[9] R. D. Astumian and M. Bier. Fluctuation driven ratchets: Molecular motors. *Phys. Rev. Lett.* **72** (11):1766, 1994. Cited on p. 13, 21, 27, 96, 101, 102, 103, 112, 162, 167, 193, 194, and 196.

[10] Y. Baek. Private communication. Cited on p. 162.

[11] A. C. Barato, D. Hartich, and U. Seifert. Efficiency of cellular information processing. *New J. Phys.* **16** (10):103024, 2014. Cited on p. 46.

[12] U. Basu, S. N. Majumdar, A. Rosso, S. Sabhapandit, and G. Schehr. Exact stationary state of a run-and-tumble particle with three internal states in a harmonic trap. *J. Phys. A: Math. Theor.* **53** (9):09LT01, 2020. Cited on p. 96.

[13] F. Berger, T. Schmiedl, and U. Seifert. Optimal potentials for temperature ratchets. *Phys. Rev. E* **79** (3):031118, 2009. Cited on p. 162.

[14] L. Berthier and J. Kurchan. Non-equilibrium glass transitions in driven and active matter. *Nat. Phys.* **9**:310, 2013. Cited on p. 162.

[15] B. Bijnens and C. Maes. Pushing run-and-tumble particles through a rugged channel. *J. Stat. Mech.: Theory Exp.* **2021** (3):033206, 2021. Cited on p. 162.

[16] J. J. Binney, N. J. Dowrick, A. J. Fisher, and M. E. J. Newman. *The Theory of Critical Phenomena.* Oxford University Press, Oxford, UK, 1998. Cited on p. 235 and 236.

[17] I. Bordeu, S. Amarteifio, R. Garcia-Millan, B. Walter, N. Wei, and G. Pruessner. Volume explored by a branching random walk on general graphs. *Sci. Rep.* **9** (1):1, 2019. Cited on p. 93.

[18] M. Bothe, L. Cocconi, Z. Zhen, and G. Pruessner. Particle Entity in the Doi-Peliti and Response Field Formalisms. *arXiv* 2022. 2205.10409. Cited on p. 7 and 215.

[19] M. Bothe and G. Pruessner. Doi-Peliti field theory of free active Ornstein-Uhlenbeck particles. *Phys. Rev. E* **103** (6):062105, 2021. Cited on p. 28.

[20] H. Brenner. Macrotransport processes. *Langmuir* **6** (12):1715, 1990. Cited on p. 162.

[21] D. Breoni, F. J. Schwarzendahl, R. Blossey, and H. Löwen. A one-dimensional three-state run-and-tumble model with a 'cell cycle'. *Eur. Phys. J. E* **45**:83, 2022. Cited on p. 96.

[22] P. C. Bressloff. Encounter-based model of a run-and-tumble particle. *J. Stat. Mech.: Theory Exp.* **2022** (11):113206, 2022. Cited on p. 97.

[23] P. C. Bressloff and J. M. Newby. Stochastic models of intracellular transport. *Rev. Mod. Phys.* **85** (1):135, 2013. Cited on p. 162.

[24] D. M. Busiello, J. Hidalgo, and A. Maritan. Entropy production for coarse-grained dynamics. *New J. Phys.* **21** (7):073004, 2019. Cited on p. 216.

[25] Y. Cao, H. Wang, Q. Ouyang, and Y. Tu. The free-energy cost of accurate biochemical oscillations. *Nat. Phys.* **11** (9):772, 2015. Cited on p. 46.

[26] L. Caprini, U. M. B. Marconi, A. Puglisi, and A. Vulpiani. The entropy production of Ornstein–Uhlenbeck active particles: a path integral method for correlations. *J. Stat. Mech.: Theory Exp.* **2019** (5):053203, 2019. Cited on p. 58.

[27] J. Cardy. Reaction-diffusion processes. In *Non-equilibrium Statistical Mechanics and Turbulence* (edited by S. Nazarenko and O. V. Zaboronski), pp. 108–161. Cambridge University Press, Cambridge, UK, 2008. Cited on p. 216, 217, 218, and 226.

[28] J. Cardy, G. Falkovich, and K. Gawedzki. *Non-equilibrium Statistical Mechanics and Turbulence*. Cambridge University Press, Cambridge, England, UK, 2008. Cited on p. 164, 179, and 180.

[29] M. E. Cates. Diffusive transport without detailed balance in motile bacteria: does microbiology need statistical physics? *Rep. Prog. Phys.* **75** (4):042601, 2012. Cited on p. 27 and 162.

[30] L. Cocconi, R. Garcia-Millan, Z. Zhen, B. Buturca, and G. Pruessner. Entropy Production in Exactly Solvable Systems. *Entropy* **22** (11):1252, 2020. Cited on p. 6, 45, 97, 115, 118, 170, 216, and 283.

[31] L. Cocconi, J. Knight, and C. Roberts. Optimal power extraction from active particles with hidden states. *arXiv* 2022. Cited on p. 128 and 140.

[32] L. Comtet. *Advanced Combinatorics: The art of finite and infinite expansions*. Springer Science & Business Media, 2012. Cited on p. 238, 242, and 243.

[33] S. Coppola and V. Kantsler. Curved ratchets improve bacteria rectification in microfluidic devices. *Phys. Rev. E* **104** (1):014602, 2021. Cited on p. 162.

[34] G. E. Crooks. Entropy production fluctuation theorem and the nonequilibrium work relation for free energy differences. *Phys. Rev. E* **60** (3):2721, 1999. Cited on p. 28.

[35] L. F. Cugliandolo and V. Lecomte. Rules of calculus in the path integral representation of white noise langevin equations: the onsager–machlup approach. *J. Phys. A: Math. Theor.* **50** (34):345001, 2017. Cited on p. 58.

[36] S. Das, G. Gompper, and R. G. Winkler. Confined active Brownian particles: theoretical description of propulsion-induced accumulation. *New J. Phys.* **20** (1):015001, 2018. Cited on p. 96.

[37] D. S. Dean. Langevin equation for the density of a system of interacting langevin processes. *J. Phys. A: Math. Gen.* **29** (24):L613, 1996. Cited on p. 216 and 221.

[38] J.-F. Derivaux, R. L. Jack, and M. E. Cates. Rectification in a mixture of active and passive particles subject to a ratchet potential. *J. Stat. Mech.: Theory Exp.* **2022** (4):043203, 2022. Cited on p. 96.

[39] A. Dhar, A. Kundu, S. N. Majumdar, S. Sabhapandit, and G. Schehr. Run-and-tumble particle in one-dimensional confining potentials: steady-state, relaxation, and first-passage properties. *Phys. Rev. E* **99** (3):032132, 2019. Cited on p. 96, 97, 127, and 129.

[40] R. Di Leonardo, L. Angelani, D. Dell'Arciprete, G. Ruocco, V. Iebba, S. Schippa, M. P. Conte, F. Mecarini, F. De Angelis, and E. Di Fabrizio. Bacterial ratchet motors. *Proc. Natl. Acad. Sci. U.S.A.* **107** (21):9541, 2010. Cited on p. 96 and 162.

[41] G. Diana and M. Esposito. Mutual entropy production in bipartite systems. *J. Stat. Mech.: Theory Exp.* **2014** (4):P04010, 2014. Cited on p. 50.

[42] C. R. Doering and J. C. Gadoua. Resonant activation over a fluctuating barrier. *Phys. Rev. Lett.* **69** (16):2318, 1992. Cited on p. 27, 96, and 162.

[43] M. Doi. Second quantization representation for classical many-particle system. *J. Phys. A: Math. Gen.* **9** (9):1465, 1976. Cited on p. 28, 93, and 164.

[44] C. D. Dominicis. Technics of field renormalization and dynamics of critical phenomena. In *J. Phys.(Paris), Colloq*, pp. C1–247. 1976. Cited on p. 28, 153, 216, and 245.

[45] O. T. Dyer and R. C. Ball. Influence of thermal fluctuations on active diffusion at large Péclet numbers. *Phys. Fluids* **33** (5):051904, 2021. Cited on p. 122 and 170.

[46] F. J. Dyson. The Radiation Theories of Tomonaga, Schwinger, and Feynman. *Phys. Rev.* **75** (3):486, 1949. Cited on p. 36.

[47] J. Elgeti and G. Gompper. Run-and-tumble dynamics of self-propelled particles in confinement. *Europhys. Lett.* **109** (5):58003, 2015. Cited on p. 96.

[48] M. Esposito and C. Van den Broeck. Three faces of the second law. i. master equation formulation. *Phys. Rev. E* **82** (1):011143, 2010. Cited on p. 48, 59, and 66.

[49] B. Ezhilan, R. Alonso-Matilla, and D. Saintillan. On the distribution and swim pressure of run-and-tumble particles in confinement. *J. Fluid Mech.* **781**:R4, 2015. Cited on p. 96.

[50] T. Fallesen, J. Roostalu, C. Duellberg, G. Pruessner, and T. Surrey. Ensembles of Bidirectional Kinesin Cin8 Produce Additive Forces in Both Directions of Movement. *Biophys. J.* **113** (9):2055, 2017. 29117528. Cited on p. 170.

[51] T. F. Farage, P. Krinninger, and J. M. Brader. Effective interactions in active brownian suspensions. *Phys. Rev. E* **91** (4):042310, 2015. Cited on p. 96.

[52] R. Feynman, R. Leighton, and M. Sands. *The Feynman Lecturers in Physics*. Addison-Wesley, Reading, 1963. Cited on p. 162.

[53] É. Fodor, R. L. Jack, and M. E. Cates. Irreversibility and biased ensembles in active matter: Insights from stochastic thermodynamics. *arXiv:2104.06634* 2021. Cited on p. 216.

[54] É. Fodor, C. Nardini, M. E. Cates, J. Tailleur, P. Visco, and F. van Wijland. How far from equilibrium is active matter? *Phys. Rev. Lett.* **117** (3):038103, 2016. Cited on p. 27, 58, 96, and 97.

[55] É. Fodor, C. Nardini, M. E. Cates, J. Tailleur, P. Visco, and F. van Wijland. How Far from Equilibrium Is Active Matter? *Phys. Rev. Lett.* **117** (3):038103, 2016. Cited on p. 264.

[56] R. F. Fox. Uniform convergence to an effective fokker-planck equation for weakly colored noise. *Phys. Rev. A* **34** (5):4525, 1986. Cited on p. 96.

[57] D. Frydel. Positing the problem of stationary distributions of active particles as third-order differential equation. *Phys. Rev. E* **106** (2):024121, 2022. Cited on p. 96.

[58] D. Frydel. The run-and-tumble particle model with four-states: Exact solution at zero temperature. *Phys. Fluids* **34** (2):027111, 2022. Cited on p. 96.

[59] P. Galajda, J. Keymer, P. Chaikin, and R. Austin. A wall of funnels concentrates swimming bacteria. *J. Bacteriol.* **189** (23):8704, 2007. 17890308. Cited on p. 27, 96, and 162.

[60] M. Galassi, J. Davies, J. Theiler, B. Gough, G. Jungman, P. Alken, M. Booth, and F. Rossi. *GNU Scientific Library Reference Manual*. Network Theory Ltd., 3rd edition, 2009. https://www.gnu.org/software/gsl/, accessed 27 Oct 2020. Cited on p. 75.

[61] R. Garcia-Millan, J. Pausch, B. Walter, and G. Pruessner. Field-theoretic approach to the universality of branching processes. *Phys. Rev. E* **98** (6):062107, 2018. Cited on p. 28 and 261.

[62] R. Garcia-Millan and G. Pruessner. Run-and-tumble motion in a harmonic potential: field theory and entropy production. *J. Stat. Mech.: Theory Exp.* **2021** (6):063203, 2021. Cited on p. 28, 93, 96, 97, 114, 115, 119, 129, 170, 180, and 216.

[63] C. Gardiner. *Stochastic Methods*. Springer, Berlin, Germany, 2009. Cited on p. 40 and 102.

[64] P. Gaspard. Time-Reversed Dynamical Entropy and Irreversibility in Markovian Random Processes. *J. Stat. Phys.* **117** (3):599, 2004. Cited on p. 46, 47, 48, 49, 54, 59, 91, 170, and 210.

[65] A. Gelimson and R. Golestanian. Collective dynamics of dividing chemotactic cells. *Phys. Rev. Lett.* **114**:028101, 2015. Cited on p. 216.

[66] P. K. Ghosh, V. R. Misko, F. Marchesoni, and F. Nori. Self-Propelled Janus Particles in a Ratchet: Numerical Simulations. *Phys. Rev. Lett.* **110** (26):268301, 2013. Cited on p. 162.

[67] J. W. Gibbs. Fourier's Series. *Nature* **59** (1522):200, 1898. Cited on p. 175.

[68] G. Gompper, R. G. Winkler, T. Speck, A. Solon, C. Nardini, F. Peruani, H. Löwen, R. Golestanian, U. B. Kaupp, L. Alvarez, *et al.* The 2020 motile active matter roadmap. *J. Phys.: Condens. Matter* **32** (19):193001, 2020. Cited on p. 96 and 216.

[69] I. S. Gradshteyn and I. M. Ryzhik. *Table of integrals, series and products*. Academic Press, San Diego, CA, USA, 7th edition, 2007. Cited on p. 257.

[70] P. S. Hagan, C. R. Doering, and C. D. Levermore. Mean Exit Times for Particles Driven by Weakly Colored Noise. *SIAM J. Appl. Math.* **49** (5):1480, 1989. Cited on p. 162.

[71] T. Herpich, T. Cossetto, G. Falasco, and M. Esposito. Stochastic thermodynamics of all-to-all interacting many-body systems. *New J. Phys.* **22** (6):063005, 2020. Cited on p. 68.

[72] J. A. Hertz, Y. Roudi, and P. Sollich. Path integral methods for the dynamics of stochastic and disordered systems. *J. Phys. A: Math. Theor.* **50** (3):033001, 2016. Publisher: IOP Publishing. Cited on p. 216 and 221.

[73] P. C. Hohenberg and B. I. Halperin. Theory of dynamic critical phenomena. *Rev. Mod. Phys.* **49**:435, 1977. Cited on p. 216.

[74] J. Honkonen. Itô and Stratonovich calculuses in stochastic field theory. *Invited talk presented at The 12th Small Triangle Meeting on Theoretical Physics* 2011. Cited on p. 221.

[75] J. M. Horowitz and T. R. Gingrich. Thermodynamic uncertainty relations constrain non-equilibrium fluctuations. *Nat. Phys.* **16** (1):15, 2020. Cited on p. 47.

[76] W. Horsthemke and R. Lefever. *Noise-Induced Transitions - Theory and Applications in Physics, Chemistry, and Biology*. Springer-Verlag Berlin, Heidelberg, Germany, 1984. Cited on p. 82.

[77] W. R. Inc. Mathematica, Version 13.0.0, 2021. Champaign, IL, 2021. Cited on p. 195.

[78] H.-K. Janssen. On a lagrangean for classical field dynamics and renormalization group calculations of dynamical critical properties. *Z. Phys. B: Condens. Matter* **23** (4):377, 1976. Cited on p. 28, 216, and 245.

[79] H.-K. Janssen and U. C. Täuber. The field theory approach to percolation processes. *Ann. Phys.* **315** (1):147, 2005. Cited on p. 28.

[80] C. Jarzynski. Nonequilibrium Equality for Free Energy Differences. *Phys. Rev. Lett.* **78** (14):2690, 1997. Cited on p. 28.

[81] D.-Q. Jiang, M. Qian, and M.-P. Qian. *Mathematical Theory of Nonequilibrium Steady States: On the Frontier of Probability and Dynamical Systems*. Lecture notes in Mathematics. Springer-Verlag, Berlin, Heidelberg, Germany, 2004. Cited on p. 46.

[82] P. Jung and P. Hänggi. Dynamical systems: a unified colored-noise approximation. *Phys. Rev. A* **35** (10):4464, 1987. Cited on p. 96.

[83] F. Jülicher, A. Ajdari, and J. Prost. Modeling molecular motors. *Rev. Mod. Phys.* **69** (4):1269, 1997. Cited on p. 97.

[84] N. Koumakis, C. Maggi, and R. Di Leonardo. Directed transport of active particles over asymmetric energy barriers. *Soft Matter* **10** (31):5695, 2014. Cited on p. 27 and 162.

[85] H. A. Kramers. Brownian motion in a field of force and the diffusion model of chemical reactions. *Physica* **7** (4):284, 1940. Cited on p. 97.

[86] S. Kullback and R. A. Leibler. On Information and Sufficiency. *Ann. Math. Stat.* **22** (1):79, 1951. Publisher: Institute of Mathematical Statistics. Cited on p. 50.

[87] M. Kuś, E. Wajnryb, and K. Wódkiewicz. Mean first-passage time in the presence of colored noise: A random-telegraph-signal approach. *Phys. Rev. A* **43** (8):4167, 1991. Cited on p. 125.

[88] D. Lacoste, A. W. Lau, and K. Mallick. Fluctuation theorem and large deviation function for a solvable model of a molecular motor. *Phys. Rev. E* **78**:011915, 2008. Cited on p. 73.

[89] G. Lan and Y. Tu. Information processing in bacteria: memory, computation, and statistical physics: a key issues review. *Rep. Prog. Phys.* **79** (5):052601, 2016. Cited on p. 46.

[90] G. T. Landi, T. Tomé, and M. J. de Oliveira. Entropy production in linear Langevin systems. *J. Phys. A Math. Theor.* **46** (39):395001, 2013. Cited on p. 46.

[91] A. Lazarescu, T. Cossetto, G. Falasco, and M. Esposito. Large deviations and dynamical phase transitions in stochastic chemical networks. *J. Chem. Phys.* **151** (6):064117, 2019. Cited on p. 93.

[92] M. Le Bellac. *Quantum and Statistical Field Theory [Phenomenes critiques aux champs de jauge, English]*. Oxford University Press, New York, NY, USA, 1991. Translated by G. Barton. Cited on p. 216, 223, 235, 236, and 245.

[93] P. Le Doussal, S. N. Majumdar, and G. Schehr. Noncrossing run-and-tumble particles on a line. *Phys. Rev. E* **100** (1):012113, 2019. Cited on p. 97.

[94] J. L. Lebowitz and H. Spohn. A Gallavotti–Cohen-Type Symmetry in the Large Deviation Functional for Stochastic Dynamics. *J. Stat. Phys.* **95** (1):333, 1999. Cited on p. 49 and 55.

[95] A. Lefèvre and G. Biroli. Dynamics of interacting particle systems: stochastic process and field theory. *J. Stat. Mech.: Theory Exp.* **2007** (07):P07024, 2007. Cited on p. 216 and 226.

[96] A. Lesne. Shannon entropy: a rigorous notion at the crossroads between probability, information theory, dynamical systems and statistical physics. *Math. Struct. Comput. Sci.* **24** (3), 2014. Cited on p. 59.

[97] B. Lindner, M. Kostur, and L. Schimansky-Geier. OPTIMAL DIFFUSIVE TRANSPORT IN A TILTED PERIODIC POTENTIAL. *Fluct. Noise Lett.* **01** (01):R25, 2001. Cited on p. 101 and 162.

[98] S. A. M. Loos and S. H. L. Klapp. Heat flow due to time-delayed feedback. *Sci. Rep.* **9** (1):2491, 2019. Cited on p. 47.

[99] C. Maes. The Fluctuation Theorem as a Gibbs Property. *J. Stat. Phys.* **95** (1):367, 1999. Cited on p. 46.

[100] C. Maes, F. Redig, and A. V. Moffaert. On the definition of entropy production, via examples. *J. Math. Phys.* **41** (3):1528, 2000. Cited on p. 79.

[101] C. Maggi, U. M. B. Marconi, N. Gnan, and R. Di Leonardo. Multidimensional stationary probability distribution for interacting active particles. *Sci. Rep.* **5** (10742):1, 2015. Cited on p. 96.

[102] M. O. Magnasco. Forced thermal ratchets. *Phys. Rev. Lett.* **71** (10):1477, 1993. Cited on p. 27, 101, and 162.

[103] W. Magnus, F. Oberhettinger, and R. P. Soni. *Formulas and Theorems for the Special Functions of Mathematical Physics*. Springer-Verlag, Berlin, Germany, 1966. Cited on p. 74 and 75.

[104] Y. A. Makhnovskii, V. Rozenbaum, D.-Y. Yang, S. Lin, and T. Tsong. Flashing ratchet model with high efficiency. *Phys. Rev. E* **69** (2):021102, 2004. Cited on p. 101.

[105] K. Malakar, V. Jemseena, A. Kundu, K. V. Kumar, S. Sabhapandit, S. N. Majumdar, S. Redner, and A. Dhar. Steady state, relaxation and first-passage properties of a run-and-tumble particle in one-dimension. *J. Stat. Mech.: Theory Exp.* **2018** (4):043215, 2018. Cited on p. 20, 96, 97, 126, and 127.

[106] M. C. Marchetti, J. F. Joanny, S. Ramaswamy, T. B. Liverpool, J. Prost, M. Rao, and R. A. Simha. Hydrodynamics of soft active matter. *Rev. Mod. Phys.* **85** (3):1143, 2013. Cited on p. 27, 96, and 162.

[107] U. M. B. Marconi, N. Gnan, M. Paoluzzi, C. Maggi, and R. Di Leonardo. Velocity distribution in active particles systems. *Sci. Rep.* **6** (1):1, 2016. Cited on p. 96.

[108] U. M. B. Marconi and C. Maggi. Towards a statistical mechanical theory of active fluids. *Soft Matter* **11** (45):8768, 2015. Cited on p. 96.

[109] D. Martin, J. O'Byrne, M. E. Cates, É. Fodor, C. Nardini, J. Tailleur, and F. van Wijland. Statistical mechanics of active Ornstein-Uhlenbeck particles. *Phys. Rev. E* **103** (3):032607, 2021. Cited on p. 27, 96, 97, 162, and 206.

[110] P. C. Martin, E. D. Siggia, and H. A. Rose. Statistical dynamics of classical systems. *Phys. Rev. A* **8**:423, 1973. Cited on p. 28, 153, 216, and 245.

[111] M. Molaei, M. Barry, R. Stocker, and J. Sheng. Failed escape: solid surfaces prevent tumbling of Escherichia coli. *Phys. Rev. Lett.* **113** (6):068103, 2014. Cited on p. 122.

[112] T. Munakata and M. L. Rosinberg. Entropy production and fluctuation theorems for Langevin processes under continuous non-Markovian feedback control. *Phys. Rev. Lett.* **112** (18):180601, 2014. Cited on p. 47.

[113] C. Nardini, É. Fodor, E. Tjhung, F. van Wijland, J. Tailleur, and M. E. Cates. Entropy Production in Field Theories without Time-Reversal Symmetry: Quantifying the Non-Equilibrium Character of Active Matter. *Phys. Rev. X* **7** (2):021007, 2017. Cited on p. 27, 46, 58, and 216.

[114] I. Neri, É. Roldán, S. Pigolotti, and F. Jülicher. Integral fluctuation relations for entropy production at stopping times. *J. Stat. Mech.: Theory Exp.* **2019** (10):104006, 2019. Cited on p. 82.

[115] B. Øksendal. *Stochastic Differential Equations*. Springer, Berlin, Germany. Cited on p. 38.

[116] L. Onsager and S. Machlup. Fluctuations and Irreversible Processes. *Phys. Rev.* **91** (6):1505, 1953. Cited on p. 40, 57, and 154.

[117] T. E. Ouldridge, R. A. Brittain, and P. R. t. Wolde. The power of being explicit: demystifying work, heat, and free energy in the physics of computation. In *The Energetics of Computing in Life and Machines* (edited by D. H. Wolpert). SFI Press, 2018. Cited on p. 47.

[118] J. M. R. Parrondo, J. M. Blanco, F. J. Cao, and R. Brito. Efficiency of Brownian motors. *Europhys. Lett.* **43** (3):248, 1998. Cited on p. 97, 101, and 164.

[119] J. Pausch. *Topics in statistical mechanics*. Ph.D. thesis, Imperial College, 2019. Cited on p. 6, 28, 143, 220, and 238.

[120] J. Pausch and G. Pruessner. Is actin filament and microtubule growth reaction-or diffusion-limited? *J. Stat. Mech.: Theory Exp.* **2019** (5):053501, 2019. Cited on p. 93.

[121] G. A. Pavliotis. A multiscale approach to Brownian motors. *Phys. Lett. A* **344** (5):331, 2005. Cited on p. 27, 96, and 162.

[122] G. A. Pavliotis. *Stochastic Processes and Applications - Diffusion Processes, the Fokker-Planck and Langevin Equations*. Springer-Verlag New York, 2014. Cited on p. 55 and 82.

[123] L. Peliti. Path integral approach to birth-death processes on a lattice. *J. Phys.* **46** (9):1469, 1985. Cited on p. 28, 93, and 164.

[124] P. Pietzonka, É. Fodor, C. Lohrmann, M. E. Cates, and U. Seifert. Autonomous Engines Driven by Active Matter: Energetics and Design Principles. *Phys. Rev. X* **9** (4):041032, 2019. Cited on p. 27, 46, 97, 121, 164, and 171.

[125] P. Pietzonka and U. Seifert. Entropy production of active particles and for particles in active baths. *J. Phys. A: Math. Theor.* **51** (1):01LT01, 2017. Cited on p. 56.

[126] S. Pigolotti, I. Neri, É. Roldán, and F. Jülicher. Generic properties of stochastic entropy production. *Phys. Rev. Lett.* **119** (14):140604, 2017. Cited on p. 82.

[127] W. H. Press, S. A. Teukolsky, W. T. Vetterling, and B. P. Flannery. *Numerical Recipes*. Cambridge University Press, Cambridge, England, UK, 2007. Cited on p. 174.

[128] G. Pruessner. Lecture notes on non-equilibrium statistical mechanics, 2011. Cited on p. 6, 143, 216, 217, 218, and 238.

[129] G. Pruessner and R. Garcia-Millan. Field theories of active particle systems and their entropy production. *arXiv* 2022. 2211.11906. Cited on p. 164 and 179.

[130] S. Ramaswamy. The Mechanics and Statistics of Active Matter. *Annu. Rev. Condens. Matter Phys.* **1** (1):323, 2010. Cited on p. 27.

[131] N. Razin. Entropy production of an active particle in a box. *Phys. Rev. E* **102** (3):030103, 2020. Cited on p. 96, 97, 114, 115, 119, 129, 166, and 210.

[132] C. J. Reichhardt and C. Reichhardt. Ratchet Effects in Active Matter Systems. *Annu. Rev. Condens. Matter Phys.* **8**, 2016. Cited on p. 27 and 96.

[133] P. Reimann. Supersymmetric Ratchets. *Phys. Rev. Lett.* **86** (22):4992, 2001. Cited on p. 166, 198, and 202.

[134] P. Reimann, C. Van den Broeck, H. Linke, P. Hänggi, J. M. Rubi, and A. Pérez-Madrid. Giant Acceleration of Free Diffusion by Use of Tilted Periodic Potentials. *Phys. Rev. Lett.* **87** (1):010602, 2001. Cited on p. 82, 101, and 264.

[135] H. Risken. *The Fokker-Planck Equation*. Springer, Berlin, Germany, 1996. Cited on p. 6, 31, 40, 78, 80, 83, and 84.

[136] C. Roberts and G. Pruessner. Exact solution of a boundary tumbling particle system in one dimension. *Phys. Rev. Res.* **4** (3):033234, 2022. Cited on p. 96.

[137] C. Roberts and Z. Zhen. Run-and-tumble motion in a linear ratchet potential: analytic solution, power extraction and first-passage properties. *arXiv* 2023. 2303.07880. Cited on p. 6 and 95.

[138] J. Rodenfels, K. M. Neugebauer, and J. Howard. Heat Oscillations Driven by the Embryonic Cell Cycle Reveal the Energetic Costs of Signaling. *Dev. Cell* **48** (5):646, 2019. Cited on p. 47.

[139] E. Roldán, I. Neri, M. Dörpinghaus, H. Meyr, and F. Jülicher. Decision making in the arrow of time. *Phys. Rev. Lett.* **115**:250602, 2015. Cited on p. 51.

[140] T. Schmiedl and U. Seifert. Stochastic thermodynamics of chemical reaction networks. *J. Chem. Phys.* **126** (4):044101, 2007. Cited on p. 46.

[141] J. Schnakenberg. Network theory of microscopic and macroscopic behavior of master equation systems. *Rev. Mod. Phys.* **48** (4):571, 1976. Cited on p. 46 and 49.

[142] J. Schnakenberg. Network theory of microscopic and macroscopic behavior of master equation systems. *Rev. Mod. Phys.* **48** (4):571, 1976. Cited on p. 49.

[143] M. J. Schnitzer. Theory of continuum random walks and application to chemotaxis. *Phys. Rev. E* **48** (4):2553, 1993. Cited on p. 86 and 96.

[144] U. Seifert. Entropy production along a stochastic trajectory and an integral fluctuation theorem. *Phys. Rev. Let.* **95** (4):040602, 2005. Cited on p. 46, 47, 55, 57, 98, 114, and 128.

[145] U. Seifert. Lecture notes: 'soft matter. from synthetic to biological materials', 2008. Cited on p. 56.

[146] U. Seifert. Stochastic thermodynamics, fluctuation theorems, and molecular machines. *Rep. Prog. Phys.* **75** (12):126001, 2012. Cited on p. 28, 46, 49, 55, and 56.

[147] U. Seifert. Stochastic thermodynamics: From principles to the cost of precision. *Physica A* **504**:176, 2018. Cited on p. 46 and 47.

[148] K. Sekimoto. Kinetic Characterization of Heat Bath and the Energetics of Thermal Ratchet Models. *J. Phys. Soc. Jpn.* **66** (5):1234, 1997. Cited on p. 97.

[149] C. E. Shannon. A Mathematical Theory of Communication. *Bell Syst. Tech. J* **27** (3):379, 1948. Cited on p. 47, 50, and 114.

[150] J. Singh, A. E. Patteson, P. K. Purohit, and P. E. Arratia. Sedimentation and diffusion of passive particles in suspensions of swimming Escherichia coli. *arXiv* 2017. 1710.04068. Cited on p. 170.

[151] O. Sipos, K. Nagy, R. Di Leonardo, and P. Galajda. Hydrodynamic Trapping of Swimming Bacteria by Convex Walls. *Phys. Rev. Lett.* **114** (25):258104, 2015. Cited on p. 170.

[152] A. Slowman, M. Evans, and R. Blythe. Jamming and attraction of interacting run-and-tumble random walkers. *Phys. Rev. Lett.* **116** (21):218101, 2016. Cited on p. 216.

[153] E. Smith and S. Krishnamurthy. Path-reversal, doi-peliti generating functionals, and dualities between dynamics and inference for stochastic processes. *arXiv:1806.02001* 2018. Cited on p. 93.

[154] A. P. Solon, Y. Fily, A. Baskaran, M. E. Cates, Y. Kafri, M. Kardar, and J. Tailleur. Pressure is not a state function for generic active fluids. *Nat. Phys.* **11**:673, 2015. Cited on p. 28.

[155] Y. Song, J. O. Park, L. Tanner, Y. Nagano, J. D. Rabinowitz, and S. Y. Shvartsman. Energy budget of Drosophila embryogenesis. *Curr. Biol.* **29** (12):R566, 2019. Cited on p. 47.

[156] R. Soto and R. Golestanian. Self-assembly of active colloidal molecules with dynamic function. *Phys. Rev. E* **91** (5):052304, 2015. Cited on p. 216.

[157] R. E. Spinney and I. J. Ford. Entropy production in full phase space for continuous stochastic dynamics. *Phys. Rev. E* **85** (5):051113, 2012. Cited on p. 79.

[158] U. C. Täuber, M. J. Howard, and H. Hinrichsen. Multicritical Behavior in Coupled Directed Percolation Processes. *Phys. Rev. Lett.* **80** (10):2165, 1998. Cited on p. 28.

[159] J. Tailleur and M. E. Cates. Statistical Mechanics of Interacting Run-and-Tumble Bacteria. *Phys. Rev. Lett.* **100** (21):218103, 2008. Cited on p. 162.

[160] J. Tailleur and M. E. Cates. Sedimentation, trapping, and rectification of dilute bacteria. *Europhys. Lett.* **86** (6):60002, 2009. Cited on p. 96.

[161] U. C. Täuber, M. Howard, and B. P. Vollmayr-Lee. Applications of field-theoretic renormalization group methods to reaction–diffusion problems. *J. Phys. A: Math. Gen.* **38** (17):R79, 2005. Cited on p. 6, 93, 143, 179, 217, and 219.

[162] E. Tjhung, C. Nardini, and M. E. Cates. Cluster Phases and Bubbly Phase Separation in Active Fluids: Reversal of the Ostwald Process. *Phys. Rev. X* **8** (3):031080, 2018. Cited on p. 162.

[163] D. Tong. Lecture notes on kinetic theory, 2012. Cited on p. 6 and 31.

[164] U. C. Täuber. *Critical Dynamics: A Field Theory Approach to Equilibrium and Non-Equilibrium Scaling Behavior*. Cambridge University Press, 2014. Cited on p. 28, 57, 155, 164, 216, 221, 224, 226, and 245.

[165] C. Van den Broeck and M. Esposito. Three faces of the second law. ii. fokker-planck formulation. *Phys. Rev. E* **82** (1):011144, 2010. Cited on p. 78 and 79.

[166] N. G. van Kampen. *Stochastic Processes in Physics and Chemistry*. Elsevier Science B. V., Amsterdam, The Netherlands, 1992. Third impression 2001, enlarged and revised. Cited on p. 124, 125, and 235.

[167] A. Velenich, C. Chamon, L. F. Cugliandolo, and D. Kreimer. On the brownian gas: a field theory with a poissonian ground state. *J. Phys. A: Math. Theor.* **41** (23):235002, 2008. Cited on p. 216, 221, and 245.

[168] G. Vizsnyiczai, G. Frangipane, S. Bianchi, F. Saglimbeni, D. Dell'Arciprete, and R. Di Leonardo. A transition to stable one-dimensional swimming enhances E. coli motility through narrow channels - Nature Communications. *Nat. Commun.* **11** (2340):1, 2020. Cited on p. 170.

[169] C. G. Wagner, M. F. Hagan, and A. Baskaran. Steady-state distributions of ideal active Brownian particles under confinement and forcing. *J. Stat. Mech.: Theory Exp.* **2017** (4):043203, 2017. Cited on p. 96.

[170] B. Walter, G. Pruessner, and G. Salbreux. First passage time distribution of active thermal particles in potentials. *Phys. Rev. Res.* **3** (1):013075, 2021. Cited on p. 162.

[171] A. Walther and A. H. E. Müller. Janus Particles: Synthesis, Self-Assembly, Physical Properties, and Applications. *Chem. Rev.* **113** (7):5194, 2013. Cited on p. 27.

[172] M. B. Wan, C. J. Olson Reichhardt, Z. Nussinov, and C. Reichhardt. Rectification of Swimming Bacteria and Self-Driven Particle Systems by Arrays of Asymmetric Barriers. *Phys. Rev. Lett.* **101** (1):018102, 2008. Cited on p. 96.

[173] J. Wang. Landscape and flux theory of non-equilibrium dynamical systems with application to biology. *Adv. Phys.* **64** (1):1, 2015. Cited on p. 55.

[174] C. Wissel. Manifolds of equivalent path integral solutions of the Fokker-Planck equation. *Z. Phys. B: Condens. Matter* **35** (2):185, 1979. Cited on p. 38, 53, and 83.

[175] E. Woillez, Y. Zhao, Y. Kafri, V. Lecomte, and J. Tailleur. Activated Escape of a Self-Propelled Particle from a Metastable State. *Phys. Rev. Lett.* **122** (25):258001, 2019. Cited on p. 97, 102, 109, and 162.

[176] H. Xin, Q. Liu, and B. Li. Non-contact fiber-optical trapping of motile bacteria: dynamics observation and energy estimation - Sci. Rep. *Sci. Rep.* **4** (6576):1, 2014. Cited on p. 170.

[177] S.-X. Yang and H. Ge. Decomposition of the entropy production rate and nonequilibrium thermodynamics of switching diffusion processes. *Phys. Rev. E* **98** (1):012418, 2018. Cited on p. 88.

[178] K. T. Yiu. *Entropy Production and Time Reversal.* Master's thesis, Imperial College London, 2017. Cited on p. 93.

[179] X.-J. Zhang, H. Qian, and M. Qian. Stochastic theory of nonequilibrium steady states and its applications. part i. *Phys Rep.* **510** (1-2):1, 2012. Cited on p. 62.

[180] Z. Zhang and G. Pruessner. Field theory of free run and tumble particles in d dimensions. *J. Phys. A: Math. Theor.* **55** (4):045204, 2022. Cited on p. 28, 162, and 164.

[181] Z. Zhen and G. Pruessner. Optimal ratchet potentials for run-and-tumble particles. *arXiv* 2022. Cited on p. 6, 96, and 161.

A

Right to Reproduce

A.1 Copyright permission

Some of the work presented in this thesis was published in journals.

In Chapter 2, the article [30] was reproduced. The statement on their website

Copyright and Licensing

For all articles published in MDPI journals, copyright is retained by the authors. Articles are licensed under an open access Creative Commons CC BY 4.0 license, meaning that anyone may download and read the paper for free. In addition, the article may be reused and quoted provided that the original published version is cited. These conditions allow for maximum use and exposure of the work, while ensuring that the authors receive proper credit.

In exceptional circumstances articles may be licensed differently. If you have specific condition (such as one linked to funding) that does not allow this license, please mention this to the editorial office of the journal at submission. Exceptions will be granted at the discretion of the publisher.

A.2 Approval of co-authors

This section contains the proof of approval of all co-authors to reproduce published or submitted work. Authors appear in alphabetic order.

A.2.1 Bianca Buturca

Dear Bianca, Rosalba, Gunnar and Luca,

I am completing my PhD Thesis at Imperial College London entitled “Active particles, ratchets and their field theories”. I would like to use our jointly published paper “Entropy production in exactly solvable systems” (2020) as a part of my PhD thesis and cite it as a whole and verbatim. I would like to ask you as my co-authors for your approval. Your responses to this email will be included in the thesis as evidence.

Best wishes,

Zigan

She responded as follows.

Dear Zigan,

I give my approval for you to use our paper “Entropy production in exactly solvable systems” (2020) in your PhD thesis.

Best wishes,

Bianca

A.2.2 Marius Bothe

Dear both,

I am completing my PhD thesis at Imperial College London entitled “Active particles, ratchets and their field theories". I would like to use our preprint “Particle entity in the Doi-Peliti and response-field formalisms” (2022) as a part of my PhD thesis and cite it as a whole and with minor edits. I would like to ask you as my co-authors for your approval. Your responses to this email will be included in the thesis as evidence.

Best wishes,

Zigan

He responded as follows.

Dear Zigan,

I am happy for you to do this.

Cheers,

Marius

A.2.3 Luca Cocconi

Dear Bianca, Rosalba, Gunnar and Luca,

I am completing my PhD Thesis at Imperial College London entitled “Active particles, ratchets and their field theories”. I would like to use our jointly published paper “Entropy production in exactly solvable systems” (2020) as a part of my PhD thesis and cite it as a whole and verbatim. I would like to ask you as my co-authors for your approval. Your responses to this email will be included in the thesis as evidence.

Best wishes,

Zigan

He responded as follows.

Dear Zigan,

Of course I am happy for you to include our work in your thesis (as a whole and verbatim).

Best wishes,

Luca

Dear both,

I am completing my PhD thesis at Imperial College London entitled "Active particles, ratchets and their field theories". I would like to use our preprint “Particle entity

in the Doi-Peliti and response-field formalisms" (2022) as a part of my PhD thesis and cite it as a whole and with minor edits. I would like to ask you as my co-authors for your approval. Your responses to this email will be included in the thesis as evidence.

Best wishes,

Zigan

He responded as follows.

Dear Zigan,

Feel free to use the material from our preprint as you please in your thesis. And good luck with the final stretch of the writing up!

Best wishes,

Luca

A.2.4 Rosalba Garcia-Millan

Dear Bianca, Rosalba, Gunnar and Luca,

I am completing my PhD Thesis at Imperial College London entitled "Active particles, ratchets and their field theories". I would like to use our jointly published paper "Entropy production in exactly solvable systems" (2020) as a part of my PhD thesis and cite it as a whole and verbatim. I would like to ask you as my co-authors for your approval. Your responses to this email will be included in the thesis as evidence.

Best wishes,

Zigan

She responded as follows.

Dear Zigan

I am happy for you to cite and reproduce our paper in your thesis.

All the best

Rosalba

A.2.5 Gunnar Pruessner

Dear Bianca, Rosalba, Gunnar and Luca,

I am completing my PhD Thesis at Imperial College London entitled “Active particles, ratchets and their field theories”. I would like to use our jointly published paper “Entropy production in exactly solvable systems” (2020) as a part of my PhD thesis and cite it as a whole and verbatim. I would like to ask you as my co-authors for your approval. Your responses to this email will be included in the thesis as evidence.

Best wishes,

Zigan

He responded as follows.

Dear Zigan,

I am happy for you to quote verbatim any paper we have authored together.

All the best,

Gunnar

A.2.6 Connor Roberts

Dear Connor,

I am completing my PhD thesis at Imperial College London entitled "Active particles, ratchets and their field theories". I would like to use our preprint “Run-and-tumble motion in a linear ratchet potential: analytic solution, power extraction and first-passage properties” (2023) as a part of my PhD thesis and cite it as a whole and with minor edits. I would like to ask you as my co-authorc for your approval. Your responses to this email will be included in the thesis as evidence.

Best wishes,

Zigan

He responded as follows.

Dear Zigan,

You have my approval to include our preprint in your thesis.

Kind regards,

Connor